EPFL

Thèse n° 9821

Engineering of chitosan-based derivatives for non-viral gene delivery

Présentée le 29 juillet 2022

Faculté des sciences de base
Groupe SCI SB SG
Programme doctoral en chimie et génie chimique

pour l'obtention du grade de Docteur ès Sciences

par

Laura Camille Louise NICOLLE

Acceptée sur proposition du jury

Prof. C. Heinis, président du jury
Prof. S. Gerber, directrice de thèse
Dr A. Träger, rapporteuse
Prof. J.-C. Leroux, rapporteur
Dr R. Hovius, rapporteur

École polytechnique fédérale de Lausanne

2022

Acknowledgements

I would like to express my gratitude to Prof. Sandrine Gerber-Lemaire for offering me to work on such innovative, applied and interdisciplinary projects during both my Master and PhD theses. It exactly fulfilled what I was hoping for to start my scientific career. Her guidance along those years helped me to become the scientist I am today and I am very grateful for that.

I would like to thank Dr. Anja Träger, Prof. Jean-Christophe Leroux and Dr. Rudolf Hovius for accepting to be my jury members and for the time spent to examine my thesis manuscript. I also thank Prof. Christian Heinis for chairing this PhD defense.

This project led me to work in collaboration with two external laboratories from Switzerland: the teams of Prof. Jörg Huwyler from the University of Basel, and of Prof. Beat Thöny from the University Children's Hospital of Zürich. I thank all the members of both teams for their work on this project. Special thanks to Jens Casper for his implication in this project, but also for the fun times we had during our Basel-Lausanne exchange trips.

Many thanks also to Dr. Aurélien Bornet who taught me so much about 2D-DOSY NMR, and to the teams of both shops from BCH and CH buildings, that constantly tried to fulfill at best my requests. Special thanks to Jacques Gremaud and Maurizio Maïo for our friendly chitchats over the years.

My warmest thanks go to the amaaaaazing GBF members that I had the chance to work with for the past five years. Our working atmosphere was always great, and enjoying life with you outside of the lab was definitely awesome. Besides being my colleagues, most of you became my friends over time and I am truly sad to leave you. In particular, I would like to warmly thank Raph for his guidance during my Master, but also for everything that we shared about Kaamelott, TV shows, food, good wines, books and so on. The night life in Lausanne would also have been much different without your hospitality. Many thanks to Adrian with whom the new generation (finally!) started. I am very grateful for your help over the years regarding lab maintenance, we formed a great duo. Most importantly you were always here for a drink and to have fun such as during our memorable Just Dance parties, but also during our "Food trips" with Raph and Lea. The end of this PhD would have been so much different without the lovely presence of Perrine and Alessandra. I must admit I missed a lot these girly chitchats before you arrived. Thank you Perrine, for our morning discussions about life in general, I enjoyed those routine chitchats and will miss them. And you Alex (a.k.a the Post-it Queen), please never stop being so crazy and so joyful as you are! Your friendship means a lot to me, I am really sad we did not have more overlap together. I would also like to thank my dearest Harry Potter friend François (#HogwartsLegacy), for his constant chill vibes, and his puns, sometimes pretty good, sometimes pretty lame (especially at 8:00 am!). With François, there is always a Mayoutz nearby, because these two are one of the best colleague-friends pair I have ever met. Be sure Lucas that I enjoyed our F1 discussions as much as all the office was bewildered to see us talking about it! Simon (a.k.a Simswim, a.k.a Simsouin le marsouin), I know that you are not

one of the permanent of the lab (yet !), but it honestly feels like you already are. Your “weirdness” really adds an amazing touch to our lab. I would also like to thank Céline for her help on my project and the great time we had in Lecce in conference. Thanks also to Luca for bringing Palinka in our lives and to Jérémy for his advice all along my Master thesis. We did not have so much time to get to know each other, but I am really glad I crossed your path, Alireza. I know that you will achieve great work with Perrine and wish you the best for this. Lastly, thank you Sara for this amazing Madrid-Lausanne exchange, your stay was really intense, both work- and fun-wise!

The GBF group would not be complete without the continuous flow of Master students and apprentices that we hosted along the years. Besides Adrian and Perrine, I had the opportunity to supervise several other Master students and apprentices: Justine, David, Elias and Amélie, I truly hope you learnt interesting things by my side, for sure, I learnt a lot from supervising you! Many thanks also to Elise, the Master of cupcakes, as well as Laetitia, for their delightful presences in the lab those past months.

EPFL is a huge campus where you can meet sooo many people. Amongst all of them, special thanks to Nina, Dina, and Stéphanie for our lunches togethers, as well as Christophe for all our coffee breaks at Arcadie. Thank you also MagicRaph for your contagious happiness. I would also like to thank people from UNIGE, and especially past and current members of the Matile group who always welcomed me as one of them, and with whom I enjoyed so much parties in Geneva. In particular, thank you Antoine, Florence, and Rémi for your friendship and our boomer weekends. Many thanks also to Inga, Mickaël and Lea for the great time we got to spend together.

Life would be much more boring and difficult without my dear friends from Lyon. Thank you Marie, Eugénie, Julien, Sylvain, Guillaume and Justine for our awesome weekends and holidays in France and Europe (#loveyouguys). Octavie, Mathieu and Loïs, thanks you so much for all these Friday and Saturday nights squeezed in our respective minister schedules! Lastly, I am sure to stay young forever (#teqpaf) with my ~~dear~~ shameless friends Yohan and Izia who constantly change their life plans but always make room for our friendship.

Many thanks to my father who transmitted me his curiosity for science and to my mother for her daily support, I would not be writing this PhD without you. Thank you Guillaume and Audrey, my amazing brother and sister, life is always funnier when we are together.

I am also deeply grateful to Quentin, for his love and support for soooo many years. Besides being an awesome ~~boyfriend~~ very-soon-to-be husband (\o/), you are definitely the best life coach I could have ever dreamt of. Thank you for your support during this PhD, you are always by my side to help me reach any goal I may have in mind!

And lastly, thank you to anyone reading this thesis, I hope this reading will be pleasant and you will find whatever you are looking for.

Abstract

Gene therapy offers the possibility to treat or even cure diseases originating from genetic defects by introducing a therapeutic gene in target cells or correcting the initial defective gene. Amongst different options, non-viral vectors rely on the delivery of such genes using vehicles composed of lipids, inorganic nanoparticles or polymers. These systems are designed to protect the genetic material, while efficiently delivering it to the cells of interest. The initial backbone can be complemented with various components to help it overcome the many physiological barriers it may encounter during its journey. Amongst polymers, chitosan is a polysaccharide presenting many advantages for such purpose. Besides its biocompatibility and biodegradability, its potential for functionalization, thanks to numerous primary amines and hydroxyl groups, make it a backbone of choice for the preparation of a polymeric delivery vehicle. This work describes the covalent functionalization of chitosan with other polymers, peptides, and small molecules to later form polymeric nanoparticles condensing therapeutic DNA. Each component brings additional features to the initial system, thus finely tuning it for biological applications. The final system aims at treating liver inherited diseases such as ornithine transcarbamylase deficiency and phenylketonuria.

This manuscript first exposes the preparation of a chitosan-based cationic system able to properly condense anionic DNA through electrostatic interactions. Due to its excellent DNA condensation properties, polyethylenimine was grafted to chitosan *via* a succinyl linker. The first *in vitro* investigations confirmed the potential of the resulting core system, but *in vivo* experiments highlighted toxicity coming from the remaining cationic charge on the nanoparticles.

In order to better shield this cationic charge, bifunctional polyethylene glycol chains terminated by carboxylic acid moieties were grafted to chitosan amines. The resulting polymer was used to coat the first polymeric system through electrostatic interactions between the carboxylate groups and the remaining free amines of the chitosan-polyethylenimine derivative. The newly formed core-shell complex showed sustained cell viability *in vitro* and induced higher transfection efficiency of the gene as compared to the core system alone. However, its *in vivo* evaluation *via* retrograde intrabiliary infusion did not confirm such results: although transfection efficiency was retained, the core-shell complex did not significantly decrease the toxicity previously reported.

The last part of this work includes the decoration of the core-shell system with targeting ligands making possible to perform *in vivo* assays *via* intravenous injection, for which the developed polymeric systems did not induce toxicity in preliminary experiments. So far, only a proof-of-concept with folic acid, a tumor targeting ligand, was achieved. To do so, the shell polymer was further functionalized with folic acid-derived polyethylene glycol chains through strain-promoted azide-alkyne cycloaddition. The same strategy shall be applied in the near future with a liver-specific targeting ligand. Lastly, the improvement of the system's cell-penetration features was tackled by the grafting of cell-penetrating peptides to chitosan. The application of the resulting derivatives as shell polymers being unsuccessful,

a second strategy was developed with asparagusic acid-derived polyethylene glycol chains following the same strategy than for folic acid. Asparagusic acid moieties trigger endocytosis-independent cellular uptake of their cargos, thus circumventing their acidic endosomal degradation. Both targeting and cell-penetrating abilities of the core-shell system are currently investigated *in vitro*.

The polymeric vehicles produced by the end of these four years already tackle several essential aspects for an efficient gene delivery process. The following years will focus on its optimization in order to get one step closer to clinical applications.

Keywords: chitosan, liver-inherited disease, non-viral gene delivery, polyethylenimine, polymeric vehicle, polyethylene glycol, folic acid, asparagusic acid.

Résumé

Grâce à la thérapie génique il est possible de traiter ou même de soigner les maladies d'origine génétique. Le but est soit d'introduire un gène thérapeutique dans les cellules d'intérêts ou de directement modifier le gène d'origine. Parmi les différentes options en cours de développement, les vecteurs non-viraux permettent d'administrer ce type de gènes à l'aide de véhicules composés de lipides, de nanoparticules inorganiques ou de polymères. Ces systèmes sont préparés avec l'intention de protéger le matériel génétique tout en le livrant rapidement et efficacement dans les cellules cibles. Plusieurs additifs peuvent servir à compléter le système de base afin de l'aider à affronter les différentes barrières physiologiques qu'il pourrait rencontrer au cours de son trajet. En ce qui concerne les polymères, le chitosan est un polysaccharide qui présente de nombreux avantages pour ce type d'application. Mis à part sa biodégradabilité et sa biocompatibilité, son haut potentiel de fonctionnalisation grâce à ses nombreux groupes alcools et amines primaires en fait un produit de départ idéal pour le développement d'un système polymérique de livraison de gènes. Ce travail de thèse décrit ainsi la fonctionnalisation covalente du chitosan avec d'autres polymères, mais aussi avec des peptides et des petites molécules, pour ensuite former des nanoparticules polymériques capable de condenser l'ADN. Chaque composant du système final apporte une fonction supplémentaire, permettant ainsi de l'affiner en vue d'applications biologiques. Le but final est de traiter certaines maladies héréditaires du foie comme la déficience en ornithine transcarbamylase et la phénylcétonurie.

Ce manuscrit commence par présenter la préparation d'un système cationique à base de chitosan, qui puisse condenser efficacement l'ADN par interactions électrostatiques. Grâce à ces propriétés de condensation, le polyéthylène imine a ainsi été greffé sur le chitosan *via* un linker succinyl. Les premiers tests *in vitro* ont confirmé le potentiel de ce système de base, mais les expériences *in vivo* ont souligné une certaine toxicité émanant des charges résiduelles positives après complexation.

Afin de mieux cacher ces charges positives et améliorer la stabiltié colloidale, des chaînes de polyéthylène glycol bi-fonctionnalisées et terminées par des acides carboxyliques ont été greffées sur les amines du chitosan. Le polymère correspondant a permis de recouvrir le premier système grâce à des interactions électrostatiques entre les carboxylates du polyéthylène glycol et les amines libres restantes du dérivé chitosan-polyéthylène imine. Le système noyau-enveloppe (*core-shell*) ainsi obtenu a démontré une viabilité cellulaire maintenue *in vitro* et a induit de plus hautes transfections du gène par rapport au système de base. Cependant, l'évaluation *in vivo* de ce système *via* infusion intrabiliaire rétrograde n'a pas confirmé ces résultats, avec seulement une transfection maintenue par rapport à celle d'origine. Par ailleurs, le système noyau-enveloppe n'a pas réduit de manière significative la toxicité préalablement observée.

La dernière partie de cette thèse s'est concentrée sur la décoration du système noyau-enveloppe, et notamment sur la greffe de ligands de ciblage afin d'effectuer les prochains essais *in vivo* par injection intraveineuse. D'après nos tests préliminaires, les polymères déjà développés n'induisent pas de toxicité

par cette méthode d'administration. Pour le moment, seule la conjugaison de l'acide folique, un ligand de ciblage de cellules cancéreuses, a été effectuée afin de valider la stratégie. Utilisant des chaînes de polyéthylène glycol, préalablement conjuguées avec de l'acide folique et un derivé de cyclooctyne, le polymère d'enveloppe a été fonctionnalisé avec ces dernières selon une cycloaddition alcyne-azoture. Nous prévoyons d'appliquer la même stratégie à un ligand de ciblage des cellules du foie dans un futur proche. Pour finir, des peptides sélectionnés pour leur haute capacité de pénétration cellulaire (*cell-penetrating peptides*) ont été greffés sur des chaînes de chitosan dans l'optique d'améliorer la pénétration cellulaire du système polymérique final. Cette stratégie n'ayant pas été fructueuse, une deuxième approche utilisant des chaînes de polyéthylène glycol conjuguées à de l'acide asparagusique a été développée. Il a en effet été prouvé récemment que l'acide asparagusique peut induire un mécanisme d'internalisation cellulaire qui ne dépend pas de l'endocytose, permettant ainsi à ses cargos de ne pas être dégradés par le pH acide des endosomes. Cette stratégie reprend la même que celle de l'acide folique. Les systèmes de ciblage et de pénétration cellulaire sont actuellement en cours de tests *in vitro.*

Le véhicule polymérique produit suite à ces quatre ans de thèse a d'ores et déjà abordé plusieurs points essentiels pour un procédé de livraison de gènes efficace. Les années à venir se concentreront sur son optimisation afin de se rapprocher petit à petit des applications cliniques.

Mots-clés : chitosan, maladie héréditaire du foie, vecteurs non-viraux, polyéthylène imine, véhicule polymérique, polyéthylène glycol, acide folique, acide asparagusique.

Abbreviations

A

AAV	Adeno-associated virus
Acr	Acrylate
ALP	Alkaline phosphatase
ALT	Alanine transaminase
ASGPr	Asialoglycoprotein receptor
AspA	Asparagusic acid

B

BPEI	Branched PEI

C

CA	Citric acid
CDI	1,1'-Carbonyldiimidazole
CMCS	*O*-carboxymethyl CS
CNT	Carbone nanotubes
COS	CS oligosaccharides
COVID-19	Coronavirus disease 2019
c/p ratio	Ratio dCS derivative/DNA
CPD	Cell-penetrating poly(disulfide)
CPP	Cell-penetrating peptide
CS	Chitosan
Cy3	Cyanine 3

D

DBU	1,8-diazabicyclo(5.4.0)undec-7-ene
DC-Cholesterol	3β-[*N*-(*N',N'*-dimethylaminoethane)-carbamoyl]cholesterol
DCM	Dichloromethane
dCS	Depolymerized CS
DD	Deacetylation degree
D-Gal	D-Galactose
D-GalNAc	*N*-acetyl-D-galactosamine
DIBO	Dibenzocyclooctyne
DIPEA	*N,N*-Diisopropylethylamine
DLS	Dynamic light scattering
DMAP	4-Dimethylaminopyridine
DMF	Dimethylformamide
DMSO	Dimethylsulfoxide
DMTMM	4-(4,6-dimethoxy-1,3,5-triazin-2-yl)-4-methyl-morpholinium chloride
DNA	Deoxyribonucleic acid
DOGS	Dioctadecylamido-glycylspermine
DOPE	Dioleoyl-phosphatidylethanolamine
DOSPA	Cholesterol, 2,3-dioleyloxy-*N*-[2(sperminecarboxamido)ethyl]-*N,N*-dimethyl-1-propanaminium trifluoroacetate
DOTAP	1,2-dioleoyl-3-trimethylammoniumpropane
DOTMA	*N*-[1-(2,3-dioleyloxy)propyl]-*N,N,N*-trimethyl-ammonium chloride
DPPES	Dipalmitoylphosphati-dylethanolamidospermine
DSC	*N,N'*-disuccinimidyl carbonate
DTNB	5,5'-Dithiobis(2-nitrobenzoic acid)

E

EDC.HCl	*N*-ethyl-*N*′-(3-dimethylaminopropyl)carbodii mide hydrochloride
EGFP	Enhanced GFP
ER	Endoplasmic reticulum

F

FA	Folic acid
FR	Folic acid receptor
FTIR	Fourier transform infrared

G

GD	Grafting degree
GFP	Green fluorescent protein
GPC	Gel permeation chromatography

H

HIV	Human immunodeficiency virus
HOBt	Hydroxybenzotriazole
HuH-7	Hepatocellular carcinoma cell line

L

LA	Lactobionic acid
LPEI	Linear PEI
Luc	Luciferase

M

Mal	Maleimide
miRNA	Micro RNA
MW	Molecular weight
Mn	Number average MW
Mp	MW of the peak maxima
MTS	3-(4,5-dimethylthiazol-2-yl)-5-(3-carboxymethoxyphenyl)-2-(4-sulfophenyl)-2H-tetrazolium
Mw	Weight average MW

N

n.CAG.GFP1	GFP expressing Nanoplasmid™ with the ubiquitous CAG promoter
n.CAG.Luc2	Luc expressing Nanoplasmid™ with the ubiquitous CAG promoter
NHS	*N*-Hydroxysuccinimide
NLS	Nuclear localization signal
NMR	Nuclear magnetic resonance
NP	Nanoparticle
NPC	Nuclear pore complex
n.P3.Luc1	Luc expressing Nanoplasmid™ with the liver-specific P3 promoter

P

PAMAM	Polyamidoamine
PBS	Phosphate buffered saline
PD	Polydispersity
PDI	Polydispersity index
pDNA	Plasmid DNA
PEG	Polyethylene glycol
PEI	Polyethylenimine
PEtOx	Poly(2-ethyl-2-oxazoline)
pH	Potential hydrogen
PLGA	Poly(lactide-co-glycolide)

PLL	Poly-L-lysine
PNA	Peptide nucleic acids

Q

QD	Quantum dots

R

RNA	Ribonucleic acid

S

shRNA	Short hairpin RNA
siRNA	Silencing RNA
sulfo-NHS	N-hydroxysulfosuccinimide
SV40	Simian virus 40
SYBR	Synergy Brands, Inc.

T

TAT	Transactivator of transcription
TBTU	2-(1H-Benzotriazole-1-yl)-1,1,3,3-tetramethylaminium tetrafluoroborate
THF	Tetrahydrofuran
TL	Targeting ligand
TLC	Thin layer chromatography
TLR	Toll-like receptor
TMCS	Trimethyl CS
Ts	Tosyl
2D-DOSY	2D-Diffusion ordered spectroscopy

Table of content

Chapter 1 Introduction

1.1. Gene therapy

1.1.1. Definition

While protein therapy emerged as a promising field in the 80s, its development has been hampered by several obstacles such as proteins' short half-life in blood circulation, as well as their low bioavailability, and fast degradation by enzymes *in vivo*.[1] Together with repetitive injections leading to toxicity and expensive manufacturing, protein therapy still requires some improvements to be considered as a viable long-term solution. Consequently, transfecting the gene coding for the desired protein(s) appeared as an alternative strategy. This is the basics of gene therapy.

Gene therapy primarily aims at replacing a defective gene with its healthy copy or modifying its expression through the transfection of specific RNA sequences. This method was initially envisioned for inherited genetic disorders but may also be adapted to acquired diseases linked to genetic mutations.[2] Theoretically, a single treatment should be enough to cure the patient. Additional assets of gene therapy may include a long-lasting production of the desired protein and its localized expression in targeted cells, thus avoiding potential off-target effects. So-called "germ line" gene therapy relies on the insertion or modification of a gene in an individual's reproductive cells, meaning this change may be inherited by its offspring, potentially fixing the genetic disorder on the long run. On the contrary, somatic gene therapy induces modifications that are restricted to the patient and cannot be transmitted. Due to ethical reasons, "germ line" gene therapy has not been authorized in every countries.[1]

Depending on the desired modifications, the transfected exogenous DNA/RNA sequences do not have the same goal (Figure 1).[3] The prime goal of gene therapy is to restore normal cellular function by transfecting a healthy copy of the defective or missing gene and inducing its expression. This approach is sometimes called augmentation gene therapy (Figure 1). Alternatively, the mutated gene may cause a gain-in-function which dysregulates the cellular function. In this case, gene suppression can be achieved through the transfection of DNA sequences coding for inhibitory sequences such as short hairpin RNA (shRNA) and micro (miRNA) (Figure 1). This down-regulates the target protein to restore normal levels of expression. Lastly, although not applicable yet in clinical trials, genome editing aims at directly correcting the mutated gene in a precise location through the use of genome editing tools (Figure 1).[4–6]

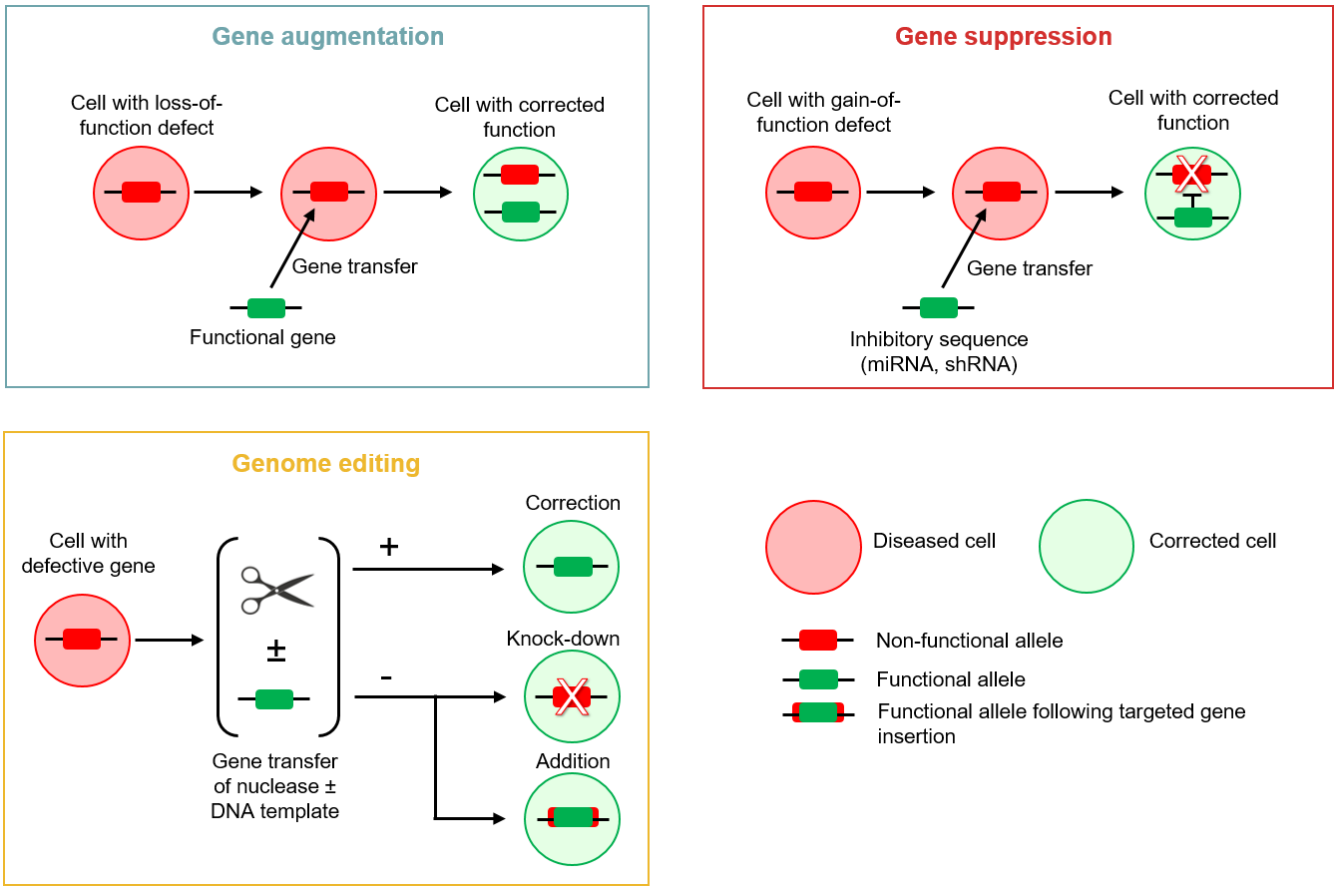

Figure 1. Schematic representation of the different gene therapy modalities.

Two strategies are possible to administer a therapeutic gene to a patient. In *ex vivo* therapies, the targeted cells are harvested from the patient and transfected with the therapeutic gene. After treatment, the cells are injected back in the patient. *In vivo* therapies consist in systemically or locally injecting the therapeutic gene, which reaches the targeted cells, gets internalized and is ultimately expressed.

Due to ubiquitous presence of endonucleases in the blood stream, the genetic material of interest is rarely administered alone to avoid fast degradation. Two main strategies have been developed over the past decades to promote efficient transfection and expression: the therapeutic gene is either incorporated into the genome of recombinant viruses, forming so-called viral vectors, or non-viral RNA/DNA sequences containing the gene of interest are engineered and protected by non-viral delivery vehicles (Figure 2).

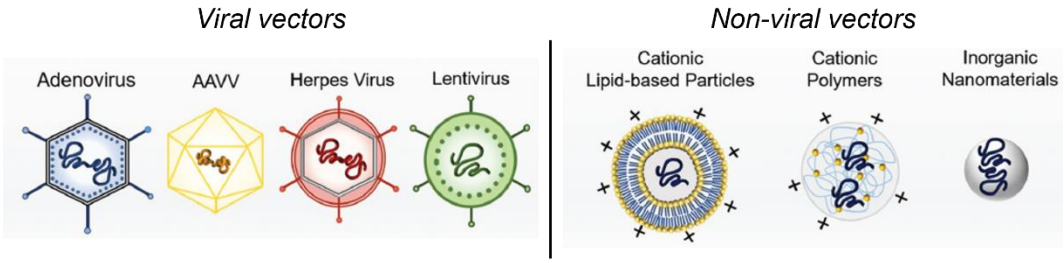

Figure 2. Spectrum of viral and non-viral vectors. Adapted from Conniot *et al.*[7]

1.1.2. Viral vectors

Due to their natural ability to invade cells and deliver a genetic cargo, viruses have been first investigated as potential gene therapy tools.[8] Gene transfer is usually achieved with replication-deficient recombinant viruses that express the desired transgene without expressing viral proteins necessary to virus assembly.[9] The spectrum of viral vectors used includes simple capsid virions such as adenoviruses or adeno-associated viruses, and others such as retroviruses and herpes viruses (Figure 2). Packaging capacity, integration ability in the host genome, or transduction capacity depend on the type of viral vector.[7] So far, retroviruses and adeno-associated viruses (AAV) have been the most successful viral vectors in clinics.

Retroviral vectors faithfully transfect cells by integrating their complementary DNA into the host genome upon reverse transcription of their RNA genome into double stranded DNA.[9] The viral genome penetrates the nucleus mainly during mitosis, during which nuclear breakdown occurs. This type of vectors is consequently more suited to address dividing cells than non-dividing or quiescent cells, such as hepatocytes. γ–Retroviral vectors are the first generation viruses that induced successful gene delivery in hematopoietic stem cells, the self-renewing cells that give rise to all blood cell lineages.[2,3] The two major drawbacks of these vectors were the risks of undesired mutations resulting from viral genome insertion, a phenomenon called insertional mutagenesis, and immune responses directed against transgenes, due to the presence of too high proportions of viral sequence. To bypass this issue, almost all the viral sequence of these vectors was replaced by target therapeutic genes, allowing the accommodation of relatively large DNA segments (up to 8 kb). In particular, retroviral vectors derived from the human immunodeficiency virus (HIV) have been used as carriers because of their ability to transfect non-dividing cells. Named lentiviruses, they are currently widely applied for *ex vivo* therapies on hematopoietic stem cells.[2]

Adeno-associated viruses (AAV) are non-enveloped parvoviruses with small (4.7 kb), single-stranded DNA.[9] Engineered AAV have a non-integrative genome which remains in an extrachromosomal state in the nucleus, thus preventing insertional mutagenesis. Their viral genes are naturally not replicating in the host, trigger only a weak immune response and can be replaced by foreign DNA at more than 95%. The immune response usually generated comes from their inactivation by neutralizing antibodies. The pre-existence of such antibodies in a significant part of the global population nonetheless restrains AAV application.[7] The small packaging size of AAV as well as their complex production processes are additional shortcomings. However, their major advantage lies in their ability to infect both dividing and non-dividing cells. Engineering of AAV is nowadays a hot topic in viral vectors research and aims at overcoming the aforementioned drawbacks.[10]

In summary, viral vectors offer excellent gene expression abilities but at cost of immunogenicity and insertional mutagenesis. Limited DNA packaging capacity and complex production processes are two common shortcomings to any viral vectors.[11] Although several viral gene therapies have reached the market (*cf.* section 1.1.4), growing interest for an alternative solution that could address their limitations has arisen over the decades.

1.1.3. Non-viral genetic material

Non-viral vectors do not contain any viral components, whether it be the genetic material or the protecting envelope, and have been engineered to overcome the limitations of viral vectors. The envelope is usually based on polymers, lipids, or inorganic nanoparticles (NPs), to cite only a few (Figure 2). A complete description of the different types of non-viral vehicles will be given in section 1.2.

Besides delivery vehicle engineering, the choice of the appropriate genetic material is also important for successful applications. While viral vectors are limited in the variety of genetic material, mostly regarding size, non-viral delivery vehicles can accommodate any size of cargo. RNA-based vectors are an interesting alternative to viral DNA due to their action external to the nucleus.[12] However they can only induce transient expression, and suffer from lower stability compared to DNA.

In this view, plasmid DNA (pDNA) hold a great potential as genetic materials for non-viral gene delivery due to their low cost, long shelf-life, as well as their ease of production, shipment and storage.[8] pDNA are large (> 10 kb), circular and non-integrative double-stranded DNA originating from bacteria. They can be easily engineered to contain a therapeutic gene.[13] The "origin of replication" of pDNA is conditional for bacteria, meaning the plasmid replicates solely in them. Due to their low immunogenicity, pDNA can be repeatedly administered to patients. Their non-integrative property also prevents insertional mutagenesis. Transient expression of the gene might however be an issue, especially in fast-dividing cells where division leads to rapid dilution of the plasmid over time. In addition, the topology of engineered pDNA and the amounts of nucleic acids of bacterial origin often lead to limitations in their applications.[13,14] Therefore, many efforts have been made to improve pDNA especially regarding the reduction of the bacterial backbone size under the 1 kb threshold.

Although mini-circles DNA have been widely investigated as successors of pDNA, the tedious removal of all the bacterial sequences, and consequently the high production costs, represent major drawbacks.[15,16] In the mini-vectors family, Nanoplasmids™ are plasmids with a minimalistic bacterial backbone, including a mini-origin of replication.[8,17] They contain less than 0.5 kb of bacterial sequence, thus standing under the limit of detection of 1 kb for endogenous gene silencing. The origin of replication allows conditional replication of these mini-vectors only in the strain of origin, which prevents random replication of the plasmid in bacteria of the host. The production process is drastically improved as compared to mini-circles, with higher yields and reduced costs, facilitating their production on industrial scales.[17] The tremendous potential of these non-viral vectors should be soon translated into gene therapy clinical trials.

Common to any non-viral genetic material, gene promoters are small non-coding DNA sequences, inserted just before the coding sequence of the therapeutic gene. They are used to induce systemic or specific expression of the desired gene by binding to transcription factors. In particular, the CAG promoter allows the expression of the gene in any type of cells, whereas the P3 promoter is specific to hepatocytes.

1.1.4. From bench to bedside

Gene therapy clinical trials started with viral vectors formulations in the 90s. The vectors issued from the first decade were supported by strong optimism but did not show significant clinical benefits. In reality, they rather produced unexpected toxicities that even turned out to be lethal in the case of an adenovirus-based ornithine transcarbamylase deficiency treatment.[18]

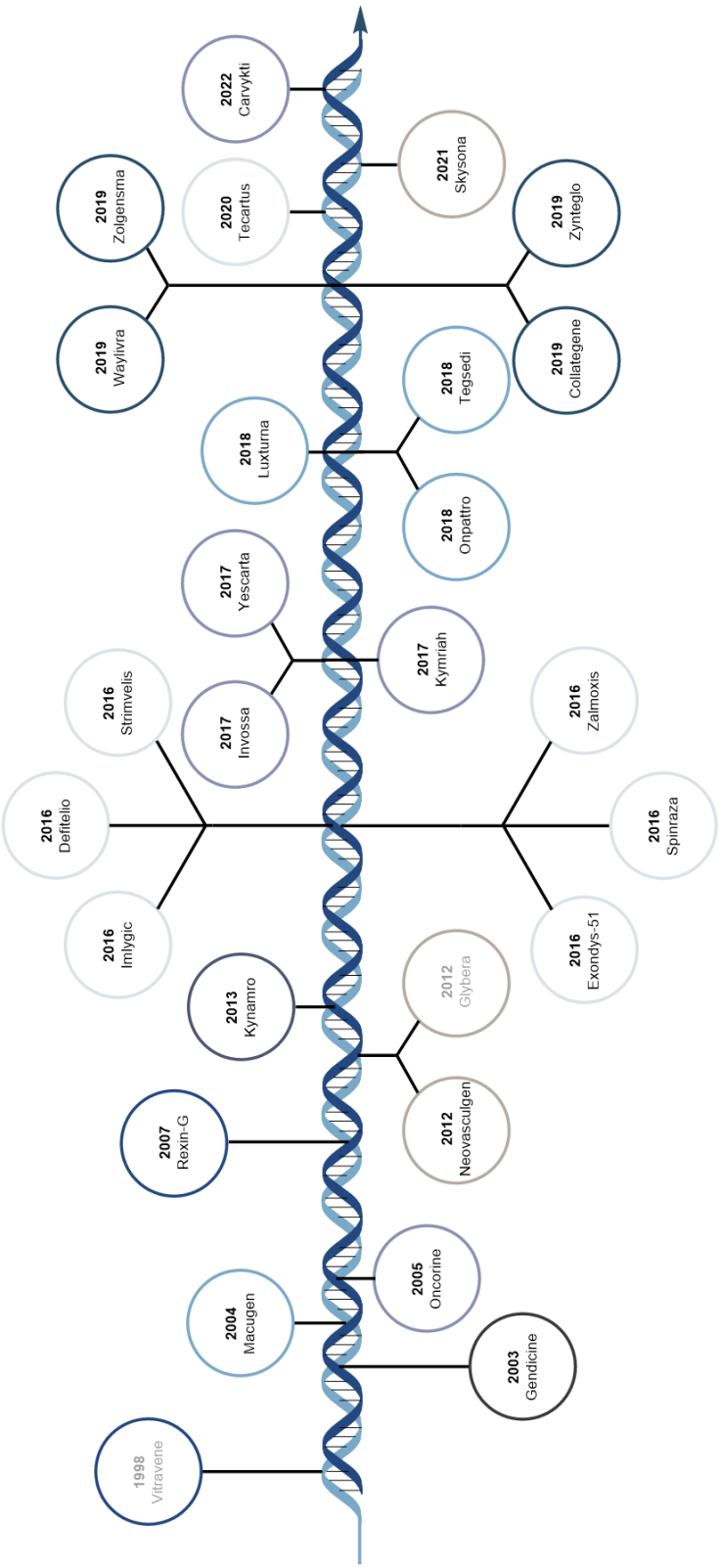

Figure 3. Timeline of approved gene therapies from 1998 to now. Most drugs are *in vivo* gene therapies, except the following ones which are *ex vivo* gene therapies: Strimvelis, Zalmoxis, Invossa, Yeskarta, Kymriah, Zyntelgo, Tecartus, Skysona and Carvykti. In grey, Vitravene (1998) and Glybera (2012) were withdrawn from the market in 2002 and 2017, respectively.

After further maturation of the field, notably on the basic science underlying gene therapies, substantial improvements were observed in clinical trials conducted in the 2000s. This led to the approval of four therapies before 2010 (Figure 3). The recombinant adeno-viral vector Gendicine was approved in 2003, after the withdrawal of Vitravene. Gendicine is considered the first officially commercialized gene therapy.[19] Since then, the number of approved therapies has steadily increased, even if it varies from one country to another, depending on their regulations. Despite a limited gene expression, the injection of naked DNA still attracted researchers for its ease of handling and safety. This led to the approval of several gene therapies, such as Neovasculgen in 2011 constituted of a plasmid encoding the vascular endothelial growth factor indicated for the treatment of peripheral vascular disease. Antisense oligonucleotides can also be injected in a similar fashion. They are short (15-30 bp), synthetic and single-stranded oliodeoxynucleotides that can alter mRNA to regulate protein expression. They reached the market several times with for example Vitravene in 1998 and Tegsedi more recently (2018). Glybera was the first gene therapy approved in Europe in 2012 and aimed at the treatment of familial lipoproteine lipase deficiency with a recombinant AAV. With a cost per patient above $1.2 million, Glybera was removed from the market in 2017 for economic reasons.[20] Most approved gene therapies target orphan diseases, but therapies for cardiovascular diseases (Neovasculgen, Collategene) and cancers (Gendicine, Oncorine, Imlygic) are also available on the market.[19] Overall, *in vivo* therapies still represent the major part of approved treatments but the proportions of *ex vivo* therapies has increased significantly in the past ten years (Figure 3).

Viral vectors represent about 70% of therapies entering clinical trials nowadays, probably due to the earlier interest they aroused.[21] The remaining 30% consist in majority in the delivery of naked DNA such as pDNA and antisense oligonucleotides. Regarding non-viral gene therapy, Onpattro has been approved in 2018 for the treatment of familial amyloid polyneuropathy. Onpattro is composed of lipid-based NPs encapsulating silencing RNA for the knockout of transthyretin, a protein produced in the liver (Figure 3). The clinical phases demonstrated a sustained decrease of protein levels, as well as decreased symptoms for the disease, having a highly positive impact on the patients' quality of life.[20] In 2020, messenger RNA COVID-19 vaccines based on lipid NPs such as Comirnaty and Spikevax, have been successfully and massively injected to the global population after conditional approval.[22] Such promising applications strongly encourages further research in non-viral gene delivery. The next sections of this introduction will focus only on DNA-based gene therapies, which have so far not reached the market.

1.2. Non-viral gene delivery vehicles

While viral vectors are based on natural systems that evolved to bypass the different biological barriers, non-viral delivery vehicles have to be wisely engineered to overcome them. They can be divided in two broad categories: physical and chemical techniques.

1.2.1. Gene delivery by physical means

Being most of the time carrier-free delivery methods, physical gene deliveries rely on the forced permeation of the cell membrane to introduce DNA by diffusion. The following paragraphs detail the major techniques used to create these transient defects at localized points of the membrane.

1.2.1.1. Gene gun

Commercialized as early as the late 90s, the gene gun employs biocompatible heavy metals like gold, silver or tungsten as DNA carriers.[1] After DNA coating *via* precipitation, the metallic NPs are loaded in a plastic tubing, accelerated and mechanically delivered into the treatment zone thanks to pressurized helium.[23] As it does not depend on receptor-mediated uptake, this technique can be applied to a wide range of cells. Being limited by the degree of penetration in tissues, this technique is usually applied to skin-related diseases. A long-lasting and high level of gene expression can be achieved as reported for the administration of green fluorescent protein (GFP)-encoding pDNA into skin dendritic cells.[24]

1.2.1.2. Electroporation

Using two electrodes, intense electric pulses can be applied to tissues of interest, causing an increase in cell membrane permeability for a short period of time and allowing DNA to freely diffuse into cells. Electroporation has been successfully applied on various tissues, and quite extensively on skin and muscles.[25] This method has been largely used in *in vitro* gene therapy studies to shortcut the issues related to delivery processes, in particular the mechanisms of nuclear internalization and DNA expression, as well as the influence of the genetic material size (*cf.* section 1.3.1).[26,27] However, the invasiveness and potential harmfulness of electroporation limit its development *in vivo*.[25] Recently, Li and coworkers reported the use of a high-density microneedle array delivering a low-voltage and a uniform electric field during the electroporation process.[28] This work demonstrated a drastic reduction of cell damage, showing promises for further developments *in vivo*.

1.2.1.3. Sonoporation

Sonoporation relies on the transient perforation of the cell membrane by ultrasounds, with frequencies usually in the MHz range.[29] Ultrasound waves create pores or acoustic cavitations in the cellular membrane, leading to its permeation and DNA penetration. The transfection efficiency being lower than for electroporation, this method has evolved in recent years towards the preparation of microbubbles composed of lipids or polymers that are submitted to sonoporation once they have reached the target cells.[30] Although more in-depth studies need to be done on the mechanism of action and potential harmfulness of sonoporated microbubbles,[31] sonoporation is considered as a promising technique for gene delivery in clinics, as it is safe and non-invasive, allowing to reach internal organs without surgery. Studies on small and large animal models are in progress.[32]

1.2.1.4. Hydrodynamic injection

Hydrodynamic injection has caught a lot of attention for its simplicity, efficiency and versatility compared to existing delivery techniques.[33,34] With this procedure, a large volume of DNA (8-10% of

the body weight) can be introduced into the blood stream and internal organs through high-speed injection for few seconds (3-7 s depending on the organ). Such high transient pressure leads to the permeation of parenchymal cells and allows DNA entry. Hydrodynamic injection has been particularly efficient and promising for DNA delivery to the liver.[35,36] Because of its simplicity, this method is still the most widely used for DNA transfection into rodents, even though it can cause temporary dysfunctions of the cardiac system, considerable increase of the blood pressure across the liver, as well as significant organ expansion.[33] Due to the risks associated with cardiac congestion in humans, this method is not advised for clinical applications.

1.2.1.5. Assets and limitations

Although physical methods promise exciting developments in the future, their application in clinical setups is hampered by serious drawbacks, including invasiveness, poor transfection efficiency or expensive instrumentation. The localized application of these techniques can either be an asset and leads to high transfection efficiency in the targeted area, or be an additional issue to overcome because the whole tissue cannot be completely transfected. The major advantage of such techniques is their possibility to bypass systemic injection and some extra- and intracellular barriers, which is well suited to the context of exploratory studies. The impossibility to target a specific cell type in a same tissue is another reason for focusing on other alternatives.

1.2.2. Gene delivery by chemical means

Non-viral vectors produced from chemicals are promising alternatives to viral vectors and physical techniques of DNA transfection. These formulations exhibit reduced toxicity, do not suffer from DNA-size limitations and are easier to produce.[7] Moreover, they are less complex to set up and less invasive, as compared to physical methods.[37] However, they lead to lower transfection efficiencies compared to viral vectors, due to the numerous biological barriers they have to face.

Non-viral vectors are composed of a carrier into or onto which DNA is loaded *via* different techniques. The nanocarriers are designed to fulfill four major objectives:

- Mask the negative charges of DNA that disfavor its interaction with the negatively charged cell-membrane
- Tightly compact DNA to limit the size of the final system
- Protect DNA from enzymatic degradation
- Prevent off-target effects

DNA packing can be achieved by electrostatic interactions or encapsulation with a cationic carrier, or surface adsorption.[1] The latter often suffers from pronounced enzymatic degradation because of the exposition of DNA at the carrier surface. Vehicles based on electrostatic interactions might lead to significant toxicity due to their positive charge, as well as poor transfection efficiency resulting from low

DNA unpacking or suboptimal cellular uptake. The biological barriers to be overcome by non-viral delivery systems will be discussed in detail in section 1.3. DNA encapsulation can be achieved through the formation of liposomes, the use of a layer-by-layer technique, or the preparation of block copolymer micelles. Independent of the selected method, the common drawback of this technique is its low encapsulation efficiency and the potential harsh conditions to be endured by the genetic material during the formation of the particles. Many types of carriers are encountered in gene delivery, including quantum dots (QD), carbon nanotubes (CNT), proteins and inorganic NPs.[1,38,39] In the next subsections, we will rather focus on lipid and polymer-based delivery systems.

1.2.2.1. Lipids

Most lipid-based delivery systems rely on cationic lipids which interact electrostatically with anionic macromolecules such as DNA and cellular membrane components. The discovery of their fusogenic potential mid-70s led liposomes to be one of the earliest strategy to deliver exogenous genetic material.[40] Even though cationic lipids may display different transfection efficiencies and toxicities, they all share the same composition: a cationic head group and a hydrophobic tail assembled through a linker. Felgner *et al.* pioneered the field in 1987 with the successful encapsulation and transfection of DNA with the synthetic cationic lipid N-[1-(2,3-dioleyloxy)propyl]-N,N,N-trimethylammonium chloride (DOTMA).[41] Since then, many lipids have been developed, with the most popular examples presented in Figure 4.

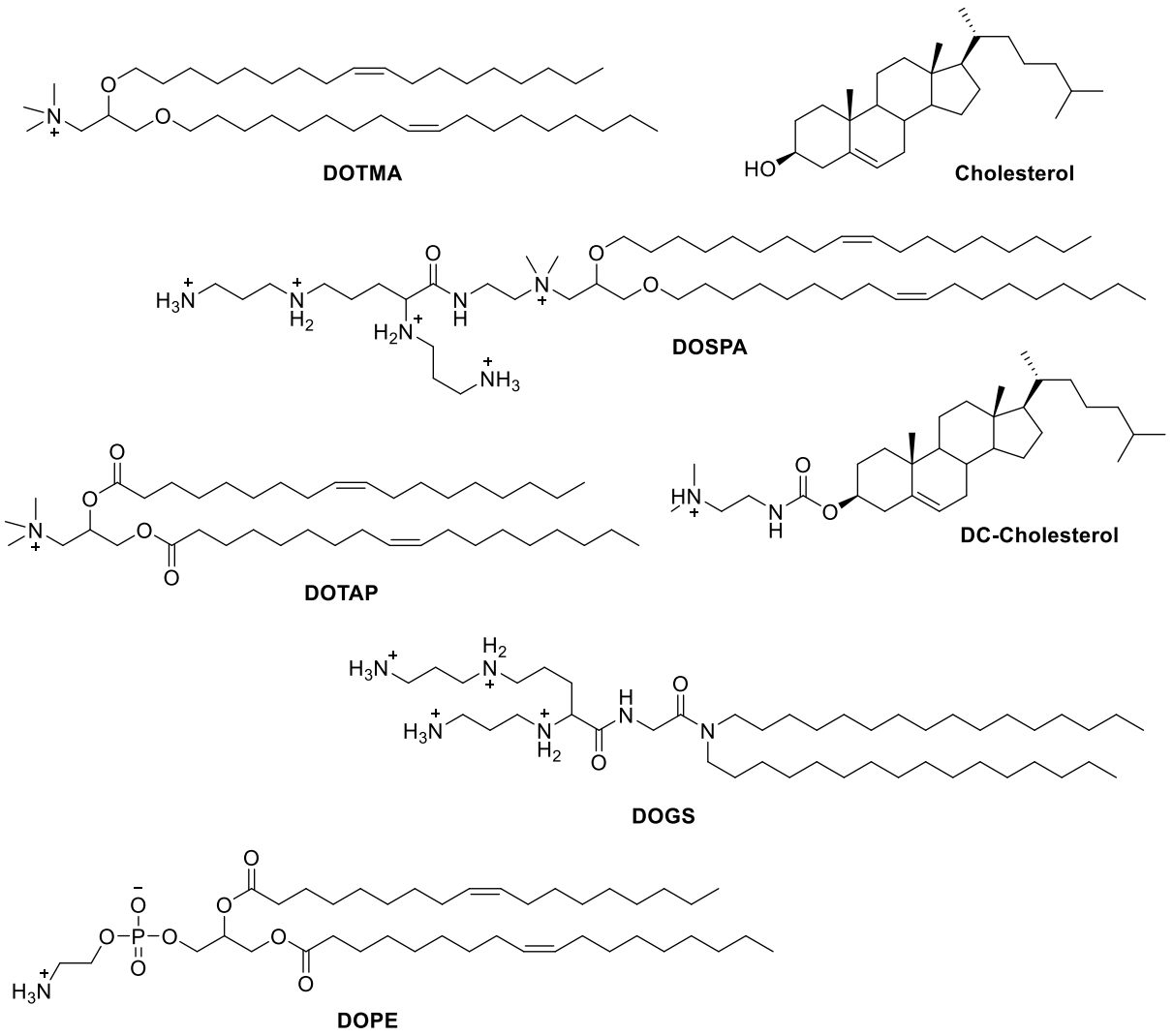

Figure 4. Structure of common cationic lipids and helper molecules in the composition of lipid-based delivery vehicles: *N*-[1-(2,3-dioleyloxy)propyl]-*N,N,N*-trimethyl-ammonium chloride (DOTMA), Cholesterol, 2,3-dioleyloxy-*N*-[2(sperminecarboxamido)ethyl]-*N,N*-dimethyl-1-propanaminium trifluoroacetate (DOSPA), 1,2-dioleoyl-3-trimethylammoniumpropane (DOTAP), 3β-[*N*-(*N′,N′*-dimethylaminoethane)-carbamoyl]cholesterol (DC-Cholesterol), dioctadecylamido-glycylspermine (DOGS), dioleoylphosphatidylethanolamine (DOPE).

Most common hydrophilic head groups are either primary, secondary, tertiary amines, or quaternary ammonium salts, and can be mono- or multi-charged.[42] The positive charges interact with the negatively charged phosphate groups of the nucleic acids and tightly compact DNA to small particles (< 100 nm). In order to improve the transfection efficiency of the resulting systems, the amines of the hydrophilic head were replaced by pyridinium groups, phosphorus and arsenic-derived moieties, or even uridine groups to form cationic nucleoside lipids.[40] As an increased density of cationic groups promoted DNA condensation, multivalent cationic head-groups were also investigated with success, with for example dioctadecylamido-glycylspermine (DOGS) and dipalmitoylphosphatidylethanolamidospermine (DPPES) (Figure 4).[43] The hydrophobic tails usually derive from aliphatic chains or cholesterol derivatives.[44] In particular, short aliphatic tails as well as multi-armed chains usually were reported to increase transfection efficiency.[40] The biodegradable character of the linker connecting the head and the tail of the lipid is determinant for the cytotoxicity of the delivery vehicle, as

it has to be cleared from the cell after DNA unpacking. Esters and disulfides are the most widely encountered linkages in this case due to their biodegradability potential, but carbamates and amides are also often used for their biocompatibility.

Developed in the late 80s, DOTMA and *N*-[1-(2,3-dioleoyloxy)propyl]-*N,N,N*-trimethylammonium methyl sulfate (DOTAP) have met a great success and were later commercialized (Figure 4).[37] 2,3-dioleyloxy-*N*-[2-(sperminecarboxamido)ethyl]-*N,N*-dimethyl-1-propanaminium trifluoroacetate (DOSPA) is the major component of Lipofectamine, a widely used commercial transfection agent (Figure 4).

Upon mixing, DNA and cationic lipids spontaneously form lipoplexes (lipid/DNA complexes) *via* electrostatic interactions. Liposomes can also be formulated from a lipidic solution and encapsulate DNA. Both strategies aim at protecting their nucleic acid cargo until it reaches the cell cytoplasm. Although early studies suggested a cellular uptake *via* lipid fusion with the cellular membrane, it was later demonstrated that lipoplexes deliver their genetic cargo mainly through endocytosis. Lipid fusion is still involved but consists in the destabilization and rearrangement of the lipid membrane of endosomal vesicles after endocytosis.[40] Due to interactions of the cationic lipid with phospholipids of the vesicle, the DNA dissociates from its carrier and is released in the cytoplasm.

Although cationic lipids demonstrated high transfection efficiency *in vitro*, very few formulations retained their activity *in vivo* due to several undesired interactions with serum.[25] Because of their unspecific uptake by the peripheral tissues and their binding to serum proteins, lipoplexes had to be formulated at higher dosage to observe an effect *in vivo*, thus leading to higher toxicity.[7]

To circumvent these issues, most formulations now associate cationic lipids with helper lipids such as neutral lipids (DOPE), cholesterol, phosphatidylcholine or also lipids functionalized with polyethylene glycol (PEG) (Figure 4).[7,42,44] These adjuvants stabilize and rigidify the resulting lipoplexes, and contribute to decrease the overall positive charge, thus reducing the toxicity of the vehicle. The cytotoxicity of lipid-based delivery systems was indeed primarily attributed to the cationic lipid component.[45] PEGylated lipids efficiently reduce the non-specific interactions of lipoplexes with blood components and increase the circulation time.[25] However, their bulkiness can cause a dose-dependent inhibition of transfection activity.

1.2.2.2. Polymers

Similarly to lipoplexes, DNA mixed to synthetic or naturally-derived cationic polymers spontaneously form polyplexes. Compared to cationic lipids, these polymers are expected to display enhanced water-solubility due to the absence of hydrophobic moieties. They also condense DNA more tightly, thus forming smaller NPs. Their high biocompatibility and potential for functionalization have attracted a lot of interest in parallel to lipid-based delivery.[21] However, the reproducibility of the composition and of the properties of polyplexes vehicles might be compromised by a too high polydispersity of the polymeric components, thus refraining their application *in vivo*. Therefore, polymers used in gene delivery systems should present a polydispersity as low as possible.

Most of cationic polymers consist of polyamine structures that strongly interact with the phosphate groups of nucleic acids. The most investigated polymers for gene delivery include poly-L-lysine (PLL), polyethylenimine (PEI), polyamidoamine (PAMAM) dendrimers, poly(lactide-co-glycolide) (PLGA), and polysaccharides such as chitosan (CS) (Figure 5).[46]

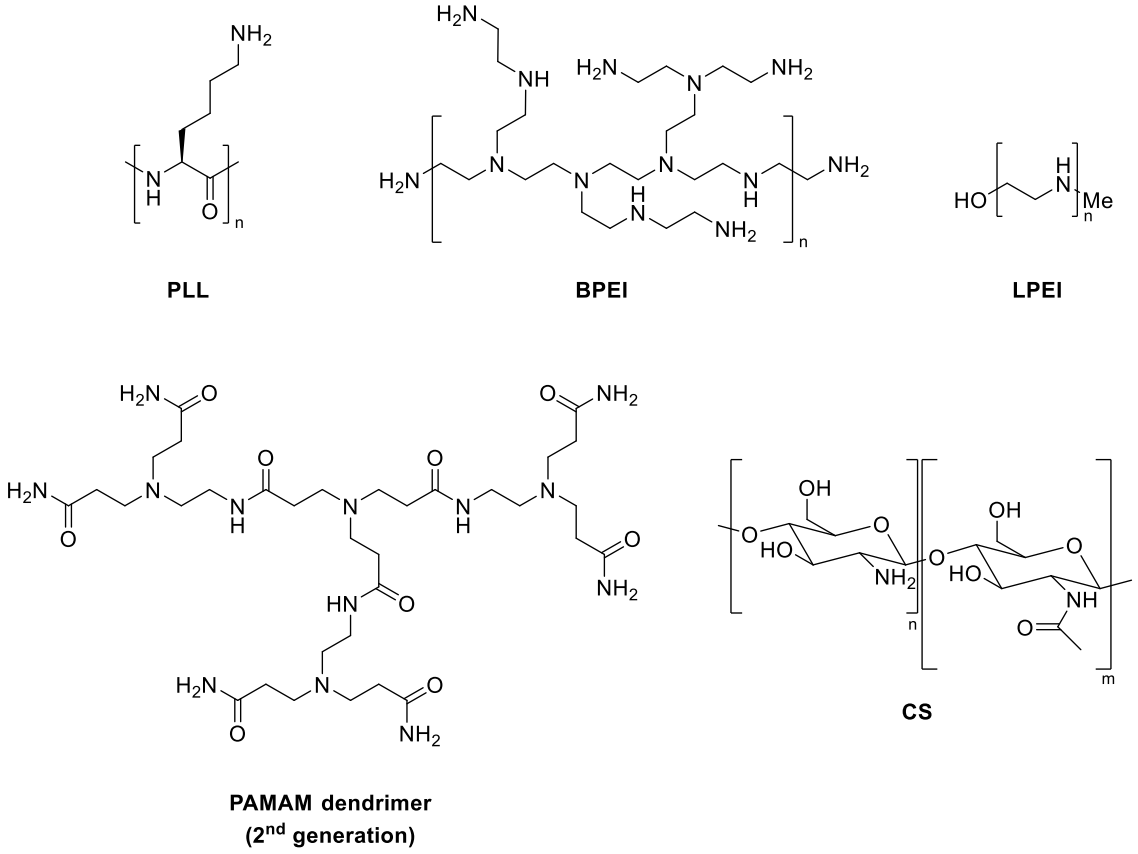

Figure 5. Common cationic polymers investigated for gene delivery: poly-L-lysine (PLL), branched and linear polyethylenimine (BPEI, LPEI), polyamidoamine (PAMAM) dendrimer of 2nd generation, poly(lactide-co-glycolide) (PLGA), and chitosan (CS).

The following subsections briefly present some of those polymers as well as their assets and drawbacks regarding gene delivery. A stronger focus is made on PEI, which is the "gold standard" polymeric transfectant in gene delivery.[47–49] CS is not described in this section as a complete introduction is given in section 1.4.

1.2.2.2.1. Poly-L-lysine

PLL was the first cationic polymer to successfully deliver pDNA to the liver *in vivo*.[50] This biocompatible polypeptide possesses excellent condensation properties. However, its successful transfection required the co-administration of chloroquine, a lysosomotropic agent that slows down the lysosomal degradation during endocytosis and helps the release of the vehicle in the cytosol.[45] As chloroquine is known to trigger significant toxicity, it limited the development of PLL as gene delivery vehicle.

1.2.2.2.2. Polyethylenimine

Thanks to its lower cytotoxicity and unique buffering properties, PEI quickly replaced PLL in

subsequent studies, and remains nowadays the most studied polymer for gene delivery.[46] Both branched and linear versions of this polymer are commercially available in a wide range of molecular weights (MW). Branched PEI (BPEI) is obtained by acid-catalyzed polymerization of aziridine monomers, leading to a randomly branched polymer constituted of primary, secondary and tertiary amines at a ratio close to 1:2:1 (Scheme 1).[51] BPEI stands as a liquid irrespective of its MW,[52] ranging from highly viscous material above 10 kDa to more fluid systems below 5 kDa. This polymer is highly water-soluble and can also be dissolved in acetone and ethanol.

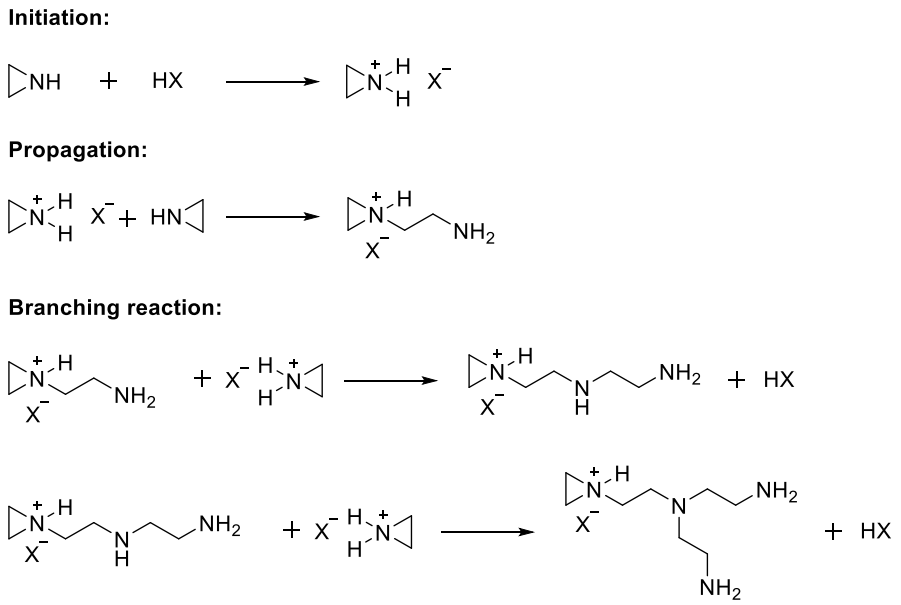

Scheme 1. Standard synthetic route to produce BPEI *via* ring-opening polymerization of unsubstituted aziridines in aqueous solution.[51]

On the other hand, commercial linear PEI (LPEI) is solid at room temperature (melting point 70-73 °C) and contains only secondary amines. Medium MW LPEI (10 to 25 kDa) are produced by ring-opening polymerization of aziridines at lower temperatures than for BPEI.[53] Higher and lower MW LPEI are however synthesized by ring-opening polymerization of 2-ethyl-2-oxazolines to afford poly(2-ethyl-2-oxazoline) (PEtOx) intermediates with a narrow range of MW (Scheme 2).[54] Subsequent acidic hydrolysis yields LPEI.

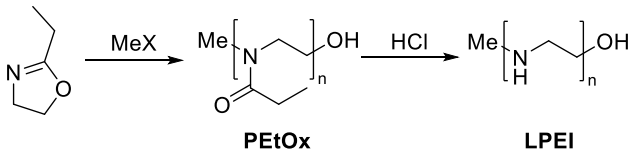

Scheme 2. Synthesis of LPEI *via* ring opening polymerization of 2-ethyl-2-oxazoline followed by acidic hydrolysis. X: Br, Cl, I.[54]

A high degree of PEtOx hydrolysis is preferred for gene delivery, in order to feature enough buffering potential on the resulting LPEI.[55] Above 95% of hydrolysis, LPEI forms however a water-insoluble crystalline phase due to the progressive building of stereoregular chain structures.[51] X-ray studies also revealed that the linear structure of LPEI leads to the formation of double-stranded helical chains stabilized by inter-chain hydrogen bonds between the two chains. Thus, a significant proportion of *N*-propionyl ethyleneimine units are necessary on the polymer backbone to maintain a sufficient solubility.

As BPEI chains cannot stack onto each other due to their branched nature, they display an excellent solubility in water. In comparison, LPEI is only soluble in water at acidic pH (pH < 5), or under heating above 50 °C in pure water. Depending on the MW, it can also be dissolved to certain extent in chloroform, DMSO and low MW alcohols like methanol and ethanol.

Theoretically one atom out of three can be protonated in a PEI chain, making it the polymer with the highest cationic charge-density potential.[56] Consequently, it tightly binds to DNA phosphate groups and still presents a significant buffering potential after polyplexes formation. This property is of utmost interest for gene delivery as the buffering of the endosome after endocytosis is believed to ultimately promote endosomal escape of the polyplex. The endosomal buffering effect of PEI is therefore believed to be responsible for the protection and successful release of the DNA cargo in the cytosol.[49] The mechanisms behind this higher transfection ability are still subject to intense debates (*cf.* section 1.3).[57–59] Because BPEI contains primary, secondary and tertiary amines, it better condenses DNA than LPEI and also has a higher buffering ability. High MW BPEI demonstrated a superior capability to form compact and stable polyplexes compared to their low MW counterparts. However, BPEI 25 kDa gives the best results compared to BPEI chains of 50 or 800 kDa, whose toxicity is detrimental to their transfection efficiency.[52] In another study, LPEI 22 kDa led to better nuclear delivery than BPEI 25 kDa, suggesting that a less stable polyplex and with a lower condensation ability favors the unpacking of DNA before its expression in the nucleus[60].

As previously illustrated with the comparison of BPEI 25, 50 and 800 kDa, high transfection efficiency is unfortunately correlated to significant toxicity. In addition to triggering endosomal escape, cationic charges have been demonstrated to cause serious side effects on the cell membrane integrity. PEI has been reported to alter the alignment of phospholipids of the lipid bilayer and to form nanoscale pores, which eventually led to necrosis.[57,61,62] Other side effects of PEI activity are linked to mitochondria dysfunction,[63] intracellular redox homeostasis,[64] or activation of the complement immune system.[65] Additional cytotoxicity is attributed to the poor degradability of PEI, which has a tendency to accumulate within cells. Small MW chains (< 5 kDa) are better tolerated, but display poorer condensation abilities, resulting in poorer stability of PEI/DNA complexes.[61,66] To combine high transfection efficiency and low toxicity, one solution is to prepare oligomers of short PEI chains linked by degradable moieties such as esters or disulfides.[67] Another interesting strategy is to graft PEI chains on biodegradable polysaccharides such as CS or heparin.

1.2.2.2.3. Polyamidoamine dendrimers

Similar to BPEI, the highly branched structure of PAMAM dendrimers and their external primary amines ensure an excellent solubility in water. Starting from a core molecule, PAMAM dendrimers are produced through a stepwise polymerization process, allowing the synthesis of monodisperse macromolecules ideal for gene delivery (Figure 5).[68] However, the stepwise synthesis of PAMAM dendrimers is tedious and results in high production costs as compared to other cationic polymers. Transfection efficiency is also generation-dependent: low generation dendrimers have a poor transfection ability and low toxicity, while high generation dendrimers exhibit more efficient

transfection but at the cost of reduced cell viability.[46] Again, the cross-linking of low-generation dendrimers with biodegradable moieties such as disulfide bridges is promising.[69] Compared to LPEI, PAMAM dendrimers remain however less efficient.

1.3. Physiological barriers to overcome as polymeric carriers

Polymeric gene delivery vehicles might represent the best compromise between viral vectors and physical gene delivery. Contrary to these two strategies, they have to overcome additional challenges due to physiological barriers (Figure 6). Before reaching the target cells, polymeric carriers must avoid immune system activation, polyplex aggregation or enzymatic degradation of the payload. Even if cellular uptake is achieved, the polyplex still has to overcome endosomal escape and DNA unpacking. The following subsections focus on the description of these various physiological barriers as well as the strategies that can be employed to bypass them. We will focus on the delivery of DNA-based payloads.

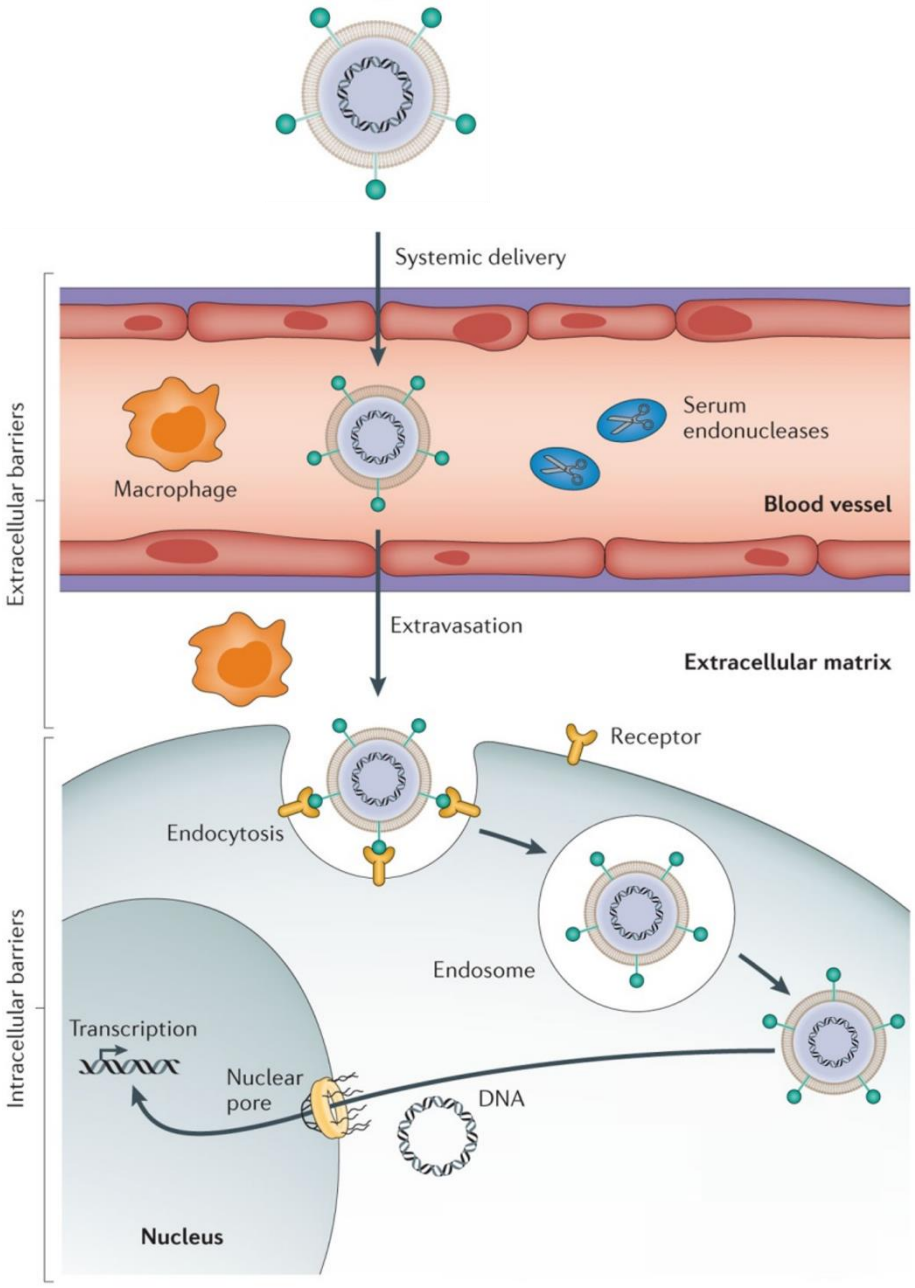

Figure 6. The successive physiological barriers to overcome by non-viral delivery vehicles during their journey towards cell nucleus upon systemic injection. Adapted from Yin *et al.*[21]

1.3.1. Extracellular barriers

1.3.1.1. Enzymatic degradation

DNAse enzymes contained in serum can degrade the payload in case of insufficient protection. One might consider first to chemically modify nucleic acids to prevent their recognition by enzymes. Such modifications have been performed on sugar moieties, phosphate groups and nucleic acid backbones.[70] Local injection to bypass the blood stream is also an attractive solution but is unfortunately not universally applicable. It is nonetheless very efficient for the treatment of some cancers and respiratory diseases.[71] The tight condensation of the genetic material by cationic polymers is for now the most convenient method to circumvent enzymatic degradation. It can be improved by the grafting of targeting

ligands on the surface of the polymeric NPs, to direct the system towards the desired cells and reduce the blood circulation time (*cf.* 1.3.1.4).

1.3.1.2. Serum-induced aggregation

The non-specific adsorption of proteins (protein fouling) on polymeric vehicles represents a challenge for both *in vivo* and *in vitro* delivery, since serum is used to cultivate immortalized cell lines and maintain primary cells. Proteins from the serum or the extracellular matrix interact with polymeric vehicles *via* electrostatic, hydrophobic or other types of interactions, and form aggregates that are rapidly cleared from the body.[72] In particular, cationic polymers employed to condense DNA *via* electrostatic interactions are often sequestered by proteins because of their resulting positive charge. Albumin, lipoproteins and macroglobulin often associate to polyplexes, further leading to immune response.[73] The formation of a protein corona around polymeric NPs also alters their size and zeta potential, which is detrimental to cell targeting and internalization. Interestingly, negatively-charged proteins, such as proteoglycans, have been reported to compete with the nucleic acid payload, thus leading to premature DNA release and disassembly of the complex.[74] In addition, high salt concentrations encountered in serum are known to impact the colloidal stability of the polymeric complexes, inducing faster clearance. Strategies to avoid aggregation and clearance from the body have been developed over the years and include surface functionalization of polyplexes with PEG,[75] fluorinated moieties,[76] or carbohydrate oligomers.[77,78]

Of particular interest, PEG leads to hydrophilic systems with a non-ionic corona thus efficiently preventing undesired interactions with proteins. These “stealth sheath” properties were described for the first time in 1977.[79] PEG chains sterically repulsing each other, the resulting polymeric NPs benefit from a thick hydration layer which protects them from serum proteins adsorption. MW and density of the PEG coating are two key parameters enabling efficient resistance towards protein fouling. The reduction of zeta potentials observed for PEGylated systems also contributes to reduced aggregation and thus increased blood circulation half-time.[72] The colloidal stability of PEGylated delivery vehicles was demonstrated to be significantly superior to non-PEGylated systems, emphasizing the positive effect of PEG in serum-based environments.[80,81]

The beneficial effect of PEG nonetheless comes with some drawbacks. One major issue concerns the decreased transfection efficiency observed for PEGylated systems.[82,83] Unfortunately, the same mechanisms favoring escape of polymeric NPs from undesired proteins interactions, also hamper their cellular uptake. This phenomenon is called the PEGylation dilemma. Ogris and coworkers nonetheless showed that moderate PEGylation did not affect the transfection efficiency of PEI-based polyplexes.[84] More recently, elicitation of immune responses from PEGylated systems has been reported and is discussed in details in a review from Gabizon and Szebeni.[85] Immune activation is also described in subsection 1.3.1.3. Two types of immune response can be triggered by PEGylated systems: either an accelerated blood clearance, or the activation of the complement system leading to an allergic reaction. Hypersensitivity to PEG was actually detected in patients that have not been previously treated with a PEG-containing formulation.[86] This observation suggests that the omnipresence of PEG in our lives

(food, cosmetics, and so on) naturally triggers the appearance of anti-PEG antibodies. This is a major drawback for the future of PEG in delivery vehicles. This polymer nonetheless remains very popular due to its otherwise excellent biocompatibility profile and its beneficial effect on colloidal stability.

1.3.1.3. Immune system activation

Non-viral gene delivery vehicles also elicit innate immunity, although to a lesser extent than viral vectors. Activation of the innate immune system first leads to the recruitment of vascular endothelial cells and platelets and the production of inflammatory cytokine. In parallel, the adaptive immune system generates antigen-specific response to nanocarriers, which contributes to their faster recognition and clearance from the body upon second administration.[72] Polymeric vectors triggers innate immunity through their interactions with toll-like receptors (TLRs) and the activation of complement immune system.

TLRs are membrane-bound proteins that specifically recognize any intruder, to help immune cells to quickly produce a tailored immunological response.[87] The human body possesses many different TLRs to fight against foreign nucleic acids from viruses and bacteria. In particular, a study reported PEI as a TLR5 agonist, meaning that nucleic acids are not the only components eliciting immune response.[88] Therefore, careful evaluation of immunostimulatory properties of polymers is recommended.

Complement proteins in the blood also recognize foreign material and initiate a proteolytic cascade which eventually leads to inflammation and phagocytosis. Both lipids and polymers can activate the complement system.[89,90] Polycations such as PLL and PEI strongly trigger this defense mechanism.[90] The MW of the polymer plays a key role in this process as short cationic polymers only induce weak activation. Neutralization of the charge with the DNA cargo or other polymeric material also efficiently reduces its activation.[91] As discussed earlier, investigations during the past decade also demonstrated the potential of PEG for immune activation, although this polymer was labelled as "generally recognized as safe" (*cf*. section 1.3.1.2).

1.3.1.4. Organ targeting

Local injections allow to reach directly the organ of interest, and are particularly convenient for delivery to the muscles.[72] However, due to the invasiveness of the corresponding techniques and their complex set up, systemic injections and modifications of polyplexes with targeting moieties represent better alternatives. Thus, gene delivery vehicles intended for systemic injections should ideally combine stealth properties and targeting moieties. The following subsections discuss two targeting ligands investigated for this project.

1.3.1.4.1. Lactobionic acid for hepatocytes targeting

In the frame of this PhD project, liver targeting was investigated. The asialoglycoprotein receptor (ASGPr) is a Ca^{2+}-dependent lectin expressed exclusively in hepatocytes or liver cancer cells, and frequently used as targeting site.[92] Distributed at the surface of parenchymal hepatocytes, this receptor directly faces the capillaries linked to the central and hepatic veins. These capillaries have fenestrations

of 100-150 nm on average, allowing polymeric complexes of this size to diffuse through them and rapidly reach the receptor.[93] ASGPr recognizes, binds and endocytoses asialoglycoproteins *via* the specific recognition of D-galactose (D-Gal) and *N*-acetyl-D-galactosamine (D-GalNAc) binding domains (Figure 7). ASGPr-mediated cellular uptake is normally triggered by triantennary ligands such as the asialofuetin glycoprotein. Di- and monovalent ligands also bind to this receptor but are less efficiently endocytosed *via* this mechanism due to a lower binding affinity. Their cargos are still endocytosed through the use of receptor-independent internalization mechanisms. Constituted of gluconic acid and galactose moieties, lactobionic acid (LA) is a monovalent and small targeting ligand of ASGPr commonly grafted on polymeric delivery vehicles (Figure 7).[94–97]

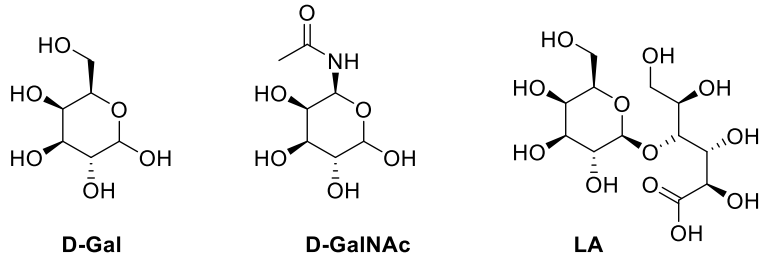

Figure 7. D-galactose (D-Gal), *N*-acetyl-D-galactosamine (D-GalNAc), and lactobionic acid (LA) structures.

1.3.1.4.2. Folic acid and cancer therapy

As it will be detailed in section 3.4.3, the grafting of folic acid (FA) was also investigated. FA is a small molecule also known as vitamin B9, involved in many biochemical processes (Figure 8). It is specifically recognized by folic acid receptors (FR) that are highly expressed in fast-dividing cells such as embryonic and cancerous cells.[98] The levels of FR are consequently much higher in cancerous cells than in the corresponding healthy cells, making these receptors promising anti-tumor targets. Cancers leading to overexpression of FR include ovarian, kidney, lung and breast cancers. Therefore, FA is often used as targeting ligand for anti-cancer gene therapies.[99–102] Thanks to its carboxylic acid moieties, amide bonds are easily formed with polymers of interest.

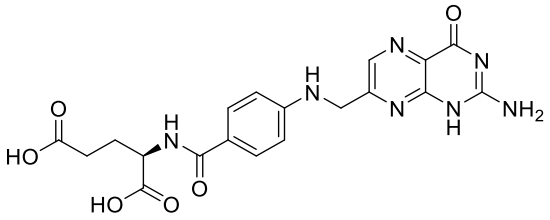

Figure 8. Folic acid (FA) structure.

1.3.2. Intracellular barriers

Irrespective of the application (e.g. *in vitro* or *in vivo*), non-viral gene delivery vehicles have to face the same intracellular barriers: cell binding and subsequent penetration, then trafficking towards the nucleus.[72] Then, DNA has to undergo unpacking from the vehicle and transfer in the nucleus.

1.3.2.1. Cellular uptake

For polyplexes grafted with a targeting ligand, specific interaction with the corresponding receptor

can initiate the cellular uptake process. For polyplexes without targeting functionality, cellular binding was initially thought to rely on electrostatic interactions with glycosaminoglycans, a subtype of proteoglycans.[40] Glycosaminoglycans are anionic and rigid polysaccharides anchored at the cell surface. Although they mediate uptake and transfection efficiency of polyplexes, they also compete with nucleic acids and prematurely disassemble the complex.[103] Mozley *et al*. suggested that cellular uptake of cationic polyplexes would depend more on the ability of syndecans, another type of proteoglycans, to recruit lipid rafts and promote their hydrophobic interactions with the polyplexes.[104] The precise mechanisms regulating the first step of cellular uptake are still under investigation and are complexified by the wide variety of proteoglycans present on the cells.

Following cellular attachment, polyplexes are generally internalized by endocytosis due to their large sizes.[72] In an effort to reduce the proportion of endosomal uptake and its deleterious effects on the polymeric complexes, thiol-mediated uptake strategies have also been investigated during the last two decades.[105]

1.3.2.1.1. Endocytosis

Clathrin-mediated endocytosis, caveolae-dependent endocytosis, macropinocytosis, and phagocytosis are the most encountered and understood endocytic pathways (Figure 9).[72] Clathrin-independent pathways are currently still under active investigation. The size of the polyplex, the nature and the MW of the polymers it contains, as well as the type of cells targeted, are the major factors determining which pathway it will undergo. However, a same polyplex is usually endocytosed through several routes at the same time.

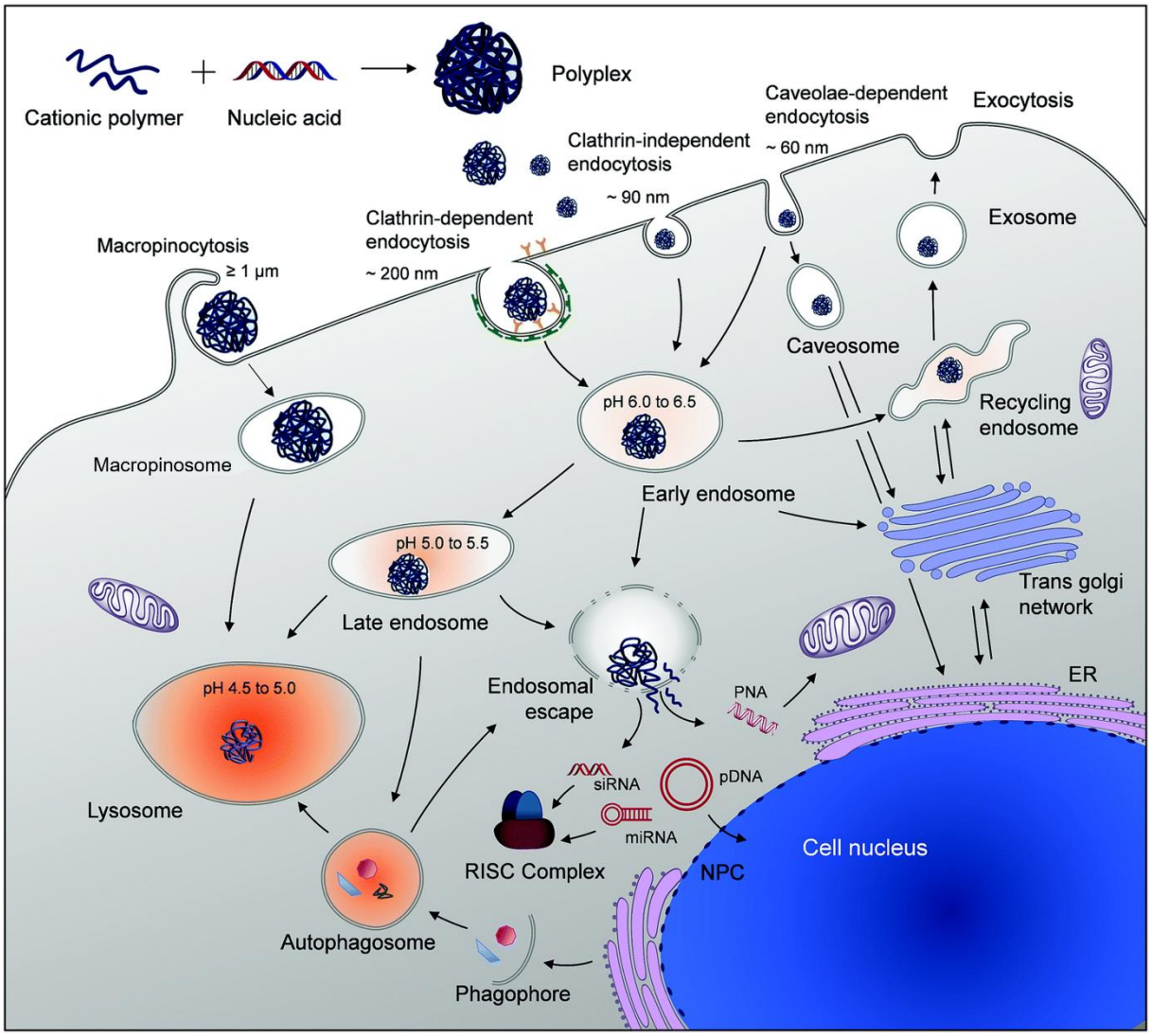

Figure 9. Endocytic pathways and cellular trafficking of polyplexes. Polyplexes can undergo different endocytosis pathways depending on their composition and size. After cellular trafficking and endosomal escape, they finally reach the perinuclear region to release DNA before nuclear uptake. ER: endoplasmic reticulum; NPC: nuclear pore complex; siRNA: silencing RNA; miRNA: microRNA; PNA: peptide nucleic acids. Adapted from Bus *et al*.[106]

Phagocytosis is mainly observed in immune cells such as macrophages, monocytes and neutrophils. Phagocytosis aims at clearing large particles (> 0.5 µm) such as cell debris or pathogens like bacteria and yeasts. Similarly, macropinocytosis non-specifically leads to the uptake of extracellular fluid, forming macropinosomes of irregular shapes and sizes (between 0.5 and 1.0 µm),[107] that rapidly evolves into lysosomes (pH 4.5-5) to degrade their content (Figure 9).

Consequently, most gene delivery vehicles are designed in order to be internalized *via* clathrin-mediated and caveolae-dependent endocytoses (Figure 9). The former is the most encountered route in mammalian cells. Clathrin-coated pits (< 200 nm in diameter) internalize extracellular and membrane components with the help of actin and dynamin. Clathrin coats are then rapidly depolymerized to lead to early endosomes (Figure 9).[103] Unlike clathrin-dependent uptake, caveolae-mediated uptake is highly regulated.[108] Caveolae are small bulb-shaped structures (60-70 nm in diameter) composed of lipid rafts and characterized by a non-acidic and non-digestive process (Figure 9). This pathway is ideal

to preserve the integrity of the polyplex. However, the density of caveolae varies a lot depending on the cell type.

1.3.2.1.2. Endosomal escape

Polyplexes endocytosis usually leads to their entrapment in early and late endosomes, which in turn become lysosomes upon acidification to pH = 4.5 (Figure 9). Endosomal escape is thus essential to allow the payload to reach the cytosol and nucleus, but remains a major challenge.[106] Compared to other cationic polymers such as PLL, PEI demonstrated excellent abilities to escape these compartments, resulting in high cytosolic delivery of its payloads.

The natural process of endosomal digestion is governed by the progressive acidification of these compartments, from approximately pH 7 to 4 (Figure 10). The high buffering potential of PEI is thought to lead to a high influx of protons and chloride ions, causing an increase in the osmotic pressure and finally their physical rupture, thus releasing the polyplex in the cytosol. This hypothesis has been coined the "proton-sponge" effect.

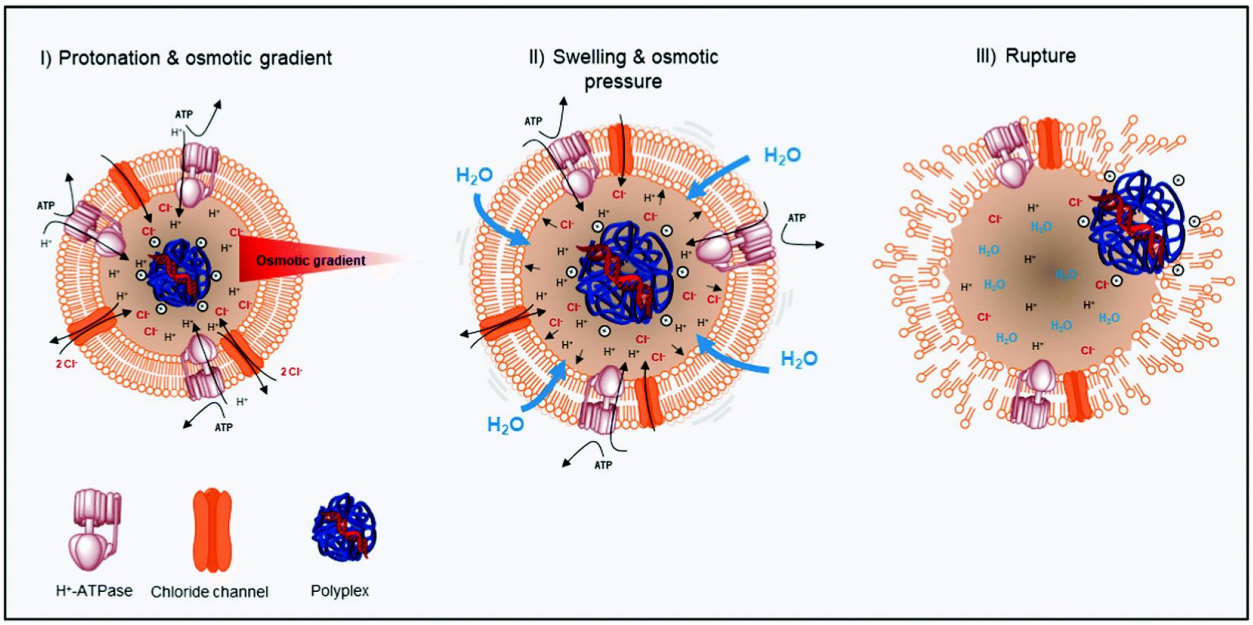

Figure 10. Illustration of the "proton sponge" hypothesis. Adapted from Bus *et al.*[106]

Several aspects of this hypothesis have been debated over the last two decades.[57–59] Many concerns have arisen on the ability of the cationic polymer to effectively buffer the pH of endosomes, as well as to induce the complete rupture of the endo-lysosomal membrane.[106] In order to better describe endosomal escape, other mechanisms were formulated. The "polyplex-mediated membrane disruption approach" theorizes that endosomal escape is mediated by a local destabilization of the membrane due to the cationic charges of the polymer. This leads to nanoscale hole formation enabling the polyplex to escape without complete rupture of the endosome. On the other hand, the "polymer-mediated membrane disruption" relies on the intercalation of free cationic polymeric chains into the endosomal membrane. Some studies revealed that the addition of free polymeric chains to the polyplex formulation had a positive impact on the transfection efficiency.[109,110] Many studies can corroborate each of the

three concepts but none of them could definitely elucidate the universal mechanism, thus remaining a major challenge.

1.3.2.2. Triggering or bypassing endocytosis

In 1988, two research groups simultaneously discovered the exceptional translocation properties of the transactivator of transcription (TAT) protein of HIV-1.[111,112] A similar observation was later made by Joliot *et al.* with the homeodomain of Antennapedia, initiating more in-depth investigations on the minimal amino acid sequences required to penetrate cells.[113] Many other minimalist peptides, called cell-penetrating peptides (CPPs), were developed in the next decades in rationalized or empirical ways, and attracted a lot of attention for payload delivery into cells.[114] Several of them have been or are nowadays under clinical evaluation.[115]

CPPs are usually 5 to 30 amino acids long and can be divided in three subclasses: cationic, amphipatic and hydrophobic.[115] While hydrophobic and amphipatic CPPs contain both polar and non-polar amino acids, cationic CPPs are mainly constituted of polar residues, with clusters of lysines and arginines. TAT-derived peptides and synthetic poylarginines are part of this last category (Figure 11). Arginine residues contribute more to cellular uptake than lysines thanks to the guanidinium group, that always remains protonated and forms bidentate hydrogen bonds with negatively charged constituents of the cell membrane.[116] In addition, Futaki *et al.* suggested that the optimal number of arginine residues for cellular uptake was 8, pointing out octaarginine (Arg_8) as an ideal CPP for gene delivery (Figure 11).[117] CPPs can transport a wide variety of biologically relevant molecules into cells, such as proteins, DNA, small drugs, and also NPs.[115] Similarly to polyplexes in general, their exact mechanism of cell penetration remains unclear, partly due to the large number of CPPs investigated and their differences in composition. As cargo-conjugated CPPs have been reported to mainly enter cells *via* endocytosis, the use of cationic CPPs is preferred to provide the final delivery vehicles with endosomal escape abilities.

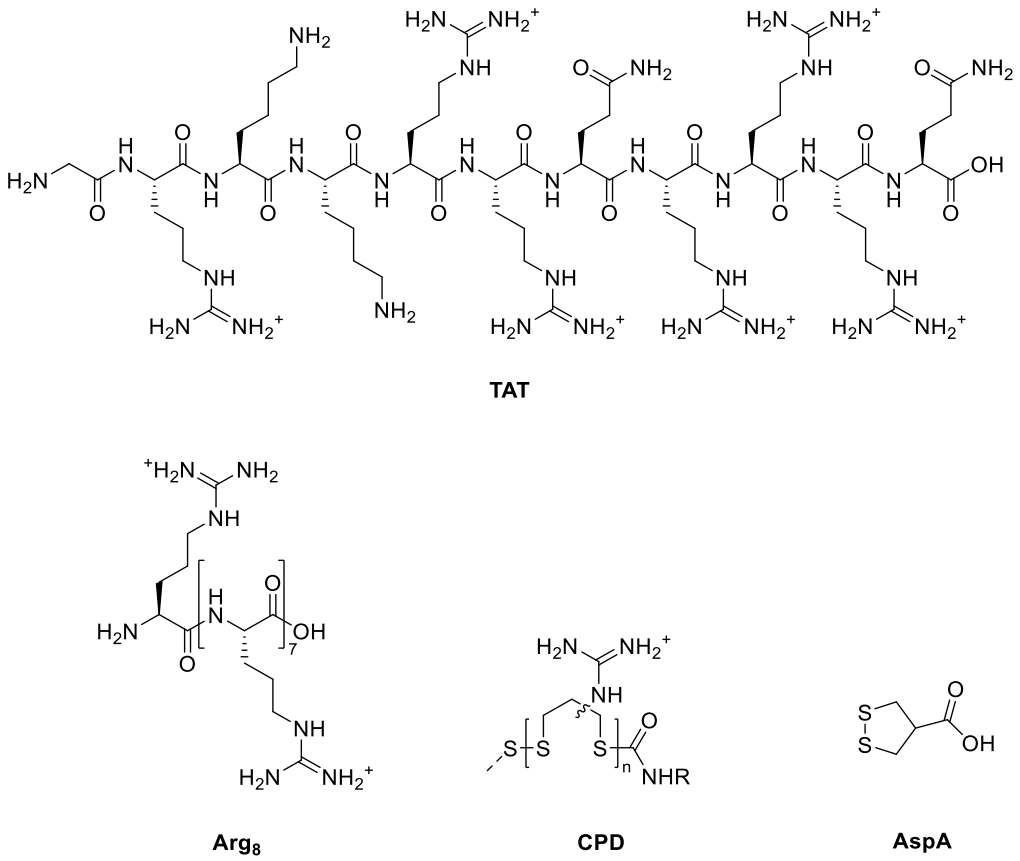

Figure 11. Structures of a TAT-derived CPP (TAT), octaarginine (Arg_8), cell-penetrating poly(disulfide) (CPD, general structure) and asparagusic acid (AspA).

Bypassing endocytosis to achieve direct cytosolic delivery can be achieved by some CPPs, but is highly cargo-dependent.[118] Other methods such as "thiol-mediated uptake", relying on reactions with cell-surface thiols and disulfides, were reported. In the 90s, the Ryser group showed that the membrane fusion of HIV depended on a thiol-disulfide exchange at the cell surface.[119] Almost two decades later, Aubry *et al.* reported a noticeably higher cellular penetration for disulfide- and thiol-containing CPPs, forming mixed disulfide bridges with membrane-bound proteins.[120] In an effort to mimic CPPs while increasing their potency, cell-penetrating poly(disulfides) (CPDs) based on lipoic acid derivatives were developed in the following years, and achieved high cytosolic delivery without relying on endocytic processes (Figure 11).[121] Despite very promising applications, notably cell delivery of large cargos such as antibodies,[122] QD,[123] and mesoporous silica NPs,[124] CPDs were limited by complex syntheses, calling for a shift towards small molecules.

Exploiting ring tension to create highly reactive disulfides, Gasparini *et al.* identified asparagusic acid (AspA) as the most potent strained disulfide for enhanced cell-penetration (Figure 11).[125] Similarly to CPDs, uptake of AspA was found to be endocytosis-independent. Its internalization was also inhibited by 5,5′-dithiobis(2-nitrobenzoic acid) (DTNB), used to mask cell-surface thiols, proving that thiol-mediated uptake was at play. Additional mechanistic studies revealed that AspA primarily targets the transferrin receptor and more specifically two cysteine residues (Figure 12).[126] A high density of AspA units was also shown to better promote AspA-induced cellular uptake.[127] Lastly, AspA was reported to

efficiently promote the cellular uptake of liposomes, polymersomes and peptides, with deep penetration in three-dimensional organoid models, suggesting thiol-mediated uptake as a promising alternative to endocytosis for drug and gene delivery applications.[128,129]

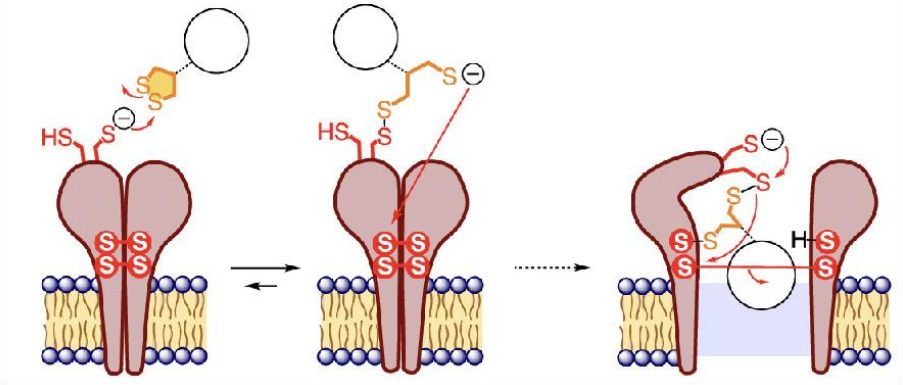

Figure 12. Proposed mechanism for the cellular uptake of AspA by the transferrin receptor. Adapted from Laurent *et al.*[105]

1.3.2.3. Cytosolic transport and nuclear uptake

The transport of the polyplexes towards the nucleus after release in the cytosol should not be underestimated. DNA greater than 250 bp have indeed been observed not to diffuse properly in the cytoplasm, thus drastically decreasing the transfection efficiency after endosomal ecape.[130] On the contrary, endocytic vesicles were shown to be actively transported along actin microtubules towards the nucleus,[131] suggesting that polyplexes should not be released too early from endosomes to better reach the perinuclear region. DNA unpacking right after endosomal escape and once in the nucleus have both been observed.[82,132] The optimal timepoint for DNA unpacking was however not clarified yet. It is nonetheless generally agreed that a fine balance has to be found between protection of the cargo and unpacking.[72] For instance, poor unpacking ability is responsible for the differences of transfection efficiencies observed between PLL- and PEI-based polyplexes. Successful expression of DNA packed with PLL could be observed only after co-administration of chloroquine, which promotes DNA release.[133] Designing polyplexes with biodegradable polymers such as polysaccharides, or containing degradable disulfide or ester bonds are popular methods to ensure DNA release after endocytosis.[67]

The journey of therapeutic DNA ends with its uptake by the nucleus, which is also protected by a phospholipid bilayer. Nuclear pore complexes (≈ 9 nm in diameter) allow small molecules, ions and double-stranded DNA up to 250-300 bp to passively diffuse through the nuclear membrane.[134,135] For larger cargos, internalization is mediated by nuclear shuttle proteins, which can be activated by nuclear localization signals (NLS). NLS are sequence-specific peptidic tags typically containing arginine and lysine residues and conjugated to DNA to favor its nuclear uptake.[136,137] The most widely used NLS is derived from the simian virus 40 (SV40) large T antigen.[138] Additionally, DNA nuclear targeting sequences can be inserted in the strand and activate the nuclear uptake of DNA upon binding to transcription factors. For example, the SV40 promoter (72 bp) has been identified to bind many transcription factors in mammalian cells, helping gene delivery.[139,140] Delivery vehicles lacking NLS or promoters can still reach the nucleus, mostly during cell division where a breakdown of the nuclear

membrane occurs. As a consequence, cancerous cell lines usually do not present severe nucleus internalization issues. However, non-dividing cells such as hepatocytes cannot benefit from this strategy. Polymer-based delivery could greatly benefit from more in-depth studies on nuclear uptake, in particular on the role played by the cationic component.

1.3.3. Features of the ideal non-viral gene delivery vehicle

Based on the previous subsections, the ideal polymeric gene delivery vehicle should display several features to circumvent the different physiological barriers it may encounter. First, for systemic injections, the focus should go on the shielding of the polyplex from blood components to avoid aggregation and detection by the mononuclear phagocyte system. Immunogenicity of the polymeric components should also be thoroughly investigated to avoid strong immune response after injection. Conjugation of targeting ligands on the surface of the polyplex should help reaching the desired cells in a short time and avoid off-target effects. As most polymeric NPs are endocytosed, they should display resistance to lysosomal conditions and promote endosomal escape. This step should not happen too fast to allow endosomal trafficking towards the nucleus, thus favoring DNA nuclear uptake after unpacking. Depending on its size and type of cells, DNA can be passively internalized through nuclear pore complexes. Otherwise, NLS and DNA nuclear targeting sequences should be respectively conjugated or inserted to DNA strands to promote their active internalization independently of the cell cycle.

In addition to physiological barriers, degradability of the vehicle after DNA unpacking is a major aspect to consider for sustained cell viability. The polymeric components should be ideally biodegradable. Manufacturing considerations such as ease of fabrication, facile purification processes, low production costs and ease of storage should also be examined.[141]

As multiple components should be combined for a successful gene delivery process, a polymeric backbone prone to multi-step functionalization such as CS would be ideal. The next section will therefore discuss this promising backbone.

1.4. Functionalization of chitosan for gene delivery

1.4.1. Origin and properties

CS is a linear polysaccharide composed of repeating β-(1,4)-2-amino-D-glucose and β-(1,4)-2-acetamido-D-glucose units linked through 1,4-β-glycosidic bonds. This compound is derived from chitin, the second most abundant biopolymer on Earth after cellulose (Scheme 3).[142] Chitin is a major component of the exoskeleton of insects, crustaceans or shellfish, and is also found in the cell walls of some fungi. Industrial production of CS is based on the deacetylation of chitin, which can be collected at low cost and in large quantities from crab and shrimp shells.[143] Considering seafood wastes are an environmental burden due to their poor recyclability and detrimental impact on local microfauna and microflora, their conversion to CS is highly eco-friendly.[144] Chitin may either be extracted by chemical or biological methods.[144,145] While chemical procedures are operated at industrial levels, biological extractions produce chitin of higher quality. Chitin is encountered in three different allomorphic forms

which depend from the source and method of extraction.[146] CS is then obtained after deacetylation of chitin under basic conditions at 110 °C.[145] The chitin source, extraction and deacetylation methods also impact the arrangement of CS units, meaning the formation of block, random or alternating copolymers.[146] This ultimately impacts the properties of the resulting CS.

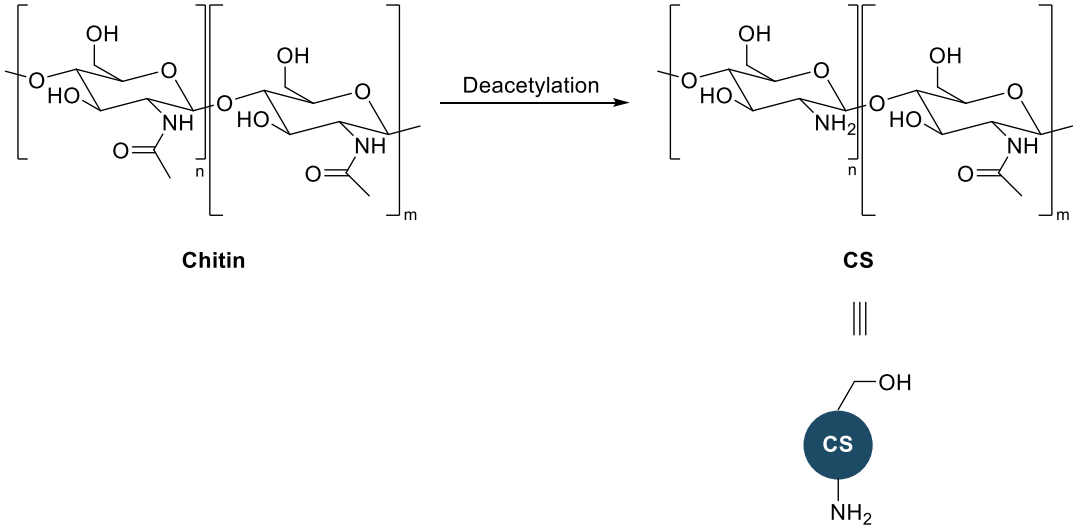

Scheme 3. Preparation of CS *via* deacetylation of chitin and simplified structure of CS.

The word "chitosan" actually embraces a whole "continuum of progressively deacetylated chitins".[147] Deacetylated chitin chains are defined as CS when more than 55% of acetylglucosamine units have been deacetylated. CS is therefore primarily characterized by its deacetylation degree (DD) which corresponds to the percentage of glucosamine units in one chain.

Along with DD, both MW and polydispersity (PD) characterize CS batches. CS is commercialized in a large range of MW starting from only a few to hundreds of kDa. In particular, chains of less than 3.9 kDa, and/or less than 20 units are defined as CS oligosaccharides (COS).[148] The PD informs on the variety of MW present in a batch and is defined by the following equation:

$$PD = \frac{Mw}{Mn}$$

with Mw referring to the weight average molecular weight and Mn referring to the number average molecular weight. PD has a minimum value of 1 which represents a perfectly monodisperse sample (e.g. proteins). In pharmaceutical applications, a PD tending towards 1 is preferred. However, the current poor characterization of commercial batches represents a major bottleneck to the development of CS in clinical applications and is partly responsible for the contradictory biological effects of CS reported in literature.[149]

Several characteristics of CS are very attractive for gene delivery, starting with its biodegradability. This polysaccharide is predominantly degraded by lysozyme and other bacterial enzymes in the colon. In addition, three human chitinases have shown biodegradation activity towards it.[150] Studies demonstrated that the degradation rate of CS was faster for compounds with low MW and DD (more "chitin-like").[150] However, *N*-substitution with derivatives other than acetyl groups may decrease the

rate of enzymatic degradation, thus increasing stability but also potentially toxicity. Therefore, a fine balance has to be reached. As regards biocompatibility, most CS derivatives are less toxic than PEI which makes CS a safer material for biomedical applications. Toxicity is usually higher for derivatives presenting higher cationic charge density and MW. In addition, red blood cell hemolysis assay did not reveal any hemolytic activity from highly purified fractions of both COS and higher MW CS (5-10 kDa and > 10 kDa).[151] The low immunogenicity of CS is another asset. From most studies, CS appears as a material with minimal toxic effects but safety evaluation of each novel CS derivatives should be considered for biomedical uses.[150] Surprisingly, CS was found to be toxic to several bacteria[152] and fungi,[153] thus opening possible applications in antimicrobial research. Lastly, the presence of numerous reactive groups along CS chains makes it an attractive backbone for functionalization. This versatility is another reason for its application in gene and drug delivery, as the properties of CS-based vehicles can be tuned according to the site of action and the desired effects.[154]

Directly linked to the MW, and to a lesser extent to the acetylation pattern and DD, the solubility of CS is however a major issue to its successful functionalization and application in gene delivery. Except for COS, known for their improved solubility in polar solvents and aqueous media,[148] longer polymeric chains are poorly soluble in basic and neutral aqueous solutions, as well as in organic solvents. The solubility limit in aqueous environment is somewhere between pH 6.5 and 6.0 thanks to the amino groups of CS, which have a pK_A value close to 6.3.[147] Even though CS is well soluble in acidic solutions (pH < 6), its functionalization is then limited by the number of reactions that can be performed in such conditions. Common methods to improve its solubility include the MW reduction through degradation procedures, which can be performed *via* irradiation,[155] enzymatic[156] or chemical treatments,[157–159] the latter being the most developed. The covalent derivatization of CS is another possibility to increase its solubility, with amines quaternization being the most popular method.[160] Additional modification of such quaternized CS are however more challenging due to a significant proportion of reactive groups already functionalized. Water-soluble CS derivatives such as trimethyl CS (TMCS) or *O*-carboxymethyl CS (CMCS) are even commercially available (Figure 13).[161,162]

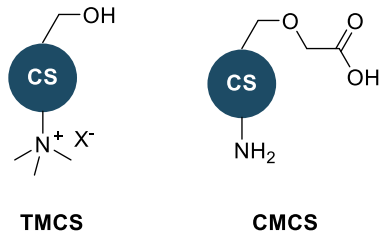

Figure 13. Structures of the commercially available TMCS and CMCS.

As thoroughly reviewed over the past decades, CS has found applications in many fields.[144,145] Asides from drug and gene delivery, CS has attracted much attention in wound healing,[163,164] tissue engineering,[165,166] food packaging,[167] waste water treatment[168,169] and even textile industry.[170] Several examples will be presented in the next subsections, with a focus on biomedical applications. The large panel of CS applications is a clear proof of its high potential, although the knowledge acquired by the different actors is not efficiently shared to build up imrpoved systems from it, which slows down its development. As regards biomedical applications, the number of CS-based products that have been

approved by health regulatory agencies or are currently under clinical investigations suggests a promising future for this polymeric backbone.[171]

CS alone cannot fulfill the different requirements and has to be derivatized to display the additional properties necessary for successful applications. The next subsections summarize the different means commonly employed to functionalize CS.

1.4.2. Covalent assemblies

A CS glucosamine unit can be covalently modified either *via* amine and primary hydroxyl groups functionalization, or upon disruption of the sugar ring integrity through oxidative cleavage. The latter leads to the formation of reactive aldehydes convenient for downstream functionalization, but at the cost of extensive and uncontrolled depolymerization. Some studies still report the use of this method for the conjugation to PEI in drug and gene delivery applications.[172,173]

1.4.2.1. Amine functionalization

The primary amines are the most reactive functionalities of CS chains. Most covalent systems are in consequence based on amine derivatization, which can be summarized around the formation of four main functionalities: amide, urea, imine and amine/ammonium (Figure 14).

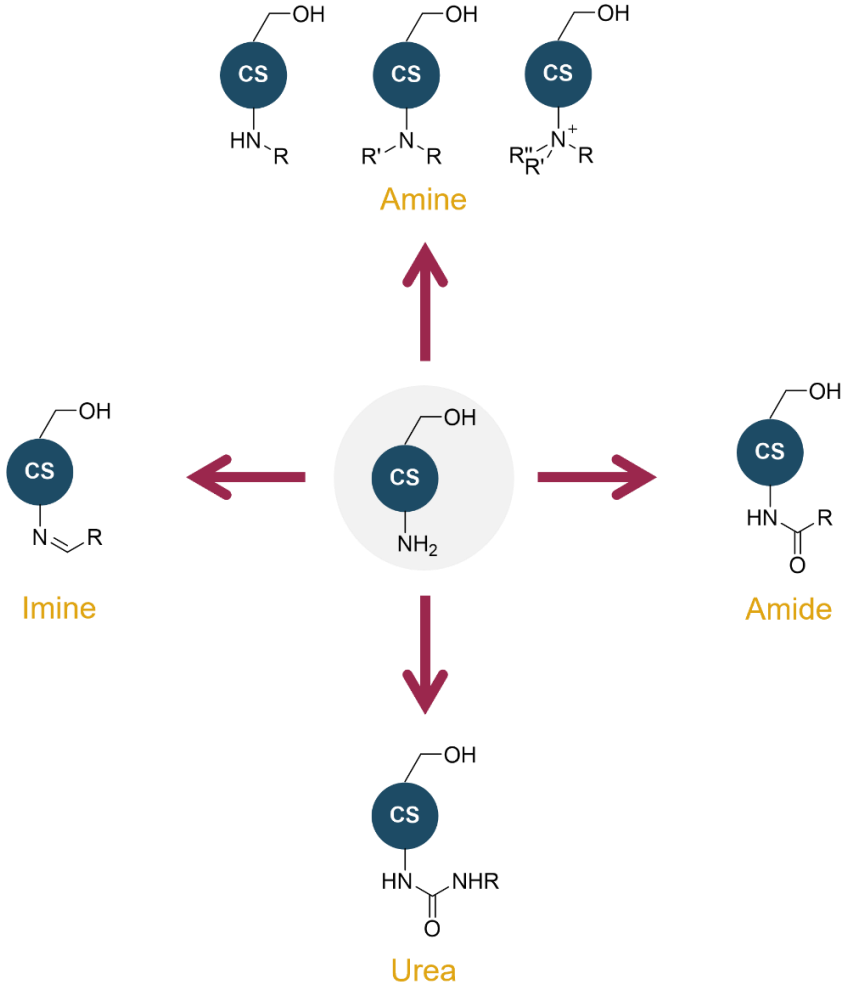

Figure 14. Covalent functionalization strategies of CS amines. Amide and urea bonds are formed upon acylation with carboxyl-based and amino-based substrates respectively, while imines are obtained after reversible 1,2-nucleophilic addition on aldehydes. Alternatively, primary amines can be converted into secondary and tertiary amines or quaternary ammoniums through alkylation and epoxide ring-opening.

Amide bonds represent the major fraction of amine functionalization due to the mild conditions required for their formation as well as their stability in aqueous solutions over a large range of pH, including physiological pH. Large and small molecules are grafted to CS either through the formation of a reactive intermediate with a coupling agent, or by reaction with anhydrides. As regards coupling agents, *N*-ethyl-*N*′-(3-dimethylaminopropyl)carbodiimide hydrochloride (EDC.HCl) is the "gold standard" and is often complemented by *N*-hydroxysuccinimide (NHS) or hydroxybenzotriazole (HOBt) to improve the reactivity of the activated intermediate prior to conjugation with CS amines.[97,174,175] Alternatively, anhydrides have long been reported for CS functionalization.[176,177] In particular, succinic anhydride provides *N*-succinyl CS derivatives with improved water-solubility and higher hydrophilicity.[178] Prior to this PhD, the succinyl group served as linker for the conjugation of BPEI to CS in the development of a gene delivery vehicle.[177]

Similarly, the formation of urea bonds stable under most biological processes were reported between CS and amino-based substrates such as BPEI (Figure 14).[179,180] To the best of our knowledge, 1,1'-carbonyldiimidazole (CDI) has been exclusively used for the formation of the acyl imidazole intermediate.

Although reversible, imine bonds formed after the condensation of CS amines to aldehydes were vastly investigated, in particular for applications requiring self-healing polymers such as wound healing (Figure 14).[163,181] Imine bonds were reported for the protection of CS amines prior to hydroxyl groups functionalization.[182] Thanks to the charge delocalization, aromatic aldehydes are more stable than their aliphatic counterparts and are consequently well suited for such strategies. Imines are also present in CS networks through their cross-linking with glutaraldehyde or the more exotic squaric acid.[183,184]

Less prevalent in literature, the nucleophilic substitution of CS amines is conducted through their alkylation with aliphatic halides or *via* ring-opening of glycidol derivatives (Figure 14).[185] In particular, the quaternization of CS amines occurs upon alkylation and provides water-soluble derivatives such as TMCS (Figure 13).[186]

1.4.2.2. Hydroxyl groups functionalization

Hydroxyl groups of CS may be selectively functionalized over amines following *N*-protection or *N*-functionalization as previously described (*cf.* section 1.4.2.1). Due to their higher accessibility, the primary alcohols are believed to be the major reactive sites for *O*-functionalization, even though this regioselectivity has not been proven. The functionalization challenge inherent to the low reactivity of hydroxyls as compared to amines is illustrated by the rather scarce publications on the matter.

The main modifications operated on primary alcohols can be categorized in two groups: acylations and nucleophilic substitutions. From acylations derive either carbamate or ester bonds. In a similar way to urea formation, CDI was used for the synthesis of carbamate functionalities between amino-based

compounds and CS. The resulting polymeric system was intended for gene delivery.[187] While the stability provided by such bonds is greatly appreciated for biomedical applications, the usefulness of the more shortly-lived ester bonds should not be underestimated. Drug delivery carriers requiring rapid degradation upon pH variation take advantage of such property, with for instance the *O*-succinylation of CS as first step towards the preparation of CS-coated gold NPs for cancer therapy.[188]

Nucleophilic substitution of hydroxyl groups refers mainly to the carboxymethylation of CS, whose in-house synthesis remains frequent despite its commercial availability.[189] The resulting CMCS (Figure 13) has been involved in applications such as wound healing,[190] cancer therapy[189] and tissue engineering.[191] Interestingly, the *O*-tosylation of CS followed by nucleophilic substitution can convert hydroxyl groups into terminal azides for further functionalization through copper-catalyzed click chemistry.[192]

1.4.3. Non-covalent assemblies

CS also forms robust functional systems *via* non-covalent interactions with small molecules, peptides, and polymers. The preparation of these assemblies advantageously bypasses the need for additional chemical reagents as well as complex and time-consuming purification steps. The association with other molecules as well the interaction patterns are however poorly controlled. Non-covalent assemblies rely on three different types of interactions: hydrogen-bonding, electrostatic interactions and chelation (Figure 15).

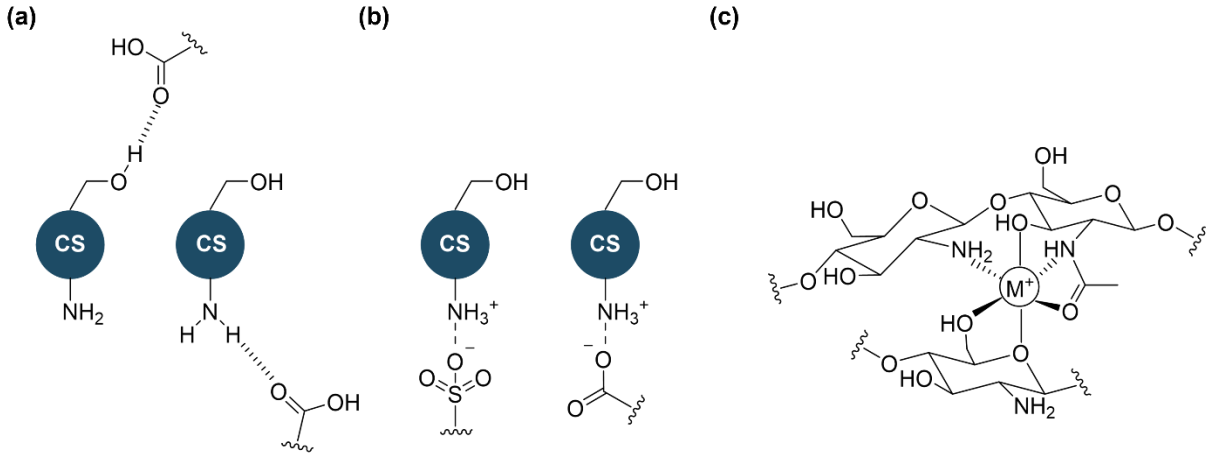

Figure 15. Non-covalent interactions with CS: (a) hydrogen bonds, (b) electrostatic interactions and (c) chelation to metal ions.

Non-covalent conjugation of ions and molecules to CS is often intended to increase the mechanical resistance and stability of the resulting derivatives, as illustrated in tissue engineering and wound dressing applications.[164,193] Metal ions can be chelated by both CS amines and hydroxyls groups, as recently explored (Figure 15c).[194] Regarding delivery systems, sodium alginate is often mixed to CS due to its gelation properties upon calcium ions addition, as reported for the treatment of inflammatory bowel disease by cell encapsulation (Figure 15a).[195] Small molecules like citric acid (CA) and sodium tripolyphosphate also form gels with CS through physical cross-linking (e.g ionic interactions, Figure 15b).[185] Compared to covalent conjugates, the resulting gels are less toxic due to dynamic interactions

which are faster degraded. Together with the antimicrobial and antioxidant properties of CA, such assemblies are well suited for biomedical applications.[196] Last but not least, the association of CS with metallic NPs, QD and CNT was reported to reduce their initial toxicity.[185]

1.4.4. Combination of covalent and non-covalent entities

While covalent CS derivatives ensure stability and precise functionalization, non-covalent assemblies offer the possibility of fast degradation, low toxicity and ease of preparation. The combination of covalent and non-covalent strategies thus provides superior delivery systems.

Dual conjugation pathways usually start with the covalent functionalization of CS amines, using the reactions described in section 1.4.2, and are followed by the spontaneous formation of non-covalent interactions upon mixing with other molecules. Figure 16a illustrates the polymeric system obtained after bulk pre-functionalization of CS with CA through amide bond formation, followed by its self-assembly in water through ionic interactions.[197] Non-covalent interactions can also form upon the addition of a second component (small molecules, polymer or proteins), bringing additional properties to the system.[185] The covalent functionalization of CS amines is often devoted to the improvement of CS water-solubility in order to facilitate any future modification. Quaternization of CS amines *via* epoxide ring opening, *N*-alkylation or quaternary ammonium substitution, is one of the most encountered methods in this case.[160,161]

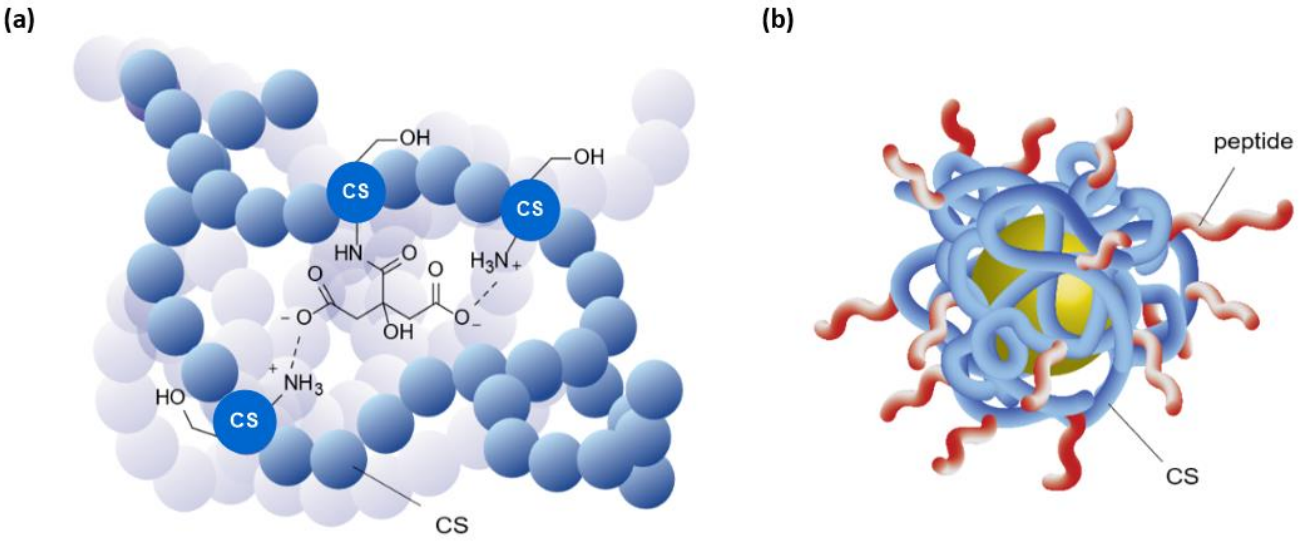

Figure 16. Illustration of CS derivatives based on dual covalent and non-covalent interactions. (a) Polymeric assembly obtained after covalent functionalization of CS with CA followed by their non-covalent assembly in solution. CS units not engaged in an interaction with CA are represented as simple blue balls. (b) Core-shell peptide-CS-Au NP formed upon non-covalent coating of CS on Au NP (yellow), followed by surface covalent functionalization with a cancer targeting peptide sequence. Adapted from Nicolle *et al*.[185]

CS was also reported to serve as coating agent of gold NPs before being grafted with a peptidic cancer targeting sequence (Figure 16b).[198] The resulting assembly displayed a core-shell structure. This post-covalent functionalization ensured the selective grafting of surface CS amines, thus ideally presenting the peptide for cell receptors recognition.

The combination of covalent and non-covalent interactions is attractive for its flexibility and versatility. In particular, core-shell systems ideally protect payloads in their core while exposing targeting ligands or shielding components at their surface.

Chapter 2 Objectives

This thesis project was devoted to the design and synthesis of multifunctional polymeric non-viral gene delivery vehicles to address the challenges encountered with viral vectors, namely toxicity, packaging limitations, and cell-type independent application. The condensation of Nanoplasmids™ as genetic material aimed at circumventing the transient character of RNA-based systems and preventing the insertional mutagenesis often observed with viral vectors.

The work herein presented is part of an interdisciplinary Sinergia project funded by the Swiss National Foundation and involved three Swiss research partners. The chemical syntheses were performed in our research group (GBF, SCI-SB-SG, EPFL, Lausanne). Formation and characterization of the resulting polyplexes were conducted in the research group of Prof. Jörg Huwyler at the University of Basel. In particular, Jens Casper (PhD student) and Dr. Pascal Detampel (post-doctoral researcher) performed these experiments, as well as the *in vitro* evaluation of the delivery vehicles. The research group of Prof. Beat Thöny (University Children's Hospital, Zürich) was involved in the *in vivo* evaluation on wild-type and model diseased mice. Hiu-Man Grisch-Chan (post-doctoral researcher) and Melanie Williman (PhD student) performed these experiments.

Although these polymeric gene delivery vectors were designed to be rather universal, the long-term objective of the project was to provide a treatment to phenylketonuria and ornithine transcarbamylase deficiency, two inborn inherited disorders resulting from deficiencies in liver enzymes.[199,200] These are exclusively produced in hepatocytes, leading the therapeutic gene and delivery vehicle to be engineered to solely express the desired proteins in those cells. *In vitro* assays were therefore focused on hepatocyte-derived cell lines.

CS was selected as polymeric backbone for its biocompatibility, biodegradability and ease of functionalization thanks to its multiple reactive groups. The project envisioned its stepwise covalent modification to reach the formation of stable NPs overtime, and in a wide set of physiological conditions. Therefore, the formation of amides and urea through the functionalization of both amines and hydroxyl groups was favored (Figure 17). We aimed at addressing each aspect of DNA delivery, that is DNA condensation, bioavailability in the blood stream, cell targeting, cellular uptake and endosomal escape. Nuclear import was not tackled in this work, as its improvement depends on DNA post-modifications and genetic engineering rather than polymer functionalization.

We sought to improve the condensation ability of CS through its covalent grafting to low MW BPEI and LPEI, which are better tolerated by cells than higher MW chains.[61,66] The condensation of Nanoplasmids™ with the resulting CS-PEI system relied on the spontaneous formation of NPs upon mixing, *via* electrostatic interactions between the cationic copolymer and the anionic DNA. This approach ensured vehicle's versatility as regards DNA cargos. In addition, the variation of the grafting degree (GD) of PEI should modulate the residual surface charge. Thanks to the high buffering character of PEI, the CS-PEI-based polyplex was also expected to efficiently escape endosomes.

To avoid undesired interactions with components of the blood and immune system, the shielding of the polyplex was investigated through the integration of low MW PEG chains on CS-PEI system. In particular, the use of heterobifunctional PEG with different cross-linking reactive moieties was intended for the spontaneous formation of covalent bonds during NPs formation, thus conferring additional stability to the polyplex (Figure 17).

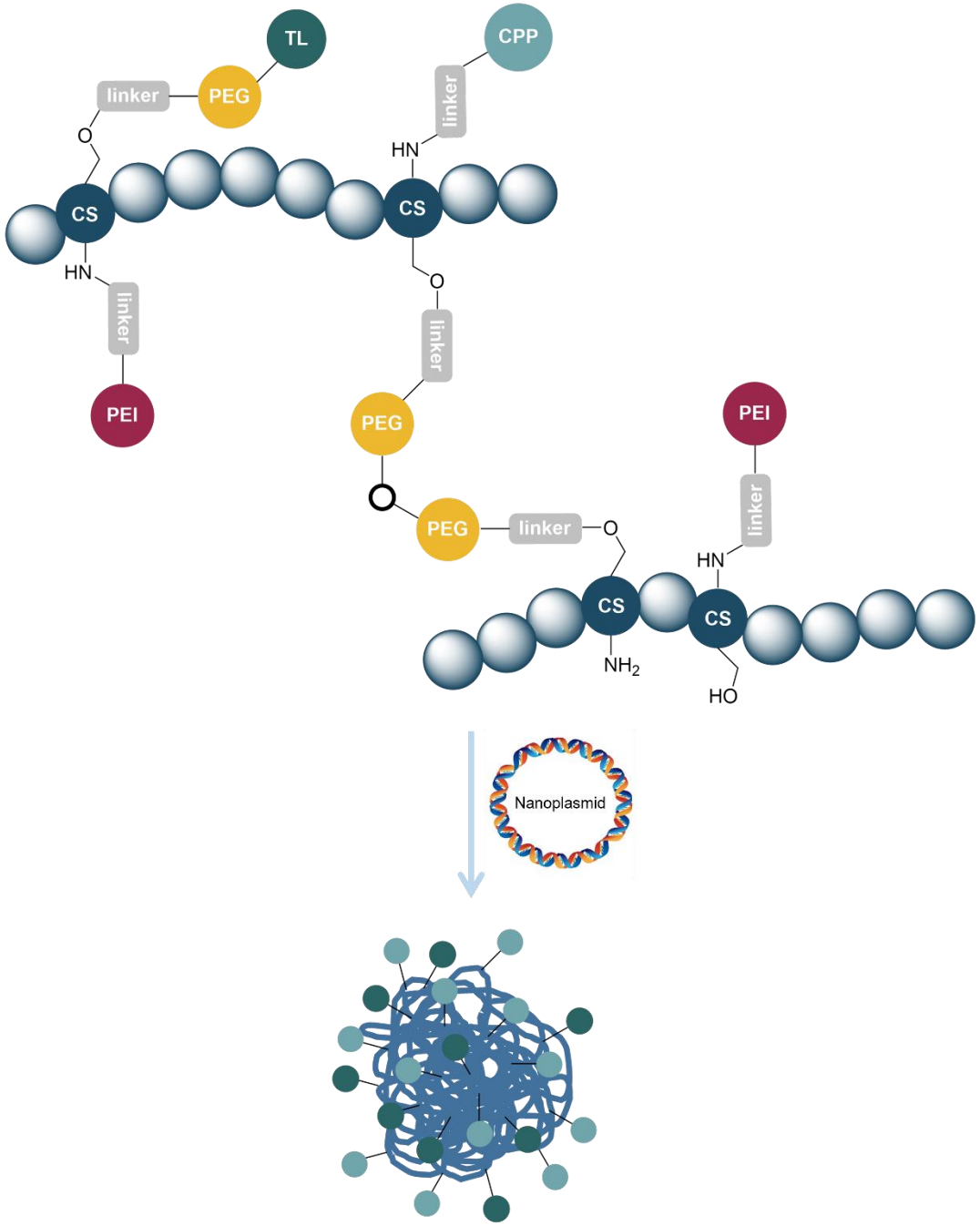

Figure 17. Schematic representation of the envisioned cross-linked CS derivatives conjugated to PEI (red), PEG (yellow), CPP (light blue) and targeting ligand (TL, dark green). CS units not functionalized with any additive are represented by empty blue balls. CS chains are cross-linked through the cross-reactive ends of PEG chains (bold black circle). Upon mixing to DNA, polymeric NPs (blue) spontaneously form, with the TL (dark green) and CPP (light blue) components pointing at its surface, and PEI and DNA compacted in the inner core.

Following optimization of the cross-linked polymeric core, we planned to decorate it with additional

components promoting cell targeting and cellular uptake (Figure 17). In view of hepatocytes-targeted applications, lactobionic acid was the targeting ligand of choice. To broaden the applications of our gene delivery vehicle, the grafting of folic acid, an anti-cancer targeting ligand, was also considered. Moreover, the conjugation of CPP based on polyarginines and TAT-derived sequences was expected to enhance the cellular uptake of the resulting polymeric vehicle. Depending on the optimal polymeric core, those new components would be grafted either to end groups of PEG spacers or directly on the CS backbone thanks to the remaining free amines and hydroxyl groups.

As illustrated in Figure 17, we envisioned to conjugate PEI, PEG and additional small components to the same CS backbone. We also aimed at exploring the formation of core-shell systems, with CS-PEI polymer forming the core to properly condense DNA, and CS-PEG polymer as a shell polymer to shield the core and stabilize the NP. Targeting and cell-penetrating components would be exposed at the surface of the resulting core-shell structure.

As regards DNA vectors, luciferase- (n.CAGLuc2) and GFP-expressing (n.CAG.GFP1) Nanoplasmids™ were both selected as reporter genes for *in vitro* cellular experiments. Doing so, we assessed the polyplexes transfection efficiency *via* bioluminescence or fluorescence, respectively. For *in vivo* experiments, a reporter Nanoplasmid™ expressing luciferase (n.P3Luc1) was selected. The replacement of the universal CAG promoter by a P3 promoter ensured specific expression in mice liver.

Chapter 3 Results and Discussion

3.1. Commercial chitosan and its depolymerization

In this first section, we expose the challenges encountered to functionalize commercial CS and the solution developed in return. In particular, the development of a robust depolymerization method leading to water-soluble CS chains, with a narrow distribution of MW, is detailed. All functionalization strategies were then developed with **depolymerized CS** (**dCS**) as starting material. This section is based on the paper: "Journot *et al.*, *Polymers*, **2020**, *12*, 1274".[201]

3.1.1. Initial observation

As presented in Chapter 1, CS was selected as polymeric backbone for the development of gene delivery vehicles. CS chains with a MW of less than 150 kDa were reported to be more suitable for gene delivery than higher MW.[202] Although polyplexes generated with high MW CS are more stable, they suffer from poor DNA unpacking once in the cell cytoplasm, thus hampering proper DNA expression. Low MW CS were found to form less stable polyplexes and to lead to higher transfection efficiency. The challenge is to find a balance between stability and effective DNA unpacking. Therefore, we performed the first tests of CS functionalization with a low MW commercial batch from Tokyo Chemical Industries displaying the following characteristics: viscosity of 5–20 mPa.s (0.5% w/v in 0.5% acetic acid, 20 °C) and DD of 75-85%. Compared to similar commercial batches characterized with a viscosity of 20 mPa.s and a MW of 50 kDa, we estimated a MW of less than 50 kDa in our case. Later on, the characterization by a GPC equipped with triple detection revealed that the sample was composed of a mixture of three distributions (Mw 478.9, 88.41 and 44.80 kDa) with a global polydispersity of 1.87. Such heterogeneity, which was also observed for other commercial batches, was not suitable for the development of biomedical products. Prior to any functionalization procedure, the homogeneity of the starting polymer had to be improved.

In addition, commercial CS was found to be insoluble in a variety of organic solvents including DMF, DMSO, acetonitrile and THF (1 mg/mL, 25 °C). A suspension formed in water but rapidly led to the sedimentation of the polymer over the time of NMR analysis. The only way to properly dissolve and analyze CS required the use of weakly acidic solutions such as mixtures of acetic acid and water, as reported by Lu *et al.*[203] However, the number of chemical reactions compatible with such mixtures was extremely limited. CS functionalizations attempted in pure water were not successful (*cf.* details in section 3.2.2), which urged us to develop a process to produce CS with suitable properties (water-solubility, low MW, low PD) for downstream functionalization and gene delivery applications.

3.1.2. Depolymerization of CS

Besides DD and pattern of acetylation, the MW is the most important factor governing CS solubility. Therefore, reducing the MW is a common strategy to improve it and can be achieved by several

techniques. As CS was meant to serve as starting material, we needed a robust and cost-effective depolymerization method. Irradiation and enzymatic treatment were quickly put aside because of their expensive price.[155,156] Chemical depolymerization methods were more promising and advanced in their development. While depolymerization under basic conditions is known to remove acetyl groups faster than the MW decreases, oxidative degradation was reported to oxidize reactive moieties of the polymeric chains concomitantly to their depolymerization.[157,158] On the contrary, acidic depolymerization favors reduction of the MW over the DD increase. We therefore explored a chain degradation procedure in acidic conditions that would deliver water-soluble **depolymerized CS** (**dCS**) chains. Water-solubility was indeed an essential property to consider for biological applications. Adrian Gheata (MSc student) and I contributed to these experiments, but Dr. Céline Journot (postdoctoral researcher) led this part of the project.

3.1.2.1. Microwave-assisted acid-based depolymerization of CS

Depolymerization of CS was first attempted in 1 M HCl solution (1% w/v) under conventional reflux for 48 h. After neutralization to pH 7 and two cycles of centrifugation, the liquid phase containing the water-soluble chains was collected and afforded 50% yield of **dCS** on average. However, **dCS** could not be efficiently separated from the insoluble fraction of degraded CS, even after extensive filtration over 0.22 mm polyethersulfone filters.

In order to reduce reaction times and avoid the formation of degradation materials, we turned our attention towards microwave-assisted heating to promote acidic degradation of CS (1 M HCl, 1% w/v). After 19 min at 100 °C (optimized reaction time), the resulting clear solution was neutralized and centrifuged twice. The soluble fractions were further dialyzed and lyophilized to afford **dCS** as a pure white aerated solid, with an overall yield of 15%. Due to the limited capacity of the microwave reactor, the procedure could only be performed on batches of 200 mg of CS at a time. Thanks to the short reaction times, the repetition of successive microwave-assisted depolymerization cycles allowed the production of several grams of **dCS**, presenting highly reproducible characteristics and excellent sample homogeneity (*cf.* section 3.1.2.2).

We precisely estimated the effect of depolymerization on the solubility of the polymer by progressively dissolving CS and **dCS** in pure water (10 mg/mL), and adding dropwise a solution of 1 M HCl until their complete dissolution. pH values before the addition of HCl (aq.) were similar for CS and **dCS** (6.40 and 6.86 respectively). The dissolution of CS and **dCS** was reached at pH 2.19 and 5.97 respectively, suggesting improved properties for **dCS**.

3.1.2.2. Analyses of dCS

All **dCS** batches produced by microwave-assisted acidic degradation were systematically characterized for their MW (Mn, Mp, Mw) and PD *via* GPC analysis, while their DD was calculated on the basis of ^{1}H NMR analysis.

3.1.2.2.1. GPC analysis

We report in Table 1 a representative fraction of all the **dCS** batches produced by different operators over the past two years and following the optimized microwave-assisted procedure. (*cf.* section 5.2.1, **dCS** procedure). All samples were analyzed on the same GPC machine, equipped with triple detection (Multiangle light scattering, Viscometer and Refractive index), thus enabling the determination of absolute values. The samples were prepared and run in acetate buffer (0.3 M aqueous acetic acid, 0.2 M aqueous sodium acetate, 0.3 M aqueous sodium nitrate, pH 4.4) with a concentration of 10 mg/mL.

Table 1. Estimation of MW and PD of **dCS** obtained *via* microwave-assisted depolymerization.

Entry[1]	Operator (#)[2]	Mn (Da)	Mp (Da)	Mw (Da)	PD
1	2	6760	7230	8420	1.25
2	1	6900	6300	8300	1.20
3	4	6270	6750	7560	1.21
4	3	5850	7000	7410	1.27
5	2	5870	6280	7230	1.23
6	4	6830	6650	7120	1.04
7	3	6750	6200	6900	1.02
8	3	6610	6100	6780	1.03
9	2	5130	5550	6590	1.29
10	3	6260	6100	6440	1.03
11	2	5840	5820	6190	1.06
12	3	5700	5390	5940	1.04
13	2	5470	5060	5750	1.05

[1]Entries are ranked by decreasing Mw. Mw is the MW value representing at best a polymeric batch. [2]There were 4 different operators, each of them is represented by a number from 1 to 4. 1: Perrine Robin, MSc student; 2: Elias Troxler, chemistry apprentice; 3: Amélie Girardin, chemistry apprentice; 4: Laura Nicolle.

Each batch was the result of the combination of 10 successive samples. Overall, this depolymerization procedure led to narrow MW ranges, between 8.5 kDa and 5.5 kDa (Table 1). The PD obtained for each batch was drastically reduced from 1.87 (value of the commercial batch) to 1.1 on average. Batches with a higher Mw displayed a higher PD value. Interestingly, the trend was not the same for the corresponding Mn values. These results suggested that the batches with a higher Mw contained some residual very large chains. The moderate variations observed between the different batches was attributed to the heterogeneity of the commercial stock (500 g, PD 1.87), from which only 2 g were collected for each series of depolymerization cycles (200 mg, 10 times). The robustness and reproducibility of the protocol was demonstrated by the similar **dCS** characteristics obtained by the different operators (Table 1).

Entries 12 and 13 were typical batches of **dCS** that presented a Mw too low for further functionalization. In order to work with long enough **dCS** chains, we set a minimal threshold of 6 kDa for Mw and put aside the batches that did not meet this requirement.

3.1.2.2.2. ^{1}H NMR analysis

Along with GPC, **dCS** batches were analyzed by ^{1}H NMR to determine their DD values. As mentioned in section 1.4, primary amines on glucosamine units represent the most interesting reactive moieties

for downstream functionalization. DD values were thus of utmost interest to calculate the amount of reactive units (e.g. glucosamine) that could be engaged in the next chemical reactions.

The DD value of each **dCS** batch was deducted from ^{1}H NMR spectrum acquired in pure D_2O. Systematic analysis in a mixture of D_2O/acetic acid-d_4 1/1 was also performed to facilitate the assignment of overlapping signals in the next synthetic steps.

A typical spectrum of **dCS**, dissolved in D_2O (3 mg/mL), is presented in Figure 18.

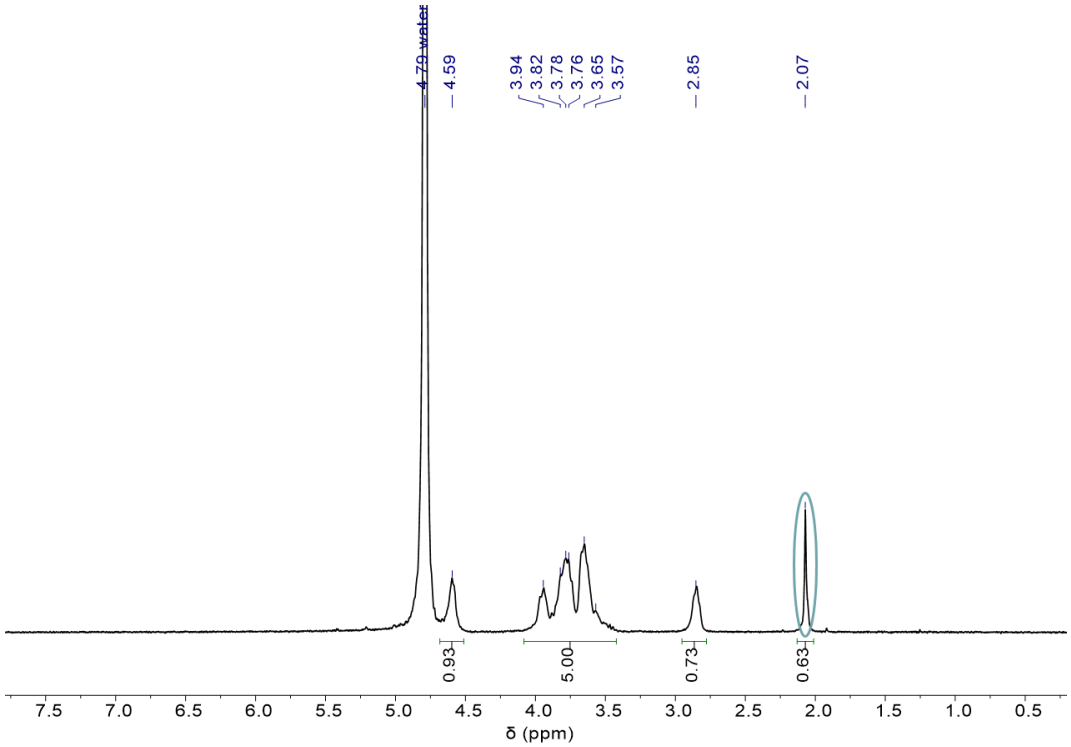

Figure 18. ^{1}H NMR spectrum of **dCS** in D_2O. The acetyl peak on the acetylglucosamine units of **dCS** is circled in pale blue.

The peak at δ 2.07 ppm (circled in pale blue) is assigned to the methyl group of the acetylglucosamine unit and represents the only isolated signal which differs between glucosamine and acetylglucosamine units (Figure 18). If **dCS** chains were composed of 100% of acetylglucosamine units, this peak should integrate for 3 H. As $\int \delta(2.07) = 0.63$ on Figure 18, this means that DD = $(1 - \frac{\int \delta(2.07)}{3})$ x 100 = 79%. In other words, 79% of **dCS** units displayed free amine groups, while the remaining 21% displayed acetamide groups. Over the different **dCS** batches, the DD values extended from 72 to 88 %, in agreement with the indicative value given by the supplier for the commercial batch. We therefore confirmed that the optimized depolymerization procedure did not induce further deacetylation of the polymeric chains. The complete analysis of **dCS** by ^{1}H NMR is described in section 5.2.1.

3.1.3. Conclusions

The heterogeneity and poor solubility of commercial CS (from Tokyo Chemical Industries) in organic solvents and aqueous solutions was not suited to the development of robust functionalization pathways

and prevented the preparation of relevant formulations for biological assays. The acidic depolymerization of CS under microwave heating led to the production of **dCS** batches presenting reproducible characteristics, improved solubility, and Mw ranging from 5.5 to 8.5 kDa. The data collected from GPC and ^{1}H NMR analyses were also key to adjust the parameters for the polyplexes formation (University of Basel).

3.2. Covalent functionalization of dCS to engineer binary polyplexes

This section discusses the covalent functionalization of **dCS** with PEI and PEG. After a brief introduction on the use of 2D-Diffusion Ordered Spectroscopy (2D-DOSY) NMR technique to evaluate the covalent character of the polymeric derivatives, the different conjugation strategies are discussed. Several final compounds were further engaged in the formation of polyplexes with Nanoplasmids™ and were evaluated *in vitro* and *in vivo* for their toxicity and transfection efficiency. This section is based on the paper: "Nicolle *et al.*, *Int. J. Mol. Sci*, **2021**, *22*, 3828".[204]

3.2.1. 2D-DOSY NMR and covalent bonding

2D-DOSY NMR is a technique relying on the measurement and comparison of the diffusion constant of every molecule present in a liquid sample. Each molecule is naturally diffusing in solution with its own diffusion rate. In 2D-DOSY NMR, the diffusion constant assigned to each ^{1}H NMR peak of the analyzed sample is measured and plotted in 2D (Figure 19). In the case of a covalent polymeric derivative, the spots arising from the different components of the system appear on the same line (i.e. same diffusion constant). On the contrary, non-covalent assemblies are characterized by non-aligned spots (i.e. different diffusion constants).

For example, we present below the 2D-DOSY NMR spectrum of **dCS-NSuc** (synthesis discussed in section 3.2.2.1) (Figure 19). The peak for the succinyl group (δ 2.6 ppm, yellow circle) gives a spot on the 2D spectrum that is aligned with the spots arising from the peaks of **dCS** (dark blue circles), attesting for the covalent character of **dCS-NSuc**. On the contrary, the residual water peak (δ 5.7 ppm, dark red circle) leads to a spot with a different diffusion constant.

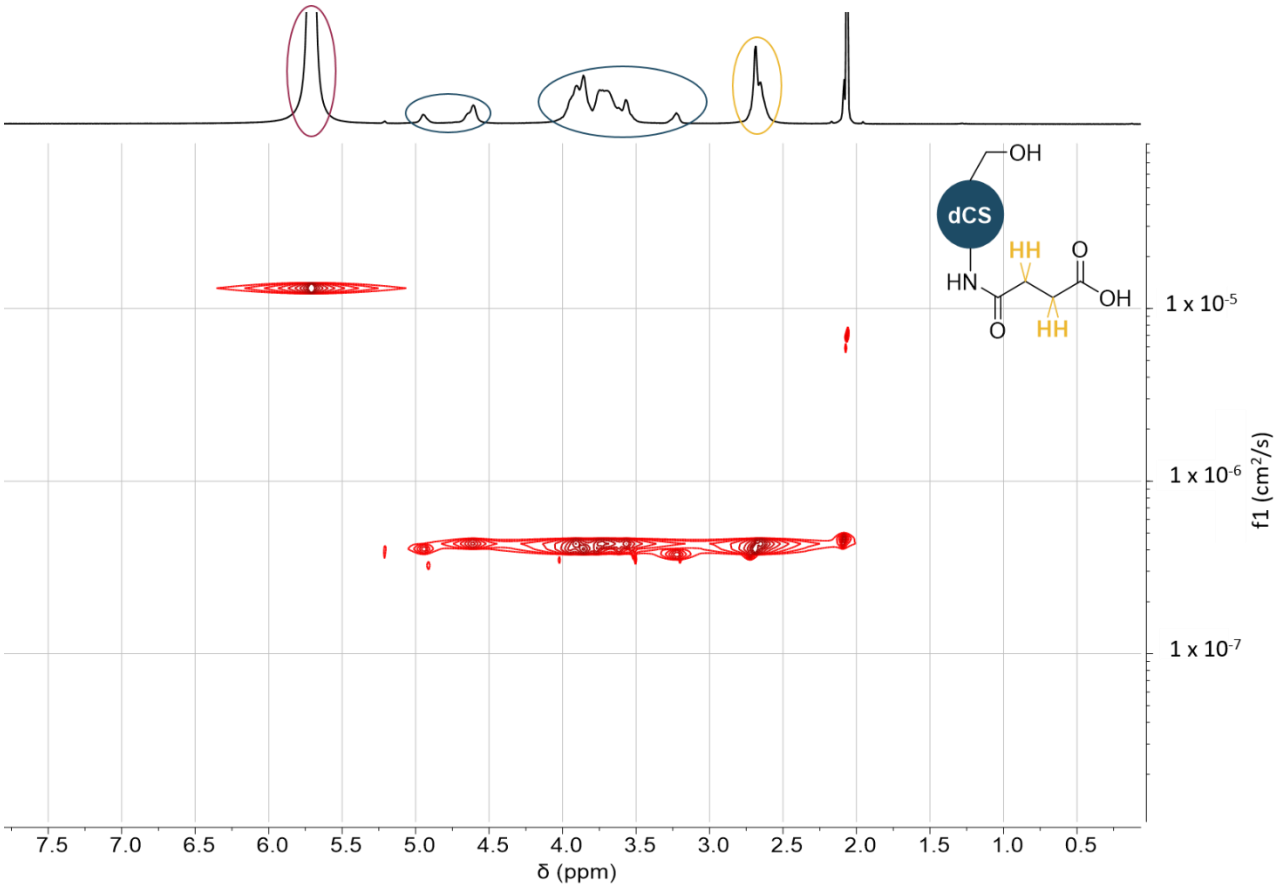

Figure 19. Illustration of the 2D-DOSY interpretation with the spectrum of **dCS-NSuc**.

Non-covalent and stable polymeric systems are often reported throughout literature but cannot be differentiated from covalent assemblies using solely ^{1}H NMR analysis. All polymeric derivatives developed in this project were thus analyzed by 2D-DOSY NMR to probe their covalent character. We strongly recommend this straightforward method for the characterization of similar systems.

3.2.2. Conjugation of dCS to PEI

3.2.2.1. First developments with BPEI

The first functionalization attempts on **dCS** aimed at the covalent conjugation of its amine moieties with BPEI (1.2 kDa) which is known to tightly condense DNA (*cf.* section 1.2.2.2.2). The less reactive hydroxyl groups were expected to remain intact. Two options were investigated: either the direct reaction of **dCS** with BPEI using carbonate-based coupling agents to form ureas, or the functionalization of **dCS** with a small linker such as a succinyl group and the subsequent grafting of BPEI using peptide coupling chemistry (Scheme 4). Both ureas and amides are stable in physiological conditions. Adrian Gheata (MSc student) contributed to this study.

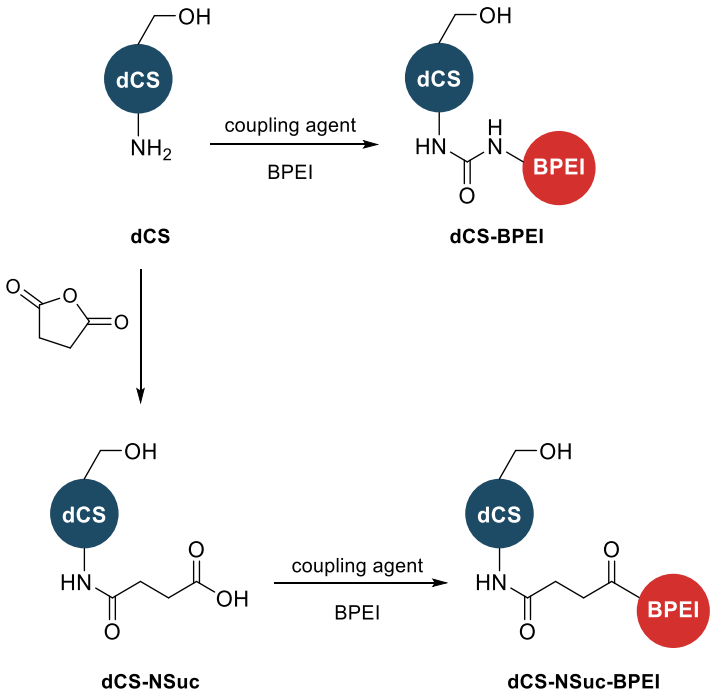

Scheme 4. Direct and stepwise conjugation of **dCS** to BPEI**.**

The direct coupling of BPEI to **dCS** was attempted with CDI, as previously reported,[180,203] and *N,N′*-disuccinimidyl carbonate (DSC) (Table 2, entries 1 and 2). None of the tested conditions led to significant grafting on the amino groups. While the imidazolide intermediate was suspected to degrade too rapidly in the reaction mixture, the use of DSC led to the formation of a stable intermediate that could be isolated and characterized by ^{1}H NMR analysis. However, the conjugation of BPEI on this intermediate was not successful, leading solely to trace amounts of **dCS-BPEI** (Scheme 4).

Table 2. Screening of coupling agents for the grafting of BPEI to **dCS**.

Starting material	Coupling agent	Reaction conditions[1]	Comments
dCS	CDI	1) DMSO, 80 °C, 30 min 2) BPEI, 80 °C, 18 h	Low grafting
dCS	DSC	1) PBS, 80 °C, 18 h 2) BPEI, H_2O, 80 °C, 17 h	Poor reactivity of dCS-DSC intermediate
dCS-NSuc	EDC/sulfo-NHS	1) DIPEA, H_2O, rt, 1 h 2) BPEI, rt, 24 h	Mixture of covalent and non-covalent conjugates
dCS-NSuc	DMTMM	DMTMM, BPEI, DIPEA, H_2O, rt, 3 h	Covalent grafting

[1]Characteristics of commercial BPEI used in these screening studies: 1.2 kDa (50 wt% in H_2O, Sigma Aldrich), Mn ≈ 1.2 kDa, Mw ≈ 1.3 kDa, determined by light scattering.

The second strategy to functionalize **dCS** with BPEI involved its prior derivatization with succinic anhydride (Scheme 4). Based on the works of Dmour *et al.* and Aiedeh and Taha,[176,205] the procedure was optimized for **dCS**, particularly regarding the purification steps. The reaction mixture was purified *via* dialysis instead of precipitation in acetone which was not suitable for such small polymeric chains. Non-water-soluble fragments were removed by centrifugation after dialysis, and the resulting supernatant was further lyophilized to afford pure **dCS-NSuc**. Such purification procedure was then

applied to all **dCS** derivatives produced during the project, as it proved to significantly improve the homogeneity of the final polymers. At that stage, the repeatability of the reaction and of the purification steps was assessed on several batches of 1 g of starting **dCS**, leading to GD values of the succinyl group (GD_{Suc}) ranging from 45 to 63%.

The carboxyl functionalities of the succinyl spacer were used to conjugate BPEI to **dCS-NSuc** through amide bonds (Scheme 4). Activation with EDC combined to NHS or to its water-soluble version N-hydroxysulfosuccinimide (sulfo-NHS), is a "gold standard" for CS functionalization, and is widely reported.[175,191,206] However, in our case, these conditions mostly resulted in the formation of non-covalent systems (Table 2, entry 3). We thus turned our attention to the water-soluble coupling agent 4-(4,6-dimethoxy-1,3,5-triazin-2-yl)-4-methyl-morpholinium chloride (DMTMM). Although **dCS** was much more soluble in organic solvents than commercial CS, water remained the solvent of choice for **dCS** functionalization. The use of DMTMM led to the successful preparation of the covalent **dCS-NSuc-BPEI** derivative within short reaction time (Table 2, entry 4).

3.2.2.2. Optimized preparation of dCS-PEI derivatives

Having identified a stepwise conjugation protocol for the covalent derivatization of **dCS**, we applied this strategy to both BPEI (1.8 kDa) and LPEI (2.5 kDa), with a specific focus on the production of batches with various GD values and reproducible scaled up procedures.

3.2.2.2.1. Optimization of dCS-NSuc-BPEI

Starting from 200 mg batches of **dCS**, a series of **dCS-NSuc-BPEI** derivatives were produced with GD values of 11, 13 and 67% to evaluate the influence of the cationic charge on the physicochemical properties and cytotoxicity of the polyplexes (Scheme 5).

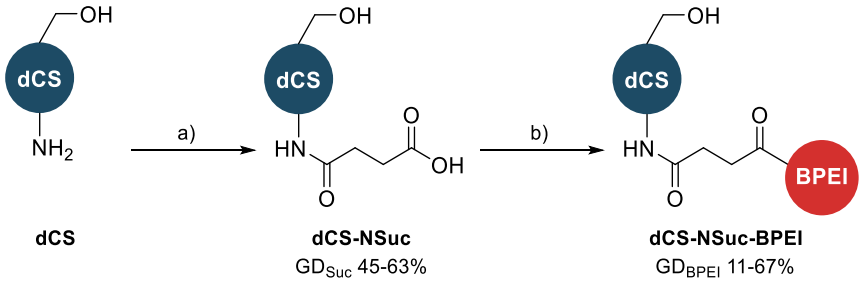

Scheme 5. Optimized two-step synthesis of **dCS-NSuc-BPEI**. a) succinic anhydride, pyridine, 0.3% aq. HCl, rt, 1.5 h. b) DMTMM, BPEI, H_2O, rt, 3 h.

Based on the promising results observed on test scales with DMTMM, the second step of **dCS-NSuc-BPEI** synthesis could also be scaled up to 650 mg of desired final product (GD_{BPEI} 18%) (Scheme 5).

3.2.2.2.2. Optimization of dCS-NSuc-LPEI

Due to the poor water-solubility of LPEI,[51] some adjustments were necessary for the preparation of **dCS-NSuc-LPEI**. As LPEI is soluble in water at 55 °C (10 mg/mL), the synthesis of **dCS-NSuc-LPEI** from **dCS-NSuc** was performed at 60 °C to ensure a homogenous reaction mixture, thus favoring LPEI's reactivity (Scheme 6).

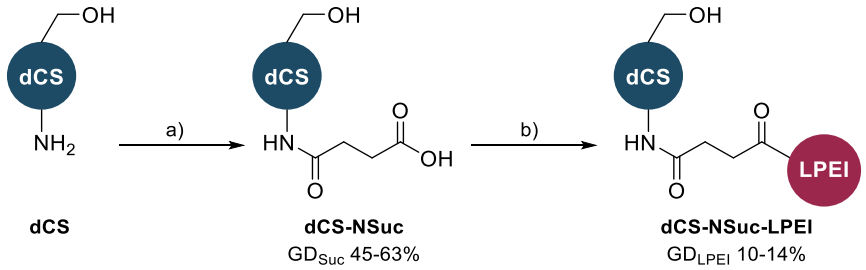

Scheme 6. Optimized two-step synthesis of **dCS-NSuc-LPEI**. a) succinic anhydride, pyridine, 0.3% aq. HCl, rt, 1.5 h. b) DMTMM, LPEI, H_2O, 60 °C, 3 h.

Because of the crystalline character of LPEI, GD_{LPEI} had to be tightly controlled to avoid the formation of a polymeric derivative insoluble in acidic water (pH 6-4), thus preventing its use for biological tests. Sufficient amounts of LPEI were nonetheless required to induce a significant effect on DNA condensation and on endosomal escape, we therefore optimized GD_{LPEI} between 10 and 15% (Scheme 6).

3.2.2.2.3. Biological assessment

The minimal solubility in water required for *in vitro* tests was set at 5 mg/mL. Except for **dCS**, all batches were soluble in water (acidified down to pH 4 when required) with a minimal concentration of 7.5 mg/mL for **dCS-NSuc-BPEI** (GD 13%), and above 10 mg/mL for the others. The physical characterization and *in vitro* assessment of these batches were performed by Jens Casper (University of Basel) with two different Nanoplasmids™ (n.CAGLuc2 and n.CAG.GFP1) in the hepatocellular carcinoma cell line HuH-7, and are summarized in Table 3.

Table 3. Physico-chemical characterization and *in vitro* assessment of **dCS-NSuc-BPEI** and **dCS-NSuc-LPEI** batches.

Polymers	c/p ratio at optimal colloidal stability[1]	ζ-potential (mV)[2]	Hydrodynamic diameter (nm)[2]	PDI[2]	Luc x GFP normalized to dCS c/p 32 (fold)[3]	MTS (% viable cells)[4]
dCS	32	22 ± 4	68 ± 5	0.23 ± 0.03	1 ± 1	111 ± 5
dCS-NSuc-BPEI, GD 11%	2	19 ± 3	68 ± 2	0.22 ± 0.01	415 ± 24	81 ± 1
dCS-NSuc-BPEI, GD 13%	4	16 ± 4	62 ± 1	0.22 ± 0.01	1174 ± 6	81 ± 7
dCS-NSuc-BPEI, GD 67%	1	24 ± 2	79 ± 1	0.21 ± 0.01	3488 ± 160	63 ± 2
dCS-NSuc-LPEI, GD 11%	2	23 ± 1	87 ± 1	0.16 ± 0.01	71'567 ± 1592	101 ± 9

[1]DNA loading degree is defined by the c/p value (ratio **dCS** derivative/DNA; w/w). Polyplex stability was determined by gel retardation assay (data not shown). The optimized colloidal stability defined the c/p ratio that was later used for *in vitro* experiments. [2]ζ-potential was determined by electrophoretic light scattering, and hydrodynamic diameter and polydispersity index (PDI) were determined by dynamic light scattering (DLS). A complex with a PDI equal or below 0.2 was considered to be monodisperse. [3]The *in vitro* gene expression was determined in HuH-7 cells using two reporter genes (n.CAGLuc2 and n.CAG.GFP1). Their transfection values were merged to give a complementary overview. [4]Cytotoxicity was assessed using a MTS assay. Values are means ± SD, $n \geq 3$.

From results in Table 3, only the binary complex **dCS-NSuc-LPEI**/DNA met all the desired criteria for gene delivery, e.g. chemical properties, physico-chemical characteristics and *in vitro* performance. Its

low c/p ratio (**dCS** derivative/DNA; w/w) limited as much as possible the potential cytotoxic effects inherent to the use of cationic polymers as delivery vehicles. The overall ζ-potential remained slightly positive, which was desirable for cellular membrane interactions and endosomal escape. The merged transfection value Luc x GFP gave a complementary view on transfection efficiency by combining the results from two reporter genes, and was the highest for **dCS-NSuc-LPEI**. Lastly, cell viability was greater for **dCS-NSuc-LPEI**, suggesting that the higher toxicity observed for the three **dCS-NSuc-BPEI** derivatives came mainly from BPEI. The decrease of cell viability observed from **dCS-NSuc-BPEI** (GD 13%) to **dCS-NSuc-BPEI** (GD 67%) also supported this hypothesis.

3.2.2.3. Lead compound and *in vivo* evaluation

3.2.2.3.1. Scale up of the lead compound

Following *in vitro* assessment, **dCS-NSuc-LPEI** was chosen as the lead compound. In order to repeat and confirm the data obtained *in vitro,* as well as to perform *in vivo* evaluation, this procedure was scaled up. Starting from 4 g of **dCS,** up to 900 mg of final polymer were produced (Table 4). The procedure was performed on several batches to assess its reproducibility, which was confirmed by ^{1}H and 2D-DOSY NMR analyses. The average GD_{LPEI} obtained from the combination of the seven batches of **dCS-NSuc-LPEI** was estimated at 14% by ^{1}H NMR analysis (Table 4).

Table 4. Scale up of **dCS-NSuc-LPEI**.

Product	Starting amount of precursor (g)	Final amount of desired product (g)	Yield (%)	GD (%)
dCS	24.6	4.40	18	-
dCS-NSuc	4.0	3.65	67	63
dCS-NSuc-LPEI	1.4	0.916	35	14

3.2.2.3.2. In vivo evaluation

In vivo studies on wild-type mice were performed by Dr. Hiu-Man Grisch-Chan and Melanie Williman (Children's University Hospital of Zürich). *In vivo*-jetPEI, a commercially available polymeric delivery vector, was used as a control. The polyplexes were formed with the Nanoplasmid™ n.P3Luc1 expressing luciferase from the liver-specific promoter P3. The GFP encoding Nanoplasmid™ could not be used because of the liver autofluorescence. As optimized *in vitro*, DNA was complexed with **dCS-NSuc-LPEI** at a c/p ratio of 2, while *in vivo*-jet PEI was used at a c/p ratio of 1.1, as advised by the supplier. The resulting polyplexes were then administered by retrograde intrabiliary infusion through the gallbladder, ensuring an efficient distribution to the hepatocytes even without the presence of a targeting ligand. Another strong asset of this technique is the low amount of DNA required, and therefore of **dCS** derivative, that has to be injected. In this case, only 1 µg of DNA was complexed with the polymeric vector.

In vivo bioluminescence imaging was followed over 3 days (Figure 20). Luciferase expression was localized in the liver, as illustrated in Figure 20b. A ten-fold difference of expression was observed between *in vivo*-jetPEI and **dCS-NSuc-LPEI** injected mice (6.4×10^{6} photons/s and 7.9×10^{7} photons/s

respectively), showing the superiority of the **dCS**-based gene delivery vehicle (Figure 20a).

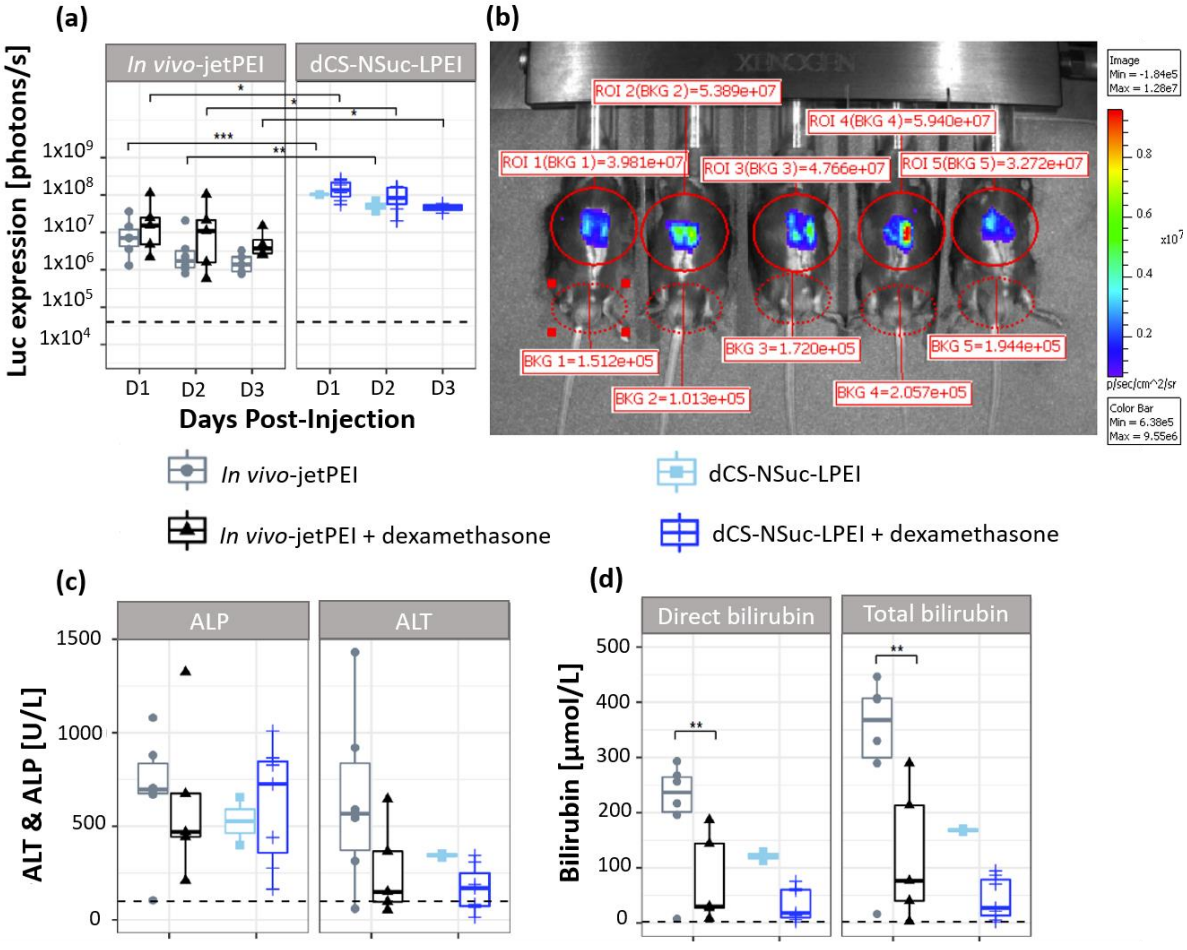

Figure 20. *In vivo* evaluation of **dCS-NSuc-LPEI** upon retrograde intrabiliary infusion into wild-type mice. (a) Luciferase expression up to three days post-infusion with polyplexes containing 1 µg of Nanoplasmid™ encapsulated with a c/p ratio of 2 (for **dCS-NSuc-LPEI**) and 1.1 (for *in vivo*-jetPEI). Animals were pre-treated without (n = 6) or with dexamethasone (n = 5) for *in vivo*-jetPEI, and without (n = 2) or with dexamethasone (n = 5) for **dCS-NSuc-LPEI**. (b) Detection of liver-associated bioluminescence in mice three days post-infusion (1 µg DNA/**dCS-NSuc-LPEI** + dexamethasone). (c-d) Serum markers for hepatotoxicity, including alkaline phosphatase (ALP), alanine transaminase (ALT), total bilirubin, and direct bilirubin. Statistical differences by Student's two tailed t-test: * = p<0.05, ** = p<0.01, *** = p<0.001. Dashed line = untreated mice. Values are means ± SD, n ≥ 3.

Moreover, pre-treatment of mice with the anti-inflammatory drug dexamethasone aimed at reducing liver toxicity and jaundice. Serum markers reporting for hepatotoxicity, such as alkaline phosphatase (ALP), alanine transaminase (ALT), and total and direct bilirubin, were monitored. Without dexamethasone, elevated levels of these biomarkers were observed 3 days post-injection (Figure 20c,d). Pre-treating mice with dexamethasone was however clearly beneficial as levels of ALT, direct and total bilirubin decreased for both **dCS-NSuc-LPEI**- and *in vivo*-jetPEI-based polyplexes.

Via this preliminary *in vivo* assessment, we could confirm the validity of our approach. Polyplexes based on **dCS-NSuc-LPEI** outperformed the ones made from the commercial *in vivo*-jetPEI, showing their potential for gene delivery *via* retrograde intrabiliary infusion. In addition, inflammatory response leading to liver toxicity and jaundice could be down-regulated with the pre-administration of dexamethasone. The results showed that the combination of **dCS** and LPEI is promising for the

preparation of gene delivery vehicles. Therefore, the next sections of this subchapter aim at further improving the features of the initial polyplex.

3.2.3. Orthogonal functionalization of dCS-PEI derivatives

The grafting of **dCS-NSuc-BPEI** and **dCS-NSuc-LPEI** with linear PEG (2 kDa, 44 ethylene glycol units) was investigated with the primary goal of improving cell viability and shielding of the delivery vehicle. In addition, functionalizing **dCS** with heterobifunctional PEGs bearing cross-linking moieties (thiol, maleimide (Mal) and acrylate (Acr)) would allow to further generate a large covalent polymeric network upon cross-linking during NPs formation (Figure 21). Thiols are known to react with Mal or Acr moieties *via* 1,4-addition (Michael addition) in a bioorthogonal way, with in theory no additional reagent required.[207,208] They can also be oxidized to form disulfide bridges.

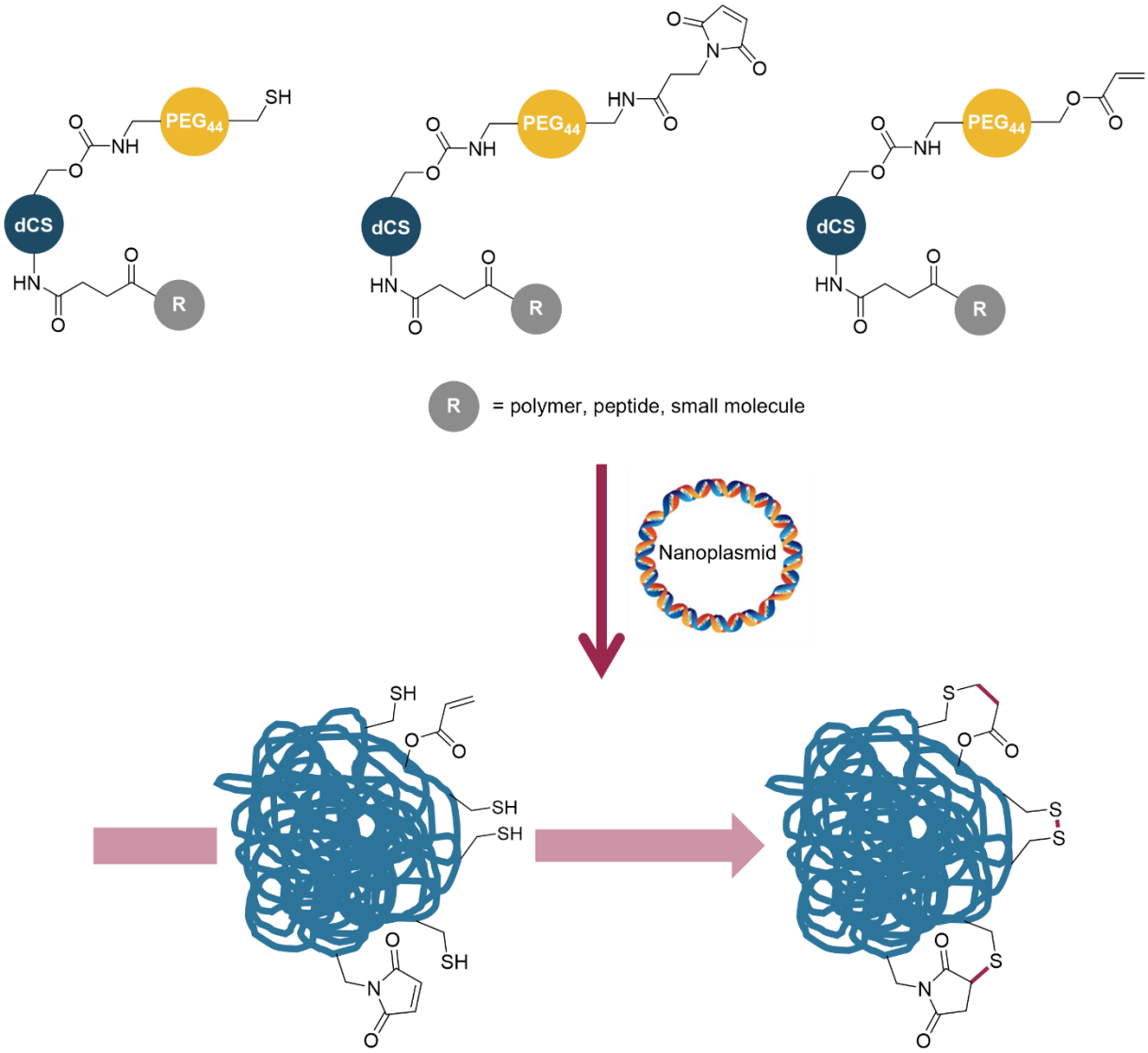

Figure 21. Cross-linking strategy with dCS-NSuc-R-OPEG$_{44}$-X derivatives (R = polymer, peptide, small molecule; X = –SH, –Mal or –Acr). Two types (or more) of the synthesized derivatives would be mixed to the Nanoplasmid™ to form binary complexes (**dCS** derivatives/DNA). Cross-linking of the different reactive moieties (–SH, –Mal or –Acr) should occur during NPs formation.

Therefore, the grafting of **dCS** to amino-PEG$_{44}$-thiol (HCl.H$_2$N-PEG$_{44}$-SH), amino-PEG$_{44}$-maleimide

(H_2N-PEG_{44}-Mal) and amino-PEG_{44}-acrylate (H_2N-PEG_{44}-Acr) was investigated (Figure 22). The primary amines of **dCS** being functionalized with BPEI or LPEI, we aimed at functionalizing the hydroxyl groups of **dCS** through carbamate linkages that would ensure sufficient stability of the resulting polymer in physiological conditions.

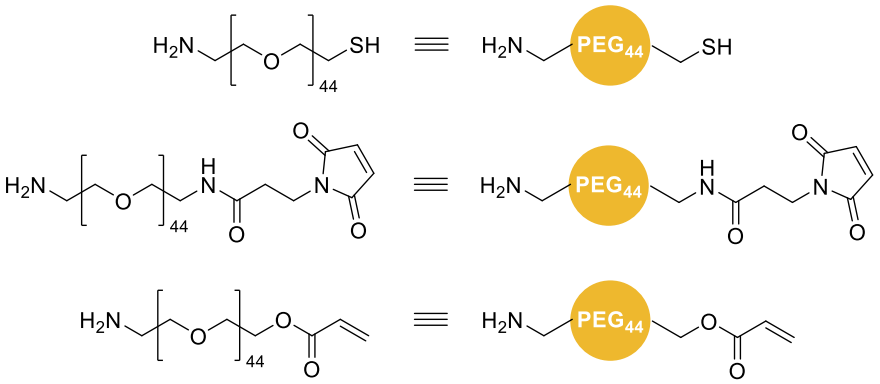

Figure 22. Simplified structures of H_2N-PEG_{44}-SH (top), H_2N-PEG_{44}-Mal (middle) and H_2N-PEG_{44}-Acr (bottom).

3.2.3.1. Functionalization with amino-PEG_{44}-thiol

In a first approach, only the grafting of HCl.H_2N-PEG_{44}-SH was attempted on **dCS**. **dCS-NSuc-BPEI-OPEG$_{44}$-SH** and **dCS-NSuc-LPEI-OPEG$_{44}$-SH** were synthesized following two sequences, either grafting PEG to **dCS-NSuc** followed by conjugation to LPEI/BPEI or the other way around (Scheme 7). These syntheses were not necessarily performed with the optimized conditions developed for **dCS-NSuc-BPEI** and **dCS-NSuc-LPEI**.

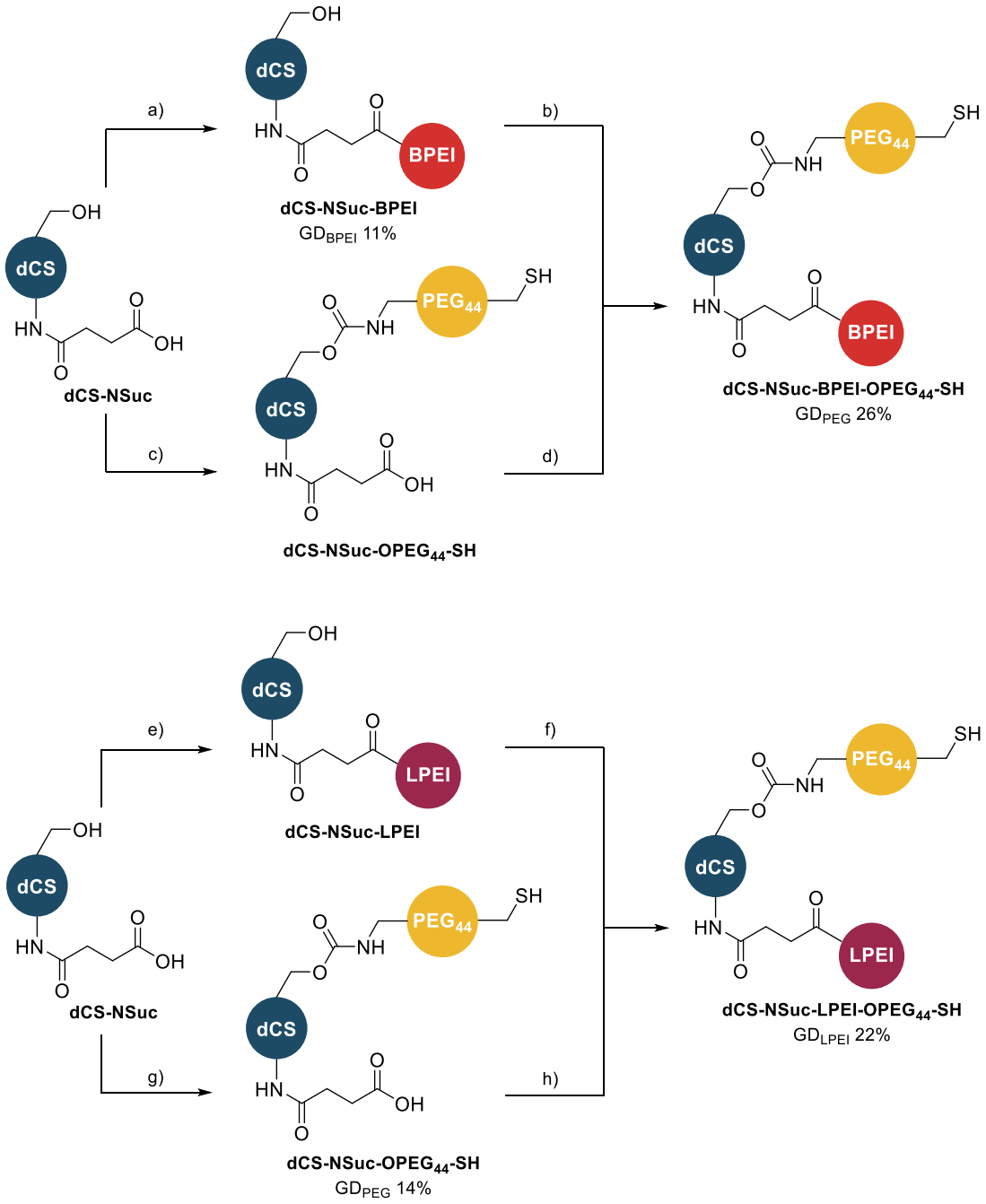

Scheme 7. Dual orthogonal functionalization of **dCS-NSuc** with HCl.H_2N-PEG$_{44}$-SH and BPEI/LPEI *via* different routes. a) DMTMM, DIPEA, BPEI, H_2O, rt, 3 h. b) CDI, HCl.H_2N-PEG$_{44}$-SH, DMSO, rt, 19 h. c) CDI, HCl.H_2N-PEG$_{44}$-SH, DMSO, rt, 16 h. d) DMTMM, BPEI, H_2O, rt, 3 h. e) DMTMM, DIPEA, LPEI, H_2O, 60 °C, 3 h. f) CDI, HCl.H_2N-PEG$_{44}$-SH, DMSO, rt, 17 h. g) CDI, DIPEA, HCl.H_2N-PEG$_{44}$-SH, DMSO, rt, 17 h. h) DMTMM, DIPEA, LPEI, H_2O, 60 °C, 3 h.

Interestingly, the optimal pathway varied depending on the nature of PEI (Table 5). For BPEI-based systems, the desired product was obtained by first grafting BPEI to **dCS-NSuc** then grafting HCl.H_2N-PEG$_{44}$-SH. On the contrary, **dCS-NSuc-LPEI-OPEG$_{44}$-SH** could be produced solely by first grafting HCl.H_2N-PEG$_{44}$-SH then LPEI (Scheme 7). When the PEG$_{44}$ chain was grafted in the first step, the challenge was then to functionalize in a second step the succinyl moieties, in spite of their hindered environment. Because of its branched character, BPEI is bulkier than LPEI, thus disfavoring the formation of a covalent bond with the activated **dCS-NSuc**. This was illustrated by the different results

observed between entries 2 and 4 in Table 5: only a small fraction of BPEI was grafted on **dCS-NSuc-OPEG$_{44}$-SH** whereas this sequence was the most efficient for LPEI.

Table 5. Selection of the optimal pathways for the functionalization of **dCS** backbone with HCl.H$_2$N-PEG$_{44}$-SH and BPEI/LPEI.

Derivatives	Functionalization sequence (steps)	Results	Grafting degrees (%)
dCS-NSuc-BPEI-OPEG$_{44}$-SH	1 – BPEI 2 – PEG$_{44}$	Covalent dual grafting	Suc: 47 BPEI: 11 PEG$_{44}$: 26
	1 – PEG$_{44}$ 2 – BPEI	Mixture of covalent and non-covalent conjugates	Suc: 45 PEG$_{44}$: 28 BPEI: -
dCS-NSuc-LPEI-OPEG$_{44}$-SH	1 – LPEI 2 – PEG$_{44}$	Mixture of covalent and non-covalent conjugates	Suc: 43 LPEI: 8 PEG$_{44}$: -
	1 – PEG$_{44}$ 2 – LPEI	Covalent dual grafting	Suc: 44 PEG$_{44}$: 14 LPEI: 22

Similarly, for entries 1 and 3, the hindrance of **dCS-NSuc-LPEI** and **dCS-NSuc-BPEI** and the inherent lower reactivity of hydroxyl groups compared to amines, might have hampered the conjugation of HCl.H$_2$N-PEG$_{44}$-SH (Table 5). The grafting was nonetheless successful on **dCS-NSuc-BPEI**, while only trace amounts of **dCS-NSuc-LPEI-OPEG$_{44}$-SH** were obtained. We suspected that the primary amines of BPEI were actually also activated with CDI. The activation of those amines most probably favored the grafting of HCl.H$_2$N-PEG$_{44}$-SH on BPEI, in particular because they were more accessible than hydroxyl groups (Figure 23).

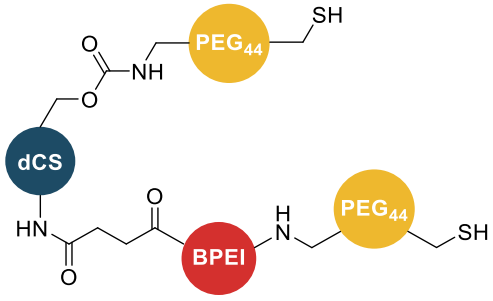

Figure 23. Alternative structure for **dCS-NSuc-BPEI-OPEG$_{44}$-SH**.

In conclusion, the functionalization of **dCS-NSuc** first with the PEG$_{44}$ fragment, then the PEI component was selected as the optimal pathway to ensure formation of the desired product.

3.2.3.2. Functionalization with amino-PEG$_{44}$-maleimide and amino-PEG$_{44}$-acrylate

Following the successful preparation of **dCS** derivatives with amino-PEG$_{44}$-thiol, our synthetic efforts focused on the preparation of **dCS-NSuc-OPEG$_{44}$-Mal** and **dCS-NSuc-OPEG$_{44}$-Acr** in order to later functionalize them with PEI polymers.

The synthesis of **dCS-NSuc-OPEG$_{44}$-Mal** was inspired from the procedure developed for **dCS-NSuc-OPEG$_{44}$-SH** and slightly optimized (Scheme 8). The thorough analysis of these batches by ^{1}H and 2D-

DOSY NMR techniques, demonstrated the presence of both grafted and free PEG_{44} fragments with **dCS-NSuc**. Additional dialysis to remove excessive PEG_{44} trapped in the polymeric network was not conclusive.

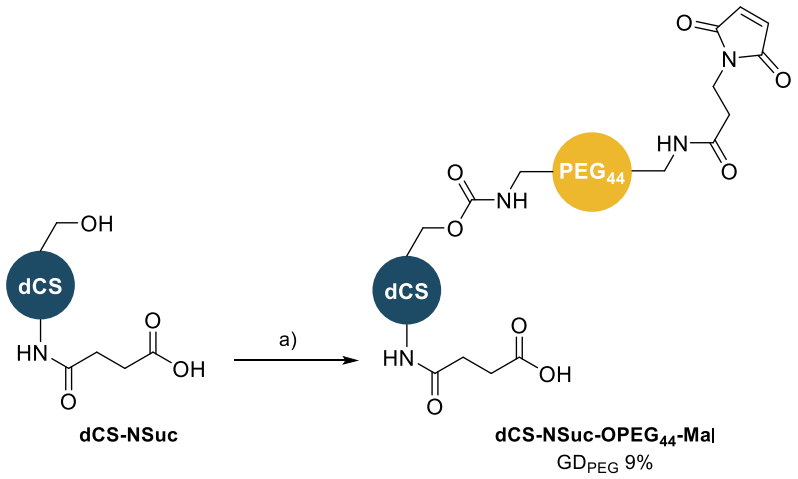

Scheme 8. Synthesis of **dCS-NSuc-OPEG$_{44}$-Mal**. a) CDI, DIPEA, H_2N-PEG_{44}-Mal, DMSO, rt, 2 h.

Moreover, GD_{PEG} was not reproducible over different batches. For some batches, partial or complete degradation of the maleimide functionality was also observed. This was not related to a problem of stability from H_2N-PEG_{44}-Mal, implying the action of undetermined factors.

A similar procedure was tested for H_2N-PEG_{44}-Acr (Scheme 9). 2D-DOSY NMR analyses of the resulting batches showed that H_2N-PEG_{44}-Acr mainly formed non-covalent interactions with **dCS-NSuc** and only trace amounts of desired product were present in the sample.

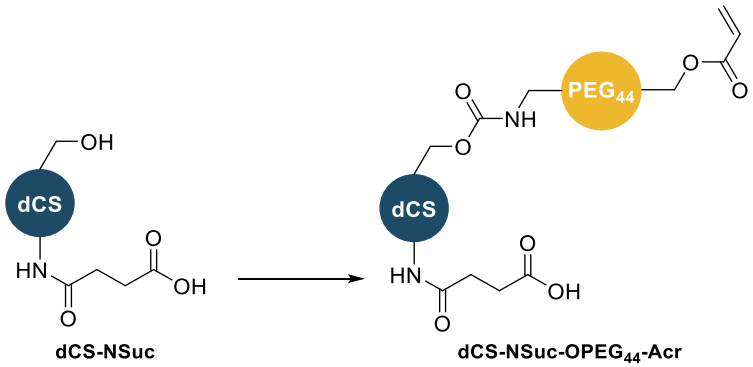

Scheme 9. Synthesis of **dCS-NSuc-OPEG$_{44}$-Acr**. a) CDI, base, H_2N-PEG_{44}-Acr, DMSO, rt, 2 h.

Hydroxyls being less nucleophile than amines, we looked for strategies to increase their reactivity towards CDI. Bases stronger than DIPEA such as 1,8-diazabicyclo(5.4.0)undec-7-ene (DBU), sodium hydride and potassium *tert*-butoxide were consequently tested (Scheme 9). Using up to 5 equivalents of base and screening conditions for the activation time of CDI and its number of equivalents, several batches were produced and analyzed. Despite a wide screening, none of these conditions led to covalent **dCS-NSuc-OPEG$_{44}$-Acr**.

3.2.3.3. Biological assessment

As the synthesis of **dCS-NSuc-OPEG$_{44}$-Acr** and **dCS-NSuc-OPEG$_{44}$-Mal** was not successful, only **dCS-NSuc-BPEI-OPEG$_{44}$-SH** and **dCS-NSuc-LPEI-OPEG$_{44}$-SH** were assessed *in vitro*. Being both soluble in water (> 10 mg/mL), they were used to form NPs with two different Nanoplasmids™ (n.CAGLuc2 and n.CAG.GFP1). These experiments were performed by Jens Casper (University of Basel). Their physico-chemical characteristics and *in vitro* assessment are presented in Table 6.

Table 6. Physico-chemical characterization and *in vitro* assessment of dCS derivatives functionalized with BPEI/LPEI and H_2N-PEG_{44}-SH.

Polymers	c/p ratio at optimal colloidal stability[1]	ζ-potential (mV)[2]	Hydrodynamic diameter (nm)[2]	PDI[2]	Luc x GFP normalized to dCS c/p 32 (fold)[3]	MTS (% viable cells)[4]
dCS	32	22 ± 4	68 ± 5	0.23 ± 0.03	1 ± 1	111 ± 5
dCS-NSuc-LPEI	2	23 ± 1	87 ± 1	0.16 ± 0.01	71'567 ± 1592	101 ± 9
dCS-NSuc-BPEI-OPEG$_{44}$-SH	2	13 ± 1	121 ± 1	0.21 ± 0.01	0 ± 0	91 ± 2
dCS-NSuc-LPEI-OPEG$_{44}$-SH	2	18 ± 1	85 ± 1	0.17 ± 0.01	0 ± 0	91 ± 1

[1]DNA loading degree is defined by the c/p value (ratio **dCS** derivative/DNA; w/w). Polyplex stability was determined by gel retardation assay (data not shown). The optimized colloidal stability defined the c/p ratio that was used later *in vitro*. [2]ζ-potential was determined by electrophoretic light scattering, and hydrodynamic diameter and PDI were determined by DLS. A complex with a PDI equal or below 0.2 was considered to be monodisperse. [3]The *in vitro* gene expression was determined in HuH-7 cells using two reporter genes (n.CAGLuc2 and n.CAG.GFP1). Their transfection values were merged to give a complementary overview. [4]Cytotoxicity was assessed using a MTS assay. Values are means ± SD, n ≥ 3.

Binary complexes based on **dCS-NSuc-BPEI-OPEG$_{44}$-SH** and **dCS-NSuc-LPEI-OPEG$_{44}$-SH** displayed similarities with **dCS-NSuc-LPEI** regarding optimal c/p ratio and PDI. As expected, the conjugation of H_2N-PEG_{44}-SH on **dCS-NSuc-BPEI** and **dCS-NSuc-LPEI** systems decreased the ζ-potential whereas the NPs had a similar or slightly bigger in size. Unexpectedly, their toxicity was higher than for **dCS-NSuc-LPEI**. More importantly, the transfection efficiency was completely lost for PEG_{44}-based derivatives (Table 6). This result might be linked to the final polymeric structure that brought PEG_{44} and PEI components too close to each other with fewer degrees of freedom: the proper DNA condensation by PEI polymers was hampered by the presence of the PEG_{44} component, which in turn did not efficiently shield the cationic charges. Therefore, this strategy was not appropriate and abandoned.

3.2.4. Conclusions

In summary, we developed a robust strategy to produce on large scales covalent assemblies of **dCS** and PEI, using a succinyl linker. The first *in vitro* studies demonstrated the higher potential of **dCS-NSuc-LPEI** for gene delivery. In order to improve the cell viability and shielding of this delivery vehicle, the grafting of heterobifunctional PEGs with cross-linking moieties was attempted on both **dCS-NSuc-BPEI** and **dCS-NSuc-LPEI**. While the functionalization was successful with HCl.H_2N-PEG_{44}-SH, mitigated results were obtained with H_2N-PEG_{44}-Mal. Regarding H_2N-PEG_{44}-Acr grafting, the desired product could not be obtained, despite a large screening of conditions. As the biological assessment of **dCS-NSuc-**

BPEI-OPEG$_{44}$-SH and **dCS-NSuc-BPEI-OPEG$_{44}$-SH** was not conclusive, this cross-linking strategy was put aside. The polyplex based on **dCS-NSuc-LPEI** being the most promising overall, we decided to rather investigate a core-shell strategy that would bring additional features around the polymeric core while maintaining proper DNA condensation.

3.3. Core-shell ternary complexes

The notion of core-shell complexes based on **dCS** is introduced in this subchapter. The focus is first made on the synthesis of shell polymers containing CPPs. Based on the physico-chemical characterization of those new systems, an optimized shell polymer was designed and synthesized. It was further used for the formation of core-shell ternary complexes.

3.3.1. Introduction on the core-shell complex

Based on the *in vitro* and *in vivo* experiments performed in section 3.2, **dCS-NSuc-LPEI** fulfilled several of the key standard criteria required for a gene delivery vehicle: efficient DNA condensation, low cytotoxicity, and efficient transfection and expression of the reporter gene.

This core system could benefit from the addition of other features such as shielding from blood components, cell-penetration, or targeting ability. We thus aimed at forming an additional layer containing those components. These new derivatives would "cap" the **dCS-NSuc-LPEI**/DNA polyplex (Figure 24). The binary complex was defined as the *core* system, and the resulting ternary complex (shell polymer/core polymer/DNA) as the *core-shell* system.

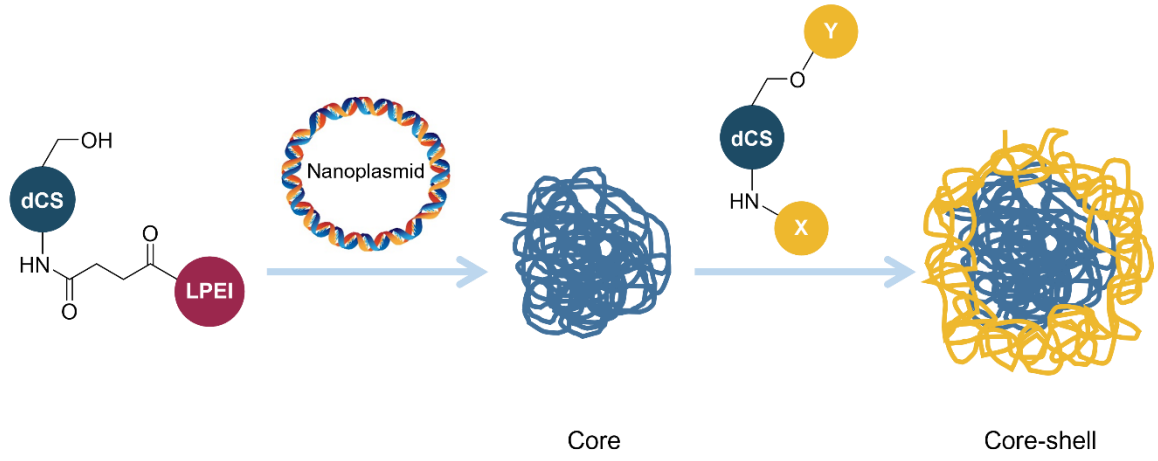

Figure 24. Formation of a core-shell system based on **dCS** derivatives. First, **dCS-NSuc-LPEI** would be mixed to the Nanoplasmid™ to form the core system (blue). Then, a second **dCS** derivative displaying additional properties such as cell-penetration enhancement, cell targeting, or shielding effect (represented by X and Y groups) would be added to the core system. This would form a shell around it, thus leading to a *core-shell* polyplex (blue-yellow).

3.3.2. Grafting of CPPs on dCS

As presented in Chapter 1, CPPs are small peptidic sequences that can favor the cellular uptake of their cargo thanks to their translocation properties. In order to increase the cell penetration of the core complex, the grafting of cationic CPPs to **dCS** backbone was investigated. Perrine Robin (MSc student) contributed to this study.

Being part of the cationic CPPs class, Arg_8 and a TAT-derived peptide were selected for such purpose (Figure 25). Two peptides from the TAT family were tested: the first peptide was terminated by a methyl ester (TAT-OMe) instead of a free carboxylic acid, in order to prevent its cyclization or oligomerization (Figure 25). The grafting of the second peptide (TAT-Cys) was meant to rely on thiol-maleimide click-chemistry thanks to its terminal cysteine residue (Figure 25).

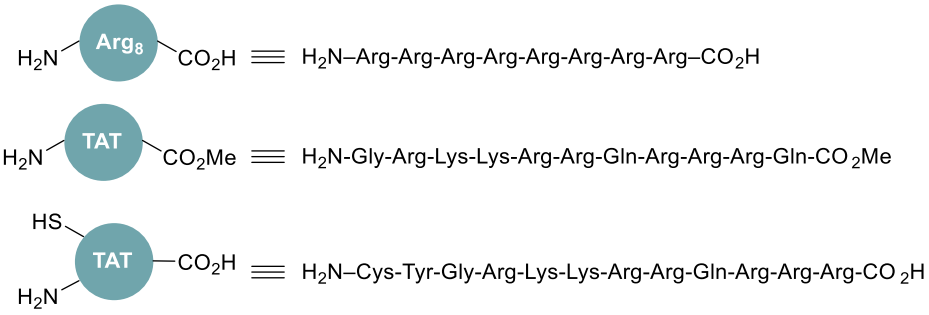

Figure 25. Amino acids sequences of Arg_8, TAT-OMe and TAT-Cys peptides.

Those peptides being quite expensive, we first optimized the grafting to **dCS-NSuc** with a model amino acid before grafting the full-length peptide.

3.3.2.1. Synthesis of dCS-NSuc-Arg_8

As model reaction, L-arginine methyl ester grafting to **dCS-NSuc** was performed with the water-soluble coupling agent DMTMM and led to amide bond formation with a GD_{Arg} of 10% (Scheme 10).

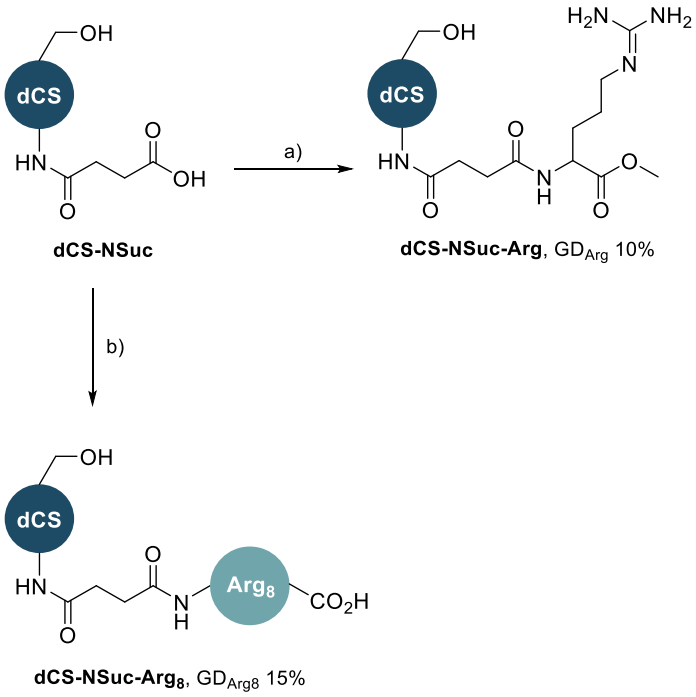

Scheme 10. Synthesis of **dCS-NSuc-Arg_8**: model reaction and full-length peptide conjugation. a) DMTMM, DIPEA, L-arginine methyl ester, H_2O, rt, 24 h. b) DMTMM, DIPEA, Arg_8 (in 4 portions every 10 min), H_2O, rt, 24 h.

This reaction was repeated in the presence of Arg_8 (Scheme 10). To overcome the potential oligomerization or cyclization of Arg_8, the peptide was added in 4 portions to a solution of activated **dCS-NSuc**. The amount of Arg_8 being in default compared to **dCS-NSuc** quantities, the grafting of the peptide

was favored. **dCS-NSuc-Arg$_8$** was successfully produced with a GD_{Arg8} of 15% (Scheme 10).

3.3.2.2. Synthesis of dCS-NSuc-TAT-OMe

In a similar fashion, we first grafted to **dCS-NSuc** glycine *tert*-butyl ester hydrochloride, to model the reaction with the terminal glycine residue of the full-length TAT-OMe peptide (Scheme 11). In this case, optimized conditions led to the desired product with a GD_{Gly} of 31%. The grafting of TAT-OMe was then performed following the same conditions and yielded **dCS-NSuc-TAT-OMe** with a $GD_{TAT\text{-}OMe}$ of 13% (Scheme 11).

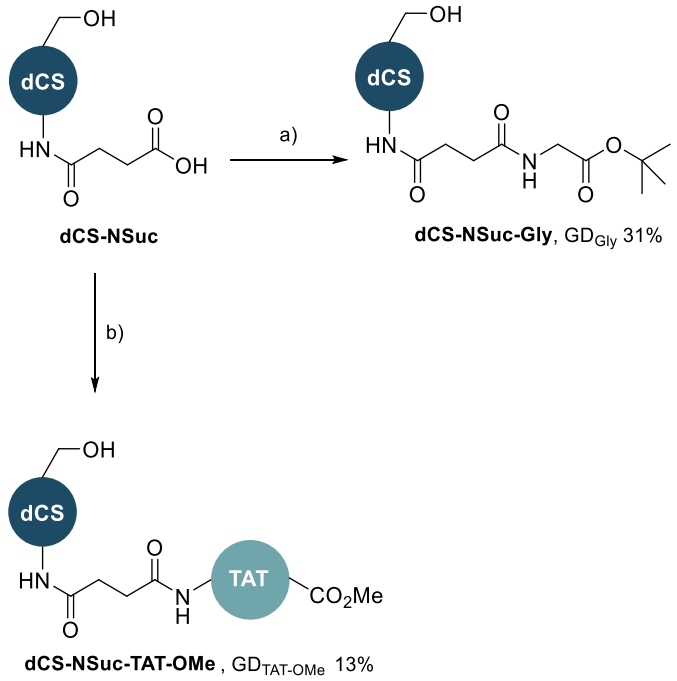

Scheme 11. Synthesis of **dCS-NSuc-TAT-OMe**: model reaction and full-length peptide conjugation. a) DMTMM, DIPEA, glycine *tert*-butyl ester hydrochloride, H_2O, rt, 16 h. b) DMTMM, DIPEA, TAT-OMe, H_2O, rt, 19 h.

Some cross-linking was however suspected between the different chains of **dCS-NSuc-TAT-OMe,** due to the presence of additional amino groups on the side chains of lysine and glutamine residues. The protection of the terminal carboxylic acid of TAT peptide only prevented its oligomerization or cyclization. As the cross-linking of **dCS-NSuc-TAT-OMe** chains might hamper the proper folding of the peptide in physiological conditions, a second derivative was developed.

3.3.2.3. Synthesis of dCS-NSuc-$OPEG_{44}$-Mal-Cys-TAT

The TAT-Cys peptide was grafted to **dCS-NSuc-OPEG$_{44}$-Mal** (GD_{PEG} 18%, synthesis detailed in section 3.2) through thiol-maleimide click chemistry, in order to circumvent the regioselectivity issues encountered with **dCS-NSuc-TAT-OMe.** (Scheme 12).

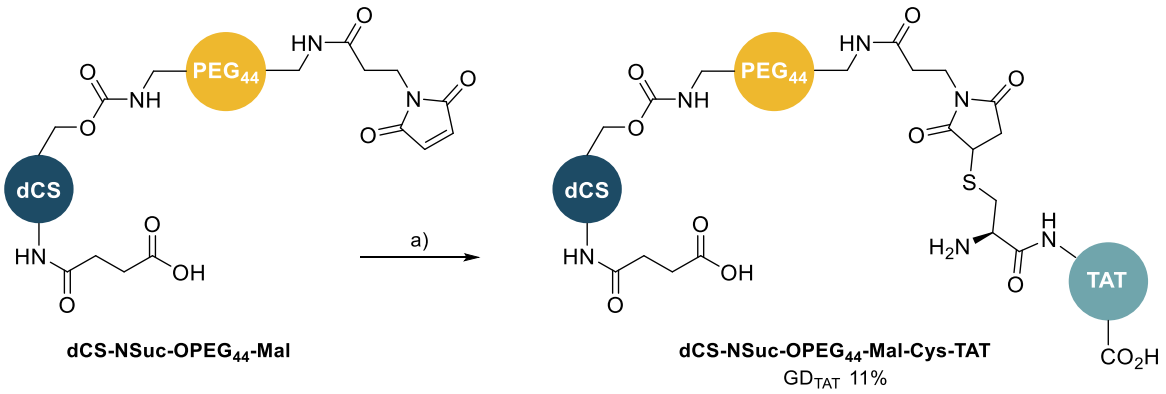

Scheme 12. Thiol-maleimide click reaction between **dCS-NSuc-OPEG$_{44}$-Mal** and TAT-Cys. a) TAT-Cys, H_2O, rt, 3 h.

Upon simple mixing of the two reactants in distilled water, spontaneous 1,4-addition led to the formation of **dCS-NSuc-OPEG$_{44}$-Mal-Cys-TAT** with a GD_{TAT} approximating 11% (Scheme 12). Compared to TAT-OMe, this conjugation strategy was expected to lead to higher cell-penetration as it ensured the proper folding of TAT-Cys in physiological medium. In addition, the presence of PEG_{44} chains might bring an additional shielding effect to the core-shell structure.

3.3.2.4. Physico-chemical characterization of dCS-CPP derivatives

These derivatives were then used to "cap" the binary complex **dCS-NSuc-LPEI**/DNA. The experiments were performed by Jens Casper (University of Basel). The physico-chemical characterizations of **dCS-NSuc-Arg$_8$**, **dCS-NSuc-TAT-OMe** and **dCS-NSuc-OPEG$_{44}$-MAL-Cys-TAT** are presented in Table 7 and are compared to the values obtained for the binary complex alone.

Table 7. Physico-chemical characterization of core-shell structured ternary complexes with dCS-CPP derivatives.

Complex	Polymer	Hydrodynamic diameter (nm)[1]	PDI[1]	DNA encapsulation in H_2O (%)[2]	Stability[3]
Binary	**dCS-NSuc-LPEI**	87 ± 1	0.16 ± 0.01	78 ± 6	**yes**
Ternary	**dCS-NSuc-Arg$_8$**	182 ± 3	0.33 ± 0.03	71 ± 11	**no**
	dCS-NSuc-TAT-OMe	105 ± 1	0.21 ± 0.01	72 ± 1	**no**
	dCS-NSuc-OPEG$_{44}$-MAL-Cys-TAT	106 ± 1	0.18 ± 0.01	77 ± 1	**no**

DNA loading degree is defined by the c/p value (ratio **dCS** derivative/DNA; w/w). All values displayed refer to a core polymer/DNA c/p of 2 and to a shell polymer/DNA c/p of 1. Nanoplasmid™ used: n.CAGLuc2. [1]Hydrodynamic diameter and PDI were determined by DLS. A complex with a PDI equal or below 0.2 was considered to be monodisperse. [2]DNA encapsulation displays the nucleic acid fraction that was shielded by the polymers, and was determined with SYBR Gold staining. Values are means ± SD, n ≥ 3. [3]Polyplex stability was determined by gel retardation assay.

The general applicability of the three shell polymers was tested at c/p 1. Table 7 reports their influence on the properties of the final complex. As expected, the hydrodynamic diameters of ternary complexes were larger to that of the binary complex, but remained under the 200 nm threshold.[40] Except for **dCS-NSuc-Arg$_8$** which led to a PDI value of 0.33, the other systems were monodisperse.

Surprisingly, the DNA encapsulation of the three core-shell systems decreased compared to **dCS-NSuc-LPEI**.

Most importantly, the ternary complexes were not colloidally stable (Table 7). The stability of polyplexes was monitored by gel electrophoresis (Figure 26). A polymeric NP is usually considered stable when the DNA is immobilized on the gel baseline after its condensation by the polymer. This state was observed starting from c/p 4 for **dCS-NSuc-LPEI** (Figure 26a). Further optimization, as reported in Nicolle *et al.*,[204] allowed to lower this value to 2. For the core-shell systems, the stabilization of the NP with **dCS-NSuc-Arg$_8$** or with **dCS-NSuc-TAT-OMe** was however only observed at high c/p ratios which led to significant cytotoxicity (Figure 26b,c). Regarding **dCS-NSuc-OPEG$_{44}$-MAL-Cys-TAT**, the Nanoplasmid™ could not even be immobilized in the range of ratio tested (c/p: 0.1 to 64) (Figure 26d).

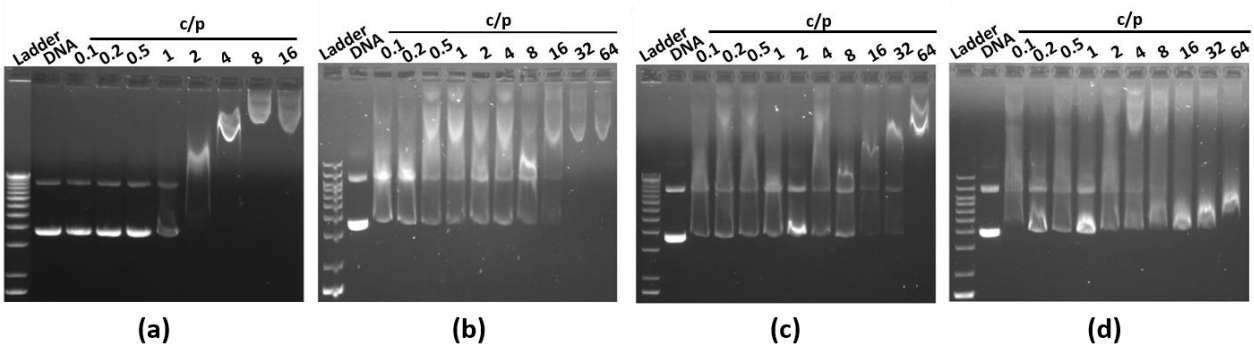

Figure 26. Gel electrophoreses of (a) the binary polyplex (c/p ratio varied from 0.1-16), and the ternary polyplexes using (b) **dCS-NSuc-Arg$_8$**, (c) **dCS-NSuc-TAT-OMe**, or (d) **dCS-NSuc-OPEG$_{44}$-MAL-Cys-TAT** as shell polymers. For the core-shell structures, the c/p ratio of core polymer/DNA was set at 2 and the c/p of shell polymer/DNA varied from 0.1-64. Naked Nanoplasmid™ was used as mobile control.

Figure 26 clearly proved that the addition of dCS-CPP systems to the core polyplex disrupted its colloidal stability, most probably due to positive charge repulsion between the core and shell polymers. Proper core-shell structures could not be obtained with cationic CPPs. Therefore, we intended to prepare a second-generation shell copolymer based on **dCS** grafted to a slightly negatively charged polymer, in order to favor electrostatic interactions with the core polyplex.

3.3.3. Towards a more negatively charged shell polymer

HOOC-PEG$_6$-COOtBu (6 ethylene glycol units) was selected for the grafting to **dCS** in order to introduce negative charges while better shielding the core complex (Figure 27). The resulting NPs were expected to display an enhanced colloidal stability which is essential for *in vivo* evaluation. The use of a low MW PEG aimed at limiting the size increase of the NPs.

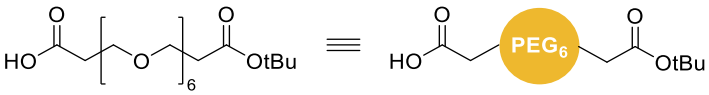

Figure 27. Simplified structure of HOOC-PEG$_6$-COOtBu.

3.3.3.1. Development, optimization and scale up of dCS-NPEG$_6$-COOH

HOOC-PEG$_6$-COOtBu and **dCS** were linked through amide bonds (Scheme 13). Several coupling agents were tested to produce the desired product (Table 8). Test reactions were run in DMSO unless stated

otherwise. The products were further analyzed by 2D-DOSY NMR to evaluate their covalent character.

Table 8. Screening of coupling agents for the synthesis of **dCS-NPEG$_6$-COOtBu**.

Entry	Coupling agents	2D-DOSY NMR results
1	EDC.HCl/NHS	Non-covalent
2	EDC.HCl	Covalent with traces of free PEG$_6$
3	EDC.HCl/HOBt	Covalent with traces of free PEG$_6$
4	DMTMM	Mixture of covalent and non-covalent PEG$_6$
5	DMTMM (solvent: H_2O)	Non-covalent

Following this initial screening, conditions described in entries 2 and 3 from Table 8 were repeated on a larger scale (40 mg) with a **dCS**/HOOC-PEG$_6$-COOtBu ratio of 1.25/1 to reach a higher GD$_{PEG}$. Subsequent deprotection of the *tert*-butyl ester with 3 M HCl (aq.) yielded the final product with GD$_{PEG}$ equal to 19 and 44% in presence of EDC.HCl and EDC.HCl/HOBt, respectively.

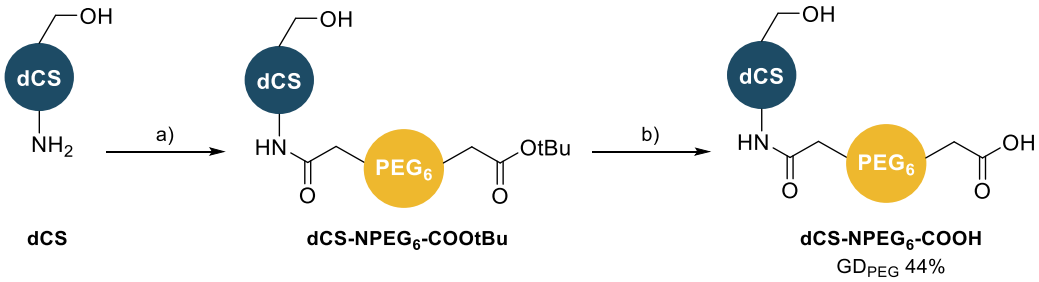

Scheme 13. Optimized two-steps synthetic pathway to prepare **dCS-NPEG$_6$-COOH**. a) HOOC-PEG$_6$-COOtBu, EDC.HCl, HOBt, DIPEA, DMAP, DMSO, rt, 17 h. b) 3 M HCl (aq), rt, 4.5 h.

Using EDC.HCl/HOBt as coupling agent system, this pathway was scaled up to 300 mg of starting **dCS**. **dCS**/HOOC-PEG$_6$-COOtBu ratio was optimized at 2/1 and provided similar GD$_{PEG}$ compared to test scale conditions (Scheme 13). From the same batch of starting **dCS**, several batches of **dCS-NPEG$_6$-COOH** were produced with very similar GD$_{PEG}$ (between 43 to 45% each time), showing great reproducibility. However, we noticed that this degree varied from one batch of **dCS** to another, with final values of GD$_{PEG}$ ranging from 36 to 48%. This highlighted the strong impact of **dCS** source on downstream functionalization procedures.

3.3.3.2. *In vitro* evaluation of the resulting core-shell ternary complex

dCS-NPEG$_6$-COOH was then used as shell polymer on core-shell structured NPs. Their characterization was performed by Jens Casper (University of Basel), and the results are reported in Table 9.

Table 9. Physico-chemical characterization of **dCS-NPEG$_6$-COOH** and comparison to the binary complex.

Complex	Hydrodynamic diameter (nm)[1]	PDI[1]	DNA encapsulation in H_2O (%)[2]	Stability[3]
Binary	87 ± 1	0.16 ± 0.01	78 ± 6	**yes**
Ternary	122 ± 1	0.22 ± 0.01	85 ± 1	**yes**

DNA loading degree is defined by the c/p value (ratio **dCS** derivative/DNA; w/w). All values displayed refer to a core polymer/DNA c/p of 2 and to a shell polymer/DNA c/p of 1. Nanoplasmid™ used: n.CAGLuc2. [1]Hydrodynamic diameter and PDI were determined by DLS. A complex with a PDI equal or below 0.2 was considered to be

monodisperse. [2]DNA encapsulation displays the nucleic acid fraction that was shielded by the polymers and was determined by SYBR Gold staining. Values are means ± SD, n ≥ 3. [3]Polyplex stability was determined by gel retardation assay.

A moderate increase of the hydrodynamic diameter was observed for the ternary complex and its PDI value close to 0.2 confirmed the formation of monodisperse NPs. In this case, DNA encapsulation was slightly increased as compared to the binary complex (Table 9). Most importantly, the ternary complex displayed a sufficient colloidal stability to be selected for further tests *in vitro*. Formation of stable NPs was indeed observed from c/p 0.5 (shell polymer/DNA; Figure 28). To ensure an efficient shielding of the core, a ratio shell/core/DNA (w/w) of 1/2/1 was set for further analyses.

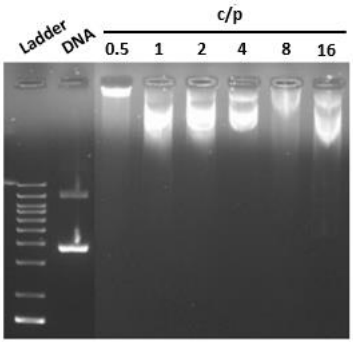

Figure 28. Gel electrophoresis of the core-shell complex based on **dCS-NPEG$_6$-COOH** as shell polymer. c/p ratio of core polymer/DNA was set at 2/1 and c/p of shell polymer/DNA varied from 0.5-16. Naked Nanoplasmid™ was used as mobile control.

In order to confirm particle integrity following formation of core-shell structures, binary and ternary complexes were visualized by cryo-transmission electron microscopy (Figure 29). For both type of NPs, polmyers seemed to be wrapped around the DNA, leading to a circular "donut-shaped" structure.

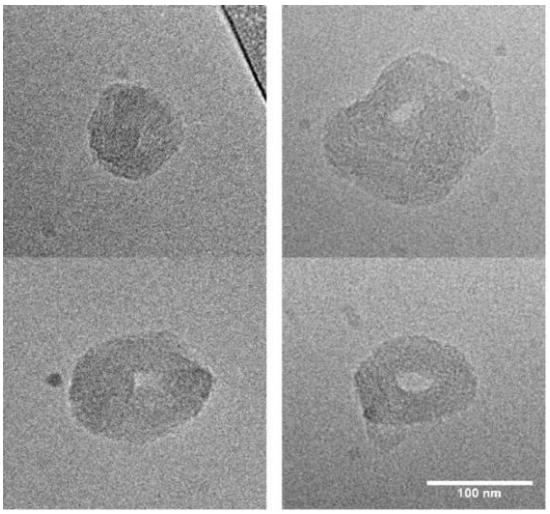

Figure 29. Transmission electron microscopy images of binary (left) and ternary (right) complexes (shell/core/DNA ratio 0/2/1 for binary and 1/2/1 for ternary complexes, scale bar: 100 nm).

In vitro evaluation of the core-shell complex based on **dCS-NPEG$_6$-COOH** aimed at comparing its transfection efficiency and cell viability to the naked core system. The results of these experiments performed by Jens Casper (University of Basel) are illustrated in Figure 30.

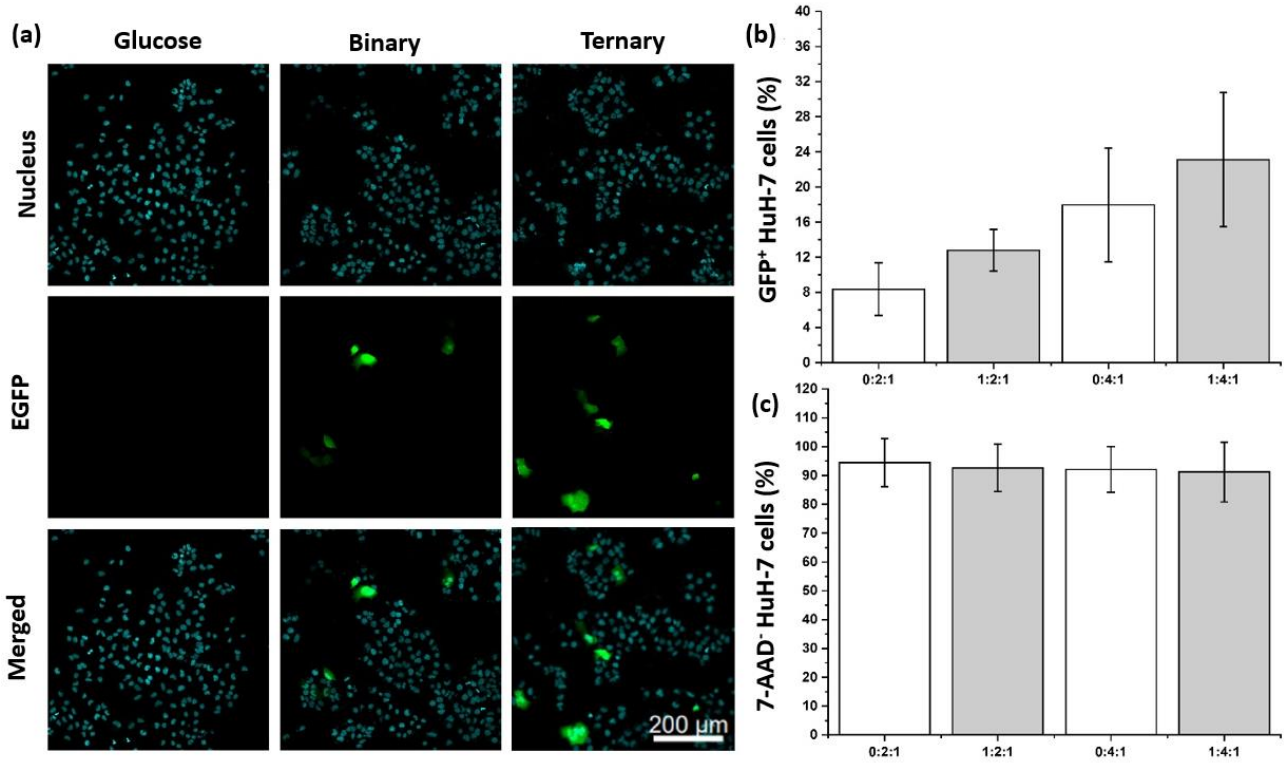

Figure 30. *In vitro* evaluation of toxicity and transfection efficiency of the core-shell system in HuH-7 cells. (a) Qualitative assessment of the transfection efficiencies of binary and ternary complexes by confocal microscopy. Left panels: untreated cells. Nuclei were stained with Hoechst 33342 (turquoise). Middle panels: Binary polyplexes loaded with Nanoplasmid™ n.CAG.GFP1 with a ratio shell/core/DNA of 0:2:1. Presence of EGFP (green). Right panels: Ternary polyplexes loaded with Nanoplasmid™ n.CAG.GFP1 with a ratio shell/core/DNA of 1:2:1. Presence of EGFP (green). Scale bar: 200 µm. In panels (b-c), the x axes represent the ratio shell/core/DNA used to prepare the ternary polyplexes. (b) Transfection efficiency quantified by flow cytometry of GFP-positive cells. (c) Cell viability assessed by 7-aminoactinomycin D (7-AAD) staining. Values are means ± SD, n ≥ 3. Statistical significance was determined by using one-way ANOVA, *** $p < 0.05$.

Based on EGFP fluorescence, efficient transfection of HuH-7 cells was observed for both binary and ternary polyplexes (Figure 30a). As measured by flow cytometry (Figure 30b), the core-shell complex led to the highest transfection efficiency. This was verified for c/p ratios 2 and 4 of the core complex, while keeping the c/p of shell polymer/DNA at 1. In addition, the cell viability was not affected by the presence of the shell polymer (Figure 30c). Contrary to the first covalent systems based on PEG_{44} fragments (*cf.* section 3.2), these new polyplexes maintained a low toxicity, while leading to higher transfection efficiencies than the binary complex (Figure 30b).

3.3.4. Fluorescent imaging of dCS derivatives

To investigate the fate of **dCS**-based delivery vehicles upon *in vitro* or *in vivo* administrations, two fluorescent **dCS** derivatives were synthesized from the commercially available Alexa Fluor 647-NHS ester (Scheme 15). This fluorophore was chosen for its emission in the far-red range (665 nm). The final aim of this project being the injection of **dCS**-based polyplexes into the liver, the use of a fluorophore emitting in the red or far-red range was required to avoid possible interferences with the natural autofluorescence of this organ (excitation between 280 and 470 nm).[209]

In a first approach, we envisioned to functionalize **dCS-NPEG$_{44}$-NH$_2$** with the Alexa Fluor 647-NHS

ester. **dCS-NPEG$_{44}$-NH$_2$** was a potential shell polymer prepared in two steps (Scheme 14).

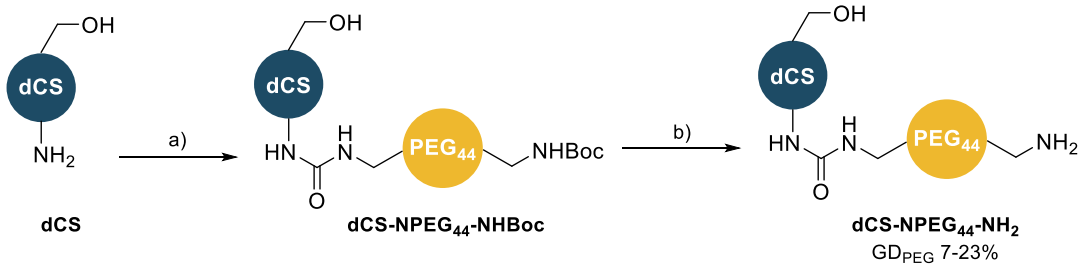

Scheme 14. Synthesis of **dCS-NPEG$_{44}$-NH$_2$**. a) CDI, DIPEA, HCl.H$_2$N-PEG$_{44}$-NHBoc, DMSO, rt, 16 h. b) 3 M HCl (aq.), rt, 45 min.

Following its activation with CDI, **dCS** was conjugated to H$_2$N-PEG$_{44}$-NHBoc overnight. The resulting polymeric derivative was deprotected using a 3 M HCl aqueous solution, leading to **dCS-NPEG$_{44}$-NH$_2$** with an optimized GD$_{PEG}$ of 23% (Scheme 14). To avoid photobleaching of the fluorophore, the conjugation of Alexa Fluor 647-NHS ester (2 mol%) to **dCS-NPEG$_{44}$-NH$_2$** was performed under dark conditions, and led to **dCS-NPEG$_{44}$-AlexaF647** with a maximum GD$_{AlexaF647}$ of 2% (Scheme 15).

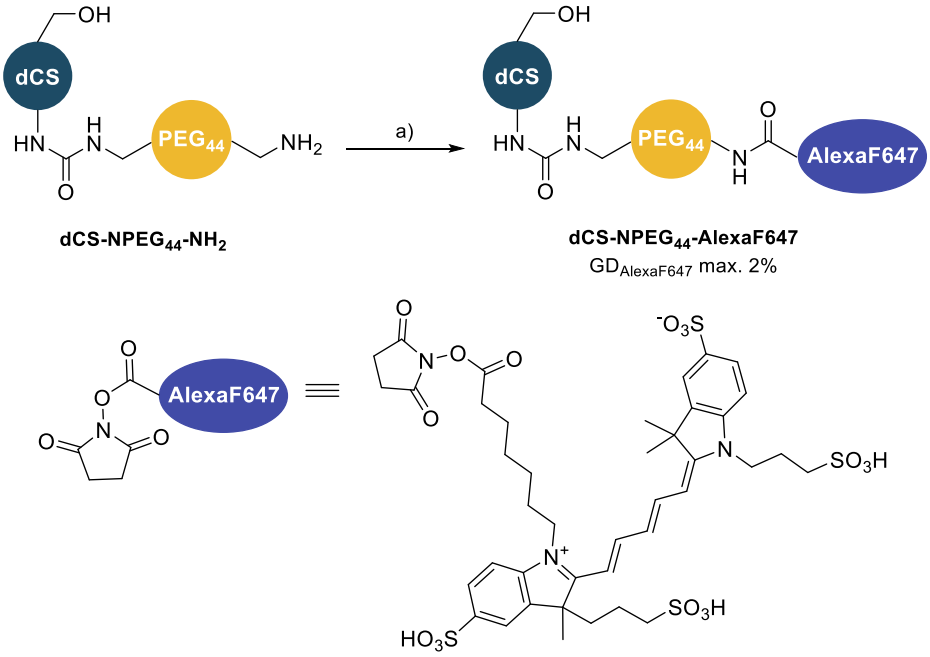

Scheme 15. Preparation of **dCS-NPEG$_{44}$-AlexaF647**. a) Alexa Fluor 647-NHS ester, Et$_3$N, *in the dark*, rt, 22 h.

The evaluation of this shell polymer unfortunately did not lead to stable NPs (University of Basel). We therefore turned to another fluorescent system based on direct conjugation to **dCS-NSuc-LPEI**.

Thanks to the numerous secondary amines of LPEI, we could successfully tag **dCS-NSuc-LPEI** with Alexa Fluor 647-NHS ester (3 mol%), yielding to **dCS-NSuc-LPEI-AlexaF647** with a maximum GD$_{AlexaF647}$ of 3% (Scheme 16).

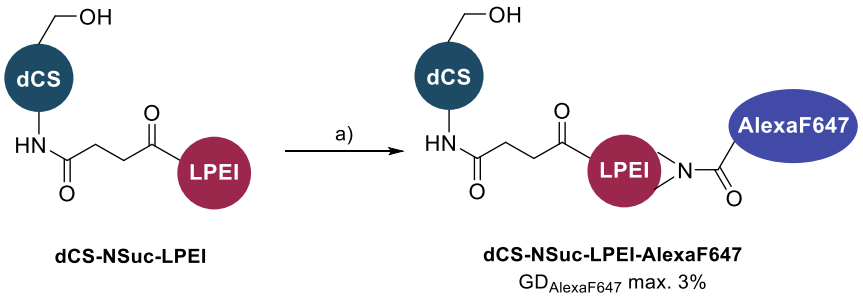

dCS-NSuc-LPEI

dCS-NSuc-LPEI-AlexaF647
$GD_{AlexaF647}$ max. 3%

Scheme 16. Synthesis of **dCS-NSuc-LPEI-AlexaF647**. a) Alexa Fluor 647-NHS ester, *in the dark*, pH 8, rt, 22 h.

During *in vitro* evaluation, a mixture of 1/5 **dCS-NSuc-LPEI-AlexaF647/dCS-NSuc-LPEI** was found to successfully condense Cyanine 3-tagged n.CAG.GFP1 Nanoplasmid™ (Cy3-DNA). The resulting fluorescent binary and ternary complexes were imaged *via* confocal microscopy to study their cellular uptake in HuH-7 cells (Figure 31a). Both binary and ternary polyplexes showed colocalized signals for Cy3-DNA and **dCS-NSuc-LPEI-AlexaF647**, resulting in a pink color on the "Merged" panels (bottom panels).

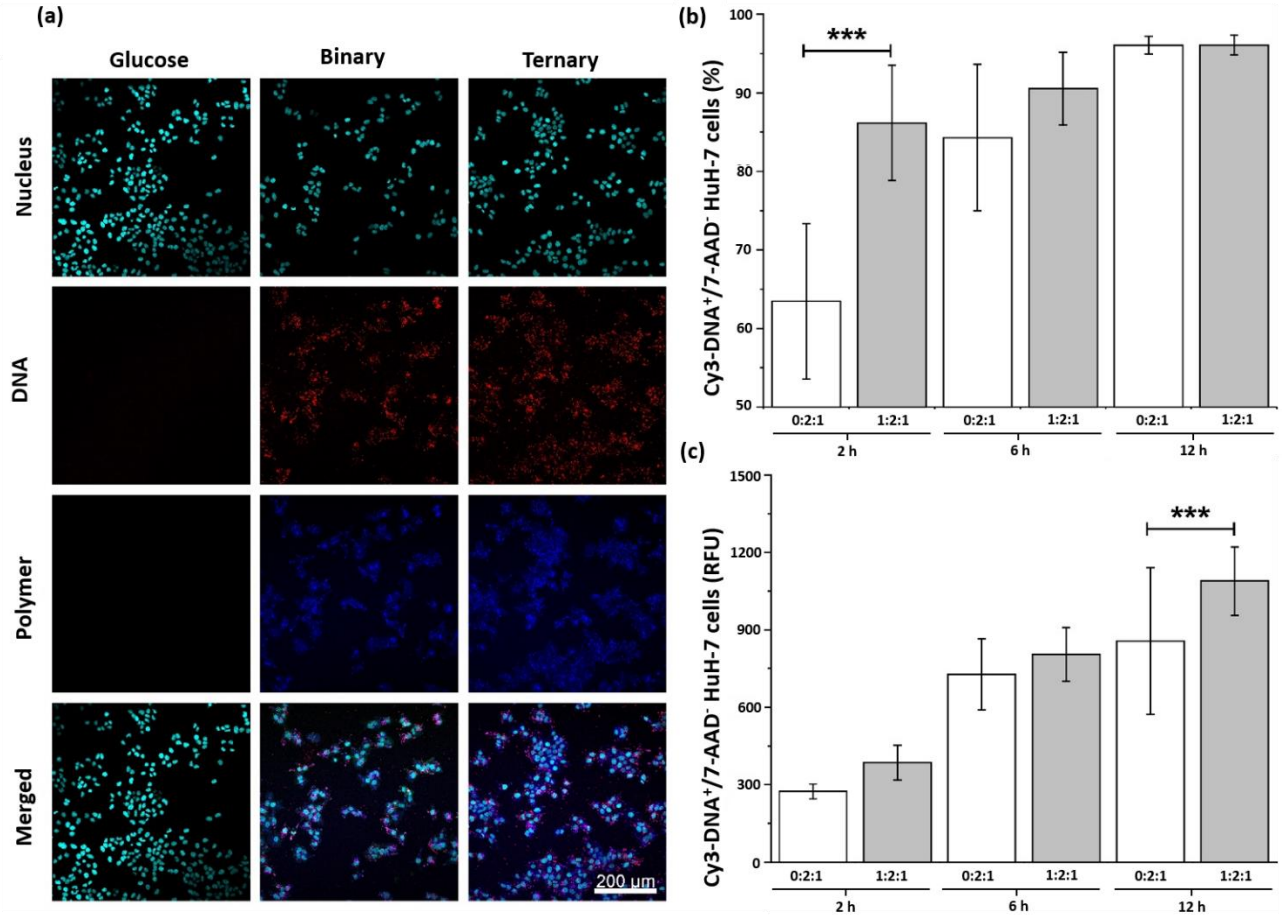

Figure 31. Cellular uptake of binary and ternary complexes in HuH-7 cells. (a) Qualitative assessment after 2 h of incubation of Huh-7 cells with the polyplexes using confocal laser scanning microscopy. Left panels: untreated control cells. Nuclei were stained with Hoechst 33342 (turquoise). Middle panels: Presence of cyanine 3-tagged n.CAG.GFP1 Nanoplasmid™ (Cy3-DNA, red) and **dCS-NSuc-LPEI-AlexaF647** (blue) 2 h after incubation with the binary complexes. Right panels: Presence of Cy3-DNA (red) and **dCS-NSuc-LPEI-AlexaF647** (blue) 2 h after incubation with the ternary complexes. Scale bar: 200 µm. (b-c) *In vitro* quantitative assessment of cellular uptake of Cy3-DNA after 2, 6 and 12 hours. The ratio shell/core/DNA of polyplexes used are displayed along the x axes.

(b) Estimation of the percentage of viable cells containing Cy3-DNA. Cell viability previously assessed using 7-AAD staining. (c) Fluorescence intensity of Cy3-DNA measured in the viable cells fraction. Values are means ± SD, n ≥ 3. Statistical significance was determined by using one-way ANOVA, *** $p < 0.05$.

Figure 31b displays the percentage of viable cells that internalized Cy3-DNA over 12 h. After 6 h, a higher percentage of HuH-7 cells had been transfected with Cy3-DNA when it was delivered by ternary complexes. However, after 12 h, the same percentage was reached for both complexes, meaning that the core-shell system was more rapidly internalized than the core complex. Figure 31c nonetheless confirmed a higher internalization of ternary complexes by HuH-7 cells. Higher levels of Cy3 fluorescence were indeed observed for the ternary systems at 2, 6 and 12 h. In conclusion, ternary complexes led to the internalization of Cy3-DNA in higher amounts and within a shorter time than binary polyplexes. This demonstrated their superior cellular uptake.

3.3.5. *In vivo* evaluation of the ternary complex

Pilot *in vivo* tests on wild-type mice were performed by Dr. Hiu-Man Grisch-Chan and Melanie Williman (Children's University Hospital of Zürich) using the n.P3Luc1 Nanoplasmid™ expressing luciferase from the liver-specific promoter P3 (Figure 32). DNA was complexed with a ratio shell/core/DNA of 1/2/1 as optimized *in vitro*, while *in vivo*-jet PEI was used at a c/p ratio of 1.1. As previously, the polyplexes were administered by retrograde intrabiliary infusion.

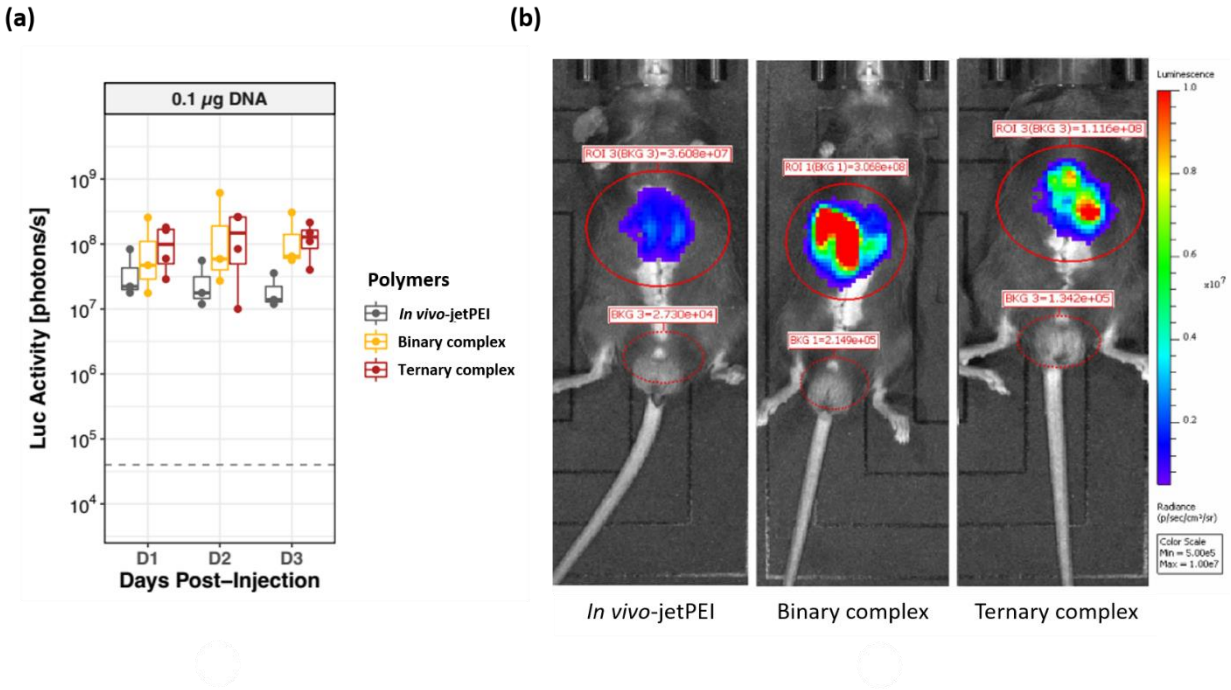

Figure 32. Retrograde intrabiliary infusion into wild-type mice of *in vivo*-jet PEI (n = 3), binary (n = 3) and ternary (n = 4) complexes. For each polyplex, 0.1 µg of n.P3Luc1 Nanoplasmid™ were encapsulated according to the following c/p ratio: 1.1/1 for *in vivo*-jet PEI, 2/1 for the core polymer **dCS-NSuc-LPEI**, and 1/1 for the shell polymer **dCS-NPEG$_6$-COOH**. (a) Luciferase expression levels up to three days post-injection. Dashed line = untreated mice. Values are means ± SD. Statistical significance was determined by using one-way ANOVA, *** $p < 0.01$. (b) Detection of liver-associated bioluminescence in mice three days post-injection.

Preliminary tests revealed that the same expression of luciferase was observed in mice for both 1 and 0.1 µg of Nanoplasmid™ injected, independently from the type of systems used (e.g binary or

ternary; data not shown). The pilot study was therefore performed on 0.1 µg of Nanoplasmid™. Both binary and ternary complexes outperformed *in vivo*-jet PEI complexes three days post-injection when assessed by i*n vivo* bioluminescence imaging (Figure 32b). Luciferase expression was also confirmed to be specific to the liver. Based on Figure 32a, luciferase activity was similar for both complexes at each time point, with 1.6 x 10^8 photons/s for the binary system and 1.3 x 10^8 photons/s for the ternary complex 3 days post-injection. *In vivo*-jet PEI only led to 3 x 10^7 photons/s of luciferase activity, demonstrating the superiority of **dCS**-based polyplexes (Figure 32a).

The monitoring of serum markers reporting for hepatotoxicity such as ALP, ALT, total and direct bilirubin revealed that neither ternary nor binary complexes had a detrimental effect on them upon administration of 0.1 µg of Nanoplasmid™. On the contrary, both complexes induced hepatotoxicity after the administration of 1 µg of DNA, showing that the toxicity of the polymeric vehicle upon retrograde intrabiliary infusion could be circumvented only with dosages similar or lower than 0.1 µg (data not shown).

This second *in vivo* assessment did not confirm the superior transfection efficiency of the ternary complex as compared to *in vitro* experiments, but did not show any negative impact. However, the possibility to use only 0.1 µg of DNA solved the toxicity issues previously encountered (*cf.* section 3.2.2.3.2).

3.3.6. Conclusions

In this section, CPP-derivatives were developed to provide higher cellular penetration but revealed to be inappropriate for the formation of core-shell structured NPs. The repulsion of cationic charges from both the core complex based on **dCS-NSuc-LPEI** and the cationic CPP derivatives was suspected to induce poor colloidal stability. Therefore, the negatively charged shell polymer **dCS-NPEG$_6$-COOH** was synthesized to shield the core polyplex *via* electrostatic interactions. Upon *in vitro* evaluation, ternary complexes displayed higher transfection efficiencies than their binary counterparts. This beneficial effect was however not clearly observed *in vivo*.

3.4. Decoration of the core-shell system

This last section details the decoration of the core-shell system, with the aim of finely tuning it to optimize the whole delivery process. In particular, the grafting of two targeting ligands and a cell penetration enhancer were investigated.

3.4.1. Strategy to decorate the core-shell system with additives

As the capping of **dCS-NSuc-LPEI**/DNA (core) with **dCS-NPEG$_6$-COOH** (shell) showed promising *in vitro* and *in vivo* results (*cf.* section 3.3.5), the functionalization of the ternary complex was explored, in order to improve its cell-targeting and cell-penetration abilities. Interest in grafting a targeting ligand on the core-shell complex arose from the rather complex injection route used *in vivo*. Although retrograde intrabiliary infusion could be adapted for humans as an endoscopic method, this technique remains less attractive than simple systemic injection. Delivering DNA intravenously thanks to a

delivery vehicle tagged with a targeting ligand would greatly facilitate the transfer of this system to clinical applications.

To graft the desired functionalities on the surface of the NPs, we aimed at the covalent functionalization of the free hydroxyl groups on **dCS-NPEG$_6$-COOH** (Figure 33). Following its formation, the core complex would be added to a mixture of **dCS-NPEG$_6$-COOH/dCS-NPEG$_6$-COOH-OX**. The resulting ternary polyplex would ideally demonstrate the same shielding properties as the non-decorated system, while displaying supplementary functionalities on its surface (represented by the –X group in the grey circle).

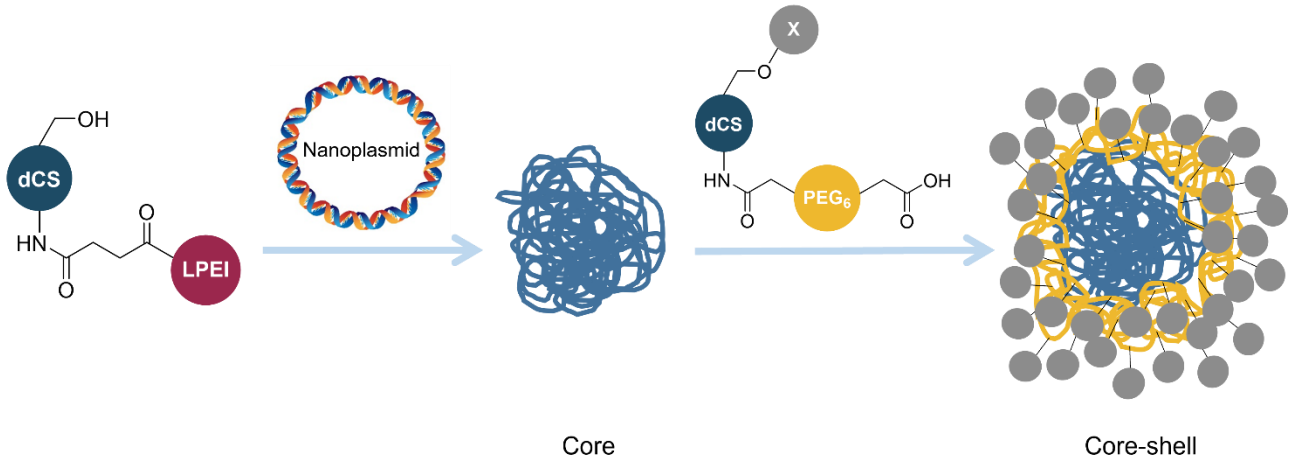

Figure 33. Decoration of the core-shell ternary complex with additives (-X groups). Additives are small molecules with cell-penetration or cell-targeting abilities. The core complex would be formed by add-mixing **dCS-NSuc-LPEI** to the Nanoplasmid™, prior to its capping with a mixture of **dCS-NPEG$_6$-COOH/dCS-NPEG$_6$-COOH-OX**. This would ensure the exposition of the new functionalities at the surface of the resulting NPs.

3.4.2. Functionalization with a hepatocyte-targeting ligand: Lactobionic acid

As presented in Chapter 1, the grafting of LA at the surface of our **dCS**-based delivery vehicle would enable the targeting of hepatocytes. The galactose moiety present on LA is indeed recognized by the ASGPr, which is selectively expressed on such cells.

Prior to the development of **dCS-NPEG$_6$-COOH**, preliminary experiments were performed with **dCS-NPEG$_{44}$-NH$_2$** (synthesis detailed in section 3.3.4) (Scheme 17), to prepare a **dCS-NPEG$_{44}$-LA** derivative to be used as shell polymer.

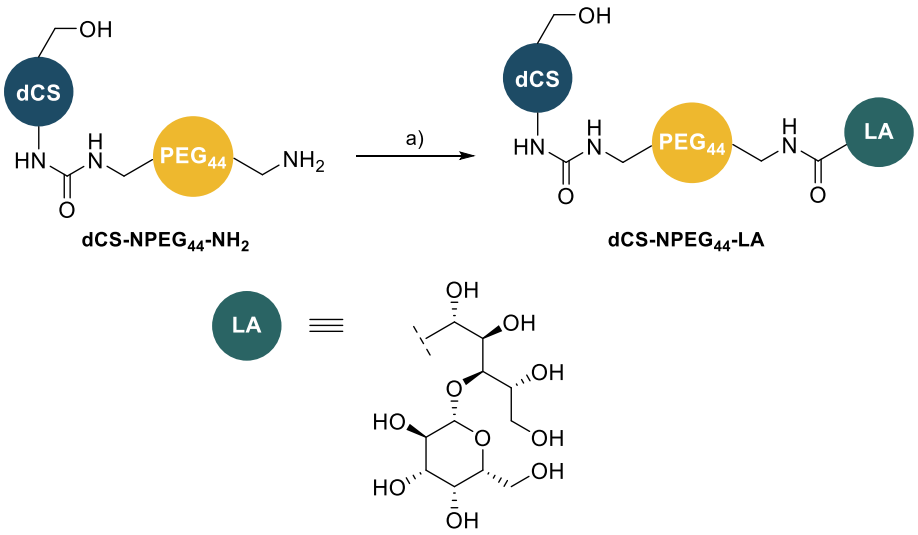

Scheme 17. Grafting of LA on **dCS-NPEG$_{44}$-NH$_2$**. a) coupling agent, LA, DMSO, rt, overnight. Coupling agents tested: EDC/sulfo-NHS, EDC.HCl/NHS, DMTMM.

dCS-NPEG$_{44}$-LA was attempted through the peptide coupling between the carboxylic acid moiety of LA and the amines on **dCS-NPEG$_{44}$-NH$_2$** (Scheme 17). As only non-covalent assemblies of LA and **dCS-NPEG$_{44}$-NH$_2$** were observed in 2D-DOSY NMR analyses, the same strategy was tried with octaacetylated LA (**LA(OAc)$_8$**, Scheme 18).

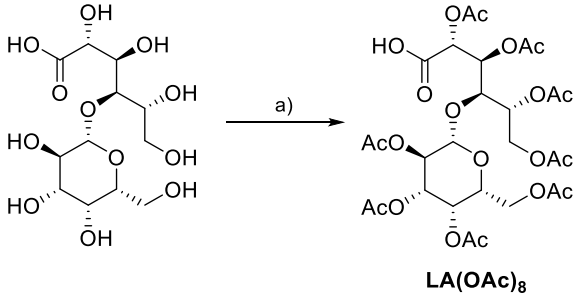

Scheme 18. Acetylation of LA. a) Ac_2O, pyridine, 0 °C to rt, 16 h, 94%. Adapted from Wahler *et al.*[210]

Unfortunately, none of coupling agents tested (DMTMM or EDC.HCl/HOBt) led to positive results, and the reverse reaction sequence was therefore tested (Scheme 19). It first required the preparation of **BocHN-PEG$_{44}$-LA**, followed by its Boc deprotection and grafting to **dCS**. The first step was tested with EDC.HCl/HOBt and TBTU as coupling agents, without success. Based on TLC monitoring, starting materials were poorly converted, and longer reaction times did not have any impact on it. The hindrance of LA protecting groups might have hampered its reactivity.

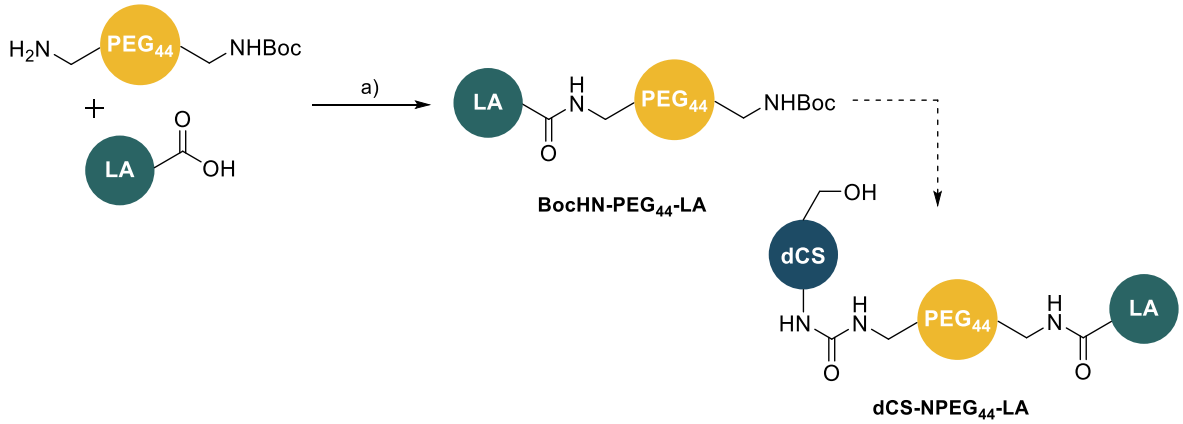

Scheme 19. Synthesis of **BocHN-PEG$_{44}$-LA**. a) TBTU, DIPEA, DMF, rt, 26 h or EDC.HCl, HOBT, DIPEA, DMAP, DCM, rt, 18 h.

The functionalization of **dCS** with FA was conducted in parallel of LA investigations. As its conjugation did not involve prior protection of its functionalities, we decided to focus on its grafting rather than LA.

3.4.3. Folic acid-derived dCS derivatives for cancer therapy

As introduced in Chapter 1, FA (Figure 34) targets FRs, which are overexpressed in cancerous tissues of lungs and breast. Although not relevant for hepatocyte-targeting, the covalent grafting of LA to **dCS** derivatives was intended to demonstrate the broad applicability of our gene delivery system.

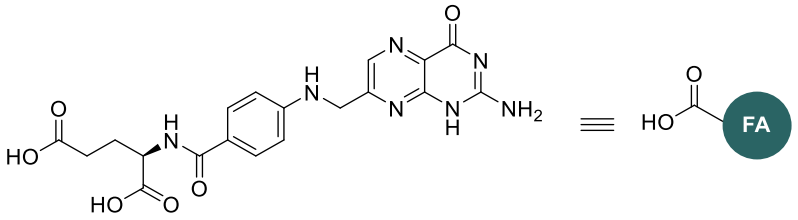

Figure 34. Schematic structure of FA.

To reach our goal, we envisioned the grafting of **H$_2$N-PEG$_6$-FA**, a small PEG derivative, onto **dCS-NPEG$_6$-COOH**.

3.4.3.1. Synthesis of H$_2$N-PEG$_6$-FA

H$_2$N-PEG$_6$-FA was obtained in two steps starting from FA and H$_2$N-PEG$_6$-NHBoc (Scheme 20). After activation of FA with TBTU, H$_2$N-PEG$_6$-NHBoc reacted on the newly formed intermediate, leading to **BocHN-PEG$_6$-FA** with 69% yield. Following deprotection under acidic conditions, the desired product was obtained with 85% yield.

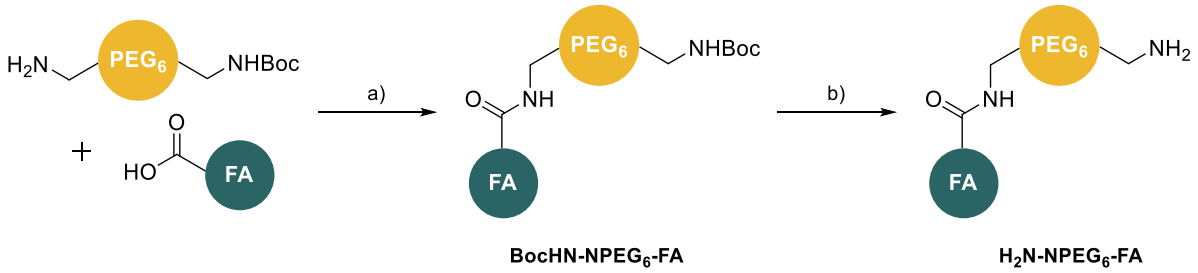

Scheme 20. Synthesis of **H_2N-PEG$_6$-FA**. a) TBTU, DIPEA, DMSO, rt, 16 h, 69%. b) 3 M HCl (aq.), rt, 3.5 h, 85%.

3.4.3.2. Covalent grafting of FA *via* carbamate bonds

H_2N-PEG$_6$-FA was then engaged in the preparation of **dCS-NPEG$_6$-COOH-OPEG$_6$-FA** (Scheme 21). Using CDI as coupling agent, we aimed at grafting **H_2N-PEG$_6$-FA** to the activated **dCS-NPEG$_6$-COOtBu**. The acidic deprotection of the resulting intermediate was expected to yield the desired product.

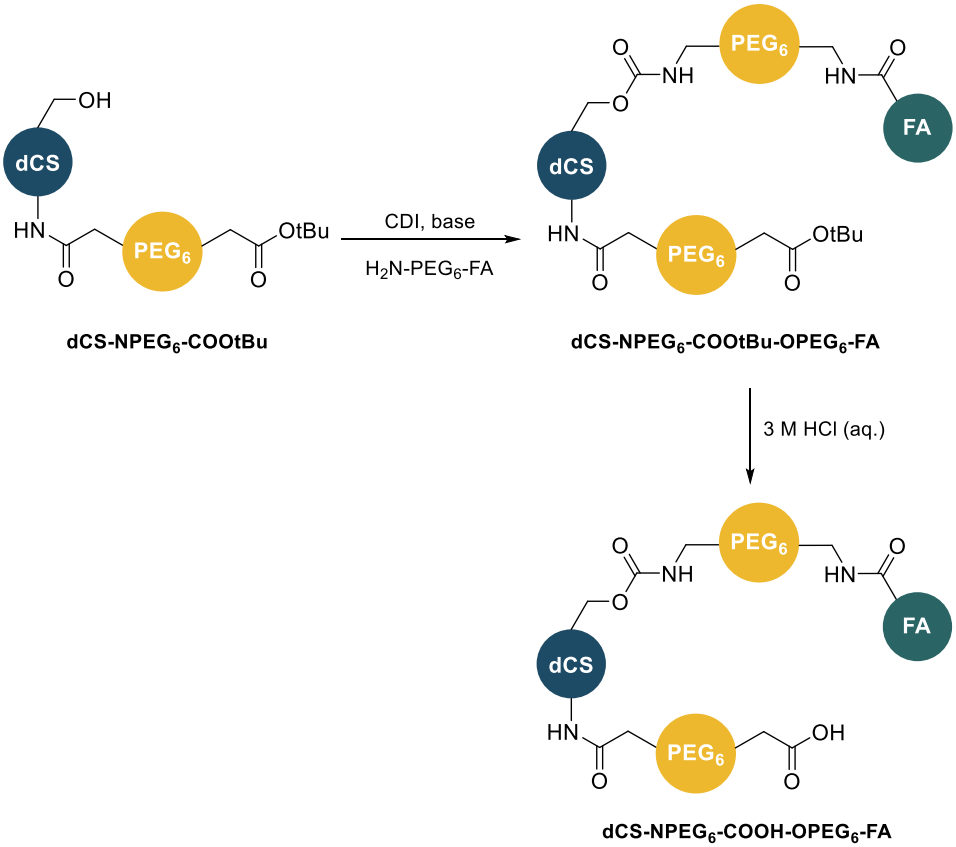

Scheme 21. Synthetic pathway for the preparation of **dCS-NPEG$_6$-COOH-OPEG$_6$-FA**.

Table 10 reports the different conditions tested for the grafting of **H_2N-PEG$_6$-FA** to **dCS-NPEG$_6$-COOtBu** (Scheme 21, first step). Following a preliminary unsuccessful test (entry 1), the procedure for entries 2 to 7 was adapted with the following order of addition: **dCS-NPEG$_6$-COOtBu** was first mixed to a base to pre-activate the hydroxyl groups. In parallel, **H_2N-PEG$_6$-FA** was activated with CDI in a second solution. Then, the former solution was added to the latter, and the resulting reaction mixture was stirred at rt.

Various bases were used for the pre-activation of **dCS-NPEG$_6$-COOtBu**, starting from DIPEA and

increasing up to stronger organic (DBU, ^{t}BuOK) and inorganic (NaH) bases (Table 10). As amine activation with CDI might take as long as 1.5 h in DMSO,[211] short and long activation times were then experimented (entries 1, 2, 5 vs 3, 4, 6, 7). Reactions were usually run overnight; one test was nonetheless performed over 3 days in order to determine whether the hindered natures of both reactants might lead to a significant decrease of reaction kinetics (entry 4). Lastly, entry 5 describes the addition of CDI in 3 portions, with 3 h of delay between each portion to investigate whether the stability of the activated intermediate of **H_2N-PEG$_6$-FA** might be the reason for such poor reactivity.

Table 10. Screening of reaction conditions for the synthesis of **dCS-NPEG$_6$-COOtBu-OPEG$_6$-FA**.

Entry	Base[1] (activation time)	CDI activation (time, number of additions)	Reaction time (h)
1[2]	DIPEA (none)	10 min, 1	16
2[3]	DBU (15 min)	5 min, 1	16
3[3]	DBU (15 min)	1.5 h, 1	16
4[3]	DBU (15 min)	1.5 h, 1	72
5[3]	DBU (15 min)	20 min, 3	16
6[3]	^{t}BuOK (15 min)	1.5 h, 1	16
7[3]	NaH 60% on oil (15 min)	1.5 h, 1	16

Tests run on 20 mg of **dCS-NPEG$_6$-COOtBu** in DMSO. [1]Base used to pre-activate the hydroxyl groups. [2]**dCS-NPEG$_6$-COOtBu** was activated with CDI and DIPEA prior to **H_2N-PEG$_6$-FA** addition to the mixture. [3]**dCS-NPEG$_6$-COOtBu** was pre-activated with a base while **H_2N-PEG$_6$-FA** reacted with CDI in a second solution; both solutions were then mixed together.

Despite a large screening, none of the tested conditions led to the desired product (Table 10). For most reactions, only **dCS-NPEG$_6$-COOtBu** was recovered after dialysis, with sometimes traces of unbound **H_2N-PEG$_6$-FA**. Test from entry 5 (three additions of CDI) afforded as major fraction a solid insoluble in every standard NMR solvent, hampering its analysis. This result suggested a potential cross-linking of **dCS** chains with each other.

One test was also performed with **dCS-NPEG$_6$-COOH** but did not yield better results. As an alternative, we attempted to first graft some **H_2N-PEG$_6$-NHBoc** on **dCS-NPEG$_6$-COOtBu**, to then deprotect the Boc and *tert*-butyl ester groups under acidic conditions, and eventually to graft FA on the newly formed free amines. As very low reactivity was encountered from the first step, this strategy was also abandoned.

In conclusion, carbamate bond formation between FA and **dCS-NPEG$_6$-COOH** could not be achieved. Although the pre-activation of the hydroxyl groups was thoroughly investigated, none of these conditions led to the desired product. The conversion of the hydroxyl groups to azides was consequently explored as an alternative solution.

3.4.3.3. Covalent grafting of FA *via* click chemistry

Based on the azidation procedure developed by Zhang *et al.*,[192] this last strategy aimed at forming **dCS-NPEG$_6$-COOH-N$_3$** in three steps, starting from the activation of hydroxyl groups of **dCS-NPEG$_6$-COO^{t}Bu** with tosyl chloride to later convert them into azides, and ending with the deprotection of the carboxylic acids to afford the desired product (Scheme 22). Based on our group's experience on dibenzocyclooctyne (DIBO) derivatives, the intermediate **DIBO-PEG$_6$-FA** would be synthesized from **H$_2$N-PEG$_6$-FA** (synthesis described in section 3.4.3.1) and **DIBO-nitrophenyl**. The latter was kindly provided by other PhD students of the group, based on a reported procedure.[212] The resulting intermediates were expected to react together through a strain-promoted azide-alkyne cycloaddition to yield **dCS-NPEG$_6$-COOH-DIBO-PEG$_6$-FA** (Scheme 22).

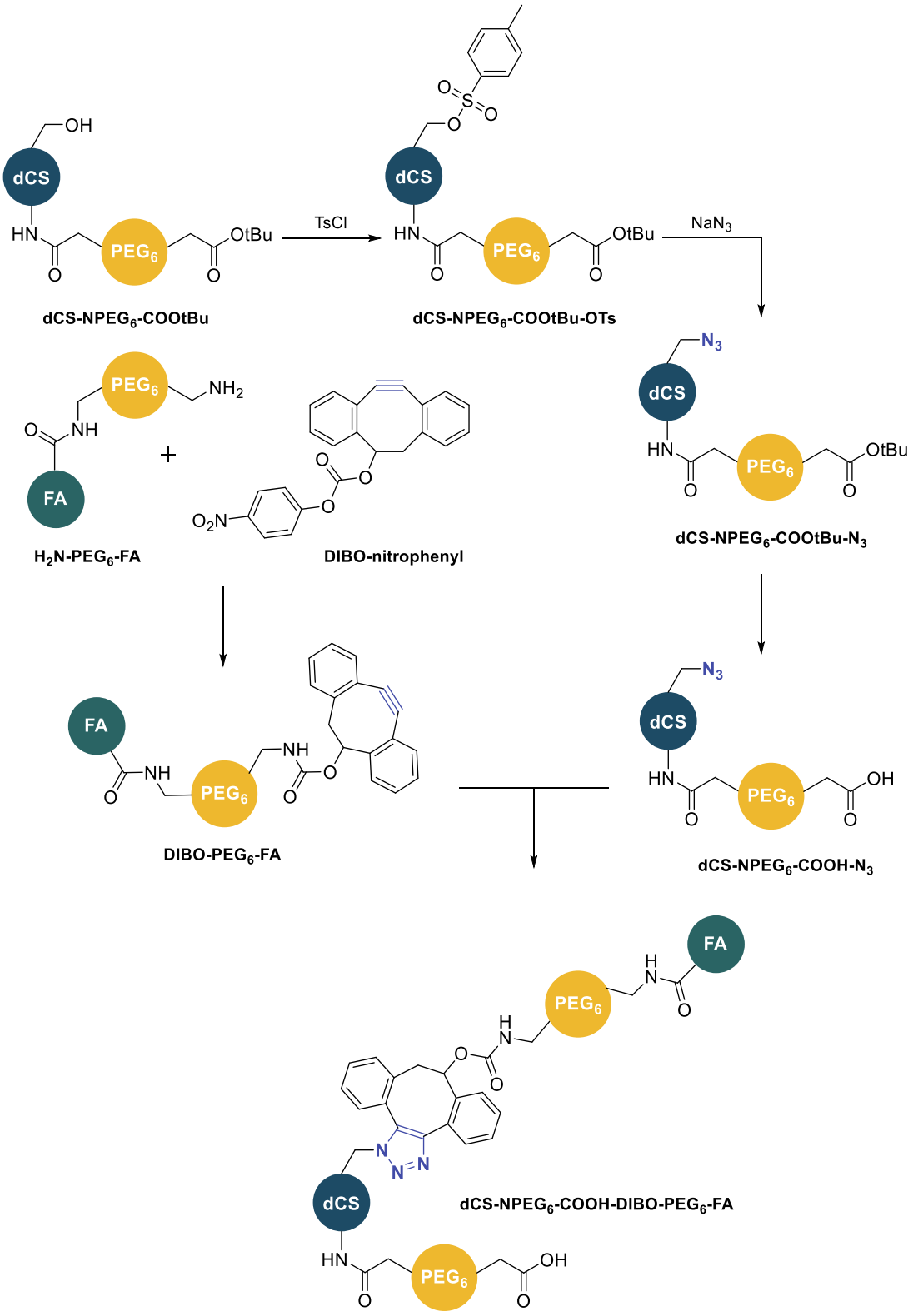

Scheme 22. Preparation of covalent FA-derived **dCS** derivative *via* strain-promoted alkyne-azide cycloaddition.

3.4.3.3.1. Synthesis of dCS-NPEG$_6$-COOH-N$_3$

Based on a reported procedure,[192] **dCS-NPEG$_6$-COO^{t}Bu** was first tosylated (Scheme 23). **dCS-NPEG$_6$-COO^{t}Bu-OTs** was obtained with a maximum grafting degree of 83%, showing almost complete conversion of the hydroxyl groups. However, the full conversion of the tosyl groups into azides in the

next step could not be reached, leaving traces of tosyl group signals on ^{1}H NMR spectra (*cf.* section 5.2.7.3). A rough value of GD_{Az} of 65% was indirectly estimated from the remaining signal of the tosyl group. The presence of the azide functionality was also assessed by FTIR analysis during which its characteristic sharp peak was observed around 2100 cm^{-1}. Lastly, deprotection of the PEG_6 fragment was carried out under acidic conditions (Scheme 23). The synthesis of **dCS-NPEG$_6$-COOH-N$_3$** was scaled up to 150 mg of starting **dCS-NPEG$_6$-COOtBu** several times and yielded about 60 mg of final product after three steps.

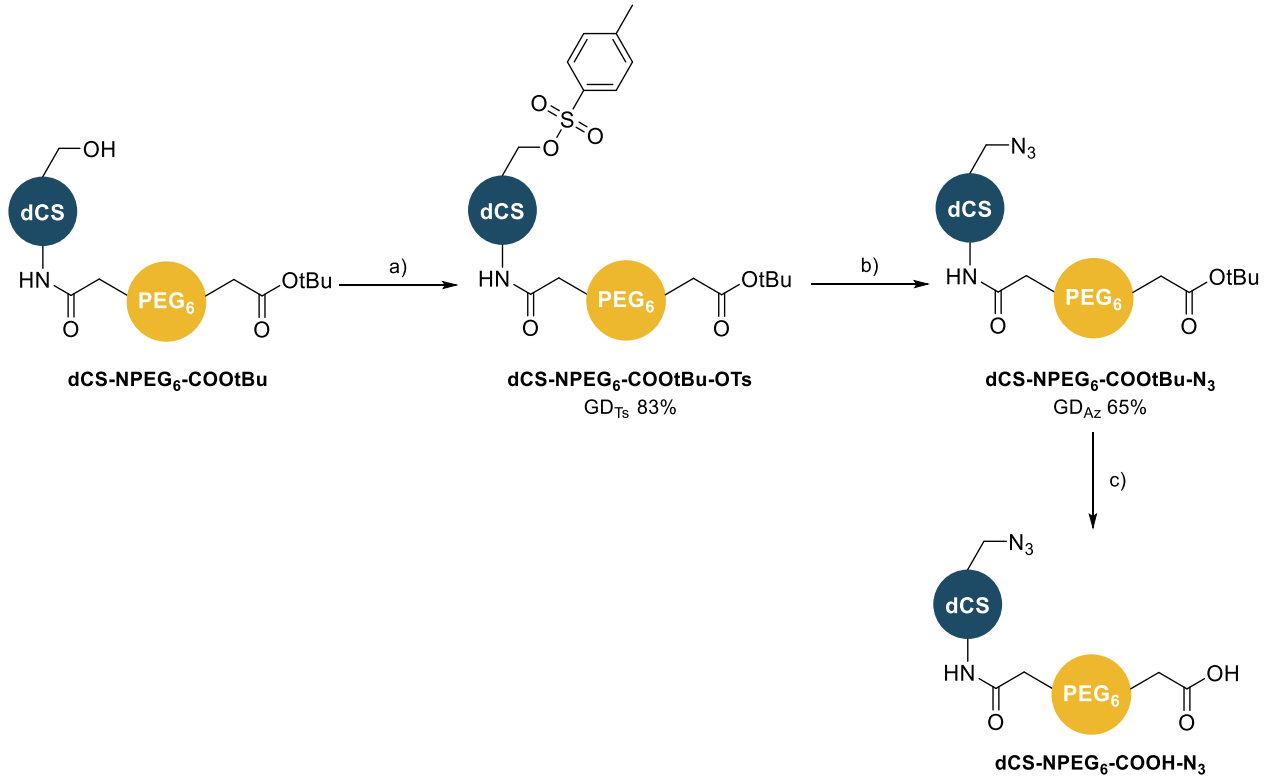

Scheme 23. Synthesis of **dCS-NPEG$_6$-COOH-N$_3$** starting from **dCS-NPEG$_6$-COOtBu**. a) TsCl, pyridine, rt, 48 h. b) NaN_3, DMSO, 60 °C, 48 h. c) 3 M HCl (aq.), rt, 5 h.

3.4.3.3.2. Synthesis of DIBO-PEG$_6$-FA

In parallel to **dCS-NPEG$_6$-COOH-N$_3$** synthesis, **H$_2$N-PEG$_6$-FA** was conjugated to our in-house **DIBO-nitrophenyl** derivative (Scheme 24). Upon activation with triethylamine, **H$_2$N-PEG$_6$-FA** reacted on **DIBO-nitrophenyl** to provide **DIBO-PEG$_6$-FA** with a yield of 40%. Longer reaction times did not have a significant impact on the yield.

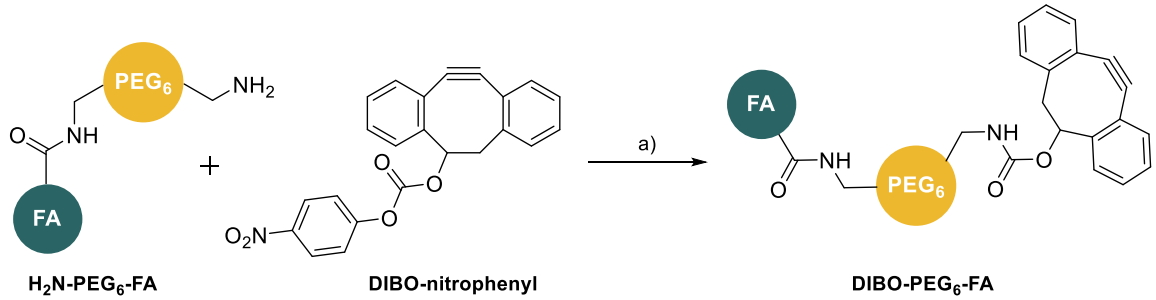

Scheme 24. Functionalization of **H$_2$N-PEG$_6$-FA** with DIBO-nitrophenyl. a) Et_3N, DMSO, rt, 17 h, 40%.

3.4.3.3.3. Synthesis of dCS-NPEG$_6$-COOH-DIBO-PEG$_6$-FA

The last step of this click chemistry-based strategy was carried out on a 40 mg scale of **dCS-NPEG$_6$-COOH-N$_3$** and yielded the final product (54 mg, GD$_{DIBO-FA}$ of 17%) upon simple mixing of the two reactants (Scheme 25). To promote azide groups reactivity, the reaction was performed at 60 °C.

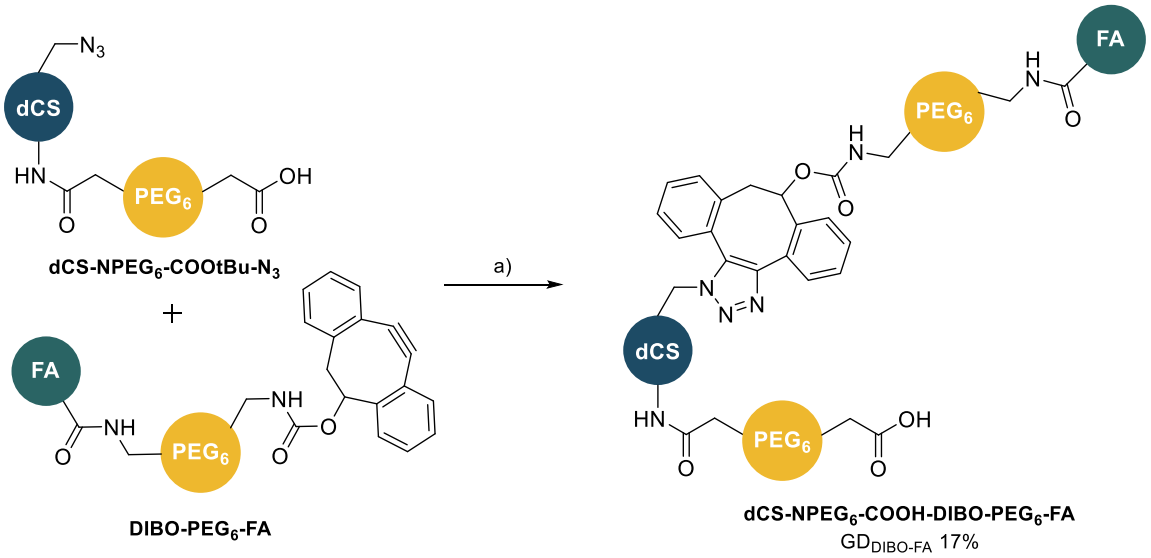

Scheme 25. Synthesis of **dCS-NPEG$_6$-COOH-DIBO-PEG$_6$-FA** *via* strain-promoted alkyne-azide cycloaddition. a) DMSO, 60 °C, 18 h.

The completion of this synthetic pathway led to **dCS-NPEG$_6$-COOH-DIBO-PEG$_6$-FA** in sufficient amounts to be later used as FA-derived shell polymer. This compound is currently under investigation in the University of Basel.

3.4.4. Improving cell-penetration with asparagusic acid

As described in Chapter 1, AspA has been reported to enhance cell-penetration of its cargos *via* the so-called thiol-mediated uptake.[105] This mechanism is endocytosis-independent, meaning that gene delivery vehicles decorated with such moieties do not suffer from endosomal escape and its side effects, thus ensuring a better protection and internalization of the genetic material. Being small, easy to graft and neutral, AspA was a ligand of choice for cell penetration enhancement. Therefore, its grafting to **dCS-NPEG$_6$-COOH** was investigated following the same strategy than with FA (Scheme 26).

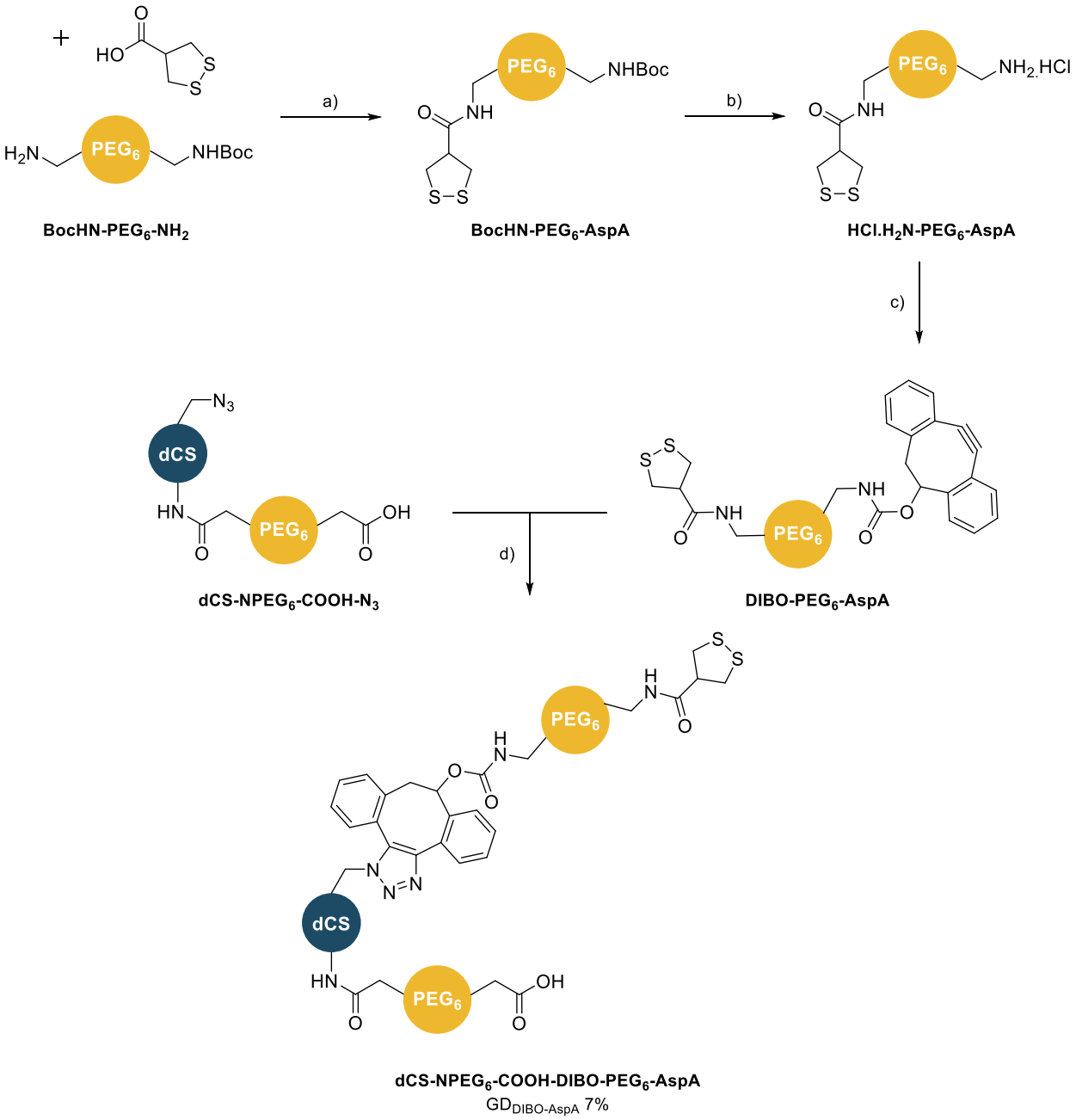

Scheme 26. Synthesis of **dCS-NPEG$_6$-COOH-DIBO-PEG$_6$-AspA**. a) TBTU, DIPEA, DMF, rt, 21 h, 52%. b) 4 M HCl in dioxane, rt, 1.5 h, quant. c) DIBO-nitrophenyl, Et_3N, DMSO, rt, 19 h, 13%. d) DMSO, 60 °C, 18 h.

Upon activation with TBTU, AspA reacted with **H$_2$N-PEG$_6$-NHBoc** to form **BocHN-PEG$_6$-AspA** with a 52% yield. Following deprotection under acidic conditions, **HCl.H$_2$N-PEG$_6$-AspA** was obtained quantitatively. Upon **DIBO-nitrophenyl** attack, **DIBO-PEG$_6$-AspA** was successfully prepared. Its mixing to **dCS-NPEG$_6$-COOH-N$_3$** led to **dCS-NPEG$_6$-COOH-DIBO-PEG$_6$-AspA** after one night of reaction at 60 °C (Scheme 26). The ^{1}H NMR spectrum revealed that on average **dCS** chains were grafted at 7% with AspA. **dCS-NPEG$_6$-COOH-DIBO-PEG$_6$-AspA** is now evaluated *in vitro* in the University of Basel to assess the impact of AspA on the cell penetration of the core-shell ternary complex.

3.4.5. Conclusions

This last subchapter described the strategies employed to decorate the ternary complexes. The free

hydroxyl groups on **dCS-NPEG$_6$-COOH** were functionalized with targeting ligands and cell-penetration enhancers. Although the first strategy relying on carbamate bond formation failed for both LA and FA, we then successfully grafted FA to **dCS-NPEG$_6$-COOH** *via* azide-alkyne click chemistry. The same strategy was then applied to AspA, thus allowing the preparation of both FA-derived and AspA-derived shell polymers. Both of them are currently under biological assessment in the University of Basel. We hope that these last polymeric derivatives will provide the ternary complex with efficient cancerous cells targeting ability and enhanced cell-penetration.

Chapter 4 Conclusions and Perspectives

The past decades have shown that many inherited and acquired disorders could benefit from therapeutic approaches based on gene therapy. The idea of treating a disease from its origin, and not only its effects, is quite appealing and could be amongst the biggest achievements of this century in the biomedical field. Promising solutions have already been proposed, starting with the simple injection of naked plasmids expressing genes of interest. Their poor bioavailability and lack of specificity were however detrimental to their further development. Viral vectors then arose as the best available solution, and went through many clinical trials, for both *in vivo* and *ex vivo* gene therapies. Some of these formulations have been approved by health regulatory agencies and bring high hopes for the treatment of orphan diseases. Although encouraging, these results were counterbalanced by significant toxicity, putting patients' lives at risk, as well as high production costs and limited genetic material packaging. Improvements of virus-based systems are still on-going and will hopefully lead to safer solutions with sustained efficiencies in the near future. In parallel, a growing interest has been observed for non-viral gene delivery over the last three decades, potentially overcoming viral vectors limitations. The use of polymers, lipids or inorganic NPs as protecting envelopes ensures low cytotoxicity. These systems can be precisely fine-tuned by versatile functionalizations. Therefore, we aimed at preparing polymeric non-viral gene delivery systems targeting liver-inherited diseases such as phenylketonuria and ornithine transcarbamylase deficiency. Based on a biocompatible and biodegradable **dCS** backbone, we successfully prepared polymeric carriers functionalized with other polymers (PEI, PEG), peptides (Arg_8, TAT), fluorophore (Alexa Fluor 647) and small molecules (folic acid, asparagusic acid) to match our requirements. The resulting core-shell polyplexes were evaluated *in vitro* and *in vivo* at different functionalization stages and demonstrated great potential for non-viral gene delivery.

The poor solubility of commercial CS represented a first challenge. Its depolymerization led to water-soluble **dCS** chains of 5-8 kDa, thus unlocking the next synthetic steps of the project. Low MW BPEI and LPEI were the first polymers to be grafted on **dCS** through a succinyl linker. Covalent linkage *via* amide bonds ensured stability towards physiological environments. The covalent character of the resulting polymers was confirmed by 2D-DOSY NMR. DNA condensation with **dCS-NSuc-BPEI** and **dCS-NSuc-LPEI** was performed at the University of Basel. After optimization and scale-up of these systems, *in vitro* cellular assays on hepatocyte-derived cell lines were conducted and identified **dCS-NSuc-LPEI** as the lead compound for further developments, with higher transfection efficiency and lower toxicity than commercially available transfecting agents. BPEI derivatives, on the other hand, were too toxic and did not reach the same transfection levels than **dCS-NSuc-LPEI**.

Following the initial objectives, we also investigated the grafting of low MW PEG chains on **dCS**. Heterobifunctional PEGs such as $HCl.H_2N\text{-}PEG_{44}\text{-}SH$, $Mal\text{-}PEG_{44}\text{-}H_2N$ and $Acr\text{-}PEG_{44}\text{-}H_2N$ were conjugated to **dCS** hydroxyl moieties through carbamate formation, **dCS** amines being already functionalized. The PEG cross-linking reactive moieties were meant to strengthen the polymeric

network stability upon NPs formation. HCl.H_2N-PEG_{44}-SH was first grafted to **dCS-NSuc-BPEI** and **dCS-NSuc-LPEI** following two different pathways, either grafting PEG to **dCS-NSuc** followed by conjugation to LPEI/BPEI, or the other way around. The first strategy proved to be more successful and was applied to other PEGs. The conjugation of Mal-PEG_{44}-H_2N and Acr-PEG_{44}-H_2N was attempted on **dCS-NSuc** but was not successful due to degradation of the cross-linking moieties and/or poor reactivity of the hydroxyl groups. Thiolated-PEG derivatives were biologically assessed and unexpectedly showed worse results for both toxicity and transfection efficiency. To explain such results, we presumed that covalently linking PEG and PEI through **dCS** prevented a proper positioning of both polymers in the NP, thus disturbing both DNA condensation by the positively-charged PEI core and surface shielding by PEG. The use of such covalent system containing cross-linking moieties was therefore not suited to this project.

Switching strategy, we therefore investigated the formation of a core-shell complex, which contained **dCS-NSuc-LPEI**/DNA polyplex in its core and additional **dCS** derivatives on its shell, held together *via* non-covalent electrostatic interactions. The new **dCS** derivatives were based on PEG and CPPs. While none of the three CPP derivatives efficiently coated the core polyplex, probably due to strong repulsive cationic interactions, **dCS-NPEG$_6$-COOH** led to colloidally stable core-shell NPs. Its carboxylate moieties ensured proper interactions with the core polyplex, while the PEG chain effectively shielded the polyplex from serum components, leading to higher transfection efficiencies as compared to the naked core. Preliminary *in vivo* experiments on wild-type mice did not corroborated those findings, although only similar transfection efficiencies were obtained.

The end of this PhD was focused on the decoration of the core-shell system with cell-penetrating and targeting moieties. In particular, the addition of a targeting ligand on the shell polymer was a promising strategy to switch from the suboptimal retrograde intrabiliary infusion setup used so far, to the more convenient intravenous injection. Lactobionic acid was selected as targeting moiety for hepatocyte-targeted treatment, but the obstacles encountered for its grafting forced us to investigate another ligand. Looking towards the project's future and additional applications, we therefore attempted the grafting of folic acid, a well-known targeting ligand for cancerous cells from breast, lung and ovarian tissues. The hydroxyl groups of **dCS-NPEG$_6$-COOH** were converted to azide functionalities by successive tosylation and nucleophilic substitution with sodium azide, leading to **dCS-NPEG$_6$-COOH-N$_3$**. Coupled with the newly synthesized **DIBO-PEG$_6$-FA**, the final **dCS-NPEG$_6$-COOH-DIBO-PEG$_6$-FA** derivative could be obtained by strain-promoted azide-alkyne cycloaddition. Using the same strategy, we also produced **dCS-NPEG$_6$-COOH-DIBO-PEG$_6$-AspA**. Asparagusic acid showing abilities for thiol-mediated uptake, ternary complexes derivatized with it are expected to bypass endocytosis, allowing them to avoid endosomal degradation. These decorated shells are currently being tested *in vitro* at the University of Basel.

Although important progress has been made so far, the non-viral delivery systems developed in the frame of this project could still be improved on several aspects (Figure 35). For example, the grafting of lactobionic acid as hepatocyte-targeting ligand is one of the first priorities (Figure 35a). Once the challenge of conjugating lactobionic acid to H_2N-PEG_6-NHBoc through amide bond coupling is overcome, the final polymeric system **dCS-NPEG$_6$-COOH-DIBO-PEG$_6$-LA** should be easy to produce. The presence

of a hepatocyte-targeting ligand at the surface of the vehicle was shown to be essential to observe expression of the reporter/therapeutic gene upon intravenous injection. Preliminary intravenous tests using the binary complex **dCS-NSuc-LPEI**/DNA and ternary complex **dCS-NPEG$_6$-COOH**/**dCS-NSuc-LPEI**/DNA did not reveal any luciferase expression with the liver-specific promoter P3 (data not shown), meaning that the NPs were not efficiently delivered to hepatocytes *via* passive targeting. Therefore, an active targeting component is necessary to reach the desired effects. In addition, intravenous administration would be safer than retrograde intrabiliary injection, as it did not induce any systemic toxicity upon administration of the binary and ternary complexes (data not shown).

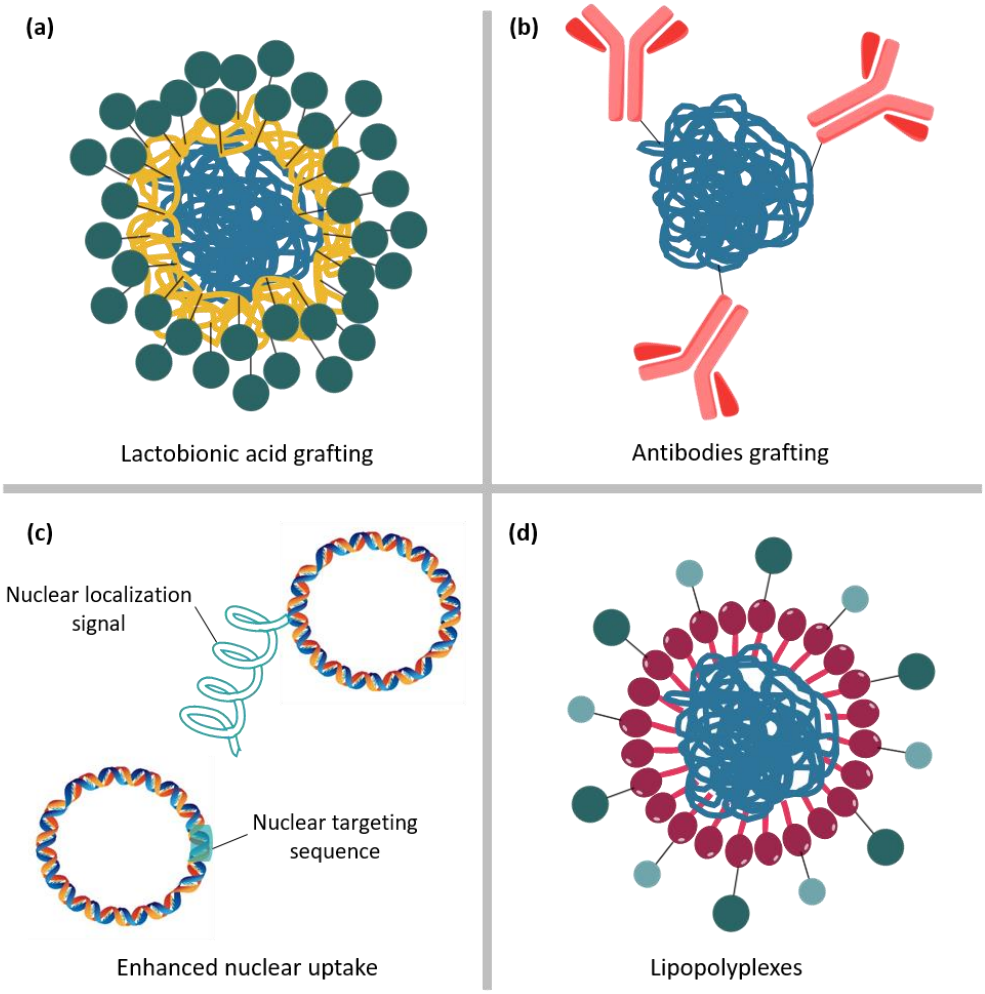

Figure 35. Perspectives of the project. (a) Grafting of lactobionic acid on the core-shell system. (b) Grafting of antibodies on the core polyplex. (c) Enhanced nuclear localization of Nanoplasmids™. (d) Preparation of lipopoylplexes.

In order to broaden its applications, the core-shell system could be functionalized with antibodies as targeting ligands for specific cells (Figure 35b). From the preliminary tests we performed, it appeared that functionalization with antibodies is more efficient when performed after formation of the polymeric NPs (data not shown). Moreover, the binary complex seems better suited to post-functionalization, probably due to the presence of residual free amines at its surface.

Grafting of NLS peptides or insertion of DNA nuclear targeting sequences in the Nanoplasmids™ could also greatly improve the overall efficiency of the system (Figure 35c). This aspect of the project could be

performed in the future by our collaborators from the University of Basel and the University Children's Hospital of Zürich.

Lastly, lipopolyplexes might be of interest for the future of this project. Lipopolyplexes are composed of cationic liposomes, polycations (cationic polymers or peptides) and nucleic acids that form a NP based on non-covalent interactions.[213] The high stability and low cytotoxicity of lipoplexes combined with the high transfection efficiency, endosomal escape ability and small size of polyplexes, make lipopolyplexes attractive for non-viral gene delivery. Applying this strategy to our system, **dCS-NSuc-LPEI** would remain the core polyplex, as it ensures excellent DNA condensation and proper endosomal escape (Figure 35d). However, the biocompatibility and bioavailability of the final system might be improved by replacing the shell polymer by a lipidic component. Similarly to the shell polymer, targeting ligands and cell-penetration moieties could be grafted to the lipid through click chemistry, with pre-functionalization of the lipid with azide groups.

The gene delivery vehicles developed over these four years have shown promising results both *in vitro* and *in vivo*. There is still much room for improvement of the final system, and several avenues to explore which could bring these systems one step closer to clinical applications.

Chapter 5 Experimental Part

5.1. General information

Reagents and solvents were purchased from commercial sources (Alfa Aesar, Acros, Fluka, Polysciences Inc., Sigma Aldrich, BioPharma PEG, TCI, ABCR, GenScript) and were used without further purification unless stated. In particular, CS was obtained from TCI (5-20 mPa·s, 0.5% in 0.5% acetic acid at 20 °C; DD 80%; mixture of three distributions with Mw 478'900, 88'410, 44'800 Da). LPEI (2'500 Da) was obtained from Polysciences Inc. and BPEI (1'800 Da, purity > 99.9%;) was supplied by ABCR. H_2N-PEG_{44}-MAL (≈ 2'000 Da, 44 units), HOOC-PEG_{44}-NHBoc (≈ 2'000 Da, 44 units), HOOC-PEG_6-COOtBu (438.5 g/mol, 6 units), were obtained from BioPharma PEG and HCl.H_2N-PEG_{44}-NHBoc (≈ 2'000 Da, 44 units) from Sigma Aldrich. The peptides Arg_8, TAT-OMe, TAT-Cys were purchased to GenScript.

Reactions were performed under inert atmosphere except when distilled water was used as solvent. Depolymerization of CS was performed using a microwave reactor (Monowave 400, Anton Paar). Centrifugations were performed in an Allegra X-30R Centrifuge (Swinging-bucket rotor, 4700 rpm, Beckman Coulter). Dialysis purifications were performed against distilled water (unless stated) at rt. Several types of dialysis membrane were used: MWCO 14 kDa (Roth, Membra Cell, regenerated cellulose (RC), dry packaged, treated with glycerine), MWCO 7 kDa (Zellu Trans 6–8 kDa, RC, dry packaged), MWCO 3.5 kDa (Spectra/Por®3 RC, dry packaged, glycerine-free), MWCO 1.0 kDa (Spectra/Por®7, RC, packaged wet in 0.1% sodium azide solution), MWCO 1.0 kDa (Spectra/Por®7, RC, packaged wet in 0.05% sodium azide solution), MWCO 0.1 – 0.5 kDa (Spectra/Por®, Biotech CE, packaged wet in 0.05% sodium azide solution). Dialysis water was changed 4 times per day. Samples were lyophilized in a VaCo 5 Zirbus technology freeze-dryer (0.4 mbar, -80 °C). Flash column chromatography was performed using Silicycle P60 silica (230-400 mesh (40-63 µm) silica) and Merck Kieselgel 60F254 aluminium for TLC monitoring. Preparative TLC was performed on glass backed plates. TLC were visualized by UV fluorescence (254 nm) and one of the following reagents: $KMnO_4$, ninhydrine, pancaldi.

^{1}H and 2D-DOSY NMR spectra were recorded at room temperature on Bruker 400 Ultrashield™ Plus, Bruker Avance Neo-500, Bruker Avance III HD-600 or Bruker Avance Neo-800 (respectively 400, 500, 600 and 800 MHz, Bruker, Billerica, MA). Spectra were analyzed using MestReNova software. Chemical shifts (δ) were reported in parts per million (ppm) relative to residual solvent peaks rounded to the nearest 0.01 ppm (ref: CD_3COOD 2.05 ppm, D_2O 4.79 ppm and DMSO-d_6 2.50 ppm). Peak multiplicities were indicated as follows: s (singlet), t (triplet), m (multiplet) and br (broad). All integrations were performed per unit of CS. Grafting degree (GD) values were determined for each derivative via ^{1}H NMR and are expressed per unit of CS (including acetylated units). The conjugation of small molecules, polymers or peptides to dCS afforded GD values below 100%. As a result, the peak integrals do not match the effective numbers of H from each components of the conjugates. In the NMR spectra description, the number of H in brackets relates to the value expected for 100% GD. The same reasoning was applied

for the reporting of H1/H1' for all dCS derivatives: the theoretical/expected integral values for H1 and H1' are reported in brackets and can be compared to the measured values highlighted on the spectra. The covalent character of each final system was confirmed by 2D-DOSY NMR. For infrared spectroscopy data, a Perkin Elmer Frontier FTIR system was used with a QUEST ATR Accessory (diamond Ext Range Accy Frontier). GPC analyses were recorded on a 1260 Infinity II Agilent GPC/SEC system equipped with a Wyatt triple detection setup: multi-angle light scattering (MALS), viscometer, and refractive index detector (DAWN8). Samples were separated using a guard column (OHpak SB-G 6B, 6 × 50 mm) and two mixed-gel columns (OHpak SB-806M HQ, 8 × 300 mm and SB-802.5 HQ, 8 x 300 mm) that were put in series (SB-G 6B → SB-806M HQ → SB-802.5 HQ). Samples of 10 mg were dissolved for 1 h in 1 mL of acetate buffer (0.3 M aqueous acetic acid, 0.2 M aqueous sodium acetate, 0.3 M aqueous sodium, pH 4.4), followed by filtration through a 0.45 µm PES membrane. The samples were injected (100 µL) into the GPC and run at 30 °C (flow rates and analysis running times varied). Pullulan P20 (180–1,220,000 Da) was used as a reference and stability control. Data were analyzed on Astra software. When necessary, data fitting was performed using exponential degree 2 and forward extrapolation. The qualitative accurate masses were measured by ESI-TOF using the Xevo G2-S QTOF (Waters) and nanoESI-FT-MS using the Elite™ Hybrid Ion Trap-Orbitrap (ThermoFisher) Mass Spectrometer.

Nanoplasmids™ were purchased from Nature Technology Corporation (Lincoln, NE). Nanoplasmid™ n.P3Luc1 (2'951 bp) encode the firefly luciferase transgene driven by a synthetic liver specific promoter P3. Nanoplasmid™ n.CAG.GFP1 (5'200 bp) consists of the CAG promoter and GFP as reporter transgene.

HuH-7 cells were obtained from RIKEN Cell Bank (Ibaraki, Japan) and cultured at 37 °C with 5% CO2 and saturated humidity. Cells were kept in Dulbecco's modified Eagle's medium (DMEM) high glucose (4500 mg/L) and additionally supplemented with 10% fetal calf serum FCS and 1% penicillin (10'000 IU/mL)-streptomycin (10'000 µg/mL). Sub-culturing was performed when cells reached 70% confluency.

Hydrodynamic diameter D and polydispersity index (PDI) were determined by dynamic light scattering (DLS) and ζ-potential was determined by electrophoretic light scattering using Zetasizer Nano-ZS Zen3600 and Zetasizer Ultra with the Zetasizer DTS and ZS explorer software, respectively (Malvern Panalytical, Worcestershire, UK). For ζ-potential measurements, polyplexes were diluted in a 5% glucose solution.

5.2. Experimental procedures

5.2.1. Starting polymers

The compounds described in this section were previously published in "Nicolle *et al.*, *Int. J. Mol. Sci*, **2021**, *22*, 3828".[204]

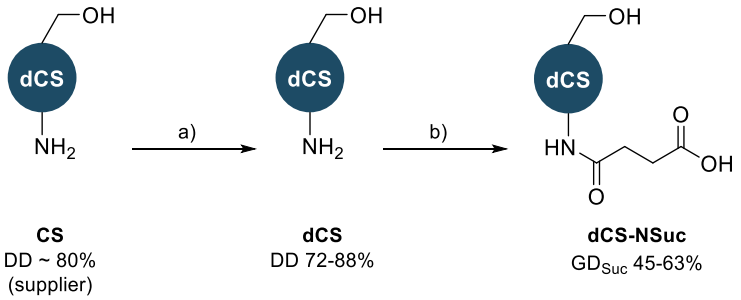

Scheme 27. Preparation of starting polymers. a) 1 M HCl (aq.), microwaves 19 min, 100 °C. b) succinic anhydride, pyridine, 0.3% HCl (aq.), rt, 1.5 h.

dCS

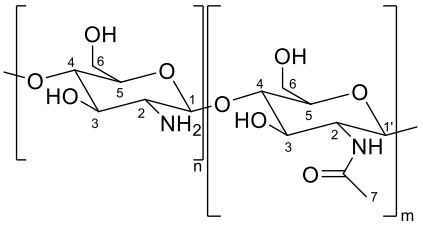

Commercial CS (200 mg) was suspended in a microwave vial containing 20 mL of 1 M HCl aqueous solution, resulting in a CS solution at 1% w/v. The vial was placed in the microwave reactor and the depolymerization program was started under a constant stirring at 300 rpm. Video monitoring of the solution showed that the sample was entirely solubilized after 1 min (T reaching 60-70 °C). The depolymerization program was composed of the following steps: heat as fast as possible to 100 °C, hold at 100 °C for 19 min, then cool down to 35 °C as fast as possible. Once the resulting dCS solution reached 30 °C, the solution was neutralized in two steps: first a 10 M NaOH aqueous solution was added dropwise until the solution started to become blurry and reached pH 6.7 (pH-meter monitoring). The suspension was left to equilibrate at rt for 15 min before being centrifuged (4700 rpm, 20 °C, 10 min). Only the liquid fraction was recovered. Its pH was then further increased to 7.0 with dropwise addition of a 0.05 M NaOH aqueous solution. The white suspension was centrifuged a second time under the same conditions to remove the second precipitate, if any. The resulting liquid part was transferred into a dialysis membrane (MWCO 3.5 kDa) and dialyzed against water for 3 days. After freeze drying, **dCS** was obtained as a white aerated solid (25 mg, DD = 79%, Mw = 8.3 kDa). **^{1}H NMR (400 MHz, D_2O/CD_3COOD 1/1)**: δ 4.94 (br, 0.79 H, H1), 4.63 (br, 0.21 H, H1') 4.10 – 3.48 (m, 5 H, H3-4-5-6), 3.25 (t, 1 H, H2).

^{1}H NMR spectrum of **dCS** (400 MHz, D_2O/CD_3COOD 1/1)

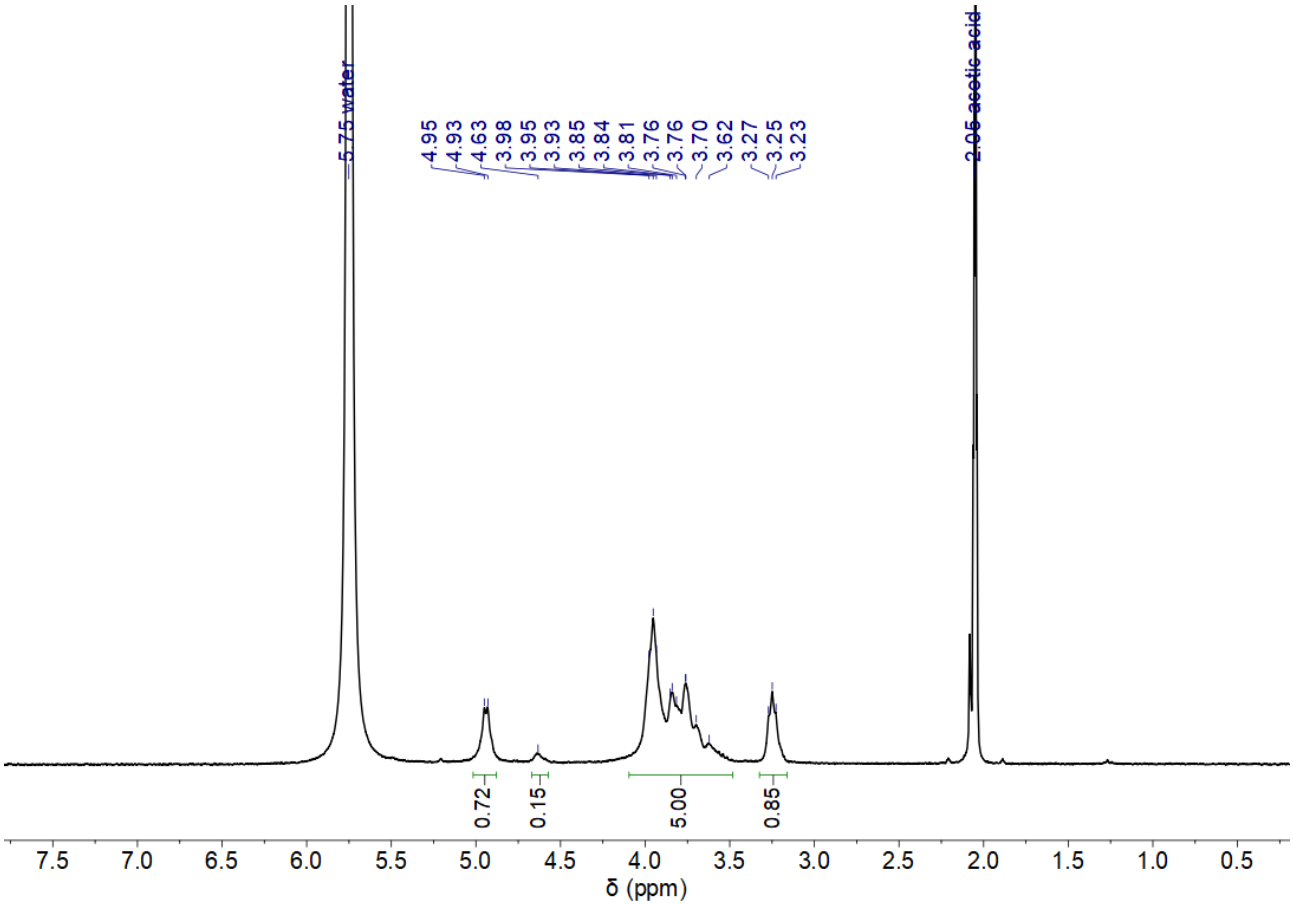

^{1}H NMR (400 MHz, D_2O): δ 4.59 (br, 1 H, H1/1'), 4.08 – 3.42 (m, 5 H, H3-4-5-6), 2.85 (br, 1 H, H2), 2.07 (s, 3 H, H7).

^{1}H NMR spectrum of **dCS** (400 MHz, D_2O)

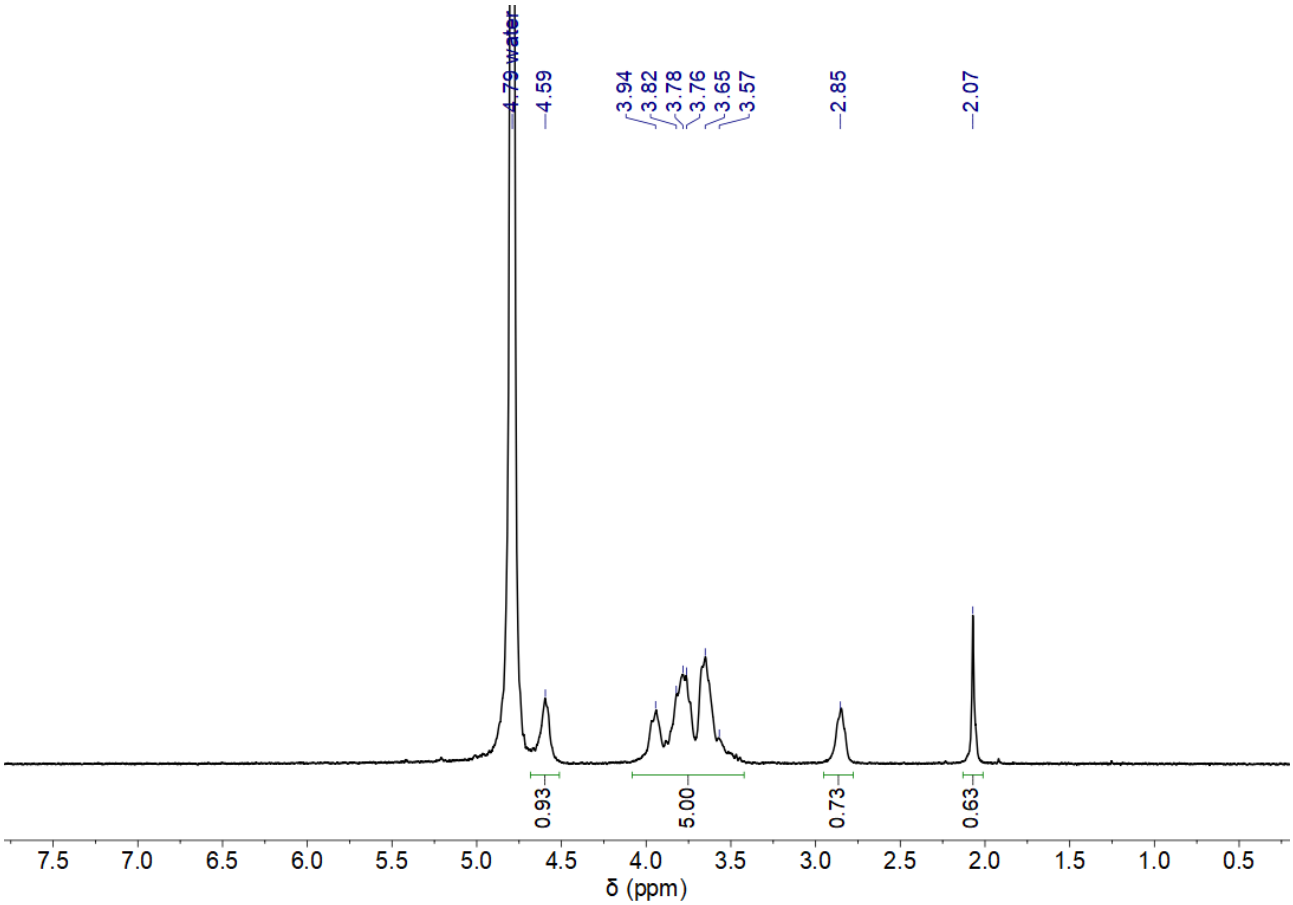

IR (cm^{-1}): 3292.45, 2876.04, 1644.11, 1376.17, 1320.32, 1151.18, 1062.07, 1029.64, 895.96, 665.85.

Determination of the molecular weight by GPC:

Mp (kDa)	Mn (kDa)	Mw (kDa)	PD[1]
6300	6900	8300	1.20

[1]Polydispersity of the polymer with a minimum value of 1 (= pure monodisperse sample).

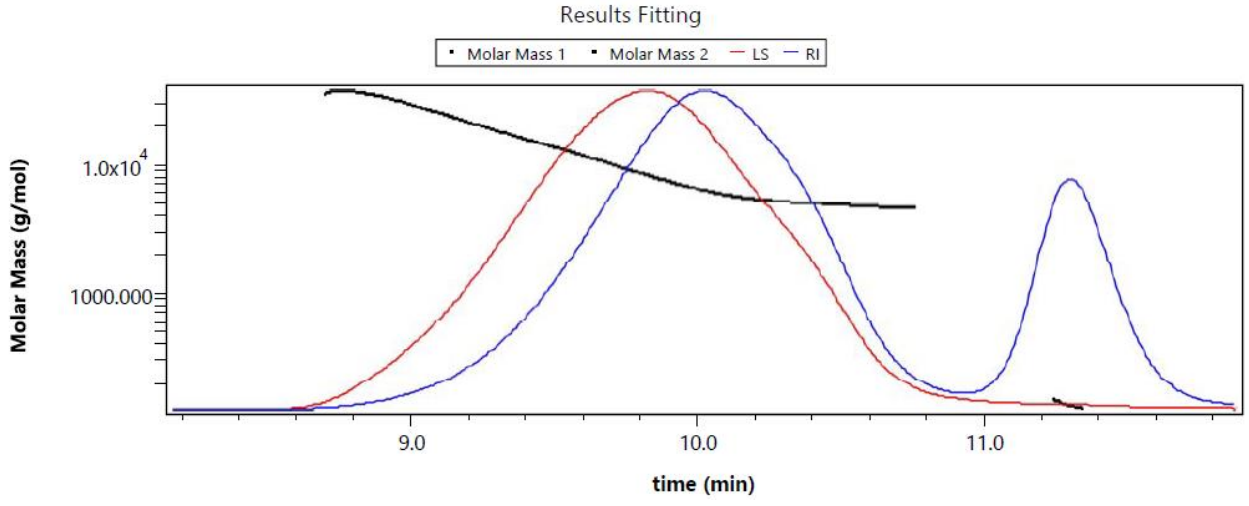

Estimation of the DD:

From the spectrum recorded in D_2O, the massif from 3.98 to 3.32 ppm is assigned to H3-4-5-6 and used as reference peak. Integration of the singlet at 1.97 ppm leads to 0.63 H. This singlet corresponds to the 3 H of the acetyl groups from the acetylglucosamine units of chitosan.

As DD = (1 – AD) x 100 where AD = $\frac{\int \delta\ (2.07\ \text{ppm})}{nb\ (H7)} = \frac{0.63}{3}$ = 0.21, hence DD = 79%

Estimation of the molar mass of one average dCS unit (M(dCS)):

M(dCS) = M(glucosamine) x DD + M(acetylglucosamine) x AD

As DD = 79%, M(dCS) = 161.2 x 0.79 + 203.2 x 0.21 = 170.0 g/mol

Estimation of the number of units per dCS chain (nb(dCS units)):

nb(dCS units) = $\frac{Mw(dCS)}{M(dCS)} = \frac{8300}{170.0} \approx 49$ units

dCS-NSuc

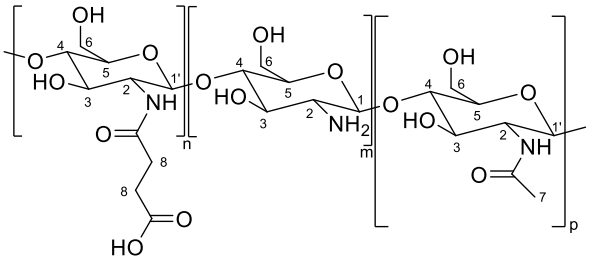

dCS (DD 79%, 1.00 g, 4.72 mmol of reactive glucosamine units, 1.0 equiv.) was dissolved in distilled water (100 mL) at rt and further acidified with HCl 37% aqueous solution (0.3 mL added dropwise to reach complete dissolution). To this solution were slowly added pyridine (5.70 mL, 70.8 mmol, 15 equiv.) and succinic anhydride (477 mg, 4.77 mmol, 1.01 equiv.). After 20 min, dissolution was complete and pH of the solution was controlled at 7. After 1 h of additional stirring at rt, the mixture was transferred to a dialysis tube (MWCO 3.5 kDa) and dialysed against water for 3 days. After centrifugation (4700 rpm, 20 °C, 10 min), the supernatant was recovered and lyophilized. **dCS-NSuc** was obtained as a white aerated solid (913 mg, GD_{Suc} = 63%). **^{1}H NMR (600 MHz, D_2O/CD_3COOD 1/1):** δ 4.94 (br, 0.16 H, H1), 4.59 (br, 0.84 H, H1'), 4.04 – 3.47 (m, 5 H, H3-4-5-6), 3.21 (br, 1 H, H2), 2.66 (br, 4 H, H8).

^{1}H NMR spectrum of **dCS-NSuc** (600 MHz, D_2O/CD_3COOD 1/1)

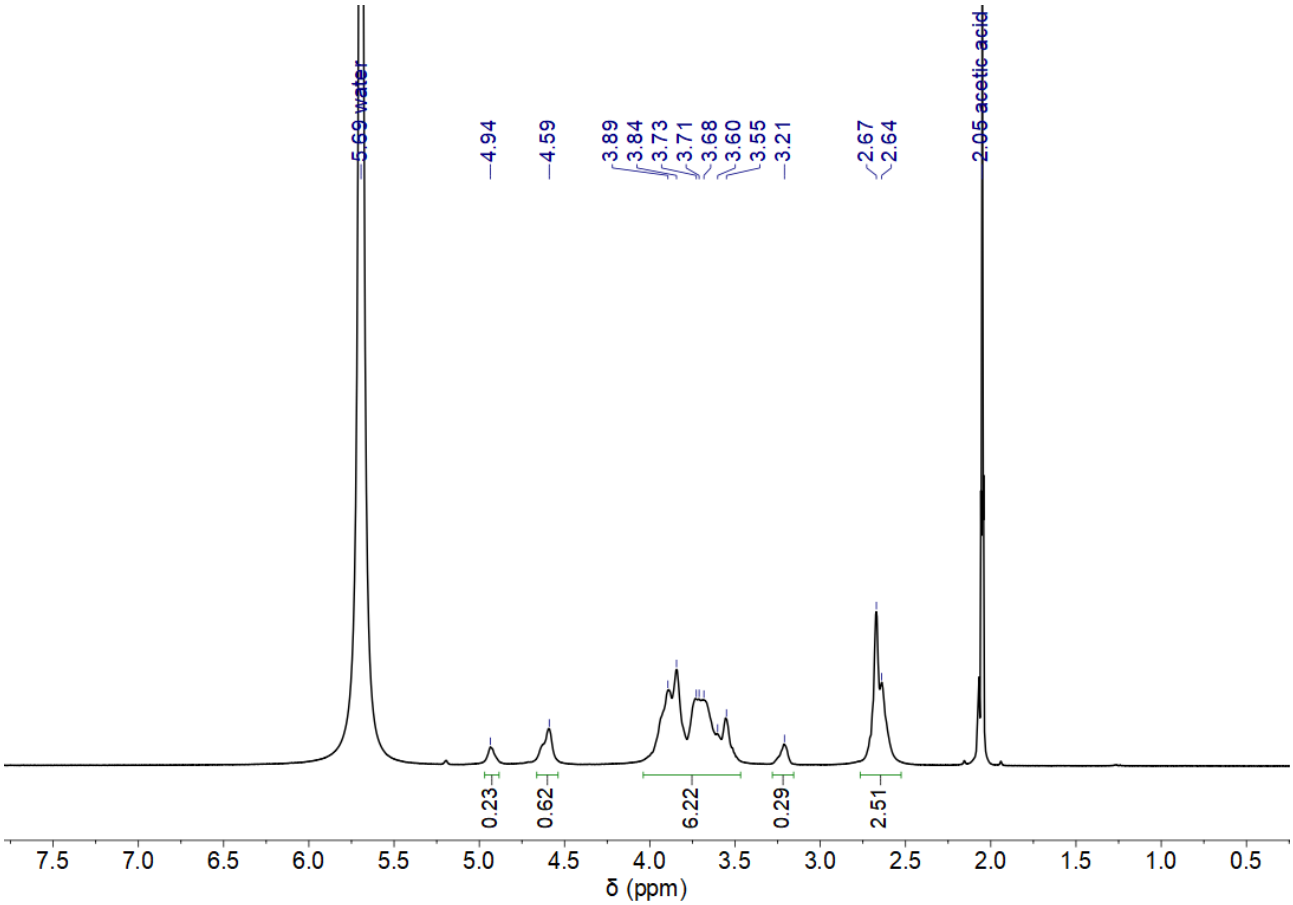

^{1}H NMR (400 MHz, D_2O): δ 4.88 (br, 0.16 H, H1), 4.58 (br, 0.84 H, H1'), 3.98 – 3.45 (m, 5 H, H3-4-5-6), 3.16 (br, 1 H, H2), 2.58 (br, 4 H, H8), 2.06 (br, 3 H, H7).

^{1}H NMR spectrum of **dCS-NSuc** (400 MHz, D_2O)

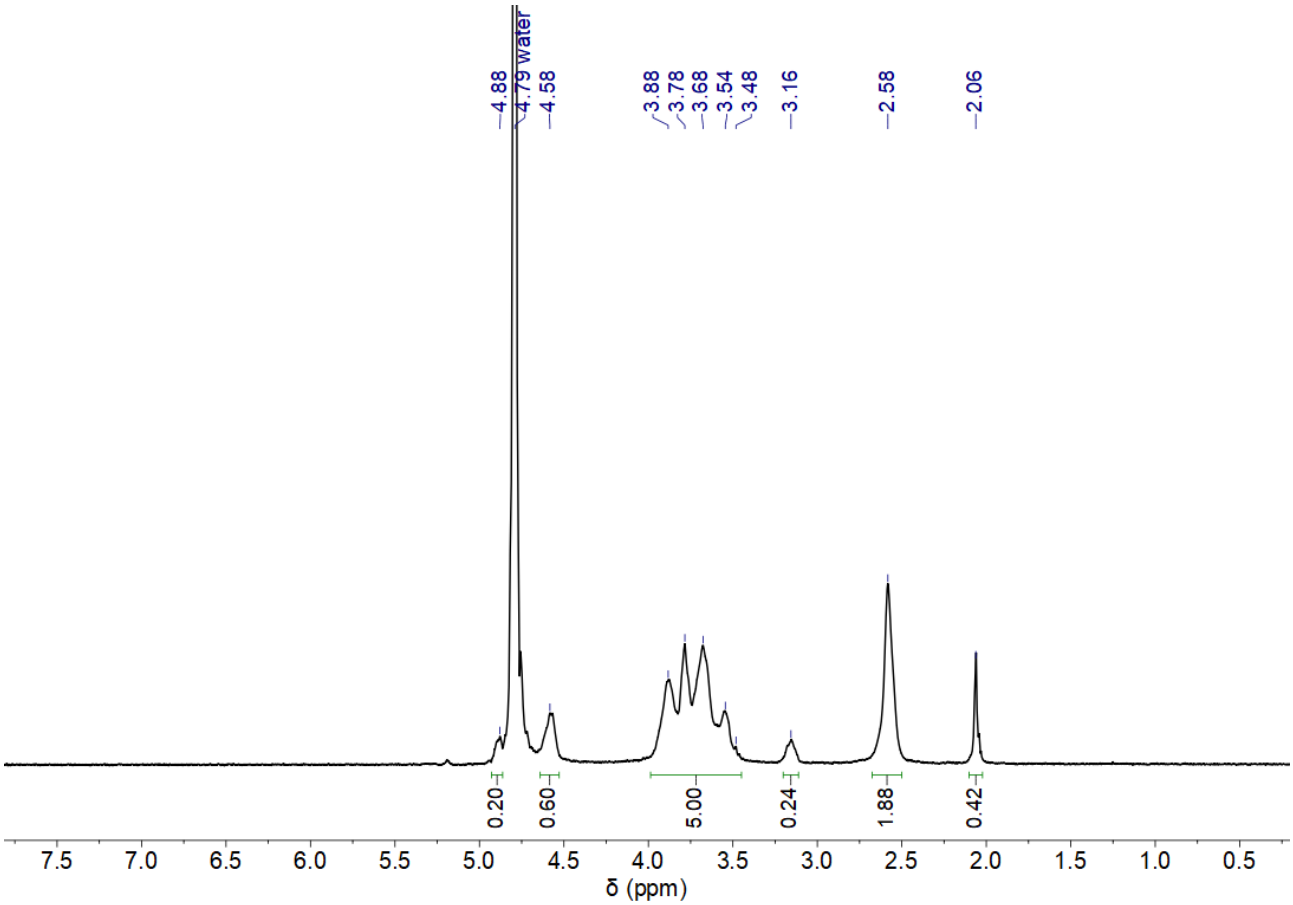

2D-DOSY NMR spectrum of **dCS-NSuc** (600 MHz, D_2O/CD_3COOD 1/1)

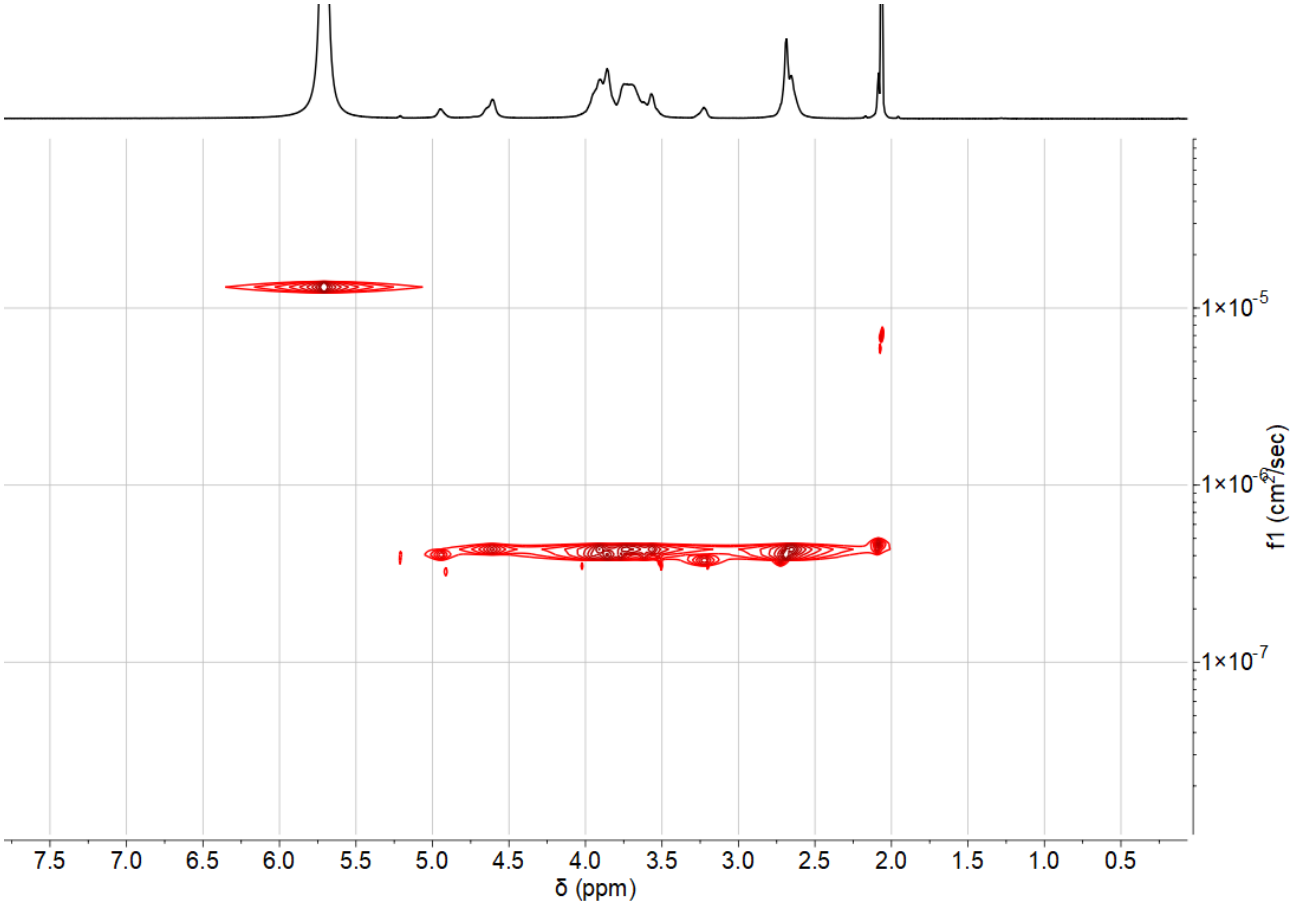

IR (cm^{-1}): 3270, 2930, 1645, 1549, 1378, 1154, 1064, 1029, 898, 622.

Calculation of the number of mol of reactive units (e.g glucosamine units) of dCS (n(glucosamine)):

m(dCS) = m(glucosamine) + m(acetylglucosamine)

= M(glucosamine) x n(glucosamine) + M(acetylglucosamine) x n(acetylglucosamine)

We know that n(acetylglucosamine) = $\frac{AD}{DD}$ x n(glucosamine)

Hence: n(glucosamine) = $\frac{m(dCS)}{M(glucosamine)+(AD/DD)\,x\,M(acetylglucosamine)}$

Here: n(glucosamine) = $\frac{1.00}{161.16 + 0.25\,x\,203.20}$ = 4.72 mmol

Estimation of grafting degree of succinyl group on dCS (GD_{Suc}):

Integrations for H1 + H1' must equal 1. From the spectrum recorded in D_2O/acetic acid-d_4 (1/1), the integration for the succinyl group (2.66 ppm) leads to 2.51 H. Each succinyl group accounts for 4 H.

Hence, GD_{Suc} = $\frac{2.51}{4}$ x 100 = 63%.

NB: GD_{Suc} can be also verified using the spectrum recorded in pure D_2O, by integrating the massif 3.98 – 3.45 ppm at 5 H and using it as a reference. In that case GD_{Suc} = $\frac{1.88}{4}$ x 100 = 47%. Both GD_{Suc} values can then be averaged and use this value as final GD_{Suc}.

Estimation of the molar mass of one average dCS-NSuc unit (M(dCS-NSuc)):

M(dCS-Suc) = GD_{Suc} x M(dCS-NSuc unit) + AD x M(acetylglucosamine) + (1 - GD_{Suc} - AD) x M(glucosamine)

= 0.63 x 261.2 + 0.21 x 203.2 + (1.00 - 0.63 - 0.21) x 161.2 = 233.0 g/mol

Estimation of the molecular weight of one dCS-NSuc chain (MW(dCS-NSuc)):

MW(dCS-NSuc) = Mw(dCS) + GD_{Suc} x M_{Suc} x nb(dCS units)

= 8300 + 0.63 x 101.1 x 49 = 11.4 kDa

with 49 being the number of units per dCS chain (see characterization of dCS for more details).

5.2.2. Core polymers

The compounds described in this section were previously published in "Nicolle *et al.*, *Int. J. Mol. Sci*, **2021**, *22*, 3828".[204]

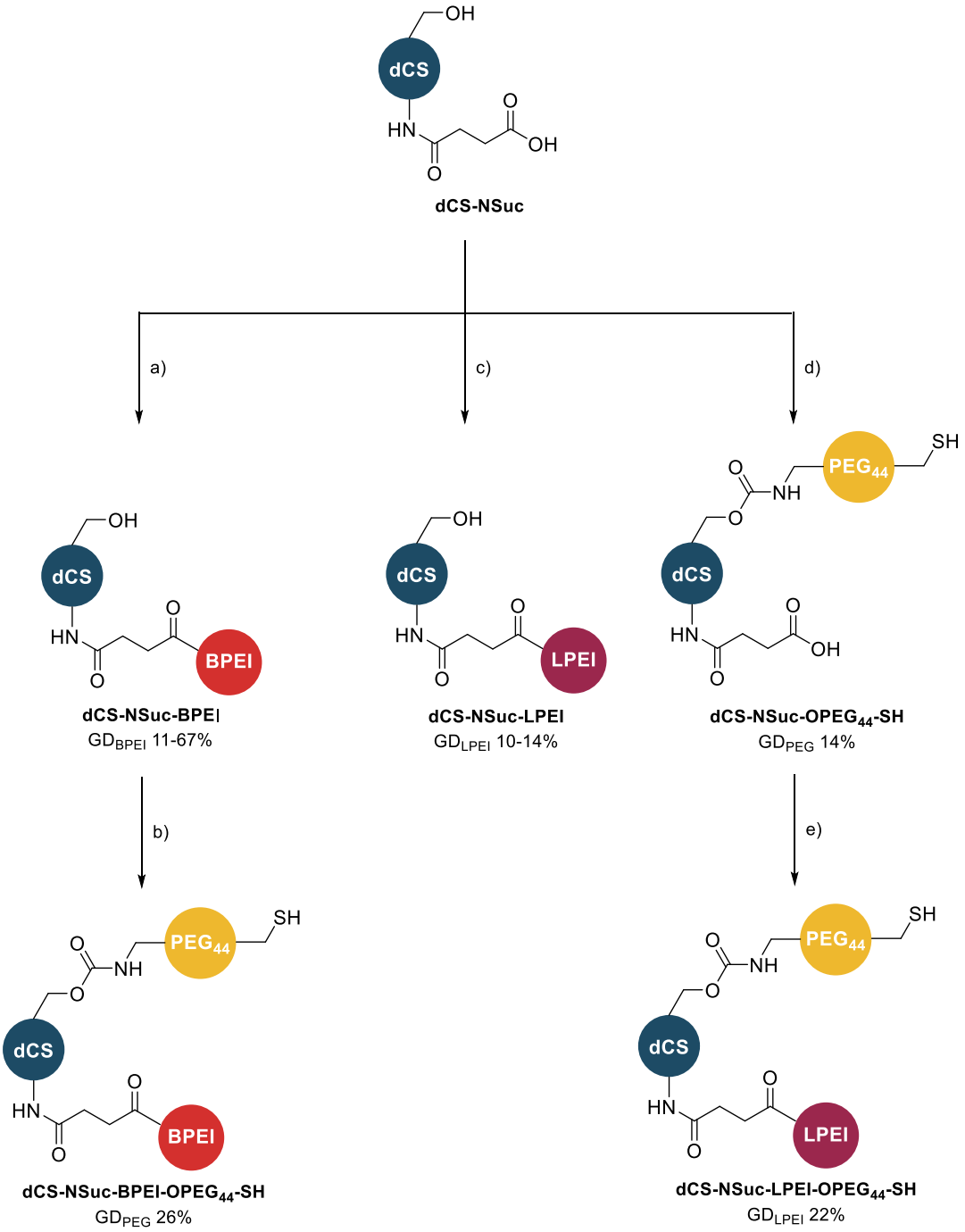

Scheme 28. Preparation of core polymers and cross-linkable assemblies. a) DMTMM, BPEI, H_2O, rt, 3 h. b) CDI, HCl.H_2N-PEG$_{44}$-SH, DMSO, rt, 19 h. c) DMTMM, LPEI, H_2O, 60 °C, 3 h. d) CDI, DIPEA, HCl.H_2N-PEG$_{44}$-SH, DMSO, rt, 17 h. e) DMTMM, DIPEA, LPEI, H_2O, 60 °C, 3 h.

dCS-NSuc-BPEI

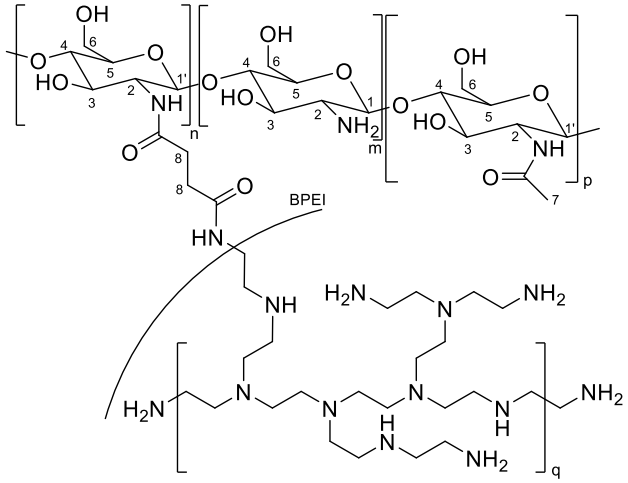

dCS-NSuc (DD 83%, GD_{Suc} 45%, 200 mg, 1.03 mmol, 1.0 equiv.) was dissolved in water (10 mL) for 15 min at rt. DMTMM (285 mg, 1.03 mmol, 1.0 equiv.) was added to this solution, which was stirred for 10 min at rt. To the clear solution was added dropwise a solution of BPEI (2.87 g, 0.638 mmol, 0.62 equiv.) dissolved in 10 mL of water. After 3 h of stirring, the very clear reaction mixture was transferred to a dialysis tube (MWCO 14 kDa) and dialysed against water for 3 days. After centrifugation (4700 rpm, 20 °C, 10 min), the supernatant was recovered and lyophilized. **dCS-NSuc-BPEI** was obtained as a white aerated solid (650 mg, GD_{BPEI} = 18%). **^{1}H NMR (400 MHz, D_2O/CD_3COOD 1:1):** δ 4.94 (br, 0.38 H, H1), 4.60 (br, 0.62 H, H1'), 4.13 – 2.75 (m, 174 H, H2-3-4-5-6 + H_{BPEI}), 2.69 (br, 4 H, H8).

^{1}H NMR spectrum of **dCS-NSuc-BPEI** (400 MHz, D_2O/CD_3COOD 1:1)

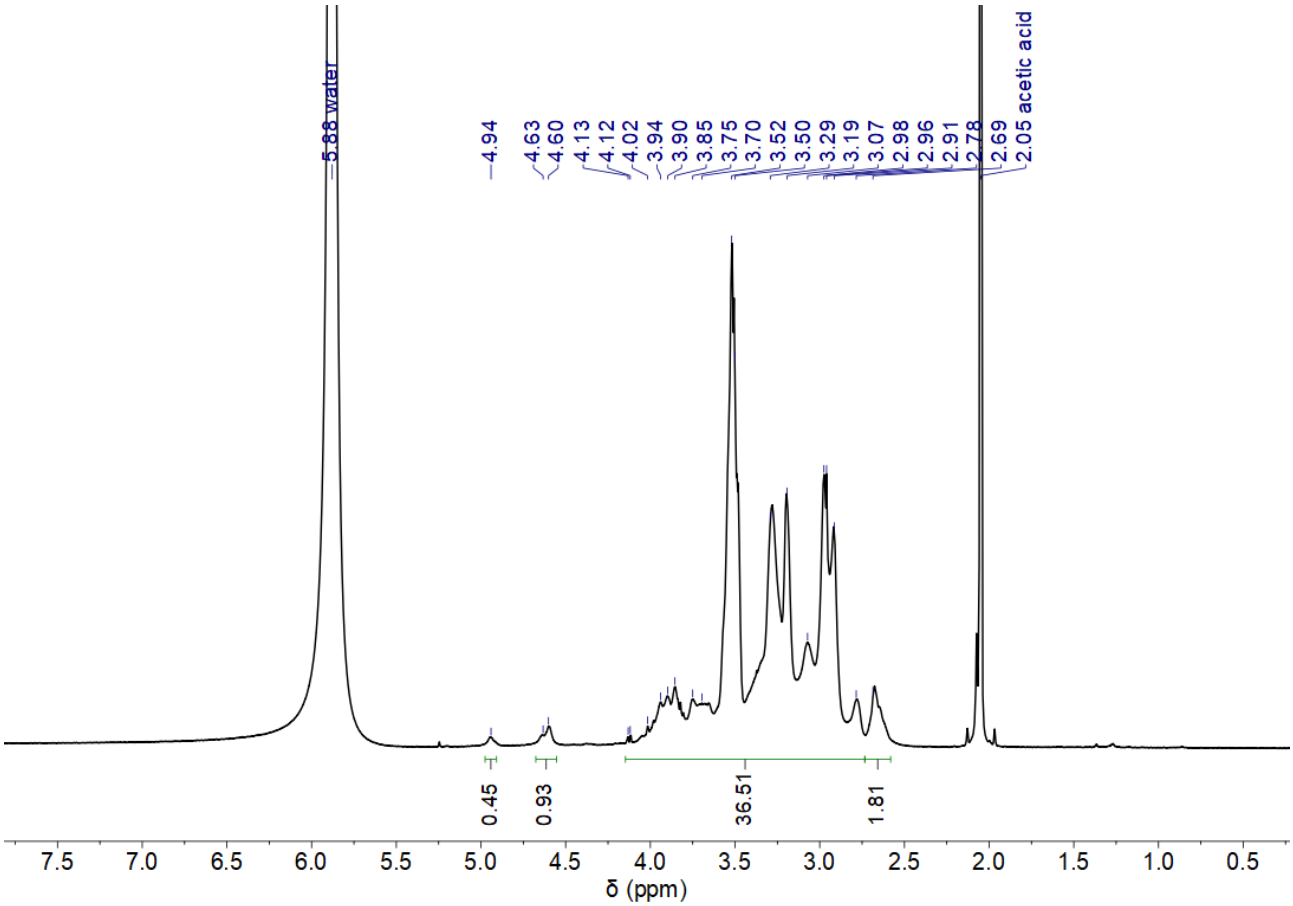

^{1}H NMR (400 MHz, D_2O): δ 4.58 (br, 1 H, H1/1'), 4.01 – 3.08 (m, 6 H, H2-3-4-5-6), 3.07 – 2.47 (br, 172 H, H8 + H_{BPEI}), 2.06 (s, 3 H, H7).

^{1}H NMR spectrum of **dCS-NSuc-BPEI** (400 MHz, D_2O)

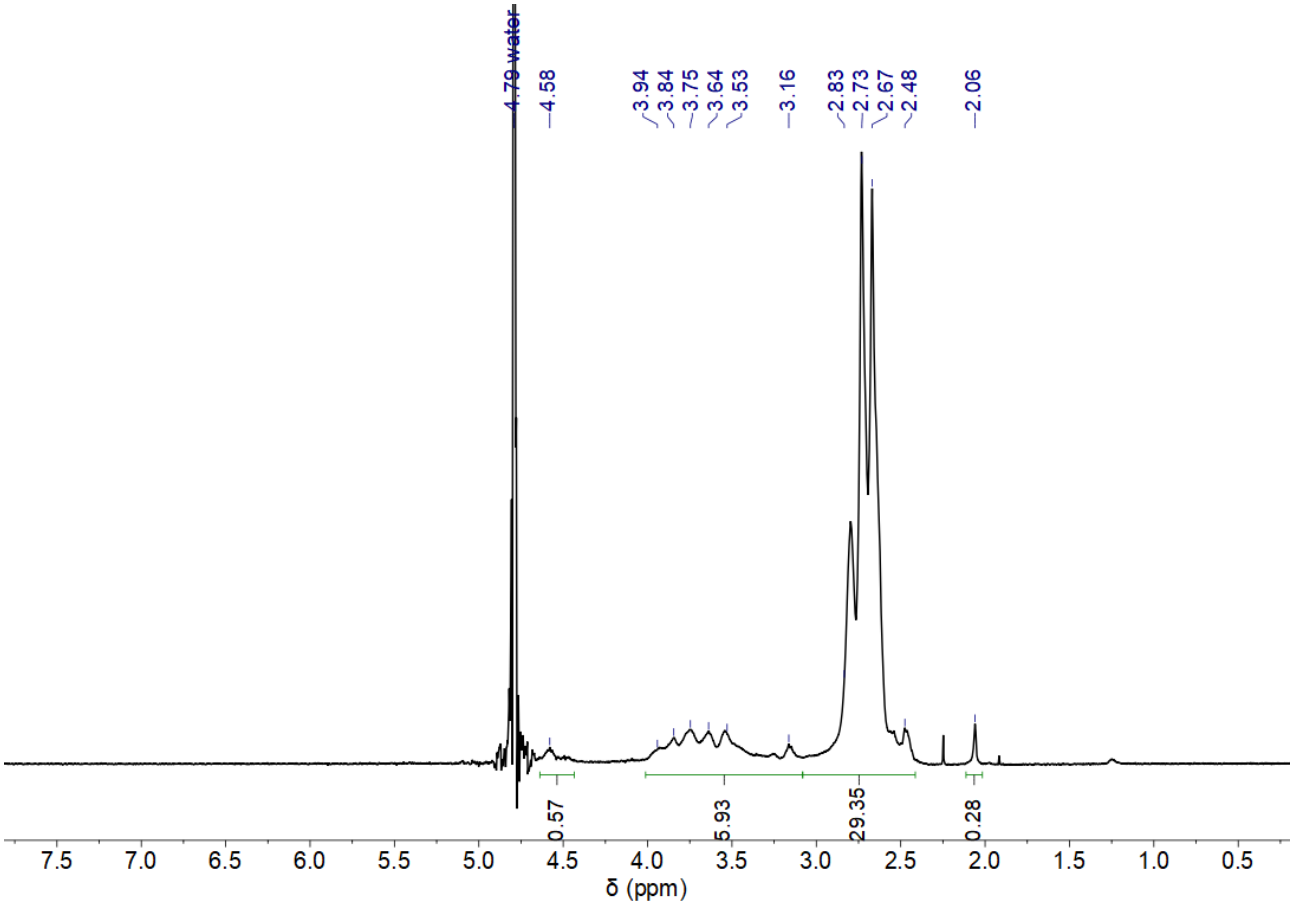

2D-DOSY NMR spectrum of **dCS-NSuc-BPEI** (800 MHz, D_2O/CD_3COOD 1:1)

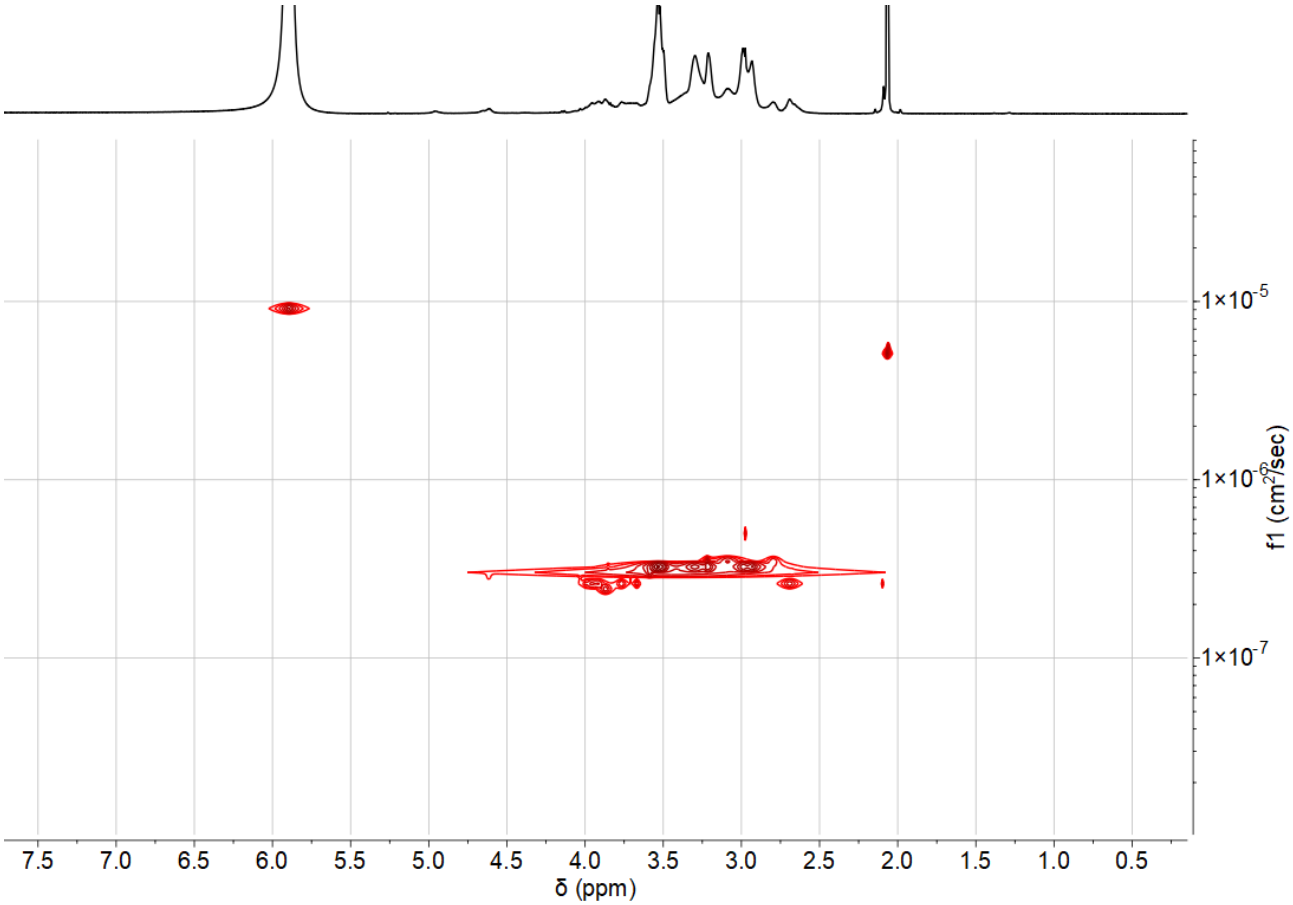

Calculation of the number of mol of dCS-NSuc (n(average)):

$$n(average) = \frac{m(dCS-NSuc)}{M(dCS-NSuc)} = \frac{0.200}{194.3} = 1.03 \text{ mmol}$$

Calculation of the mass of BPEI (m(BPEI)):

BPEI is composed of primary (I), secondary (II) and tertiary (III) amines. Due to steric hindrance, we considered that only primary amines would react. From the supplier data (Sigma Aldrich), for BPEI 1.2 kDa (50 wt% in water): I/II/III amines ratio = 1/0.6/0.9 meaning that only 40% of amino groups of BPEI are considered as reactive functionalities. This ratio was kept for BPEI 1.8 kDa.

$$n(\text{BPEI chains}) = \frac{n(reactive\ BPEI\ groups)}{ratio(I\ amines\ BPEI)} = \frac{0.638}{0.4} = 1.60 \text{ mmol}$$

$$m(\text{BPEI}) = n(\text{BPEI chains}) \times MW(\text{BPEI}) = 1.60 \times 1800 = 2.87 \text{ g}$$

Estimation of grafting degree of BPEI on dCS-NSuc (GD_{BPEI}):

From the spectrum recorded in acetic acid-d_4/D_2O (1/1), the peak from the succinyl group (δ 2.69 ppm) is used as the reference peak. From the previous step, the integration for this peak equals 1.81 H (GD_{Suc} = 45%). The integration of the massif from 4.13 to 2.75 ppm then leads to a total number of 36.5

H, assigned to H2-3-4-5-6 + H_{BPEI}. H_{BPEI} then account for 30.5 H. In one BPEI 1.8 kDa chain, there are 42 units of ethylenimine meaning 168 H in total.

Hence, $GD_{BPEI} = \frac{30.5}{168} \times 100 = 18\%$

For this calculation, we considered that each BPEI chain underwent a single grafting reaction to **dCS-NSuc**.

Estimation of the molar mass of one average dCS-NSuc-BPEI unit (M(dCS-NSuc-BPEI)):

$M(dCS\text{-}NSuc\text{-}BPEI) = GD_{Suc} \times M(dCS\text{-}NSuc\ unit) + AD \times M(acetylglucosamine) + (1 - GD_{Suc} - AD) \times M(glucosamine) + GD_{BPEI} \times MW(BPEI)$

$= 0.45 \times 261.2 + 0.17 \times 203.2 + (1.00 - 0.45 - 0.17) \times 161.2 + 0.18 \times 1800$

$= 576.0$ g/mol

Estimation of the molecular weight of one dCS-NSuc-BPEI chain (MW(dCS-NSuc-BPEI)):

$MW(dCS\text{-}NSuc\text{-}BPEI) = Mw(dCS) + GD_{Suc} \times M_{Suc} \times nb(dCS\ units) + GD_{BPEI} \times MW(BPEI) \times nb(dCS\ units)$

$= 7800 + 0.45 \times 101.1 \times 46 + 0.18 \times 1800 \times 46$

$= 24.8$ kDa

with 46 being the number of units per **dCS** chain (see characterization of **dCS** for more details).

dCS-NSuc-LPEI

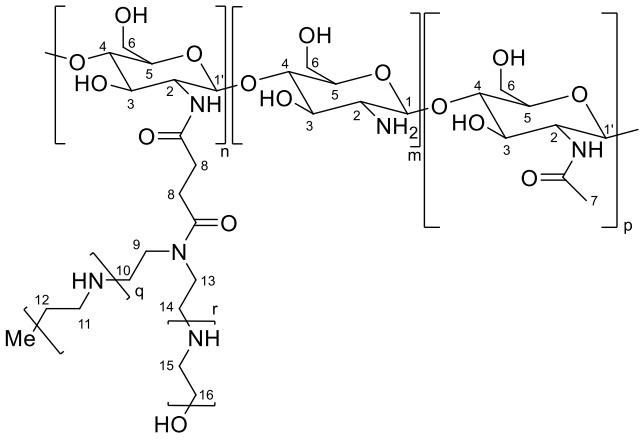

dCS-NSuc (DD 79%, GD_{Suc} 63%, 200 mg, 0.542 mmol of reactive units, 1.0 equiv.) was dissolved in water (20 mL) over 15 min from rt to 50 °C. DMTMM (150 mg, 0.542 mmol, 1.0 equiv.) was added in one portion, followed by heating of the reaction mixture at 60 °C for 10 min (clear solution). LPEI (678 mg, 0.271 mmol, 0.5 equiv.) was added in 4 equal portions and under vigorous stirring (> 500 rpm). pH was controlled at 10. After 3 h of heating at 60 °C under vigorous stirring, the mixture was cooled down and split into 6 dialysis tubes (MWCO 7 kDa). They were diluted with additional water (30 mL) and dialyzed against water for 3 days. After centrifugation (4700 rpm, 20 °C, 10 min), the supernatant was recovered and lyophilized. **dCS-NSuc-LPEI** was obtained as a white

aerated solid (135 mg, GD_{LPEI} = 14%). **^{1}H NMR (600 MHz, D_2O/CD_3COOD 1:1):** δ 4.93 (br, 0.16 H, H1), 4.60 (br, 0.84 H, H1'), 4.14 – 2.96 (m, 238 H, H2-3-4-5-6-9-10-11-12-13-14-15-16), 2.66 (br, 4 H, H8). δ 2.47, 1.25, 1.10 are impurities present in all commercial batches of LPEI.

^{1}H NMR spectrum of **dCS-NSuc-LPEI** (600 MHz, D_2O/CD_3COOD 1:1)

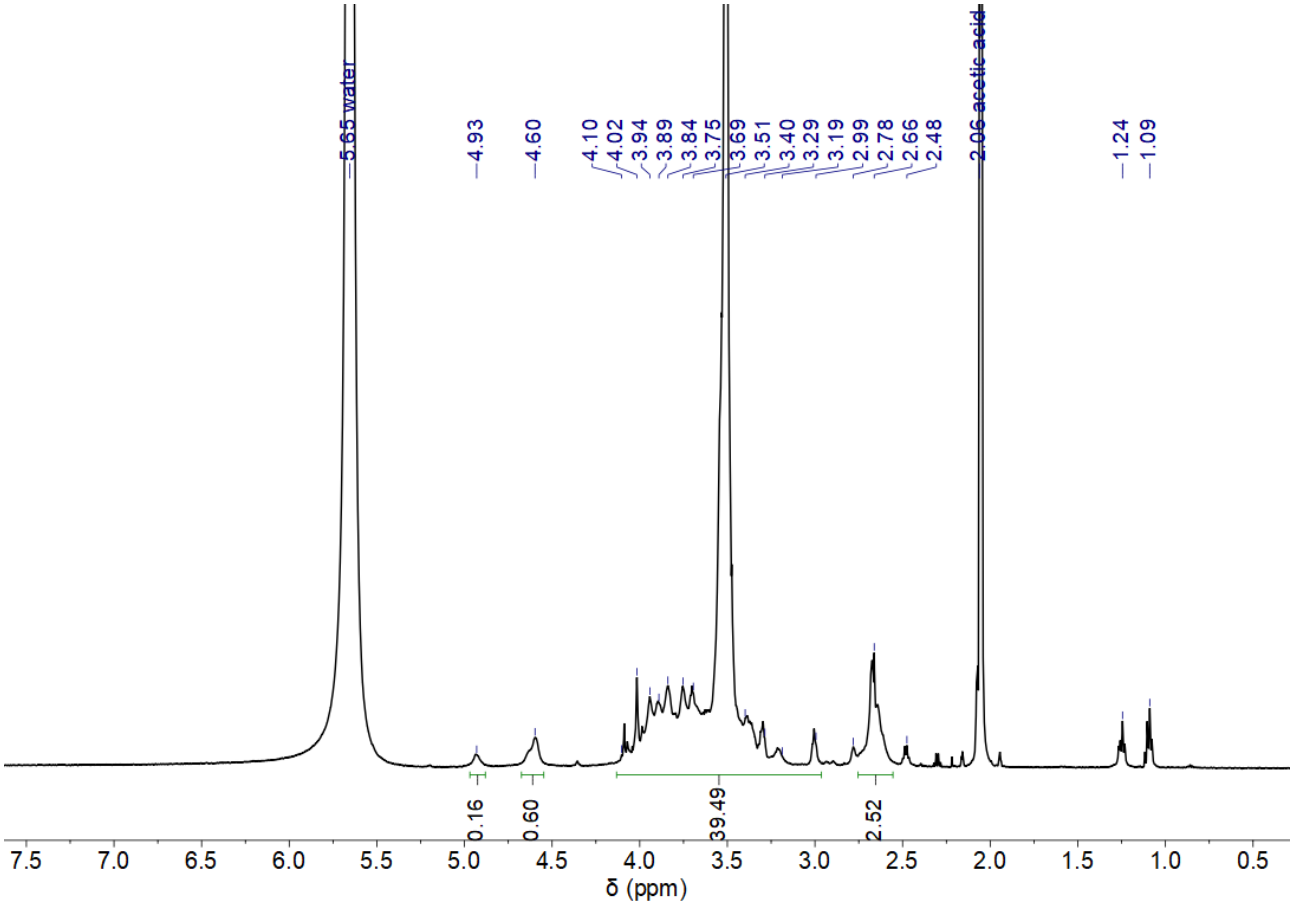

^{1}H NMR (400 MHz, D_2O): δ 4.66 – 4.45 (m, 1 H, H1/1'), 4.12 – 2.64 (m, 238 H, H2-3-4-5-6-9-10-11-12-13-14-15-16), 2.63 – 2.44 (br, 4 H, H8), 2.06 (s, 3 H, H7). δ 1.21, 1.10 are impurities present in all commercial batches of LPEI.

^{1}H NMR spectrum of **dCS-NSuc-LPEI** (400 MHz, D_2O)

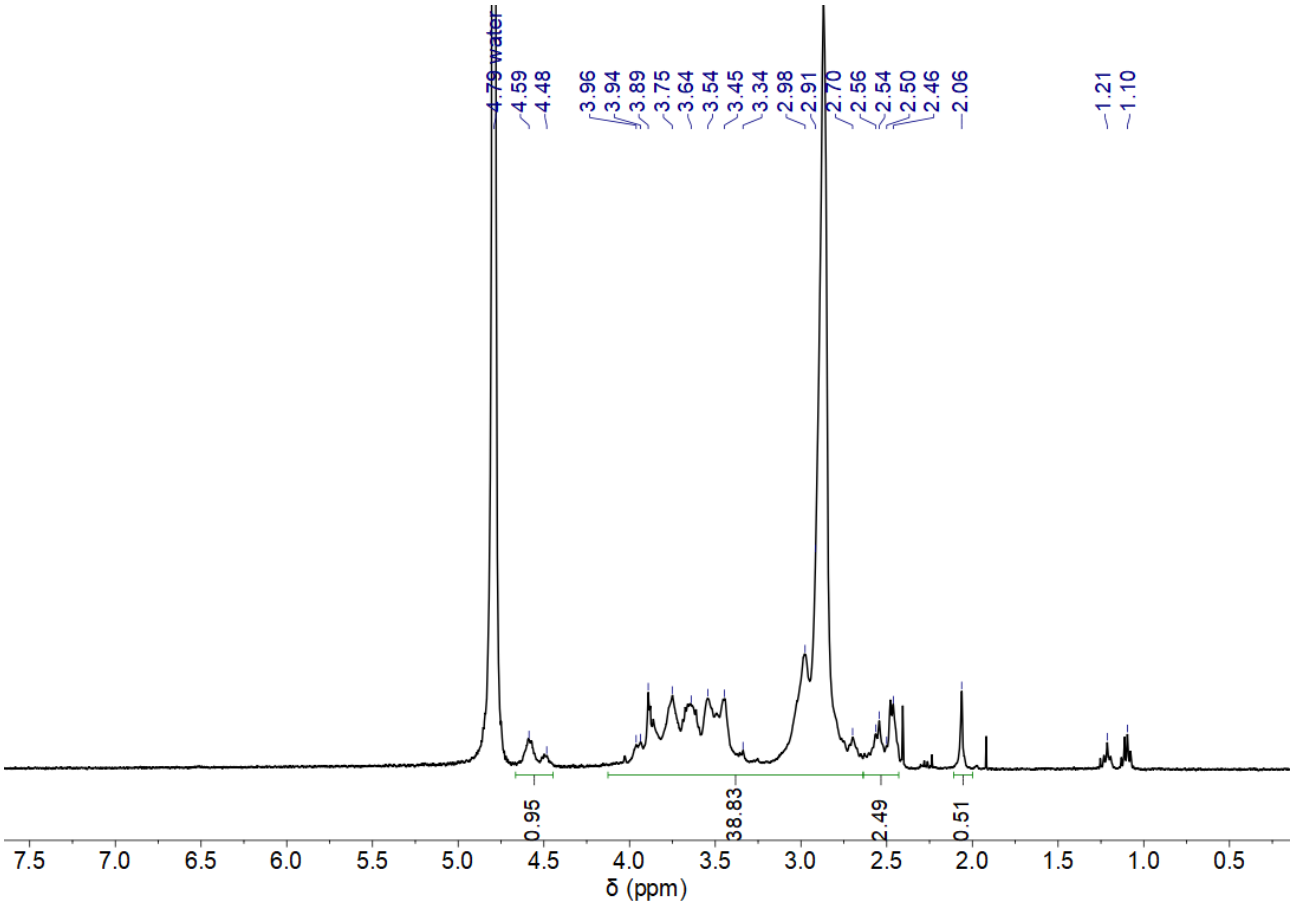

2D-DOSY NMR spectrum of **dCS-NSuc-LPEI** (600 MHz, D_2O/CD_3COOD 1:1)

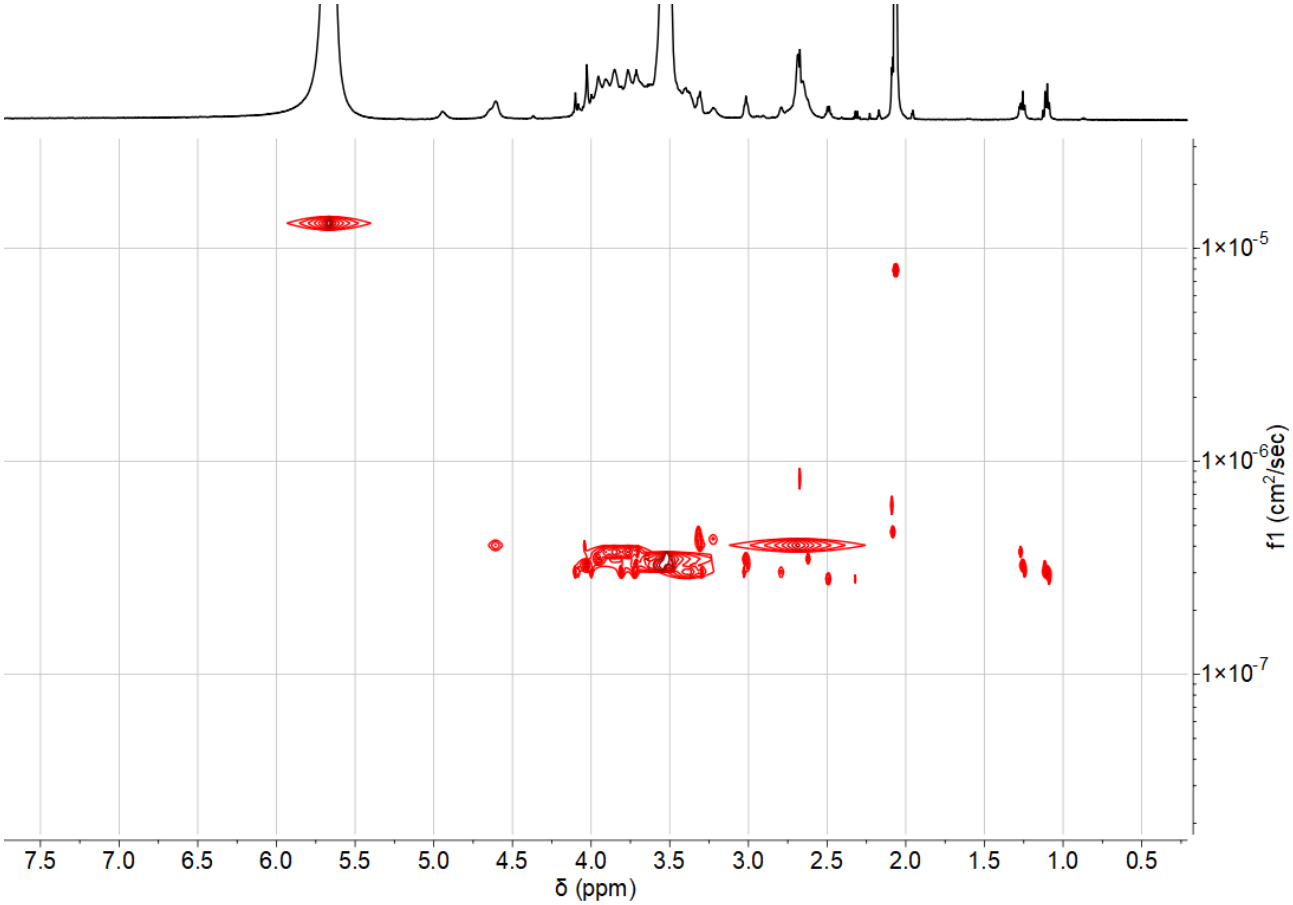

IR (cm^{-1}): 3272, 2917, 2847, 1651, 1555, 1464, 1408, 1372, 1303, 1109, 1063, 1030, 899, 812, 646.

Calculation of the number of mol of reactive units (e.g succinylated glucosamine units) of dCS-NSuc (n(reactive units)):

As GD_{Suc} = 63% and DD = 79%, the molar mass of one average unit of dCS-NSuc is M(dCS-NSuc) = 233.0 g/mol (cf. characterization of dCS-NSuc for more details), hence:

n(average units) = $\frac{m(dCS-NSuc)}{M(dCS-NSuc)} = \frac{0.200}{233.0}$ = 0.860 mmol and as only 63% of the dCS units are reactive (because GD_{Suc} = 63%), then n(reactive units) = 0.860 x 0.63 = 0.542 mmol

Estimation of grafting degree of LPEI on dCS-NSuc (GD_{LPEI}):

From the spectrum recorded in acetic acid-d^4/D_2O (1/1), the peak from the succinyl group (2.66 ppm) is used as the reference peak. From the previous step, the integration for this peak equals 2.52 (GD_{Suc} = 63%). This value is reported on the present spectrum. The integration of the massif from 4.14 to 2.96 ppm leads to a total number of 39.5 H, assigned to H2-3-4-5-6-9-10-11-12-13-14-15-16. The protons from LPEI (H9-10-11-12-13-14-15-16) account for 33.5 H. In one LPEI 2.5 kDa chain, there are 58 units of ethylenimine, accounting for a total of 232 H.

Hence, $GD_{LPEI} = \frac{33.5}{232}$ x 100 = 14%

For this calculation, we considered that each LPEI chain underwent a single grafting reaction to dCS-NSuc.

Estimation of the molar mass of one average dCS-NSuc-LPEI unit (M(dCS-NSuc-LPEI)):

M(dCS-NSuc-LPEI) = GD_{Suc} x M(dCS-NSuc unit) + AD x M(acetylglucosamine) + (1 - GD_{Suc} - AD) x M(glucosamine) + GD_{LPEI} x MW(LPEI)

= 0.63 x 261.2 + 0.21 x 203.2 + (1.00 - 0.63 - 0.21) x 161.2 + 0.14 x 1800

= 583.0 g/mol

Estimation of the molecular weight of one dCS-NSuc-LPEI chain (MW(dCS-NSuc-LPEI)):

MW(dCS-NSuc-LPEI) = Mw(dCS) + GD_{Suc} x M_{Suc} x nb(dCS units) + GD_{LPEI} x MW(LPEI) x nb(dCS units)

= 8300 + 0.63 x 101.1 x 49 + 0.14 x 2500 x 49

= 28.6 kDa

with 49 being the number of units per dCS chain (cf. dCS characterization for more details).

dCS-NSuc-BPEI-OPEG$_{44}$-SH

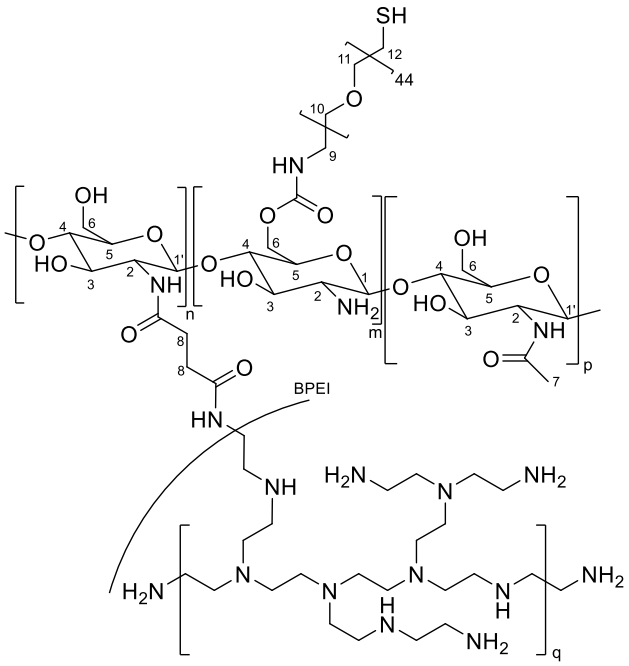

dCS-NSuc-BPEI (DD 80%, GD_{Suc} 47%, GD_{BPEI} 11%, 30.0 mg, 0.0724 mmol, 1.0 equiv.) was dissolved in dry DMSO (2.5 mL) over 15 min at rt. After addition of CDI (12.0 mg, 0.0724 mmol, 1.0 equiv.), the white suspension was stirred at rt for 30 min. A solution of HCl.H_2N-PEG$_{44}$-SH (29 mg, 0.0145 mmol, 0.20 equiv.) in 0.5 mL of DMSO was then added dropwise. The reaction mixture was stirred at rt for 19 h, before being dialyzed against water for 3 days (MWCO 14 kDa). The solution remained homogeneous over time. It was then centrifuged (4700 rpm, 20 °C, 10 min) and the supernatant was lyophilized. **dCS-NSuc-BPEI-OPEG$_{44}$-SH** was obtained as a white aerated solid (37.3 mg, GD_{PEG} = 26%). **^{1}H NMR (600 MHz, D_2O/CD_3COOD 1:1):** δ 4.94 (br, 0.33 H, H1), 4.60 (br, 0.67 H, H1'), 4.02 – 2.74 (m, 354 H, H2-3-4-5-6-9-10-11-12 + H_{BPEI}), 2.66 (br, 4 H, H8).

^{1}H NMR spectrum of **dCS-NSuc-BPEI-OPEG$_{44}$-SH** (600 MHz, D_2O/CD_3COOD 1:1)

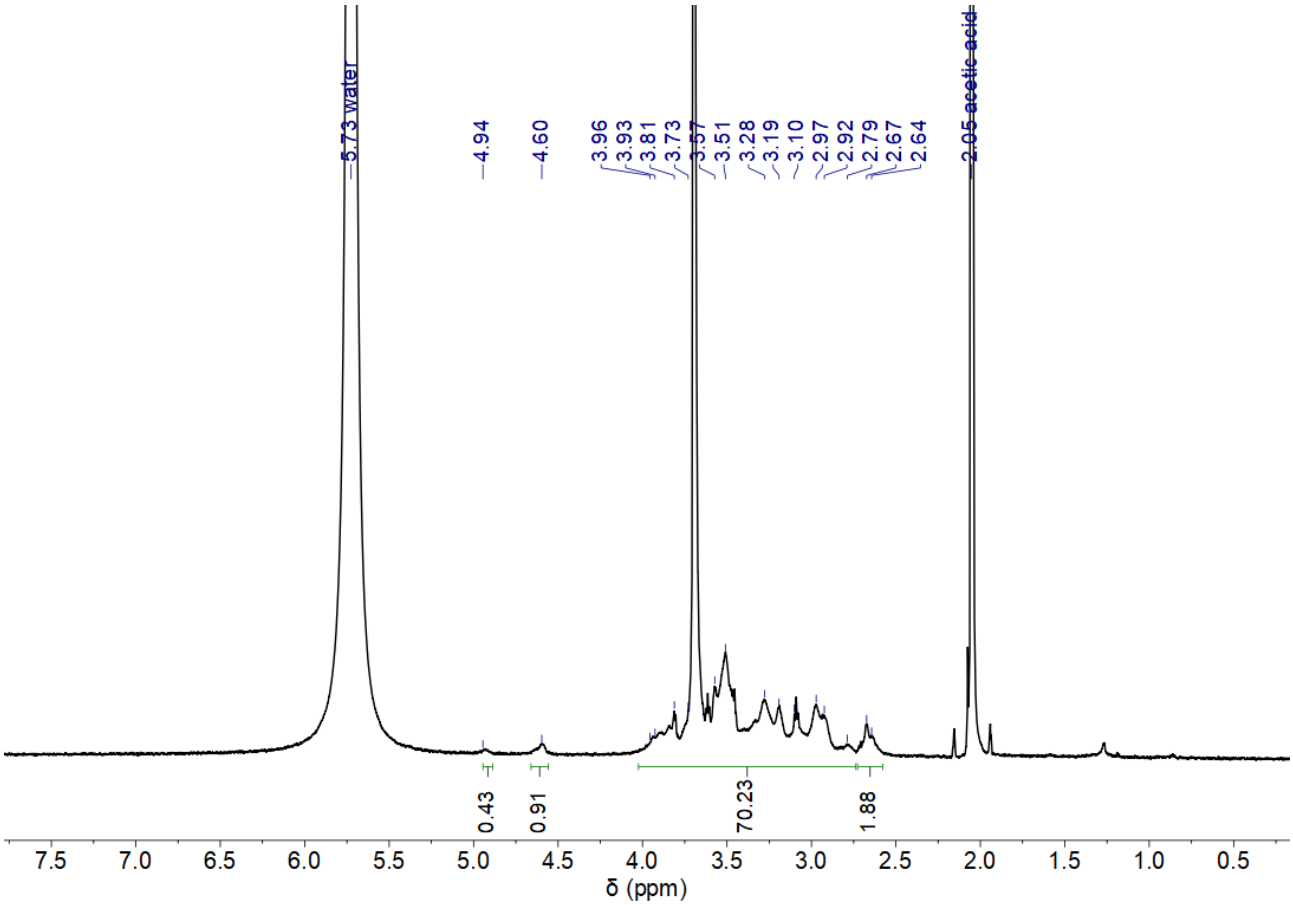

^{1}H NMR (400 MHz, D_2O): δ 4.65 – 4.43 (br, 1 H, H1/1'), 4.00 – 2.41 (m, 358 H, H2-3-4-5-6-8-9-10-11-12 + H_{BPEI}), 2.06 (s, 3 H, H7).

^{1}H NMR spectrum of **dCS-NSuc-BPEI-OPEG$_{44}$-SH** (400 MHz, D_2O)

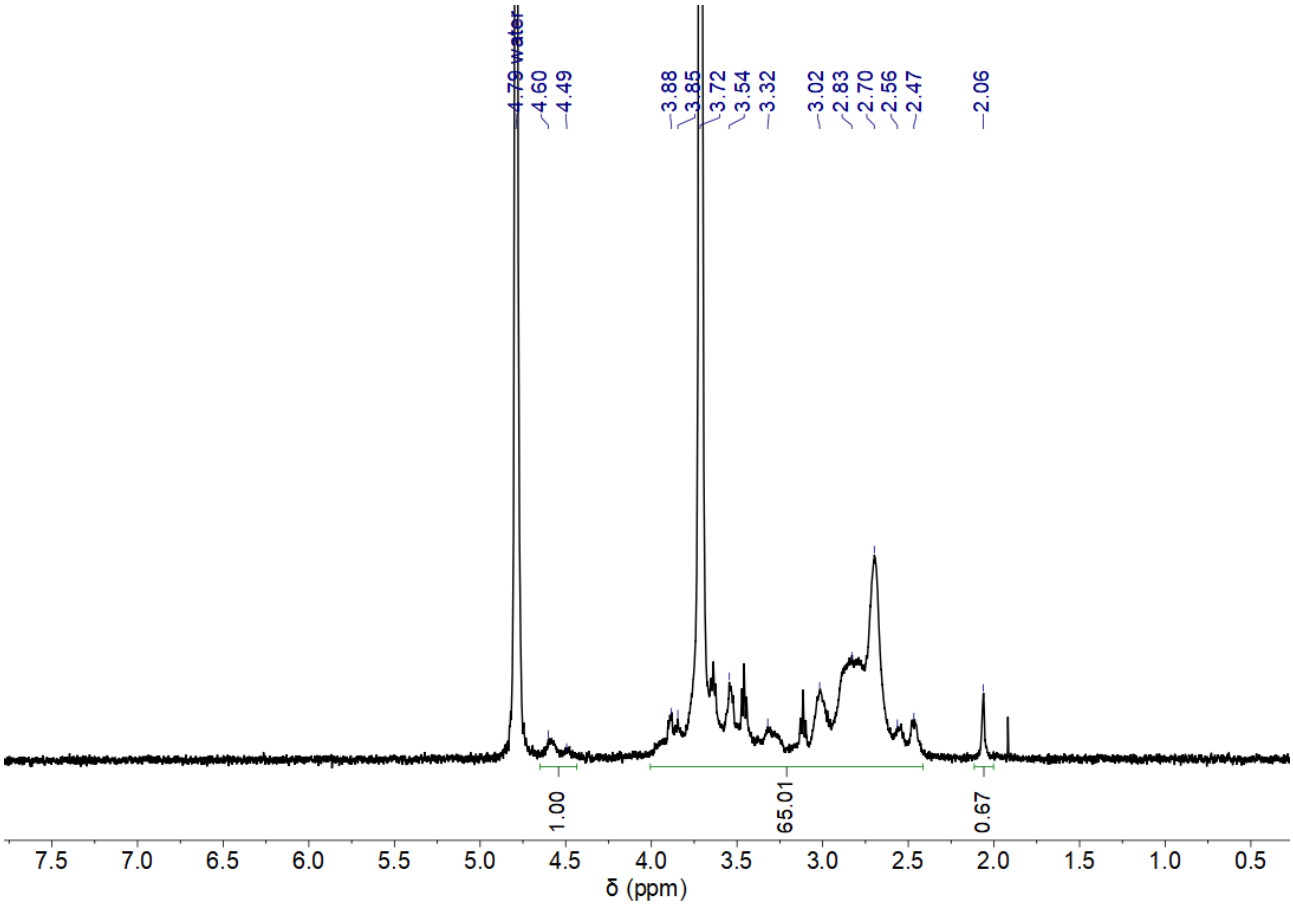

2D-DOSY NMR spectrum of **dCS-NSuc-BPEI-OPEG$_{44}$-SH** (600 MHz, D_2O/CD_3COOD 1:1)

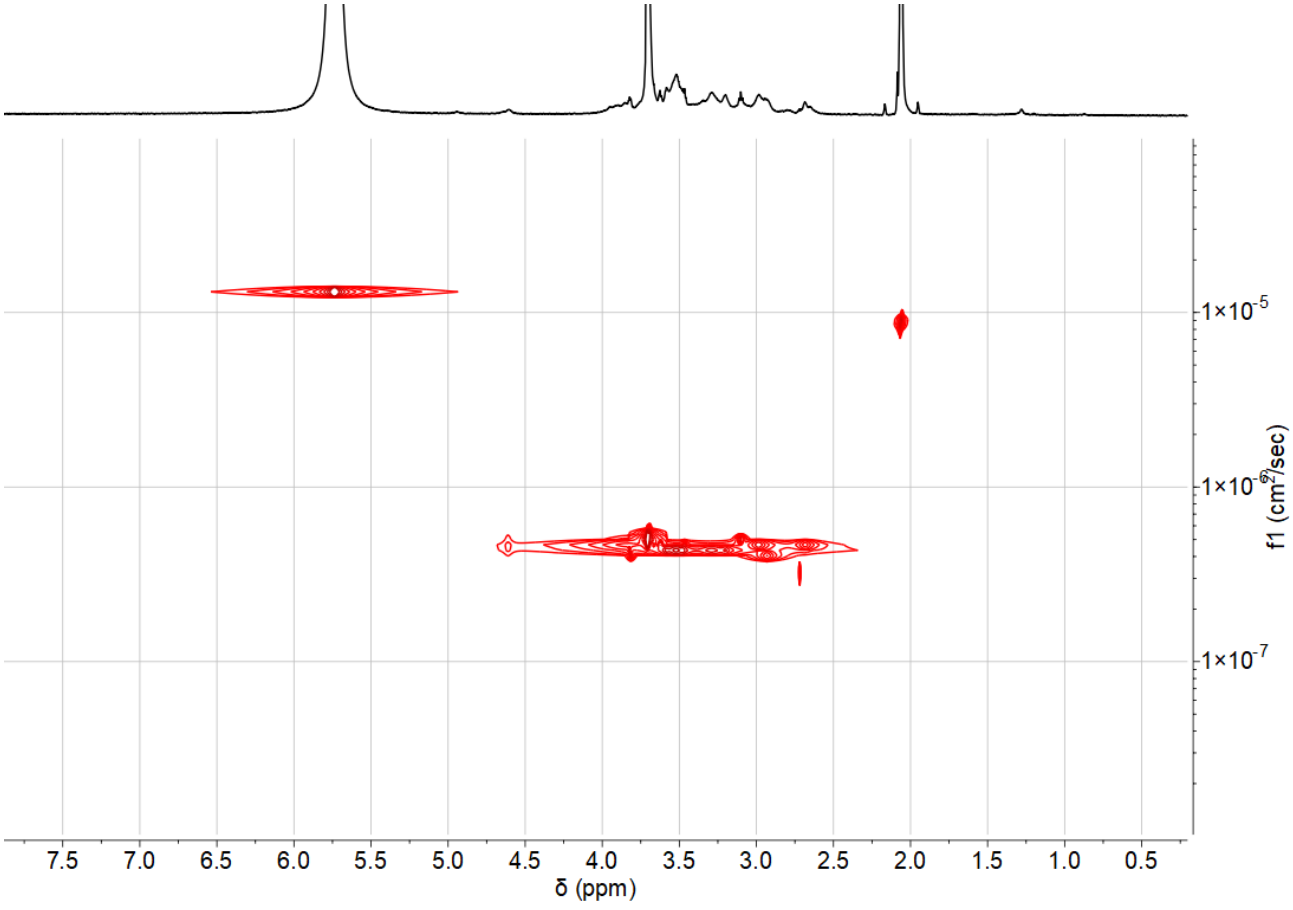

Estimation of the grafting degree of H_2N-PEG_{44}-SH on dCS-NSuc-BPEI (GD_{PEG}):

From the spectrum recorded in D_2O/CD_3COOD (1/1), the peak from the succinyl group (δ 2.66 ppm) is used as the reference peak. From the previous step, the integration for this peak equals 1.88 (GD_{Suc} = 47%). The integration of the massif from 4.02 to 2.74 ppm leads to a total number of 70 H, assigned to H2-3-4-5-6 from dCS, H9-10-11-12 from PEG and H_{BPEI} (GD_{BPEI} = 11%). There are then 46 H for H9-10-11-12. In one chain of H_2N-PEG_{44}-SH (2 kDa), there are 180 H.

Hence, $GD_{PEG} = \frac{46}{180}$ x 100 = 26%

Estimation of the molecular weight of one dCS-NSuc-BPEI-$OPEG_{44}$-SH chain (MW(dCS-NSuc-BPEI-$OPEG_{44}$-SH)):

MW(dCS-NSuc-BPEI-$OPEG_{44}$-SH) = Mw(dCS) + GD_{Suc} x M_{Suc} x nb(dCS units) + GD_{BPEI} x MW(BPEI) x nb(dCS units) + GD_{PEG} x MW(PEG) x nb(dCS units)

= 7800 + 0.47 x 101.1 x 46 + 0.11 x 1800 x 46 + 0.26 x 2042 x 46

= 43.5 kDa

with 46 being the number of units per dCS chain (cf. characterization of dCS for more details).

dCS-NSuc-$OPEG_{44}$-SH

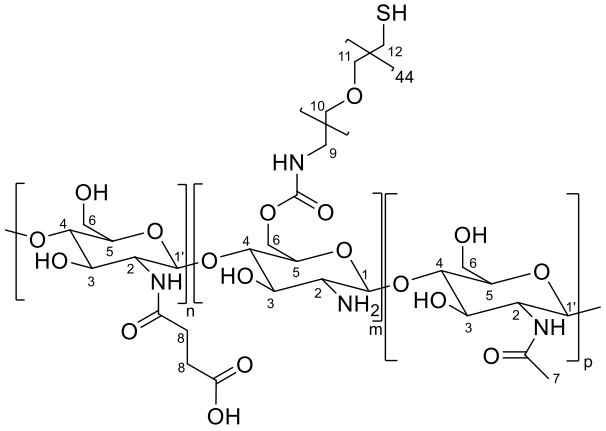

To a solution of **dCS-NSuc** (DD 85%, GD_{Suc} 44%, 100 mg, 0.473 mmol, 1.0 equiv.) in 6 mL of dry DMSO, was added CDI (77 mg, 0.473 mmol, 1.0 equiv.) at rt. The white homogenous mixture was stirred at rt for 30 min. DIPEA (41 µL, 0.236 mmol, 0.50 equiv.) was then added to the reaction mixture, followed by a dropwise addition of a solution of HCl.H_2N-PEG_{44}-SH (194 mg, 0.0946 mmol, 0.20 equiv.) in DMSO (4 mL). After 17 h of stirring at rt, the white mixture was transferred to a dialysis tube (MWCO 7 kDa) and dialyzed against water for 3 days. The solution was centrifuged (4700 rpm, 20 °C, 10 min) and the supernatant was lyophilized. **dCS-NSuc-$OPEG_{44}$-SH** was obtained as a white aerated solid (200 mg, GD_{PEG} = 14%). **^{1}H NMR (400 MHz, D_2O/CD_3COOD 1:1):** δ 4.93 (br, 0.41 H, H1), 4.60 (br, 0.59 H, H1'), 4.18 – 3.03 (m, 184 H, H2-3-4-5-6-9-10-11), 2.94 (t, 2H, H12), 2.66 (br, 4 H, H8).

^{1}H NMR spectrum of **dCS-NSuc-$OPEG_{44}$-SH** (400 MHz, D_2O/CD_3COOD 1:1)

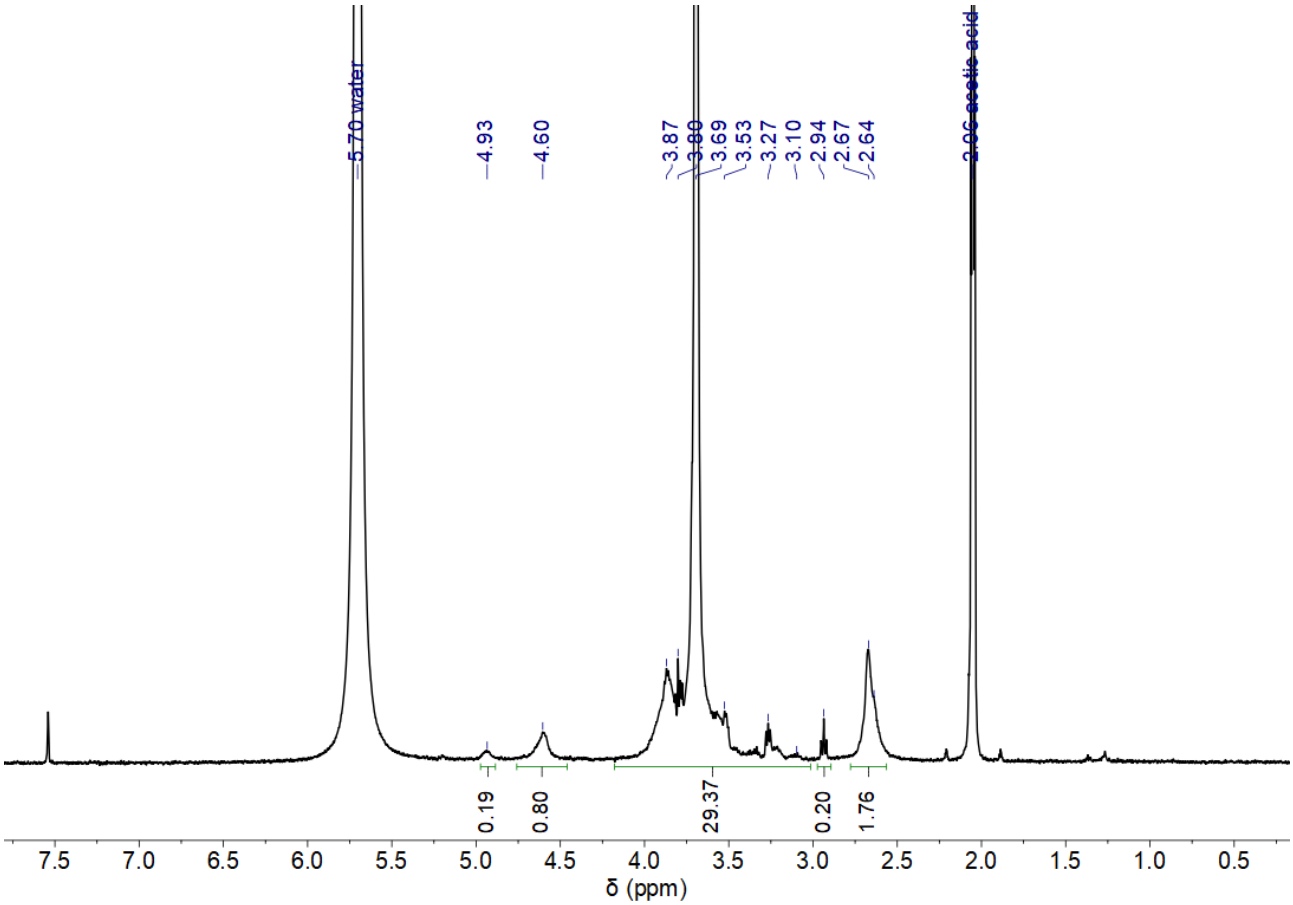

2D-DOSY NMR spectrum of **dCS-NSuc-OPEG$_{44}$-SH** (400 MHz, D_2O/CD_3COOD 1:1)

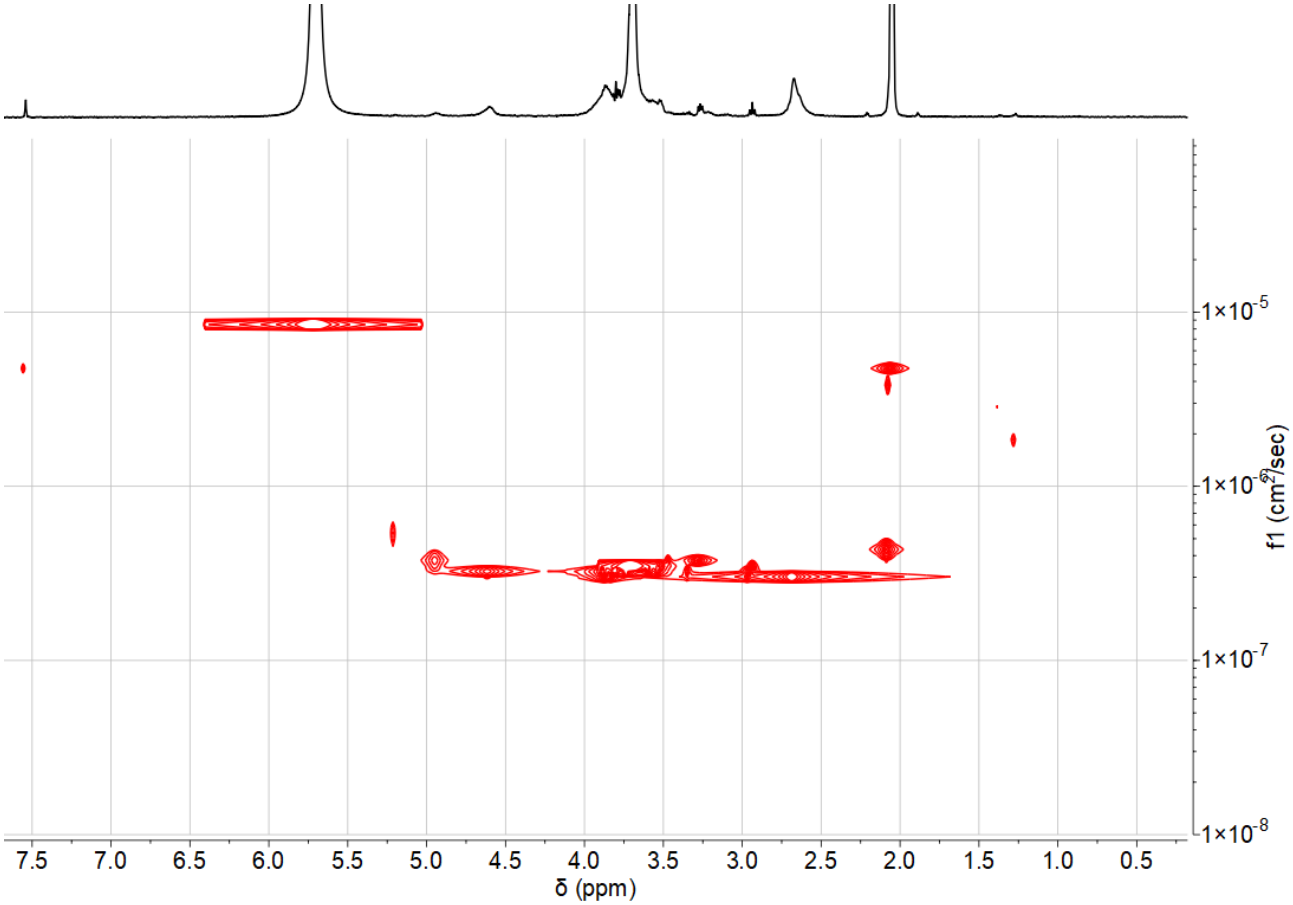

Estimation of the grafting degree of H_2N-PEG_{44}-SH on dCS-NSuc (GD_{PEG}):

From the spectrum recorded in D_2O/CD_3COOD (1/1), the peak from the succinyl group (δ 2.66 ppm) is used as the reference peak. From the previous step, the integration for this peak equals 1.76 (GD_{Suc} = 44%). The integration of the massif from 4.18 to 3.03 ppm and of the triplet at δ 2.94 ppm leads to a total number of 29.6 H, assigned to H2-3-4-5-6 from dCS and H9-10-11-12 from PEG. The protons from PEG account for 29.6 H and in one H_2N-PEG_{44}-SH chain, there are 180 H.

Hence, $GD_{PEG} = \frac{23.6}{180}$ x 100 = 14%

Estimation of the molar mass of one average dCS-NSuc-$OPEG_{44}$-SH unit (M(dCS-NSuc-$OPEG_{44}$-SH)):

M(dCS-NSuc-$OPEG_{44}$-SH) = GD_{Suc} x M(dCS-NSuc unit) + AD x M(acetylglucosamine) + (1 - GD_{Suc} - AD) x M(glucosamine) + GD_{PEG} x MW(PEG)

= 0.44 x 261.2 + 0.15 x 203.2 + (1.00 - 0.44 - 0.15) x 161.2 + 0.14 x 2042

= 498.6 g/mol

Estimation of the molecular weight of one dCS-NSuc-$OPEG_{44}$-SH chain (MW(dCS-NSuc-$OPEG_{44}$-SH)):

MW(dCS-NSuc-$OPEG_{44}$-SH) = Mw(dCS) + GD_{Suc} x M_{Suc} x nb(dCS units) + GD_{PEG} x MW(PEG) x nb(dCS units)

= 7800 + 0.44 x 101.1 x 46 + 0.14 x 2042 x 46

= 23.0 kDa

with 46 being the number of units per dCS chain (cf. characterization of dCS for more details).

dCS-NSuc-LPEI-$OPEG_{44}$-SH

To a clear solution of **dCS-NSuc-$OPEG_{44}$-SH** (DD 85%, GD_{Suc} 44%, GD_{PEG} 14%, 50.0 mg, 0.100 mmol, 1.0 equiv.) in 8 mL of water, was added at rt DMTMM (13.9 mg, 0.050 mmol, 0.500 equiv.) in one portion.

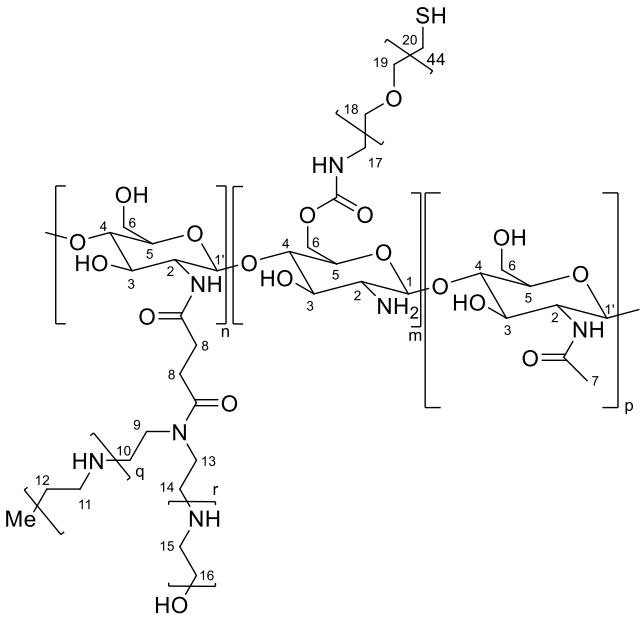

After 15 min of stirring from rt to 60 °C, LPEI (125 mg, 0.050 mmol, 0.50 equiv.) was added to the reaction mixture in 4 portions. Finally, DIPEA (3.5 µL, 0.020 mmol, 0.20 equiv.) was added and the reaction mixture was stirred at 60 °C for 3 h. After cooling down, the homogenous mixture was split into two dialysis tubes (MWCO 7 kDa) and dialyzed against water for 3 days. The solution was centrifuged (4700 rpm, 20 °C, 10 min), and the supernatant was freeze-dried to yield **dCS-NSuc-LPEI-OPEG$_{44}$-SH** as a white aerated solid (37.0 mg, GD_{LPEI} = 22%). **^{1}H NMR (600 MHz, D_2O/CD_3COOD 1:1):** δ 4.95 (br, 0.41 H, H1), 4.61 (br, 0.59 H, H1'), 4.12 – 3.20 (m, 418 H, H2-3-4-5-6-9-10-11-12-13-14-15-16-17-18-19-20), 2.67 (br, 4 H, H8). δ 2.49, 1.26, 1.10 are impurities present in the commercial batches of LPEI.

^{1}H NMR spectrum of **dCS-NSuc-LPEI-OPEG$_{44}$-SH** (600 MHz, D_2O/CD_3COOD 1:1)

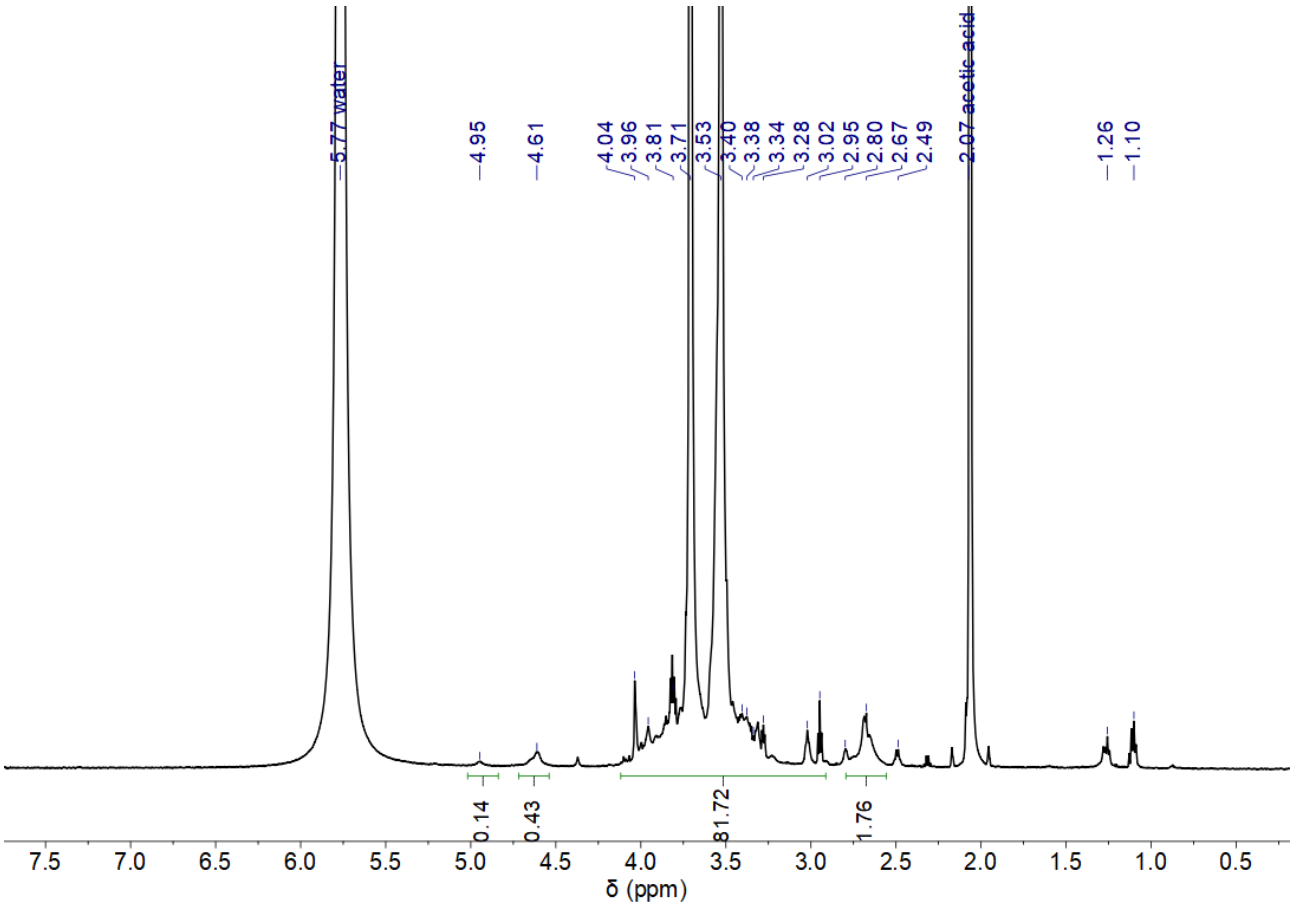

2D-DOSY NMR spectrum of **dCS-NSuc-LPEI-OPEG$_{44}$-SH** (600 MHz, D_2O/CD_3COOD 1:1)

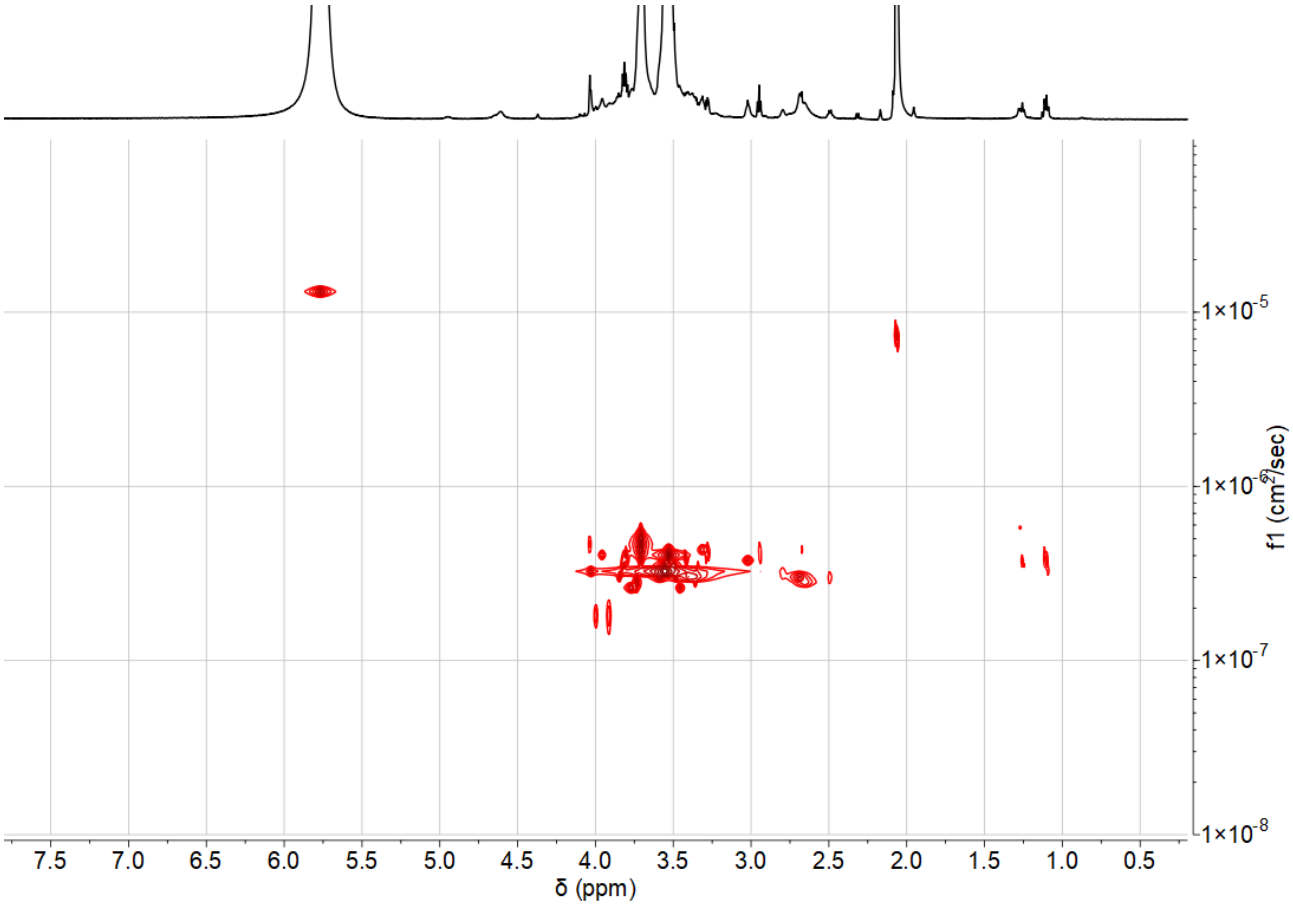

Calculation of the number of mol of reactive units (e.g succinylated glucosamine units) of dCS-NSuc-OPEG$_{44}$-SH (n(average units)):

As GD$_{Suc}$ = 44% and DD = 85%, the molar mass of one average unit of dCS-NSuc-OPEG$_{44}$-SH is M(dCS-NSuc-OPEG$_{44}$-SH) = 498.6 g/mol (cf. characterization of dCS-NSuc-OPEG$_{44}$-SH for more details), hence:

$$n(\text{average units}) = \frac{m(dCS-NSuc-OPEG44-SH)}{M(dCS-NSuc-OPEG44-SH)} = \frac{0.050}{498.6} = 0.100 \text{ mmol}$$

Estimation of the grafting degree of LPEI on dCS-NSuc-OPEG$_{44}$-SH (GD$_{LPEI}$):

From the spectrum recorded in D_2O/CD_3COOD (1/1), the peak from the succinyl group (2.67 ppm) is used as the reference peak. From the previous step, the integration for this peak equals to 1.76 (GD$_{Suc}$ = 44%). The integration of the massif from 4.12 to 3.20 ppm leads to a total number of 86.1 H, which are assigned to H2-3-4-5-6 from dCS, H17-18-19-20 from PEG (GD$_{PEG}$ = 14%) and H9-10-11-12-13-14-15-16 from LPEI. The protons for LPEI account then for 52.1 H. In one LPEI 2.5 kDa chain, there are 232 H.

Hence, $GD_{LPEI} = \frac{52.1}{232} \times 100 = 22\%$

Estimation of the molecular weight of one dCS-NSuc-LPEI-OPEG$_{44}$-SH chain (MW(dCS-NSuc-LPEI-OPEG$_{44}$-SH)):

MW(dCS-NSuc-LPEI-OPEG$_{44}$-SH) = Mw(dCS) + GD$_{Suc}$ x M$_{Suc}$ x nb(dCS units) + GD$_{LPEI}$ x MW(LPEI) x nb(dCS units) + GD$_{PEG}$ x MW(PEG) x nb(dCS units)

= 7800 + 0.44 x 101.1 x 46 + 0.22 x 2500 x 46 + 0.14 x 2042 x 46

= 48.3 kDa

with 46 being the number of units per dCS chain (cf. characterization of dCS for more details).

5.2.3. Shell polymers based on CPPs: Part 1

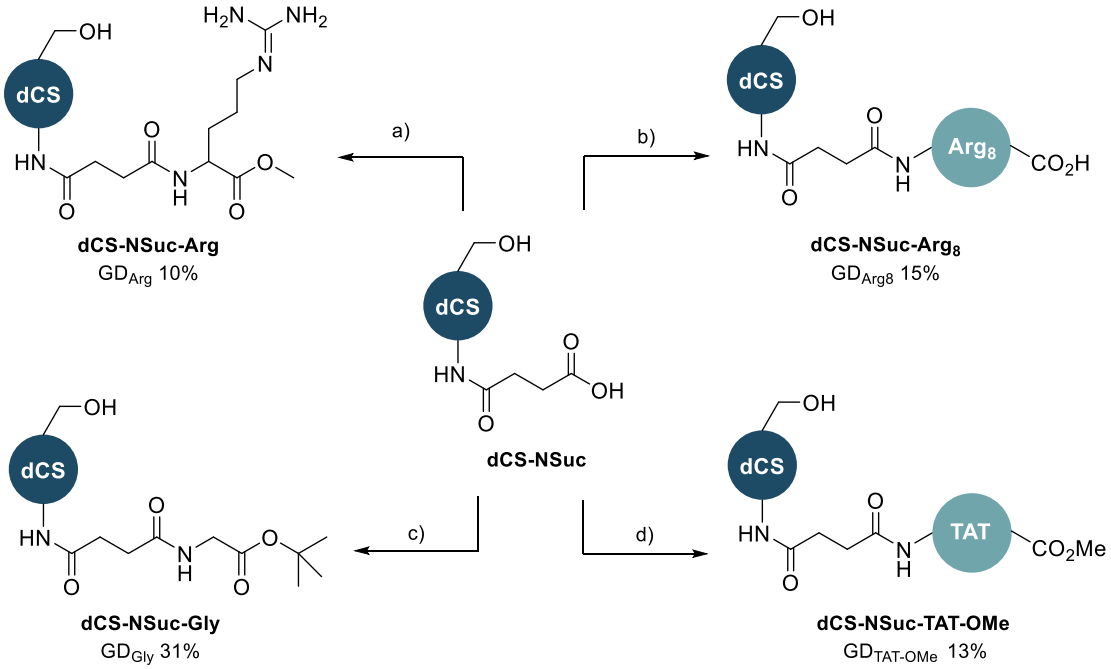

Scheme 29. Model reactions and full-length peptides conjugation of Arg$_8$ and TAT-OMe to dCS-NSuc. a) DMTMM, DIPEA, L-arginine methyl ester, H_2O, rt, 24 h. b) DMTMM, DIPEA, Arg$_8$ (in 4 portions every 10 min), H_2O, rt, 24 h. c) DMTMM, DIPEA, glycine *tert*-butyl ester hydrochloride, H_2O, rt, 16 h. d) DMTMM, DIPEA, TAT-OMe, H_2O, rt, 19 h.

dCS-NSuc-Arg

dCS-NSuc (DD 77%, GD$_{Suc}$ 43%, 49.3 mg, 0.102 mmol of reactive units, 1.0 equiv.) was dissolved at rt in 10 mL of distilled water. DMTMM (62.9 mg, 0.228 mmol, 2.2 equiv.) and DIPEA (48.2 µL, 0.277 mmol, 2.7 equiv.) were added to the solution which was stirred for 5 min at rt. Finally, L-Arginine methyl ester (Arg, 60.8 mg, 0.232 mmol, 2.3 equiv.) and dry DIPEA (40.4 µL, 0.232 mmol, 2.3 equiv.) were added to the mixture, which was stirred at rt for 24 h. The homogeneous solution was dialyzed (MWCO 3.5 kDa) against water for 2.5 days. The resulting clear solution was centrifuged (4700 rpm, 20 °C, 10 min) and the supernatant was lyophilized. **dCS-NSuc-Arg** was obtained as a white aerated solid (32 mg, GD$_{Arg}$ =

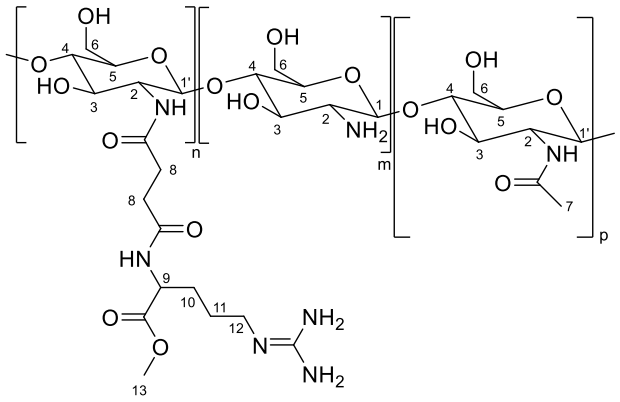

10%). **^{1}H NMR (400 MHz, D_2O):** δ 4.67 – 4.38 (br, 1 H, H1/1'), 4.10 – 3.45 (m, 9 H, H3-4-5-6-9-13), 3.23 (t, 2 H, H12), 3.14 (br, 1 H, H2), 2.68 – 2.41 (br, 4 H, H8), 2.07 (s, 3 H, H7), 1.95 (br, 2 H, H10), 1.67 (br, 2 H, H11).

^{1}H NMR spectrum of **dCS-NSuc-Arg** (400 MHz, D_2O)

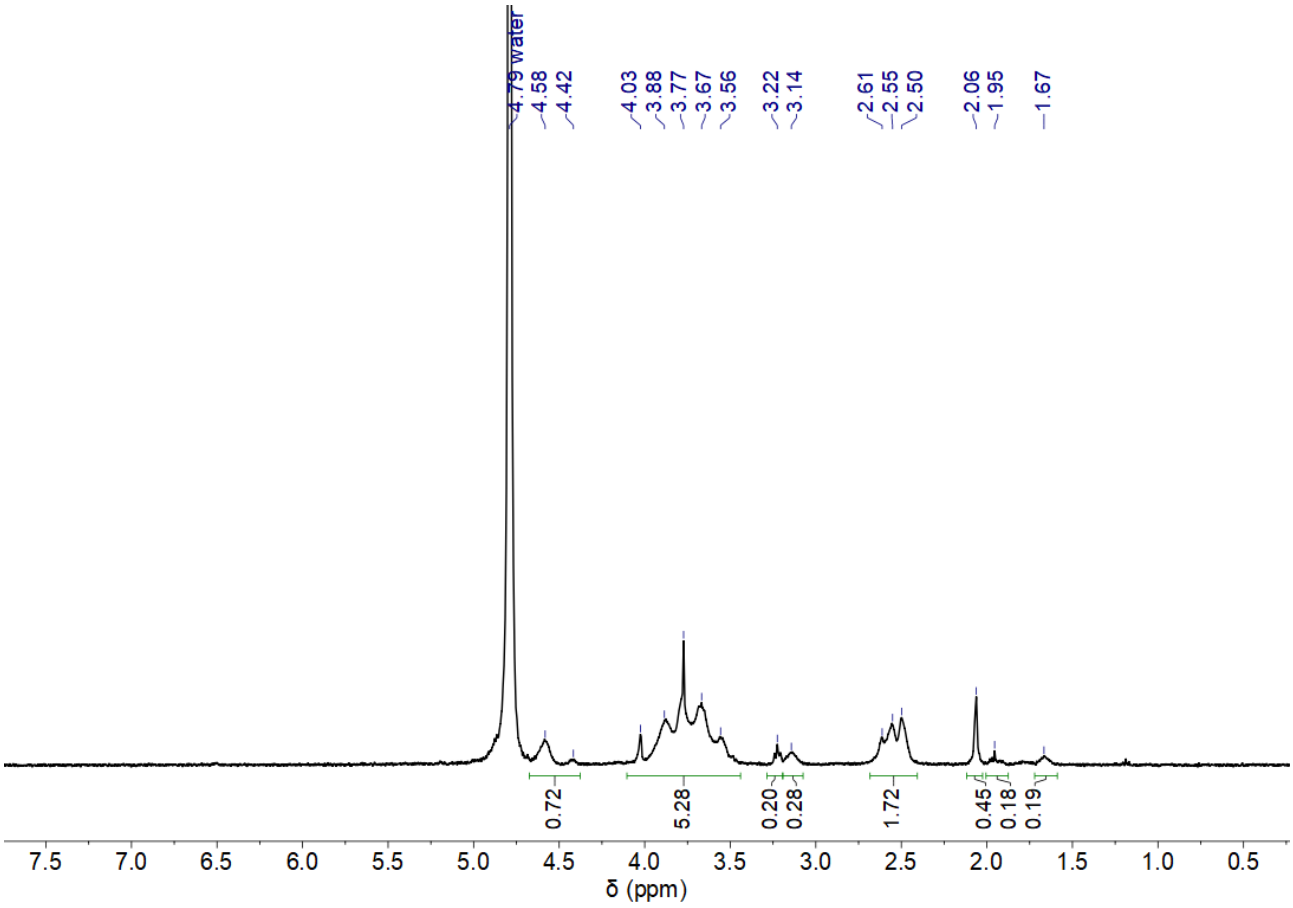

2D-DOSY NMR spectrum of **dCS-NSuc-Arg** (400 MHz, D_2O)

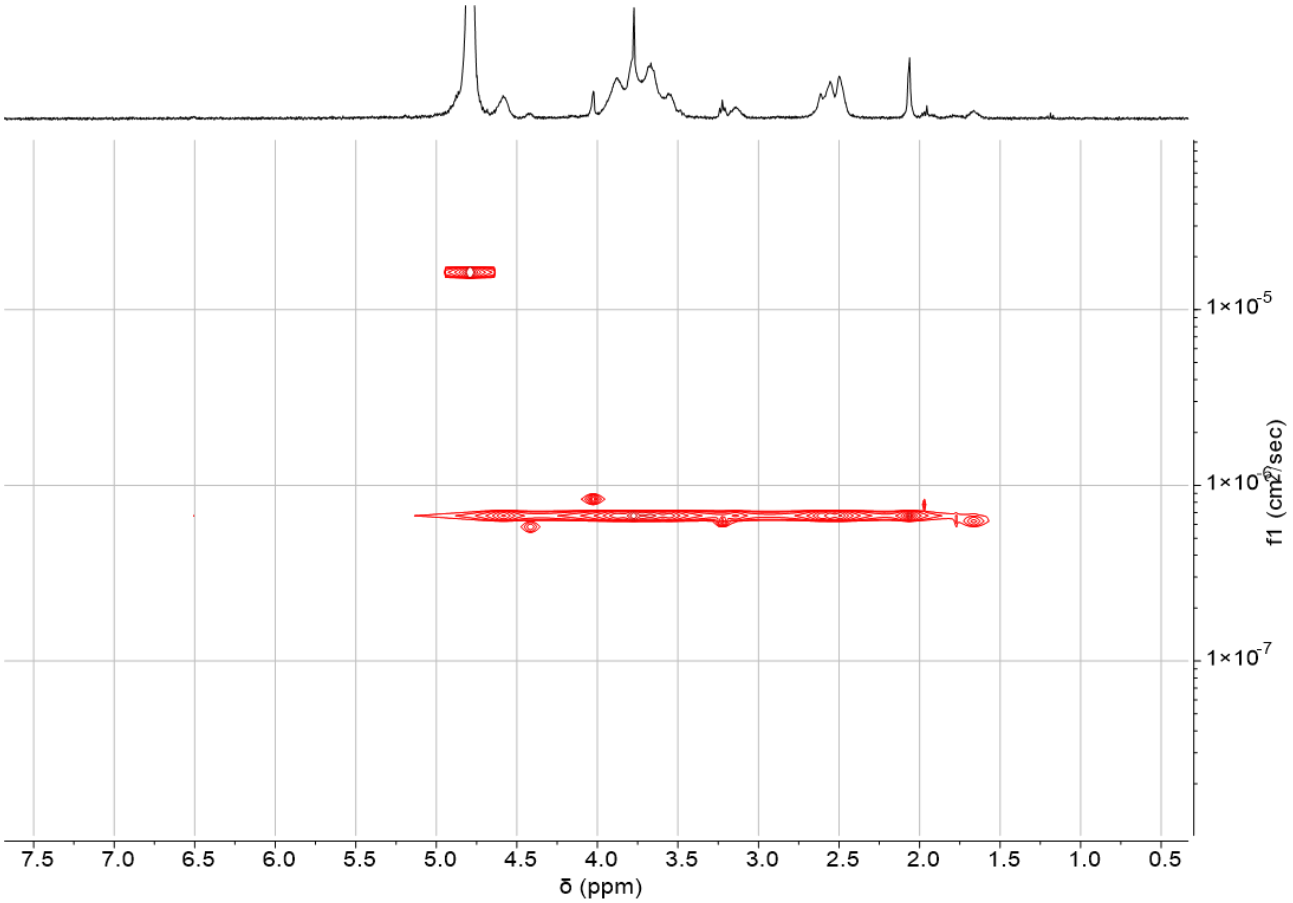

Calculation of the number of mol of reactive units (e.g. succinylated glucosamine units) of dCS-NSuc (n(reactive units)):

As GD_{Suc} = 43% and DD = 77%, the molar mass of one average unit of dCS-NSuc is M(dCS-NSuc) = 213.6 g/mol (cf. characterization of dCS-NSuc for more details), hence:

n(average units) = $\frac{m(dCS-NSuc)}{M(dCS-NSuc)} = \frac{0.0493}{213.6}$ = 0.231 mmol and as only 43% of units are reactive (because GD_{Suc} = 43%), then n(reactive units) = 0.231 x 0.43 = 0.102 mmol

Estimation of the grafting degree of Arg on dCS-NSuc (GD_{Arg}):

From the ^{1}H NMR spectrum, the peak for the succinyl group (δ 2.68 – 2.41 ppm) is used as the reference peak. As GD_{Suc} = 43%, the integration for this peak equals 1.72. The integration of the peak at δ 3.23 ppm equals to 0.20 and should account for 2 H of Arg (H12).

Hence, $GD_{Arg} = \frac{0.20}{20}$ x 100 = 10%

Estimation of the molecular weight of one dCS-NSuc-Arg chain (MW(dCS-NSuc-Arg)):

MW(dCS-NSuc-Arg) = Mw(dCS) + GD_{Suc} x M_{Suc} x nb(dCS units) + GD_{Arg} x M_{Arg} x nb(dCS units)

= 7800 + 0.43 x 101.1 x 46 + 0.10 x 243.1 x 46

= 10.9 kDa

with 46 being the number of units per dCS chain (cf. dCS characterization for more details).

dCS-NSuc-Arg$_8$

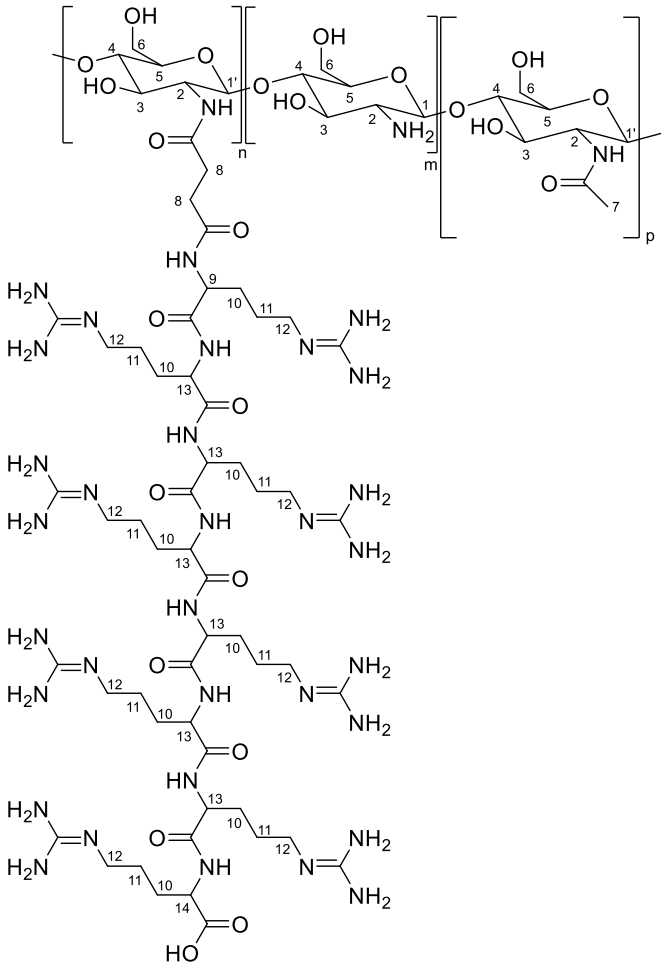

dCS-NSuc (DD 80%, GD_{Suc} 44%, 50.4 mg, 0.104 mmol of reactive units, 1.0 equiv.) was dissolved at rt in 10 mL of distilled water. To the cloudy mixture, DMTMM (65.0 mg, 0.235 mmol, 2.3 equiv.) and DIPEA (41.1 µL, 0.235 mmol, 2.3 equiv.) were added to the solution which was stirred for 5 min at rt. Arg_8 (100 mg, 0.079 mmol, 0.76 equiv.) was added portionwise (25 mg every 10 min) to this clear solution. The reaction mixture was stirred at rt for 24 h. The resulting homogeneous solution was dialyzed (MWCO 3.5 kDa) against water for 3 days before being centrifuged (4700 rpm, 20 °C, 10 min) and the supernatant was lyophilized. **dCS-NSuc-Arg$_8$** was obtained as a white aerated solid (25.7 mg, GD_{Arg8} = 15%). **^{1}H NMR (400 MHz, D_2O/CD_3COOD 14:1):** δ 4.52 (br, 1 H, H1/1'), 4.28 (m, 7 H, H9-13), 4.05 – 3.37 (m, 7 H, H2-3-4-5-6-14), 3.15 (t, 16 H, H12), 2.58 (br, 4 H, H8), 1.95 – 1.49 (m, 32 H, H10-11).

^{1}H NMR spectrum of **dCS-NSuc-Arg$_8$** (400 MHz, D_2O/CD_3COOD 14:1)

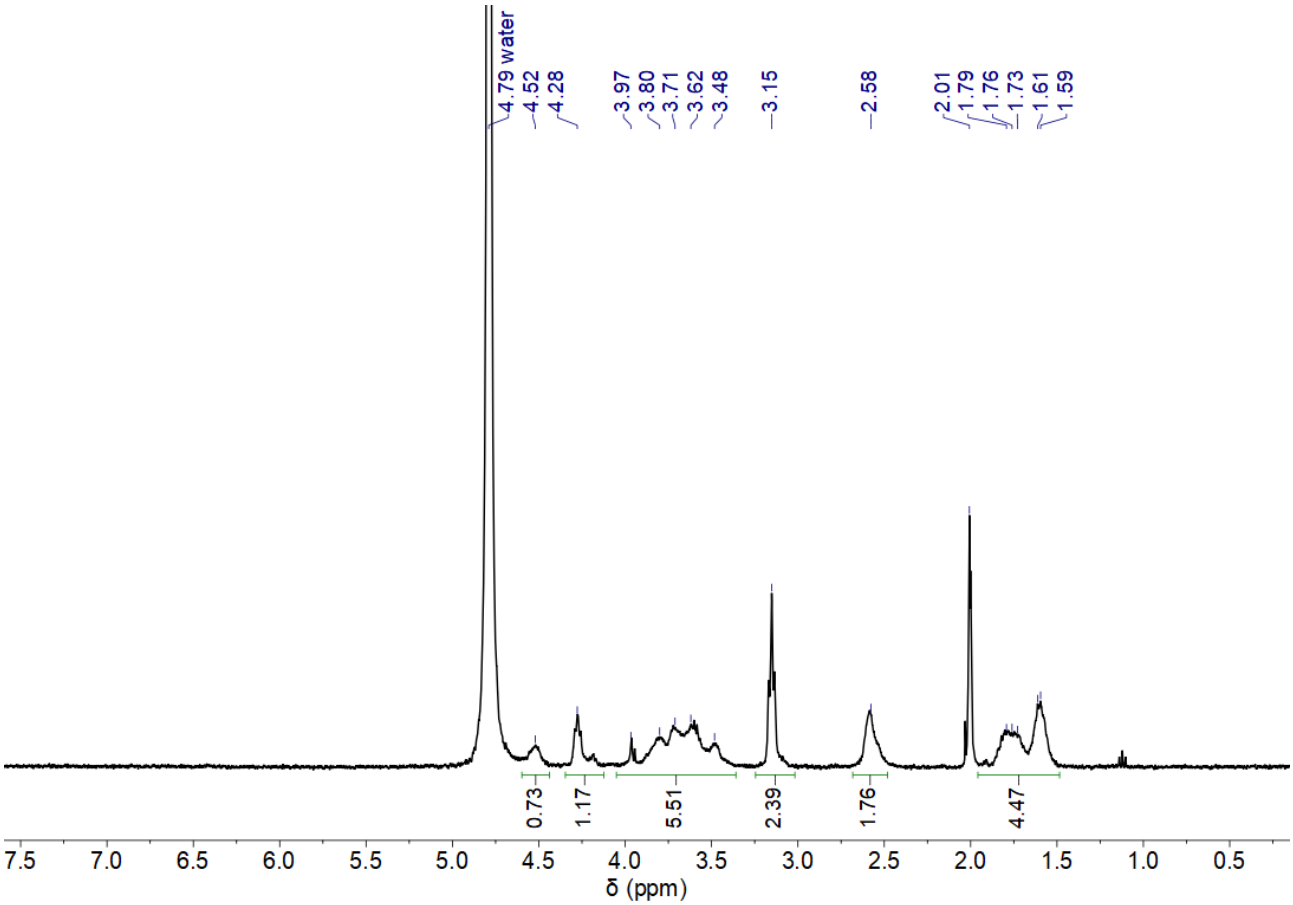

2D-DOSY NMR spectrum of **dCS-NSuc-Arg$_8$** (400 MHz, D_2O/CD_3COOD 14:1)

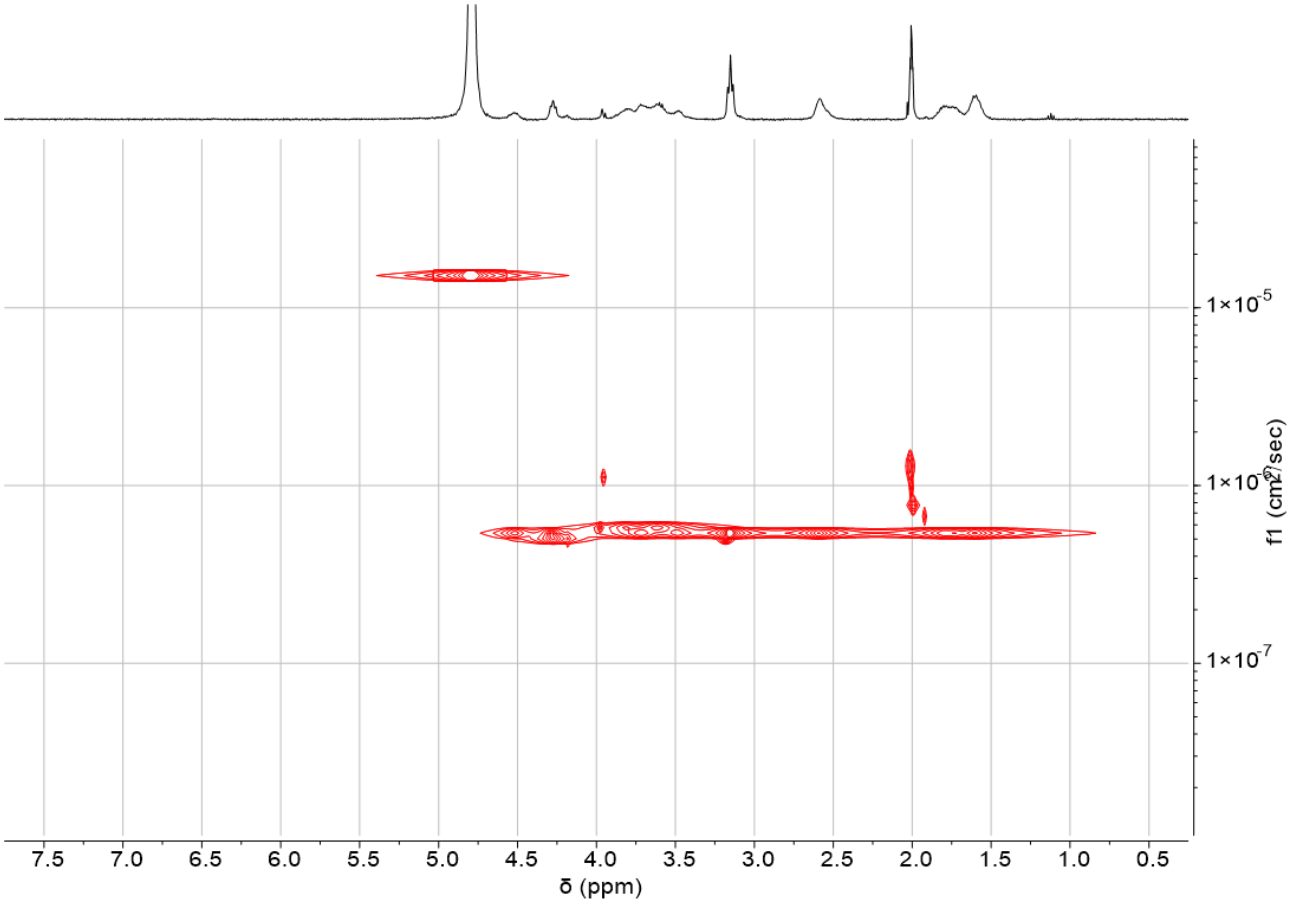

Calculation of the number of mol of reactive units (e.g. succinylated glucosamine units) of dCS-NSuc (n(reactive units)):

As GD_{Suc} = 44% and DD = 80%, the molar mass of one average unit of dCS-NSuc is M(dCS-NSuc) = 213.4 g/mol (cf. characterization of dCS-NSuc for more details), hence:

n(average units) = $\frac{m(dCS-NSuc)}{M(dCS-NSuc)} = \frac{0.0504}{213.4}$ = 0.236 mmol and as only 44% of units are reactive (because GD_{Suc} = 44%), then n(reactive units) = 0.236 x 0.44 = 0.104 mmol

Estimation of the grafting degree of Arg_8 on dCS-NSuc (GD_{Arg8}):

From the ^{1}H NMR spectrum, the peak for the succinyl group (2.58 ppm) is used as the reference peak. As GD_{Suc} = 44%, the integration for this peak equals 1.76. The integration of the peak at δ 3.15 ppm equals 2.39 and should account for 16 H of Arg (H12).

Hence, $GD_{Arg8} = \frac{2.39}{16}$ x 100 = 15%

Estimation of the molecular weight of one dCS-NSuc-Arg_8 chain (MW(dCS-NSuc-Arg_8)):

$MW(dCS\text{-}NSuc\text{-}Arg_8) = Mw(dCS) + GD_{Suc} \times M_{Suc} \times nb(dCS\ units) + GD_{Arg8} \times M_{Arg8} \times nb(dCS\ units)$

= 7800 + 0.44 x 101.1 x 46 + 0.15 x 1249 x 46

= 18.5 kDa

with 46 being the number of units per dCS chain (cf. dCS characterization for more details).

dCS-NSuc-Gly

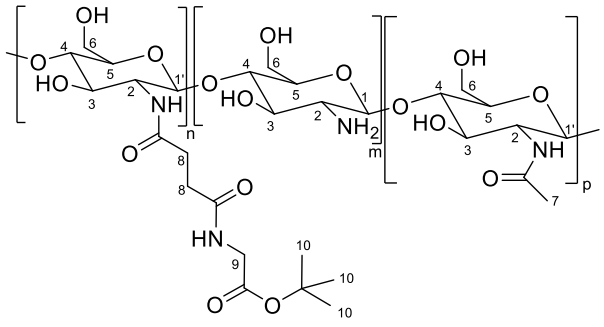

dCS-NSuc (DD 86%, GD_{Suc} 56%, 20.0 mg, 0.0502 mmol of reactive units, 1.0 equiv.) was dissolved in distilled water at rt. DMTMM (27.7 mg, 0.100 mmol, 2.0 equiv.) was added to the clear solution, followed by DIPEA (10.4 µL, 0.0602 mmol, 1.2 equiv.). Five minutes later, glycine *tert*-butyl ester hydrochloride (Gly, 5.9 mg, 0.0351 mmol, 0.70 equiv.) was added to this mixture, which was stirred at rt for 17 h. It was then dialyzed (MWCO 3.5 kDa) against water for 3.5 days before being centrifuged (4700 rpm, 20 °C, 10 min). The supernatant was lyophilized to yield **dCS-NSuc-Gly** as a white aerated solid (17.3 mg, GD_{Gly} = 31%). **^{1}H NMR (400 MHz, D_2O):** δ 4.58 (br, 1H, H1/1'), 4.05 – 3.43 (m, 6H, H3-4-5-6-9), 3.15 (br, 1H, H2), 2.71 – 2.43 (br, 4 H, H8), 2.06 (s, 3H, H7), 1.48 (s, 9 H, H10).

^{1}H NMR spectrum of **dCS-NSuc-Gly** (400 MHz, D_2O)

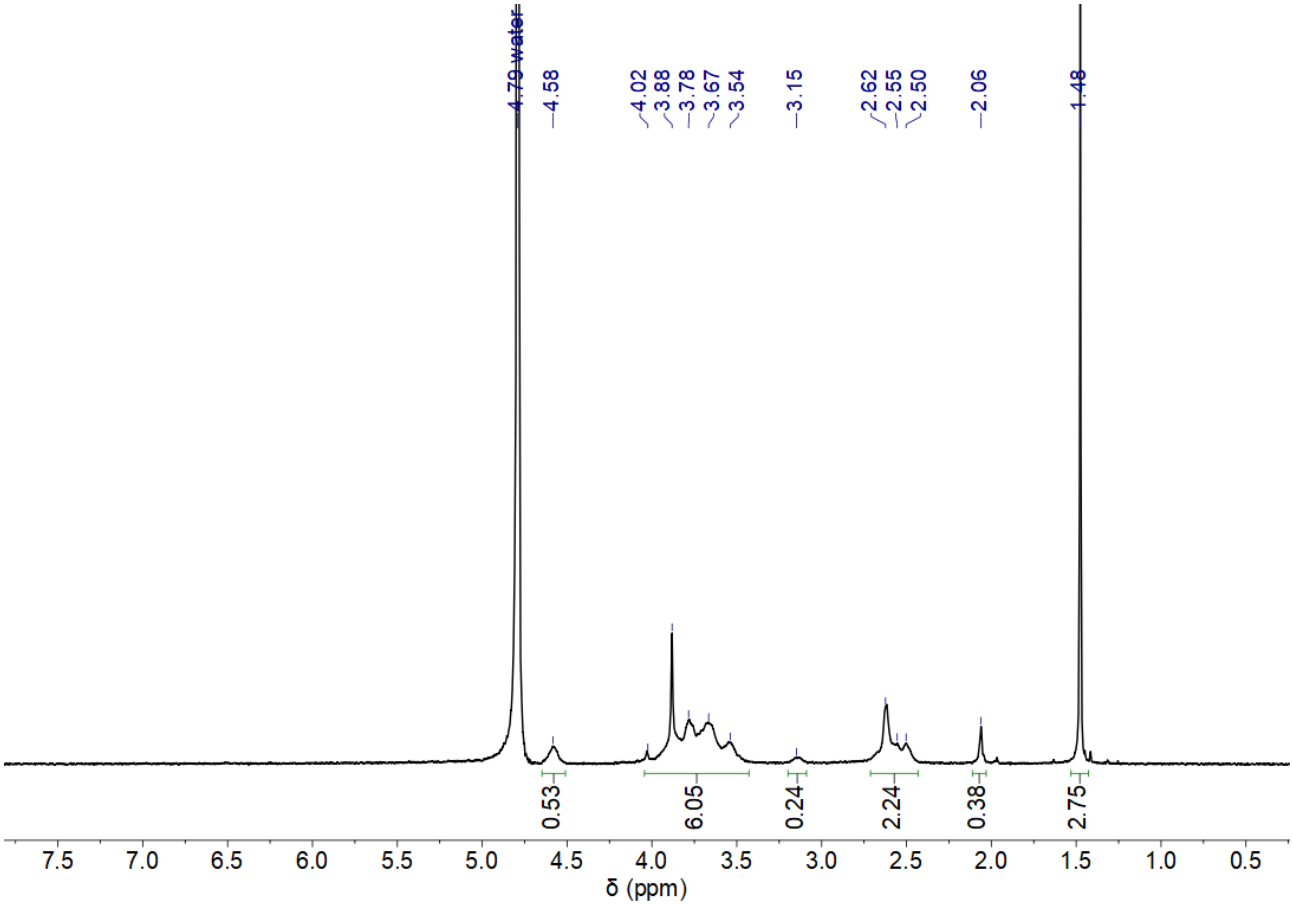

2D-DOSY NMR spectrum of **dCS-NSuc-Gly** (400 MHz, CD_3COOD/D_2O 1/1)

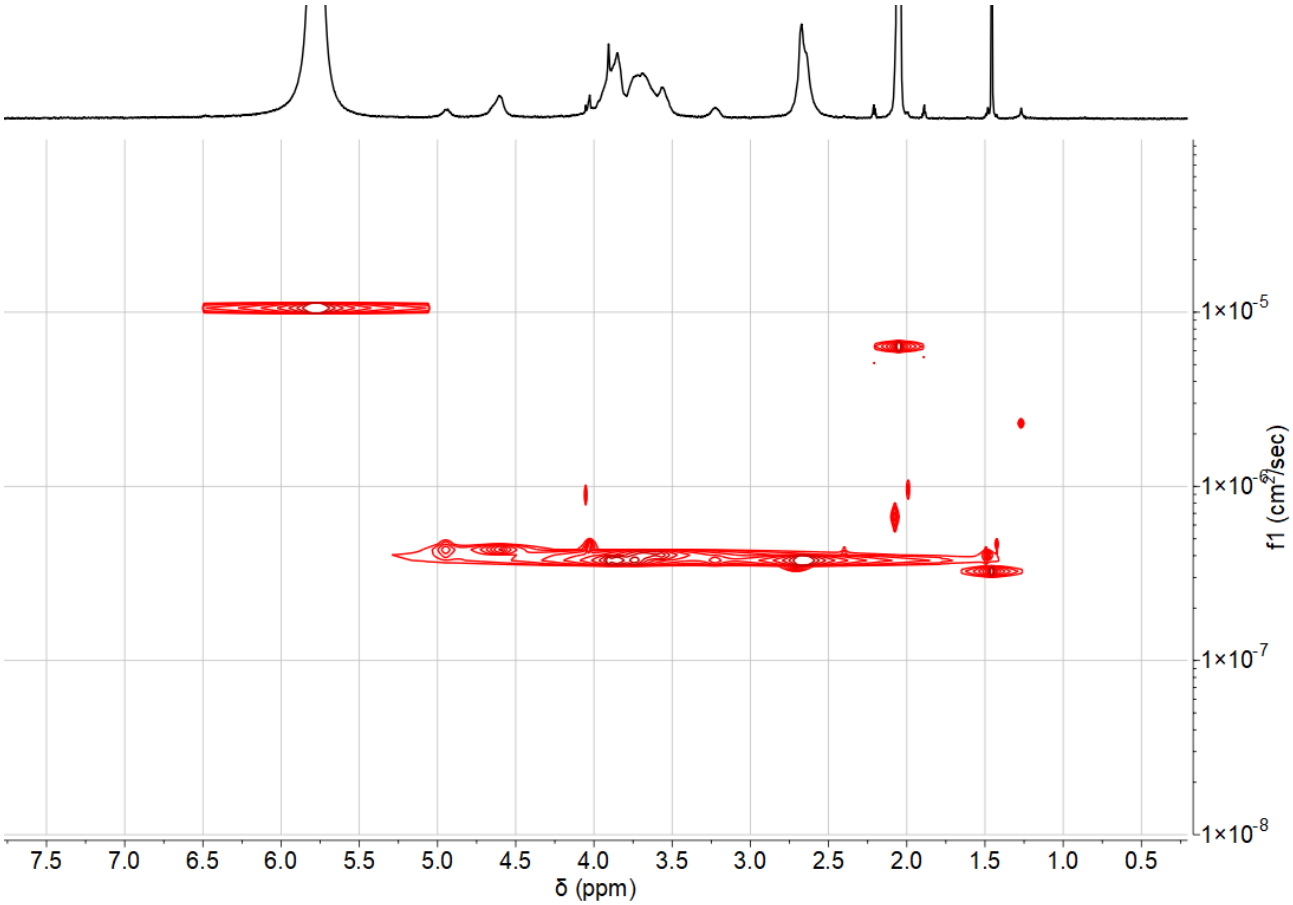

NB: this spectrum comes from a non-optimized batch of **dCS-NSuc-Gly** (GD_{Gly} 6.5%) which is why the ^1H NMR on the horizontal scale looks a bit different in particular for glycine peaks.

Calculation of the number of mol of reactive units (e.g. succinylated glucosamine units) of dCS-NSuc (n(reactive units)):

As GD_{Suc} = 56% and DD = 86%, the molar mass of one average unit of dCS-NSuc is M(dCS-NSuc) = 223.1 g/mol (cf. characterization of dCS-NSuc for more details), hence:

n(average units) = $\frac{m(dCS-NSuc)}{M(dCS-NSuc)} = \frac{0.020}{223.1}$ = 0.0897 mmol and as only 56% of units are reactive (because GD_{Suc} = 56% (in CD_3COOD/D_2O 1/1)), then n(reactive units) = 0.0897 x 0.56 = 0.0502 mmol

Estimation of the grafting degree of TAT-OMe on dCS-NSuc (GD_{TATOMe}):

From the ^1H NMR spectrum, the peak for the succinyl group (δ 2.71 – 2.43 ppm) is used as the reference peak. As GD_{Suc} = 56%, the integration for this peak equals 2.24. The peak at δ 1.48 ppm integrates for 2.75 and should account for 9 H of Gly.

Hence, $GD_{TATOMe} = \frac{2.75}{9}$ x 100 = 31%

dCS-NSuc-TAT-OMe

with TAT-OMe sequence: H_2N-Gly-Arg-Lys-Lys-Arg-Arg-Gln-Arg-Arg-Arg-Gln-CO_2Me

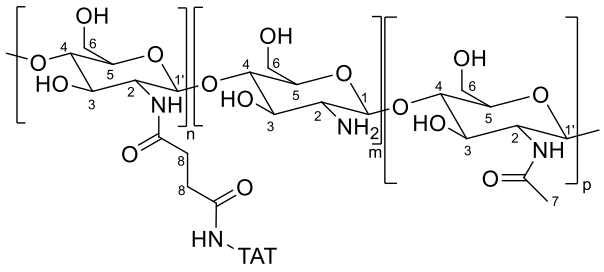

dCS-NSuc (DD 88%, GD_{Suc} 55%, 20.0 mg, 0.0497 mmol of reactive units, 1.0 equiv.) was dissolved in 3 mL of distilled water before adding successively DMTMM (26.0 mg, 0.0946 mmol, 2.0 equiv.) and DIPEA (1.6 µL, 0.00946 mmol, 0.20 equiv.). Within 5 min of stirring at rt, the mixture became clear and a solution of TAT-OMe (57.0 mg, 0.0348 mmol, 0.70 equiv.) dissolved in 1 mL of distilled water was added dropwise to it. After 19 h of stirring at rt, the solution was dialyzed (MWCO 3.5 kDa) against water for 3 days. The solution was then centrifuged (4700 rpm, 20 °C, 10 min) and the supernatant was lyophilized. **dCS-NSuc-TAT-OMe** was obtained as a white aerated solid (16 mg, GD_{TATOMe} = 13 %). **^{1}H NMR (600 MHz, D_2O):** δ 4.67 – 4.16 (m, 12 H, H1/1' + H_{TATOMe}), 4.14 – 3.39 (m, 12 H, H3-4-5-6 + H_{TATOMe}), 3.17 (br, 12 H, H_{TATOMe}), 3.04 – 2.78 (m, 5 H, H2 + H_{TATOMe}), 2.73 – 2.38 (br, 4 H, H8), 2.37 – 2.19 (m, 4 H, H_{TATOMe}), 2.11 – 1.23 (m, 45 H, H7 + H_{TATOMe}).

^{1}H NMR spectrum of **dCS-NSuc-TAT-OMe** (600 MHz, D_2O)

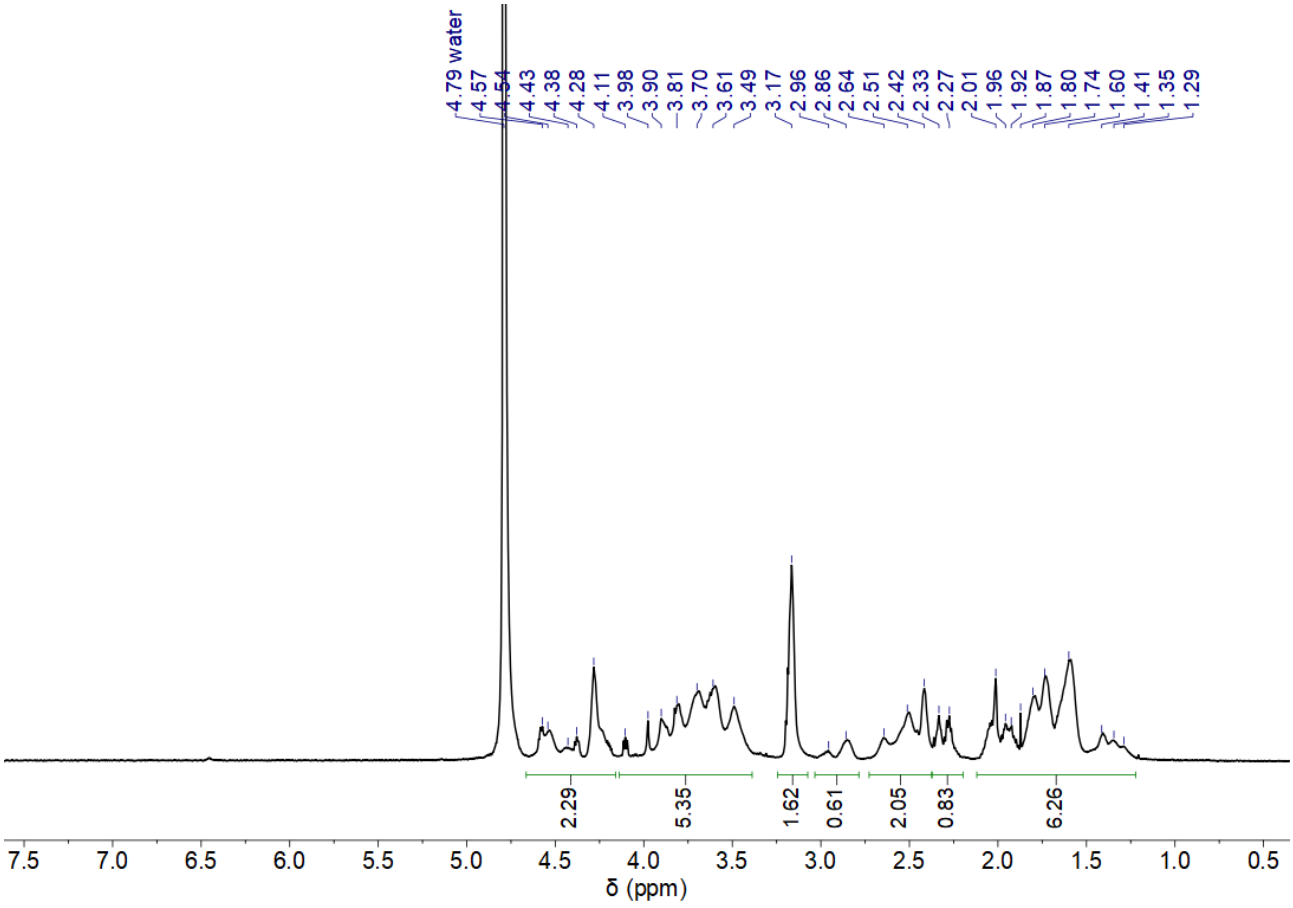

2D-DOSY NMR spectrum of **dCS-NSuc-TAT-OMe** (600 MHz, D_2O)

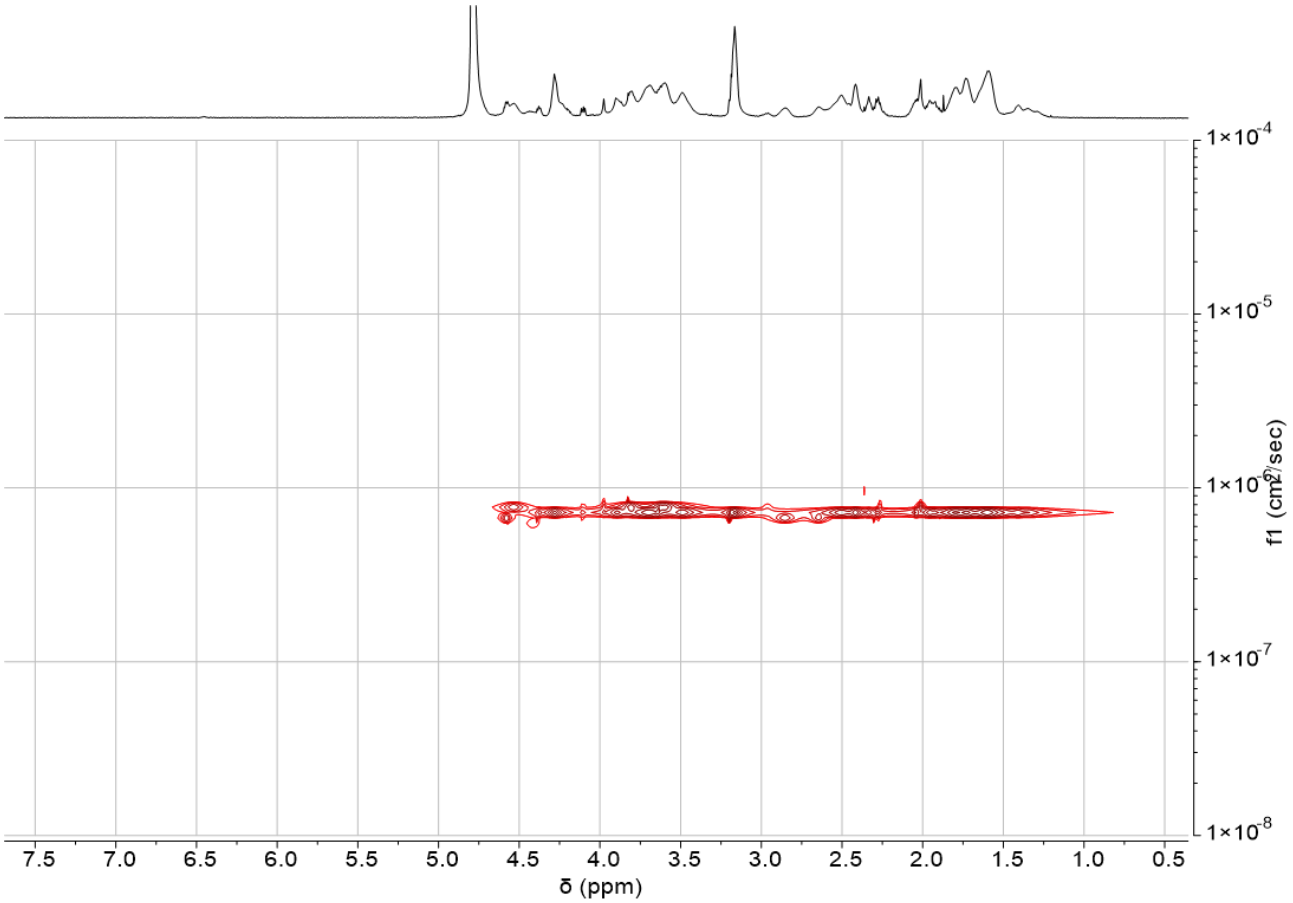

Calculation of the number of mol of reactive units (e.g. succinylated glucosamine units) of dCS-NSuc (n(reactive units)):

As GD_{Suc} = 55% and DD = 88%, the molar mass of one average unit of dCS-NSuc is M(dCS-NSuc) = 221.2 g/mol (cf. characterization of dCS-NSuc for more details), hence:

n(average units) = $\frac{m(dCS-NSuc)}{M(dCS-NSuc)} = \frac{0.020}{221.2}$ = 0.0904 mmol and as only 55% of units are reactive (because GD_{Suc} = 55% (in CD_3COOD/D_2O 1/1)), then n(reactive units) = 0.0904 x 0.55 = 0.0497 mmol

Estimation of the grafting degree of TAT-OMe on dCS-NSuc (GD_{TATOMe}):

From the ^1H NMR spectrum, the peak for the succinyl group (δ 2.73 – 2.38 ppm) is used as the reference peak. As GD_{Suc} (in D_2O) = 51%, the integration for this peak equals 2.05. The integration of the peak at δ 3.17 ppm equals 1.62 and should account for 12 H of Arg.

Hence, $GD_{TATOMe} = \frac{1.62}{12}$ x 100 = 13%

Estimation of the molecular weight of one dCS-NSuc-TAT-OMe chain (MW(dCS-NSuc-TAT-OMe)):

MW(dCS-NSuc-TAT-OMe) = Mw(dCS) + GD_{Suc} x M_{Suc} x nb(dCS units) + GD_{TATOMe} x $M_{TAT-OMe}$ x nb(dCS units)

= 8300 + 0.55 x 101.1 x 50 + 0.13 x 1618 x 50

= 21.6 kDa

with 50 being the number of units per dCS chain (*cf.* dCS characterization for more details).

5.2.4. Shell polymers based on CPPs: Part 2

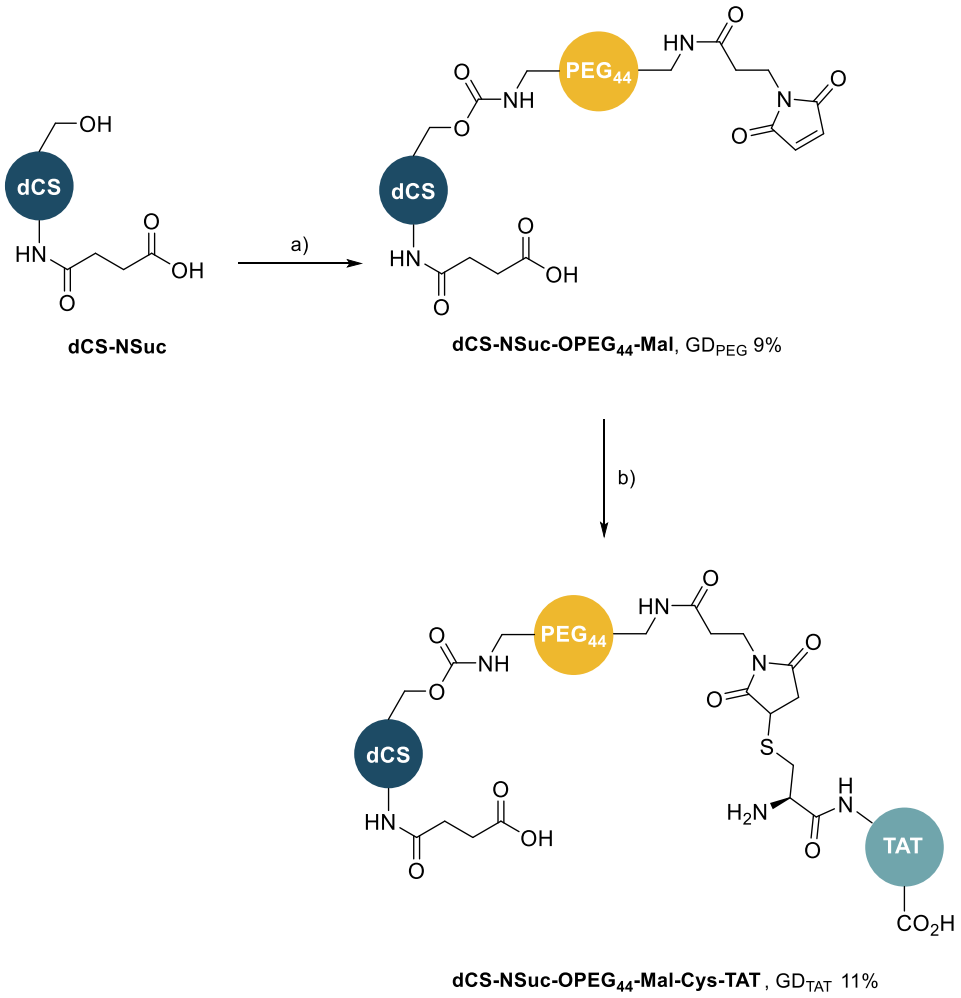

dCS-NSuc **dCS-NSuc-OPEG$_{44}$-Mal**, GD_{PEG} 9%

dCS-NSuc-OPEG$_{44}$-Mal-Cys-TAT, GD_{TAT} 11%

Scheme 30. Preparation of dCS-NSuc-OPEG$_{44}$-Mal-Cys-TAT. a) CDI, H_2N-PEG$_{44}$-Mal, DMSO, rt, 2 h. b) TAT-Cys, H_2O, rt, 3 h.

dCS-NSuc-OPEG$_{44}$-Mal

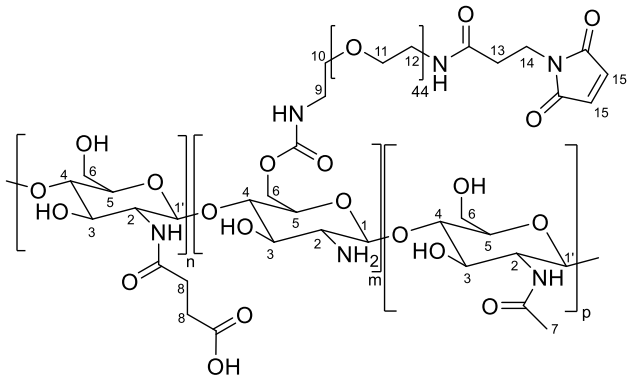

dCS-NSuc (DD 85%, GD$_{Suc}$ 52%, 30.0 mg, 0.137 mmol, 1.0 equiv) was dissolved at rt in 2.5 mL of DMSO. CDI (22.2 mg, 0.137 mmol, 1.0 equiv.) was added to the homogenous and cloudy mixture which was further stirred for 20 min at rt to allow for the activation of hydroxyls on the dCS units. Lastly, a solution of H_2N-PEG$_{44}$-Mal (59 mg, 0.0273 mmol, 0.20 equiv.) in 0.5 mL of DMSO was added to the reaction mixture. After 2 h of stirring at rt, the reaction mixture was dialyzed (MWCO 3.5 kDa) against water for 2.5 days. After dialysis, the resulting solution was centrifuged (4700 rpm, 24 °C, 10 min) and the supernatant was lyophilized. **dCS-NSuc-OPEG$_{44}$-Mal** was obtained as a white aerated solid (54.2 mg, GD$_{PEG}$ = 9%). **^{1}H NMR (500 MHz, D$_2$O):** δ 6.88 (s, 2 H, H15), 4.58z (br, 1 H, H1/1'), 4.00 – 3.08 (m, 186 H, H2-3-4-5-6-9-10-11-12-13-14), 2.73 – 2.43 (br, 4 H, H8), 2.06 (s, 3 H, H7).

^{1}H NMR spectrum of **dCS-NSuc-OPEG$_{44}$-Mal** (500 MHz, D$_2$O)

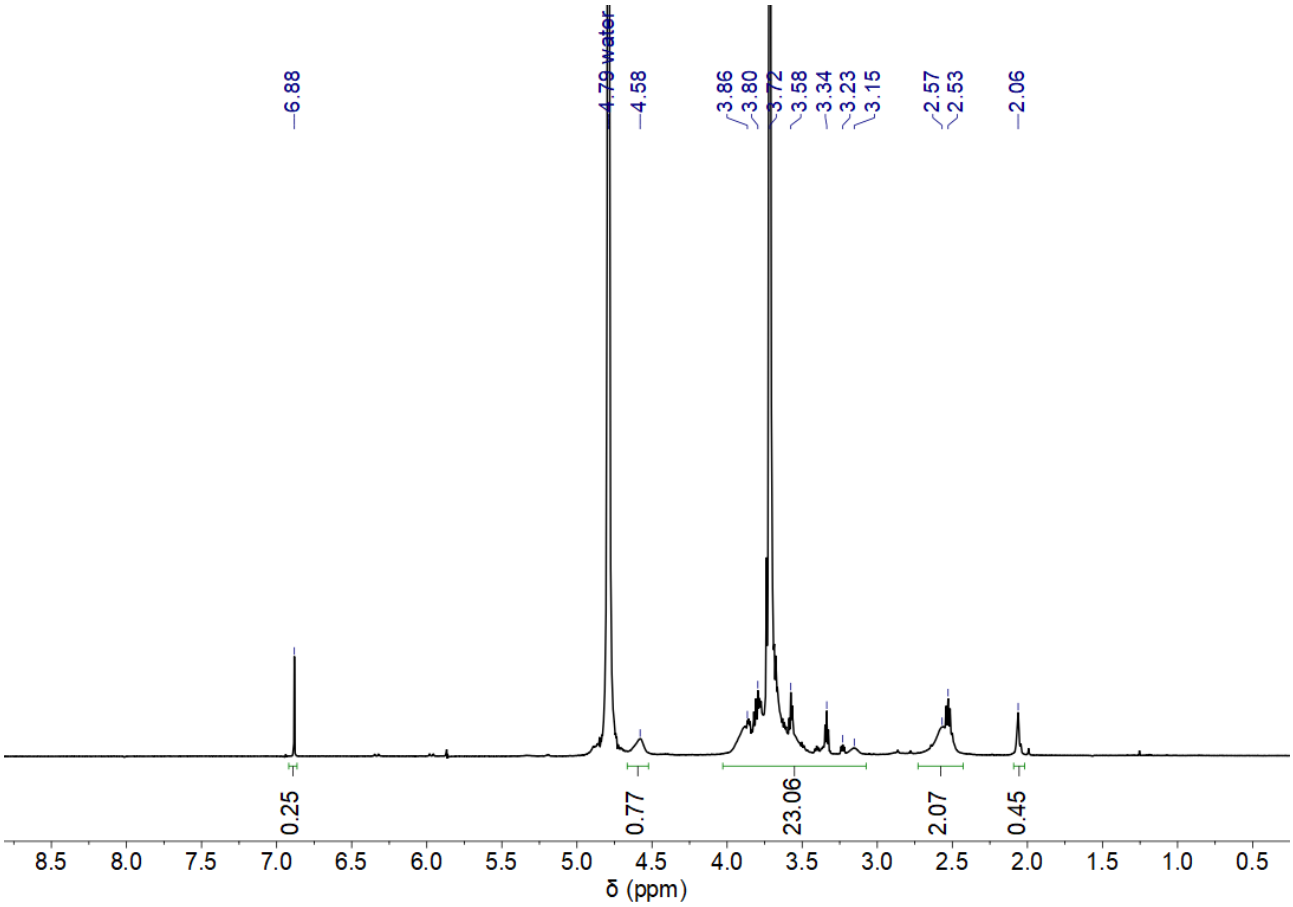

2D-DOSY NMR spectrum of **dCS-NSuc-OPEG$_{44}$-Mal** (500 MHz, D$_2$O) processed by Topspin software

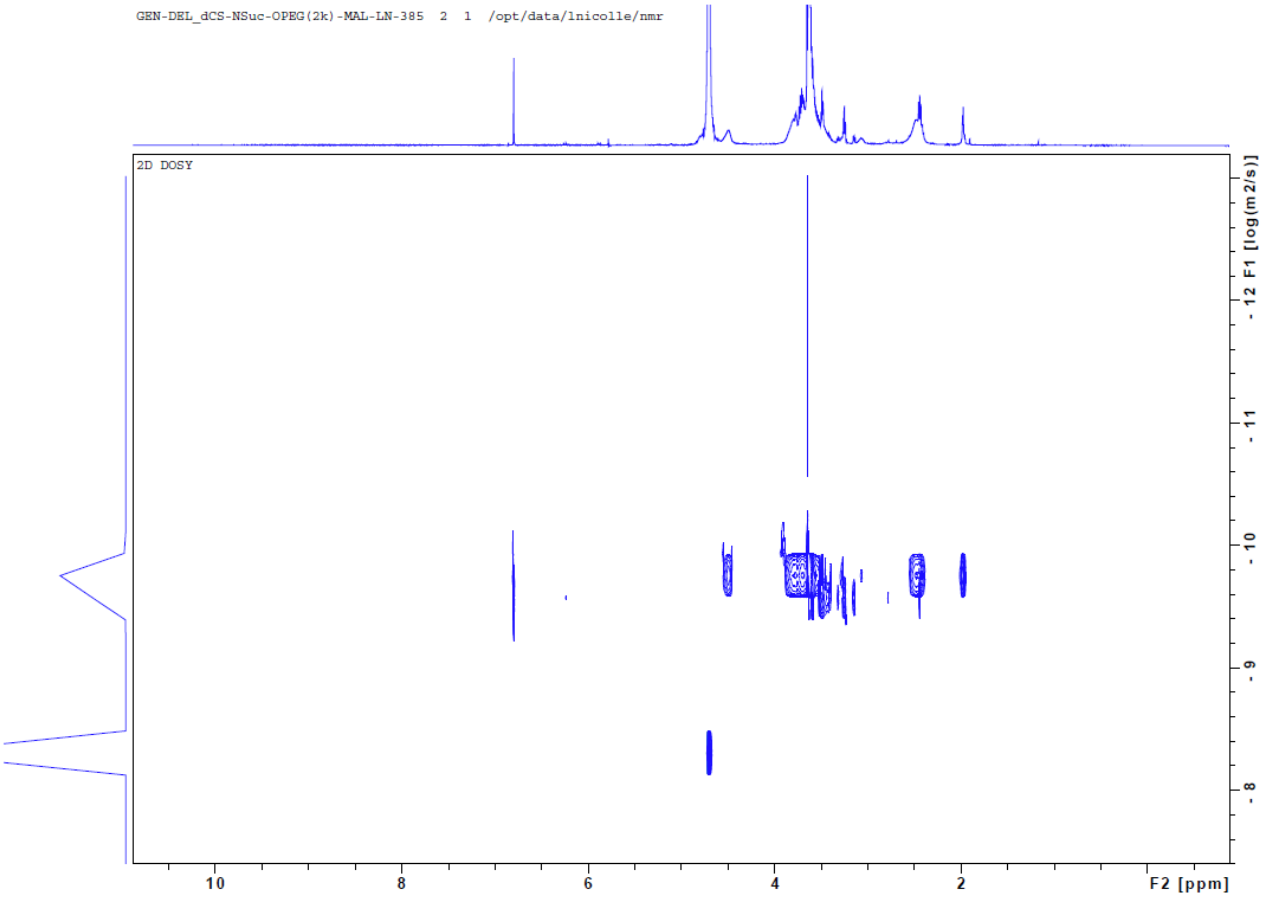

2D-DOSY NMR spectrum of **dCS-NSuc-OPEG$_{44}$-Mal** (500 MHz, D_2O) processed by Mestre Nova software

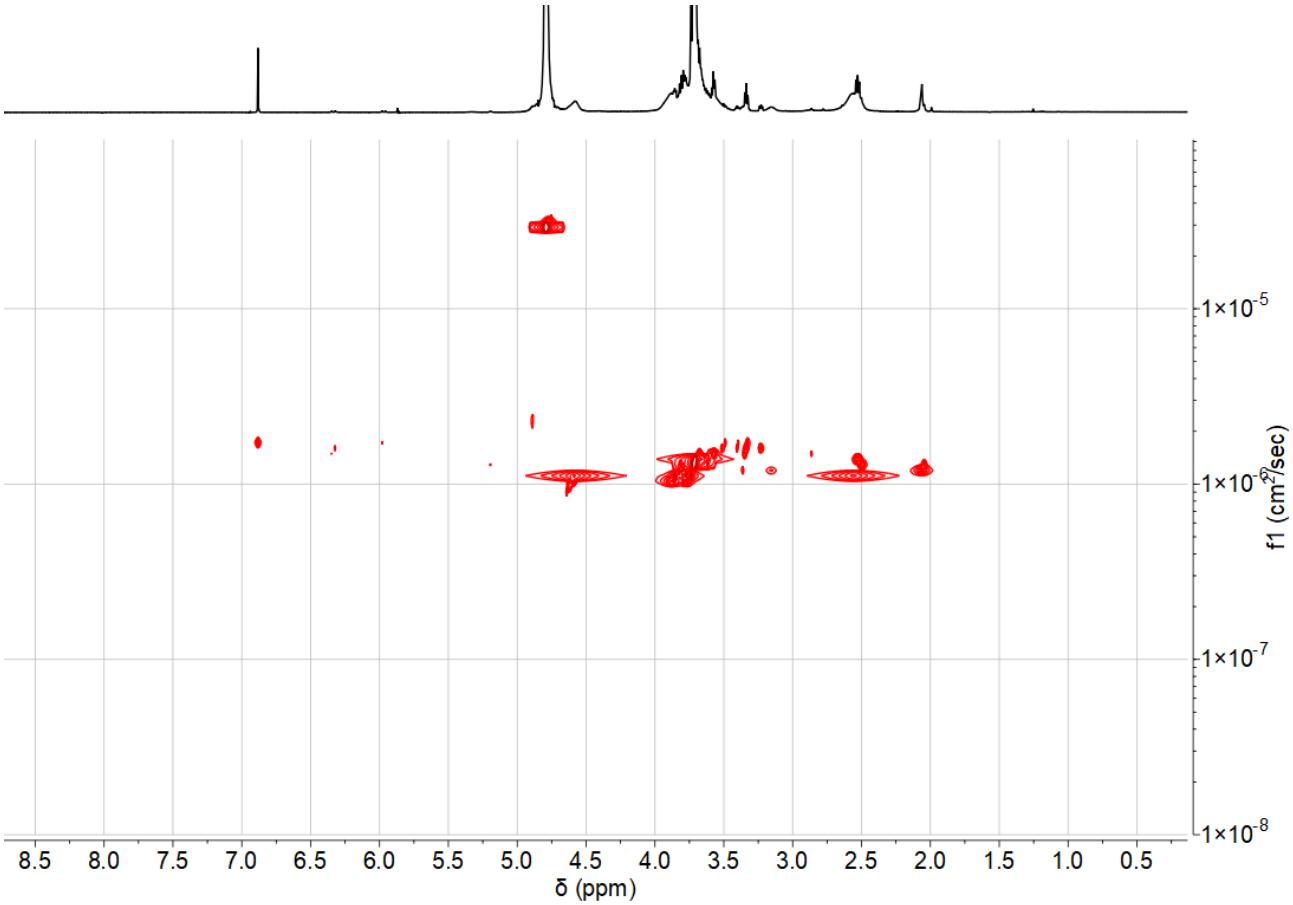

Calculation of the number of mol of dCS-NSuc (n(average units)):

As GD_{Suc} = 52% and DD = 85%, the molar mass of one average unit of dCS-NSuc is M(dCS-NSuc) = 219.5 g/mol (cf. characterization of dCS-NSuc for more details), hence:

$$n(\text{average units}) = \frac{m(dCS-NSuc)}{M(dCS-NSuc)} = \frac{0.030}{219.5} = 0.137 \text{ mmol}$$

Estimation of the grafting degree of H_2N-PEG_{44}-Mal on dCS-NSuc (GD_{PEG}):

From the ^1H NMR spectrum, the peak for the actely group (δ 2.06 ppm) is used as the reference peak. From the previous step, the integration for this peak equals 0.45 (DD = 85%). The integration of the massif from 4.00 to 3.08 ppm leads to a total number of 23.1 H, where 6 H account for H2-3-4-5-6 from dCS backbone. The remaining 17.1 H account for H-9-10-11-12-13-14 and each H_2N-PEG_{44}-Mal chain is composed of 184 H (without taking into account the 2 H from maleimide moiety).

Hence, $GD_{PEG} = \frac{17.1}{184} \times 100 = 9\%$

Calculation of the molar mass of one average unit of dCS-NSuc-OPEG$_{44}$-Mal (M(dCS-NSuc-OPEG$_{44}$-Mal)):

M(dCS-NSuc-OPEG$_{44}$-Mal) = GD_{Suc} x M(dCS-NSuc unit) + AD x M(acetylglucosamine) + (1 - GD_{Suc} - AD) x M(glucosamine) + GD_{PEG} x MW(H_2N-PEG$_{44}$-Mal)

= 0.52 x 261.2 + 0.15 x 203.2 + (1 - 0.52 - 0.15) x 161.2 + 0.09 x 2176

= 415.3 g/mol with AD = (1 – DD)

dCS-NSuc-OPEG$_{44}$-Mal-Cys-TAT

with TAT-Cys sequence: H_2N-Cys-Tyr-Gly-Arg-Lys-Lys-Arg-Arg-Gln-Arg-Arg-Arg-CO_2H

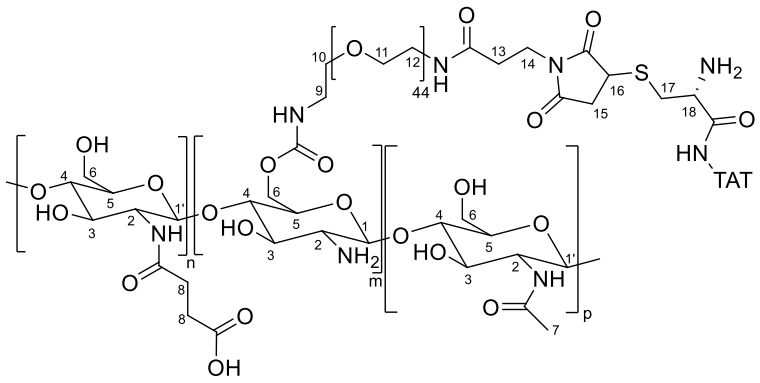

dCS-NSuc-OPEG$_{44}$-Mal (DD 85%, GD_{Suc} 49%, GD_{PEG} 18%, 20.0 mg, 0.00592 mmol of reactive units, 1.0 equiv.) was dissolved in 2 mL of distilled water (pH 6-7) at rt. After 5 min, a solution of TAT-Cys (19.7 mg, 0.0118 mmol, 2.0 equiv.) in 1 mL of distilled water was added dropwise to the clear solution. After 3 h of stirring at rt, the reaction mixture was dialyzed (MWCO 3.5 kDa) against water for 3 days. After dialysis, the mixture was centrifuged (4700 rpm, 20 °C, 10 min) and the supernatant was lyophilized. **dCS-NSuc-OPEG$_{44}$-Mal-Cys-TAT** was obtained as a white aerated solid (16.8 mg, GD_{TAT} = 11%). **^{1}H NMR (600 MHz, D_2O):** δ 7.08 (br, 2 H, H_{TAT}), 6.74 (br, 2 H, H_{TAT}), 4.61 – 4.38 (m, 2 H, H1/1'-18 + H_{TAT}), 4.36 – 4.18 (m, 10 H, H_{TAT}), 4.00 – 3.23 (m, 186 H, H3-4-5-6-9-10-11-12-13-14 + H_{TAT}), 3.22 – 2.84 (m, 22 H, H13-17 + H_{TAT}), 2.62 – 2.17 (m, 9 H, H8-15-16 + H_{TAT}), 2.08 – 1.25 (m, 39 H, H7 + H_{TAT}).

^{1}H NMR spectrum of **dCS-NSuc-OPEG$_{44}$-Mal-Cys-TAT** (600 MHz, D_2O)

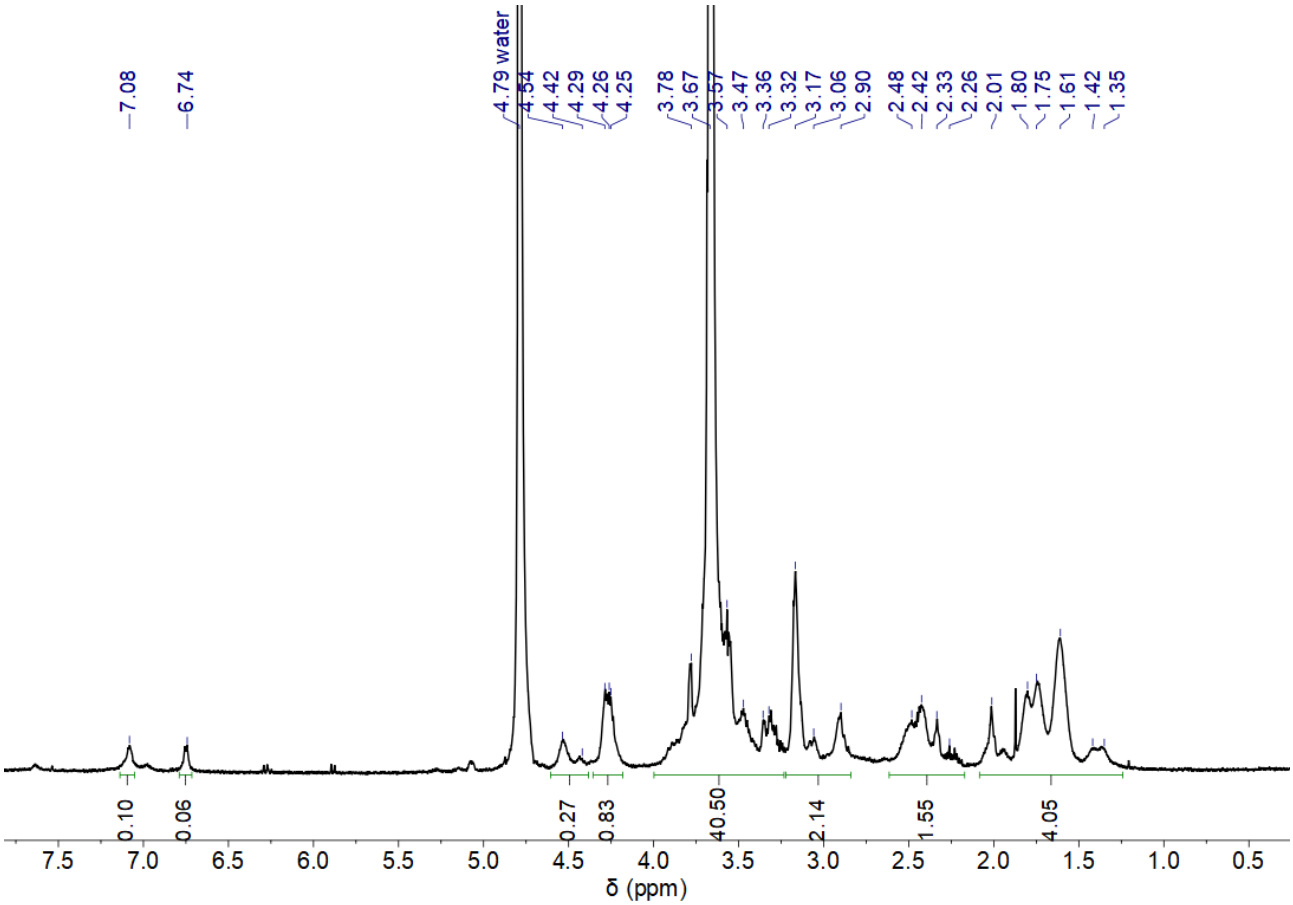

2D-DOSY NMR spectrum of **dCS-NSuc-OPEG$_{44}$-Mal-Cys-TAT** (600 MHz, D_2O)

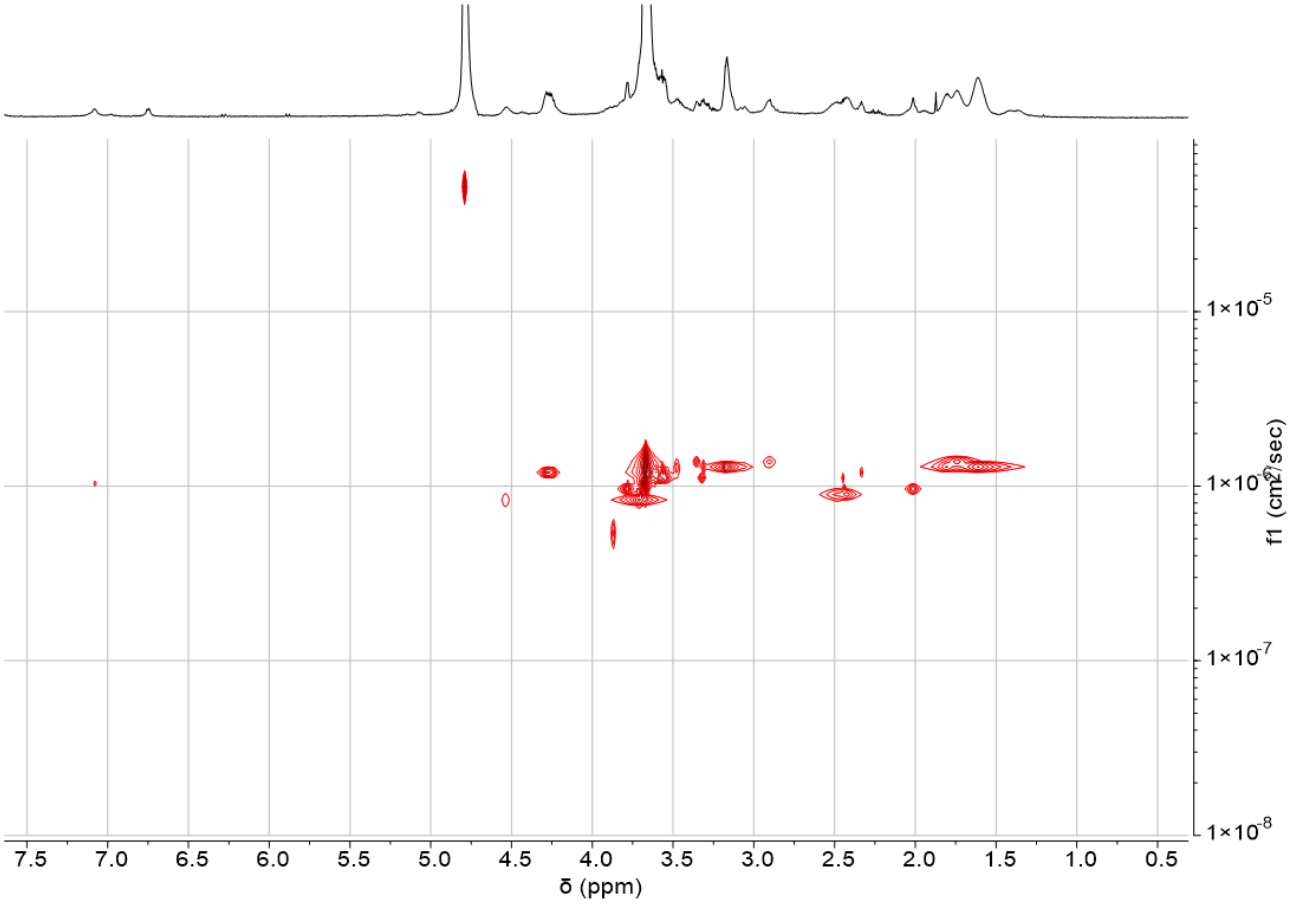

Calculation of the number of mol of reactive units (e.g. dCS units grafted with a maleimide moiety) of dCS-NSuc-OPEG$_{44}$-Mal (n(reactive units)):

As DD = 85%, GD_{Suc} = 49% and GD_{PEG} = 18%, the molar mass of one average unit of dCS-NSuc is M(dCS-NSuc-OPEG$_{44}$-Mal) = 608.1 g/mol (cf. characterization of dCS-NSuc-OPEG$_{44}$-Mal for more details), hence:

n(average) = $\frac{0.020}{608.1}$ = 0.0329 mmol and as only 18% of units are reactive (because GD_{PEG} = 18%),

n(reactive units) = 0.0329 x 0.18 = 0.00592 mmol

Estimation of the grafting degree of TAT-Cys on dCS-NSuc-OPEG$_{44}$-Mal (GD_{TAT}):

From previous step, the massif from 4.00 to 3.23 ppm is integrating for 39.6 H and includes some dCS and H_2N-PEG$_{44}$-Mal hydrogen atoms. After the grafting of TAT-Cys, this peaks is now overlapping with the peak for one of the hydrogens on the glycine residues of TAT-Cys. The integral value of the massif is then approximated at 40.5 H (knowing that GD_{TAT} is low) and the peak is used as the reference peak. Consequently, the integration of the massif from δ 3.22 to δ 2.84 ppm leads to a total number of 2.14 H, which should account for 20 H from TAT-Cys and 2 H from H_2N-PEG$_{44}$-Mal. As GD_{PEG} = 18%, 2 x 0.18 = 0.36 is removed from 2.14 leading to 1.78 H.

Hence, GD_{TAT} = $\frac{1.78}{20}$ x 100 = 9 %.

With a similar reasoning using the massif at δ 2.62 – 2.17 ppm (9 H, H8-15-16 + H_{TAT}), we can recalculate GD_{Suc}. We obtain 20% which is quite different from the estimated value from the previous steps. If GD_{Suc} is used as a reference for the calculation of GD_{TAT}, GD_{TAT} would then equal 16%. In order to approximate at best the reality, GD_{TAT} was finally set at 11%.

Estimation of the molecular weight of one dCS-NSuc-OPEG$_{44}$-Mal-Cys-TAT chain (MW(dCS-NSuc-OPEG$_{44}$-Mal-Cys-TAT)):

MW(dCS-NSuc-OPEG$_{44}$-Mal-Cys-TAT) = Mw(dCS) + GD_{Suc} x M_{Suc} x nb(dCS units) + GD_{PEG} x MW(PEG) x nb(dCS units) + GD_{TAT} x $M_{TAT\text{-}Cys}$ x nb(dCS units)

= 8300 + 0.49 x 101.1 x 50 + 0.18 x 2176 x 50 + 0.11 x 1662 x 50

= 39.5 kDa

with 50 being the number of units per dCS chain (*cf.* dCS characterization for more details).

5.2.5. Shell polymer based on PEG_6

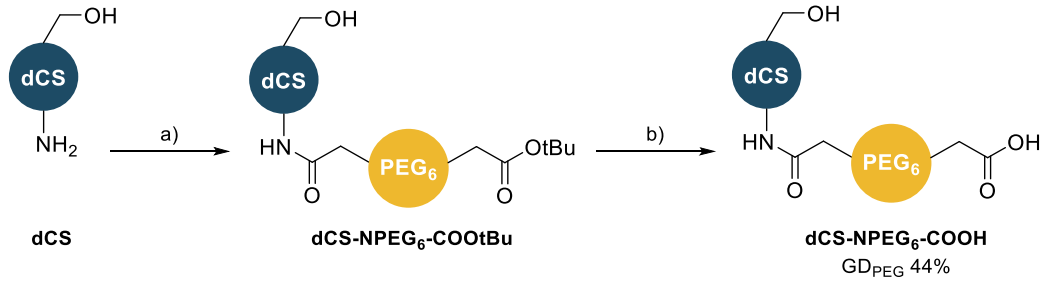

Scheme 31. Preparation of dCS-NPEG$_6$-COOH. a) HOOC-PEG$_6$-COOtBu, EDC.HCl, HOBt, DIPEA, DMAP, DMSO, rt, 17 h. b) 3 M HCl (aq), rt, 4.5 h.

dCS-NPEG$_6$-COOtBu

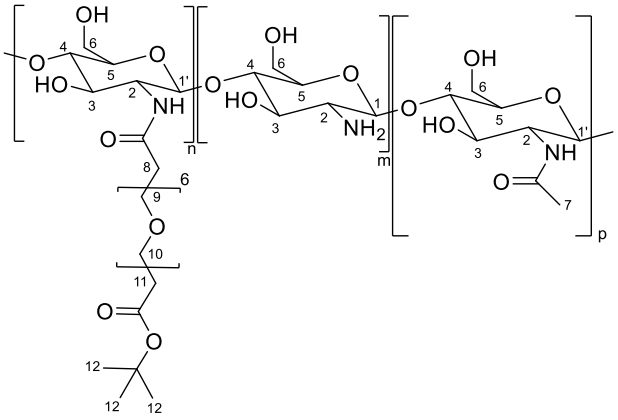

HOOC-PEG$_6$-COOtBu (184 mg, 0.420 mmol, 1.0 equiv.) was dissolved in 20 mL of dry DMSO. Dry DIPEA (219 µL, 1.26 mmol, 3.0 equiv.) and DMAP (154 mg, 1.26 mmol, 3.0 equiv.) were added to this solution. After 5 min of stirring at rt, HOBt (170 mg, 1.26 mmol, 3.0 equiv.) and EDC.HCl (241 mg, 1.26 mmol, 3.0 equiv.) were introduced. After 5 min of stirring at rt, **dCS** (DD 77%, 200 mg, 0.902 mmol of reactive units, 2.2 equiv.) was finally dissolved in the pale yellow solution. The reaction mixture was stirred at rt for 18 h. It was then split into 4 dialysis bags (MWCO 3.5 kDa) and dialyzed against water for 2.5 days. After 8 to 24 h of dialysis, NaCl solution (40 mg/mL, 10 mL in total) was added to the dialysis bags to favor removal of the remaining free HOOC-PEG$_6$-COOtBu. After dialysis, the solutions were centrifuged (4700 rpm, 20 °C, 10 min) and the supernatant was lyophilized. **dCS-NPEG$_6$-COOtBu** was obtained as a white aerated solid (233 mg, GD_{PEG} = 46%). **^{1}H NMR (500 MHz, D_2O):** δ 4.56 (br, 1 H, H1/1'), 3.97 – 3.40 (m, 29 H, H3-4-5-6-9-10), 2.68 – 2.49 (m, 5 H, H2-8-11), 2.03 (s, 3 H, H7), 1.45 (s, 9 H, H12).

^{1}H NMR spectrum of **dCS-NPEG$_6$-COOtBu** (500 MHz, D_2O)

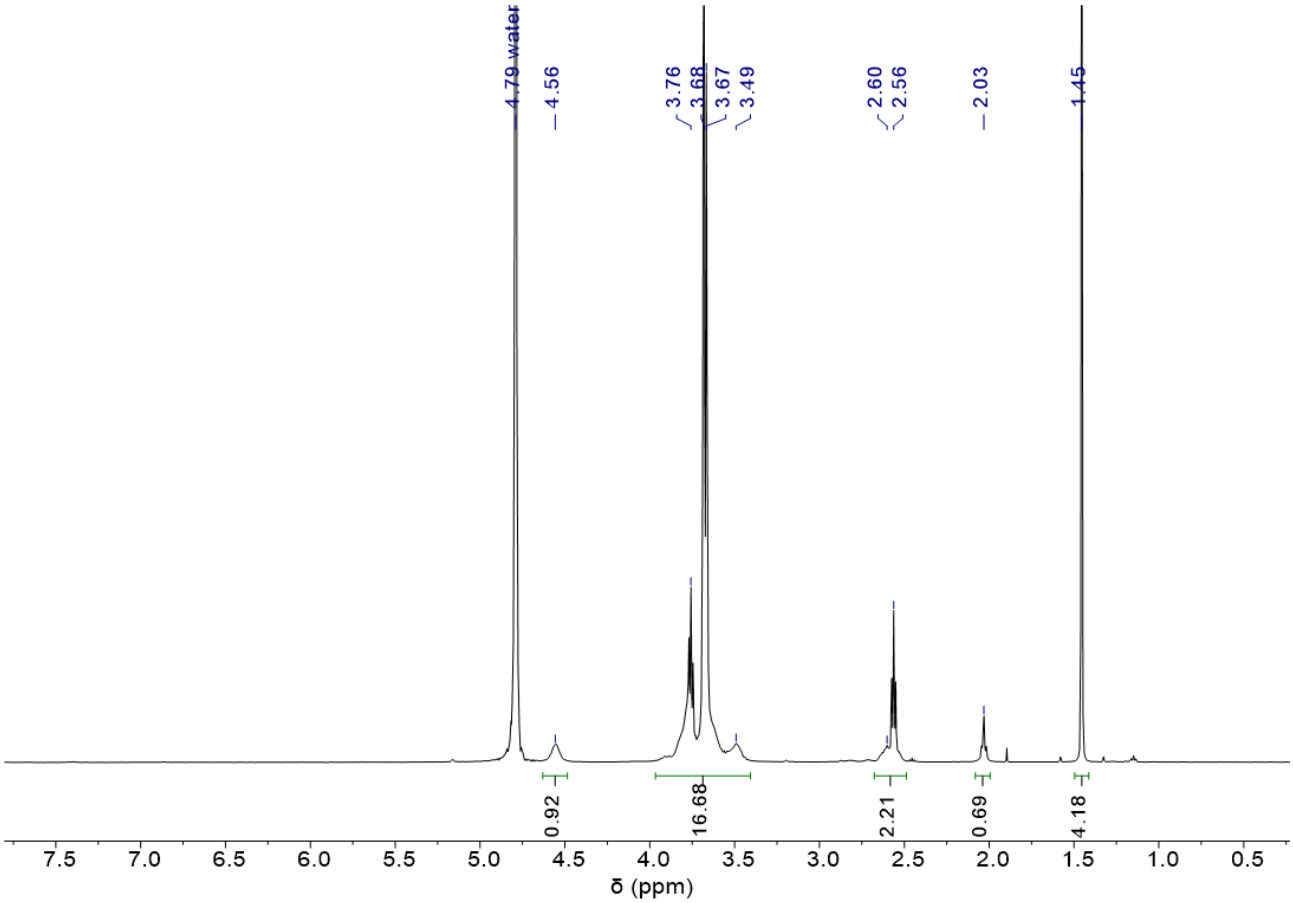

2D-DOSY NMR spectrum of **dCS-NPEG$_6$-COOtBu** (500 MHz, D_2O)

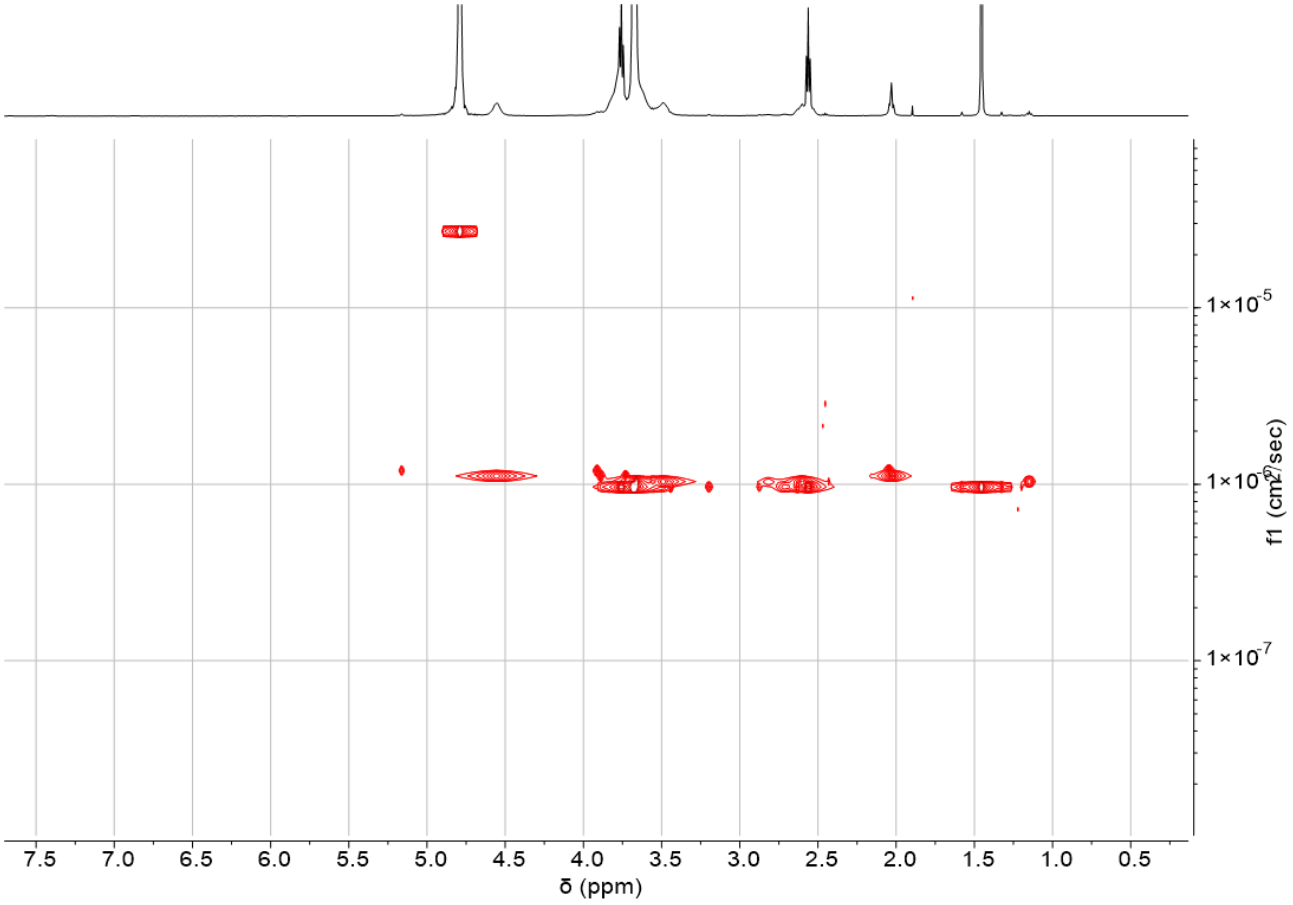

Calculation of the number of mol of reactive units (e.g. glucosamine units) of dCS (n(reactive units)):

As DD = 85%, the molar mass of one average unit of dCS is M(dCS) = 170.8 g/mol (cf. dCS characterization for more details), hence:

n(average units) = $\frac{m(dCS)}{M(dCS)} = \frac{0.200}{170.8}$ = 1.17 mmol and as only 77% of units are reactive (because DD = 77%), n(reactive units) = 1.17 x 0.77 = 0.902 mmol

Estimation of the grafting degree of HOOC-PEG$_6$-COOtBu on dCS (GD_{PEG}):

From the ^{1}H NMR spectrum, the peak for the acetyl group (δ 2.03 ppm) is used as the reference peak. As DD = 77 %, the integration for this peak equals 0.69 (cf. dCS characterization for more details). The sum of the integrations of the massifs at δ 3.97 – 3.40 ppm and δ 2.68 – 2.49 ppm leads to a total number of 18.9 H, where 6 H account for H2-3-4-5-6 from dCS backbone. The remaining 12.89 H account for H-8-9-10-11. Each HOOC-PEG$_6$-COOtBu chain is composed of 28 H (without taking into account the 9 H from *tert*-butoxyl group).

Hence, GD_{PEG} = $\frac{12.89}{28}$ x 100 = 46%

Note: The GD_{PEG} is always recalculated in the second step after removal of the Boc group (deprotection step, see below) to confirm this value.

Calculation of the molar mass of one average unit of dCS-NPEG$_6$-COOtBu (M(dCS-NPEG$_6$-COOtBu)):

M(dCS-NPEG$_6$-COOtBu) = DD x M(glucosamine) + AD x M(acetylglucosamine) + GD_{PEG} x MW(HOOC-PEG$_6$-COOtBu)

= 0.85 x 161.2 + 0.15 x 203.2 + 0.46 x 406.5

= 354.5 g/mol with AD = (1 – DD)

dCS-NPEG$_6$-COOH

dCS-NPEG$_6$-COOtBu (DD 78%, 62 mg, 10 mg/mL) was dissolved in 6 mL of 3 M HCl aqueous solution. The clear homogenous solution was stirred at rt for 4 h. The solution was then dialyzed (MWCO 3.5 kDa) against water for 3 days. The solution was centrifuged (4700 rpm, 20 °C, 10 min) and the supernatant was lyophilized. **dCS-NPEG$_6$-COOH** was obtained as a white aerated solid (38 mg, GD_{PEG} = 44%). **^{1}H NMR**

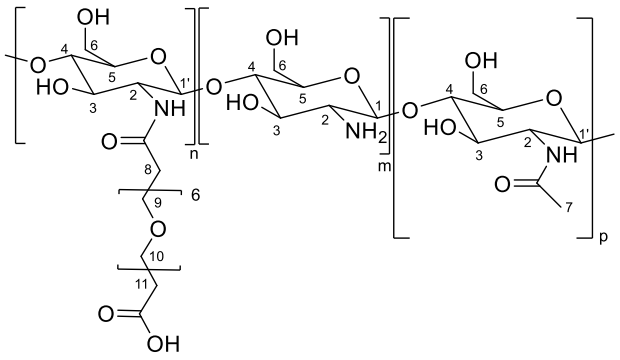

(500 MHz, D_2O): δ 4.53 (br, 1 H, H1/1'), 4.01 – 3.03 (m, 29 H, H3-4-5-6-9-10), 2.76 – 2.43 (m, 5 H, H2-8-11), 2.01 (s, 3 H, H7).

^{1}H NMR spectrum of **dCS-NPEG$_6$-COOH** (500 MHz, D_2O)

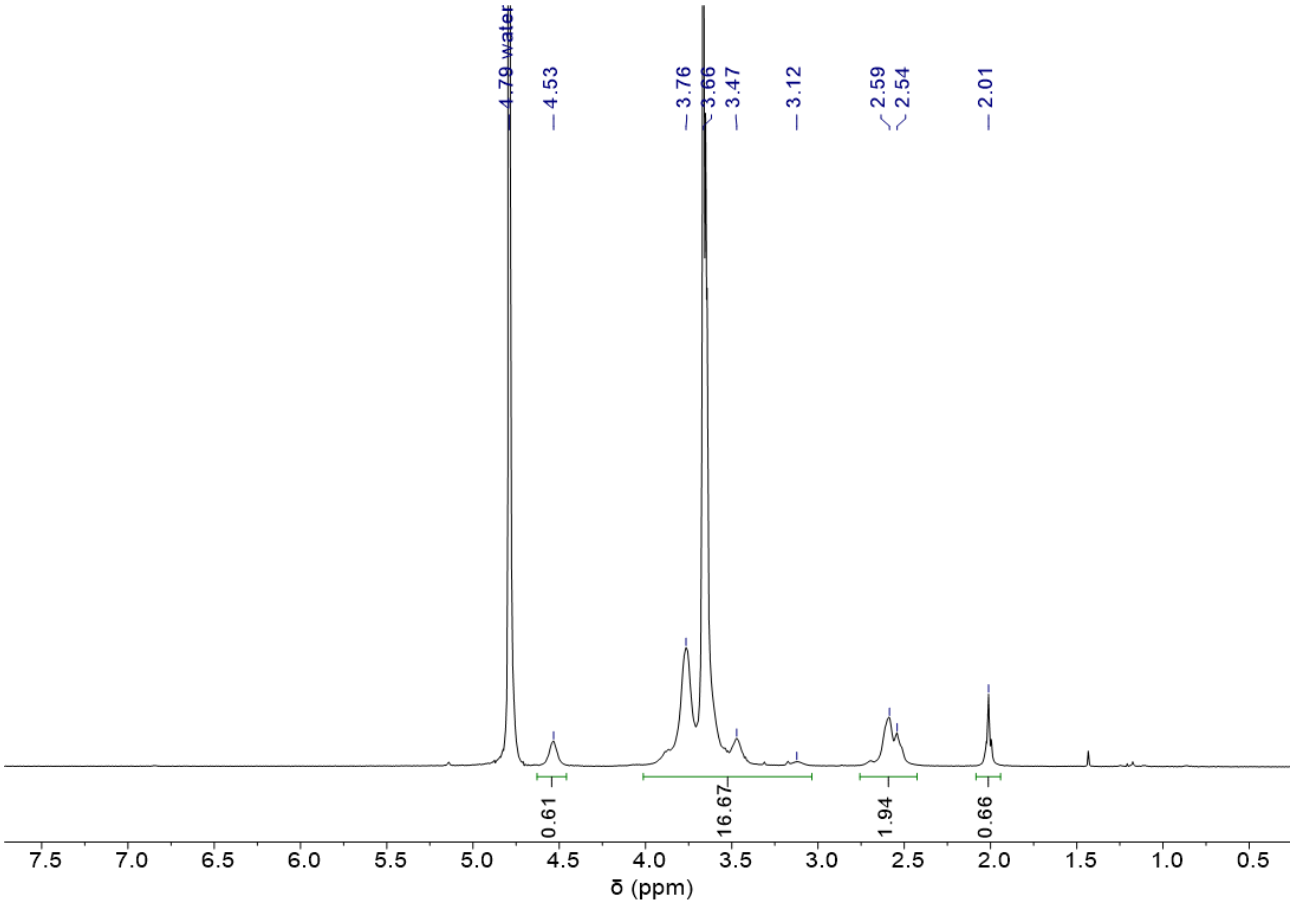

2D-DOSY NMR spectrum of **dCS-NPEG$_6$-COOH** (500 MHz, D_2O)

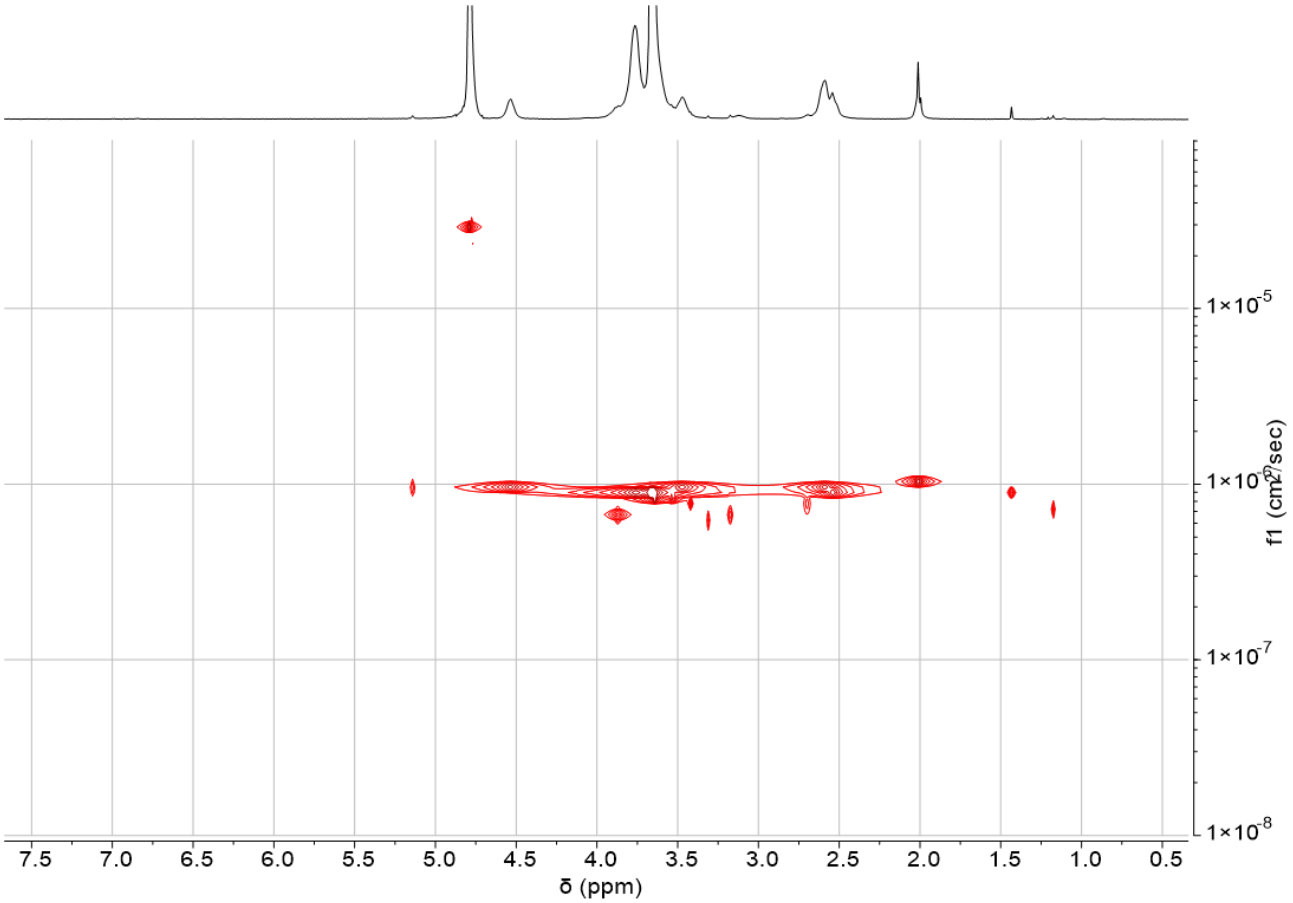

Estimation of the grafting degree of HOOC-PEG$_6$-COOH on dCS (GD$_{PEG}$):

From the ^{1}H NMR spectrum, the peak for the acetyl group (δ 2.01 ppm) is used as the reference peak. As DD = 78 %, the integration for this peak equals 0.66 (cf. characterization of dCS for more details). The sum of the integrations of the massifs at δ 4.01 – 3.03 ppm and δ 2.76 – 2.43 ppm leads to a total number of 18.6 H, where 6 H account for H2-3-4-5-6 from dCS backbone. The remaining 12.6 H account for H-8-9-10-11. Each HOOC-PEG$_6$-COOH chain is composed of 28 H visible by NMR (in D_2O).

Hence, $GD_{PEG} = \frac{12.6}{28} \times 100 = 44\%$

Estimation of the molecular weight of one dCS-NPEG$_6$-COOH chain (MW(dCS-NPEG$_6$-COOH)):

$MW(dCS\text{-}NPEG_6\text{-}COOH) = Mw(dCS) + GD_{PEG} \times MW(PEG) \times nb(dCS\ units)$

$= 5800 + 0.45 \times 364.5 \times 34$

$= 11.4$ kDa

with 34 being the number of units per dCS chain (*cf.* dCS characterization for more details).

5.2.6. Fluorescent chitosan-based derivatives

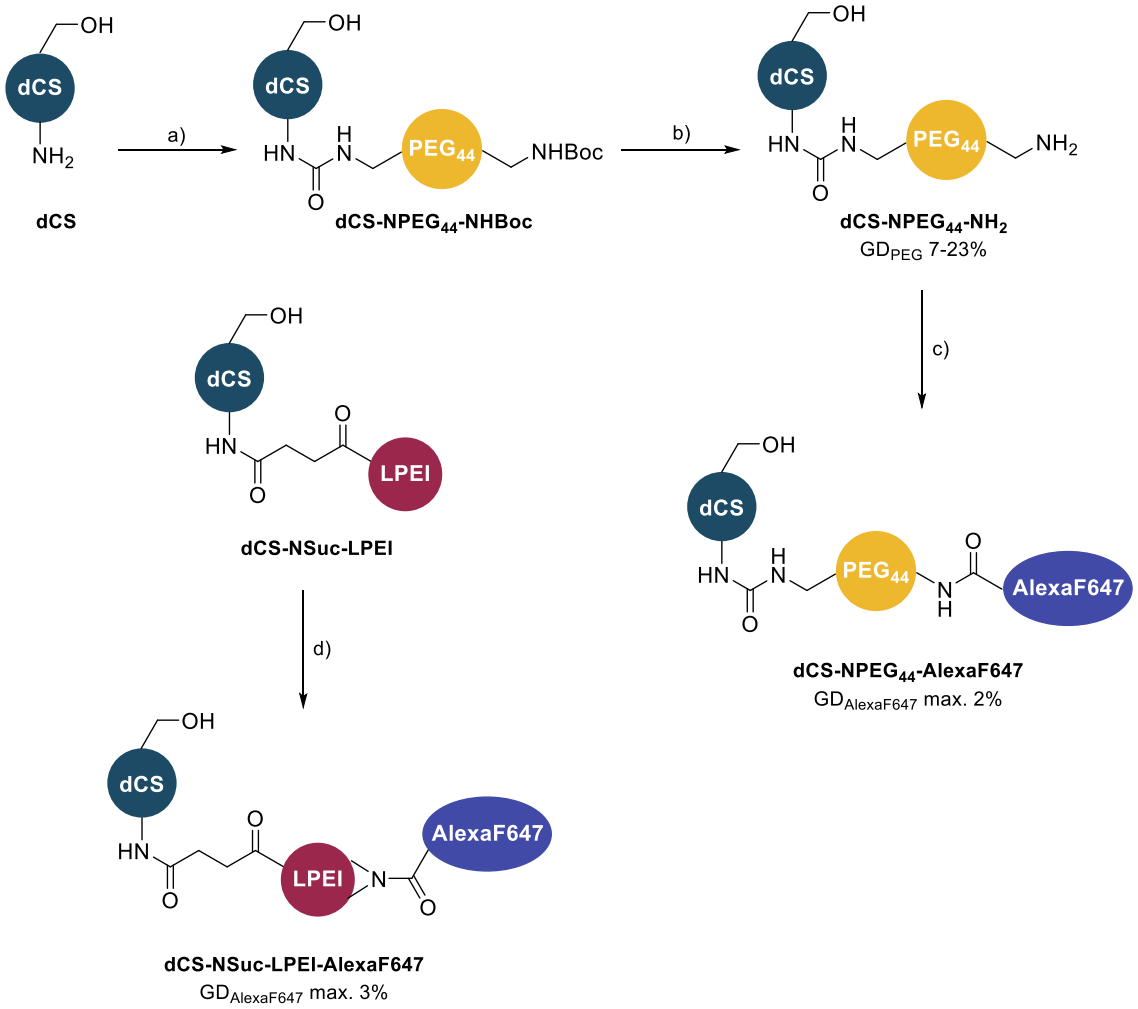

Scheme 32. Preparation of fluorescent dCS derivatives. a) CDI, DIPEA, HCl.H_2N-PEG$_{44}$-NHBoc, DMSO, rt, 16 h. b) 3 M HCl (aq.), rt, 45 min. c) Alexa Fluor 647-NHS ester, Et_3N, *in the dark*, rt, 22 h. d) Alexa Fluor 647-NHS ester, *in the dark*, pH 8, rt, 22 h.

dCS-NPEG$_{44}$-NH$_2$

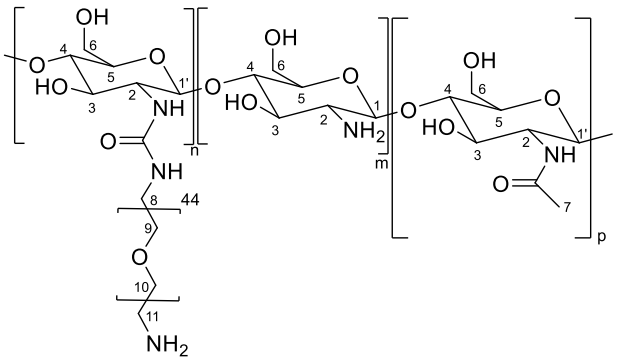

dCS (DD 72%, 46.5 mg, 0.194 mmol of reactive units, 1.0 equiv.) was dissolved in 8 mL of dry DMSO over 30 min. HCl.H_2N-PEG$_{44}$-NHBoc (82.5 mg, 0.0387 mmol, 0.20 equiv.) was added to the blurry homogenous mixture, followed by CDI (21.9 mg, 0.136 mmol, 0.70 equiv.) right after. After 15 min of stirring at rt, DIPEA (16.9 µL, 0.0970 mmol, 0.50 equiv.) was added and the reaction mixture was stirred at rt for 16 h. It was then dialyzed (MWCO 3.5 kDa) against water for 2.5 days. After 24 h of dialysis, 1 mL of 0.1 M HCl aqueous solution was added to the dialysis bag in order to favor the removal of the remaining free HCl.H_2N-PEG$_{44}$-NHBoc. Lastly, the solution was centrifuged (4700 rpm, 20 °C, 10

min) and the supernatant was lyophilized. dCS-NPEG$_{44}$-NHBoc was obtained as a white aerated solid (79.2 mg). 75 mg of dCS-NPEG$_{44}$-NHBoc were dissolved in 7.5 mL (10 mg/mL) of 3 M HCl aqueous solution and were stirred at rt with a vigorous stirring for 45 min. The white homogenous solution was then dialyzed (MWCO 3.5 kDa) against water for 2.5 days. The resulting clear solution was then centrifuged (4700 rpm, 20 °C, 10 min) and the supernatant was lyophilized. **dCS-NPEG$_{44}$-NH$_2$** was obtained as a white and aerated solid (48.3 mg, GD$_{PEG}$ = 23%). **^{1}H NMR (500 MHz, D$_2$O):** δ 4.60 (br, 1 H, H1/1'), 4.06 – 3.42 (m, 183 H, H3-4-5-6-9-10-11), 3.23 (t, 2 H, H8), 2.78 (br, 1 H, H2), 2.07 (s, 3 H, H7).

^{1}H NMR spectrum of **dCS-NPEG$_{44}$-NH$_2$** (500 MHz, D$_2$O)

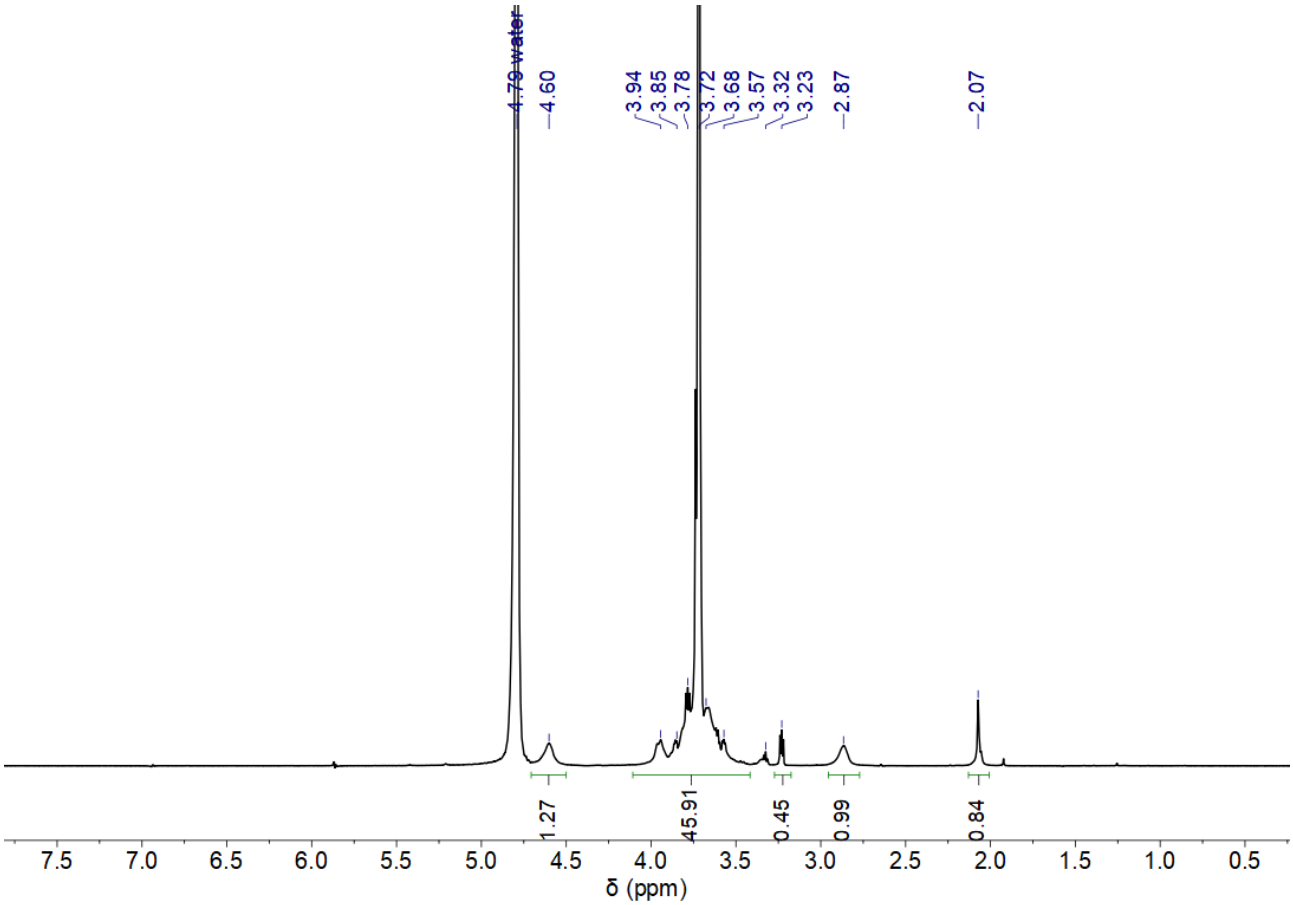

2D-DOSY NMR spectrum of **dCS-NPEG$_{44}$-NH$_2$** (500 MHz, D$_2$O)

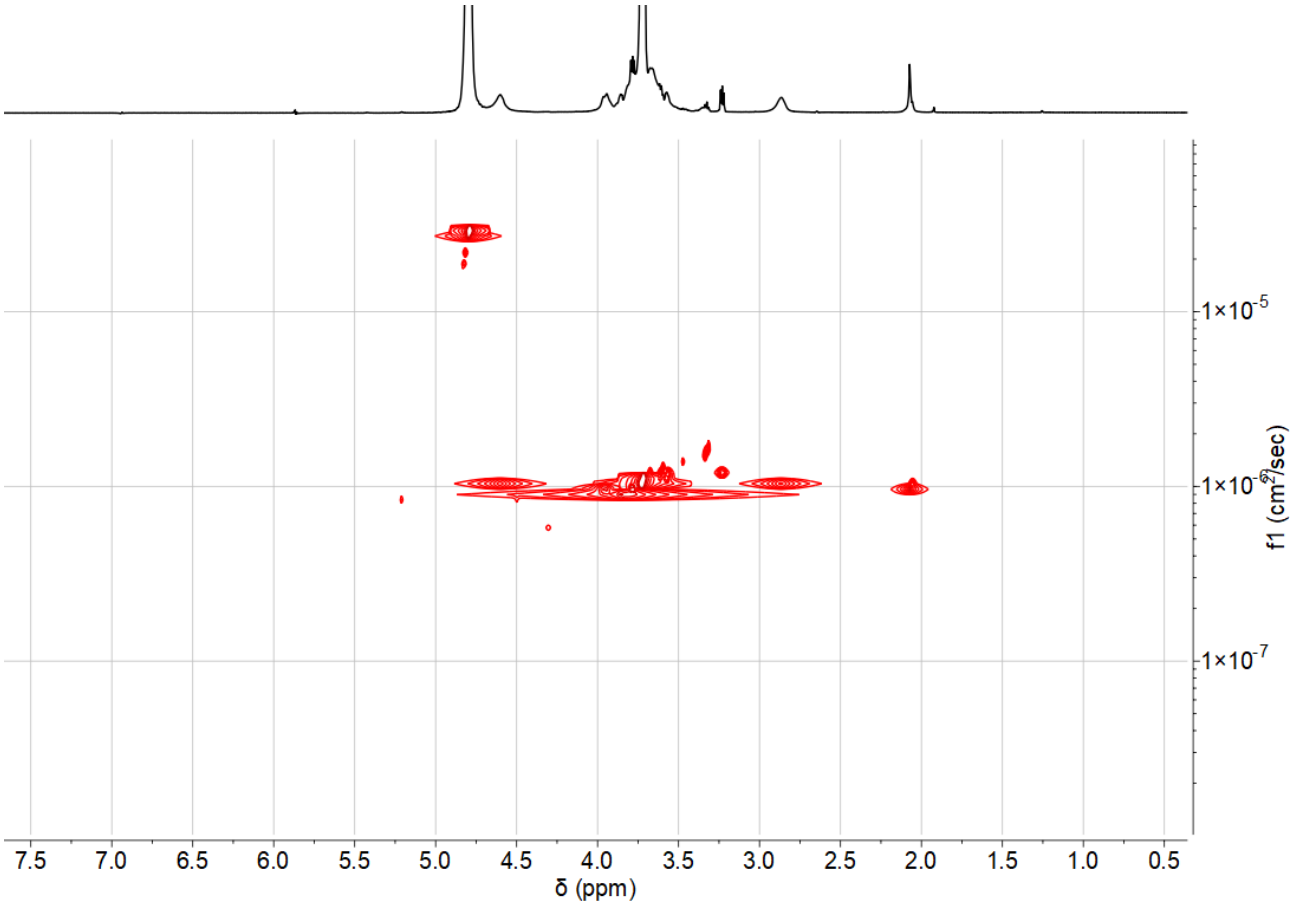

Calculation of the number of mol of reactive units (e.g. glucosamine units) of dCS (n(reactive units)):

As DD = 72%, the molar mass of one average unit of dCS is M(dCS) = 172.9 g/mol (*cf.* characterization of dCS for more details), hence:

n(average units) = $\frac{m(dCS)}{M(dCS)} = \frac{0.0465}{172.9}$ = 0.269 mmol and as only 72% of units are reactive (because DD = 72%), n(reactive units) = 0.269 x 0.72 = 0.194 mmol

Estimation of the grafting degree of H_2N-PEG_{44}-NH_2 on dCS (GD_{PEG}):

From the ^1H NMR spectrum, the peak for the acetyl group (δ 2.07 ppm) is used as the reference peak. As DD = 72 %, the integration for this peak equals 0.84 (cf. characterization of dCS for more details). The sum of the integrations of the massif at δ 4.06 – 3.42 ppm and the peaks at δ 3.23 ppm and δ 2.78 ppm leads to a total number of 47.7 H, where 6 H account for H2-3-4-5-6 from dCS backbone. The remaining 41.7 H account for H-8-9-10-11 and each H_2N-PEG_{44}-NH_2 chain is composed of 180 H.

Hence, GD_{PEG} = $\frac{41.7}{180}$ x 100 = 23%

Calculation of the molar mass of one average unit of dCS-$NPEG_{44}$-NH_2 (M(dCS-$NPEG_{44}$-NH_2)):

M(dCS-NPEG$_{44}$-NH$_2$) = DD x M(glucosamine) + AD x M(acetylglucosamine) + GD$_{PEG}$ x MW(H$_2$N-PEG$_{44}$-NH$_2$)

= 0.72 x 161.2 + 0.28 x 203.2 + 0.23 x 2024

= 638.4 g/mol with AD = (1 – DD)

dCS-NPEG$_{44}$-AlexaF647

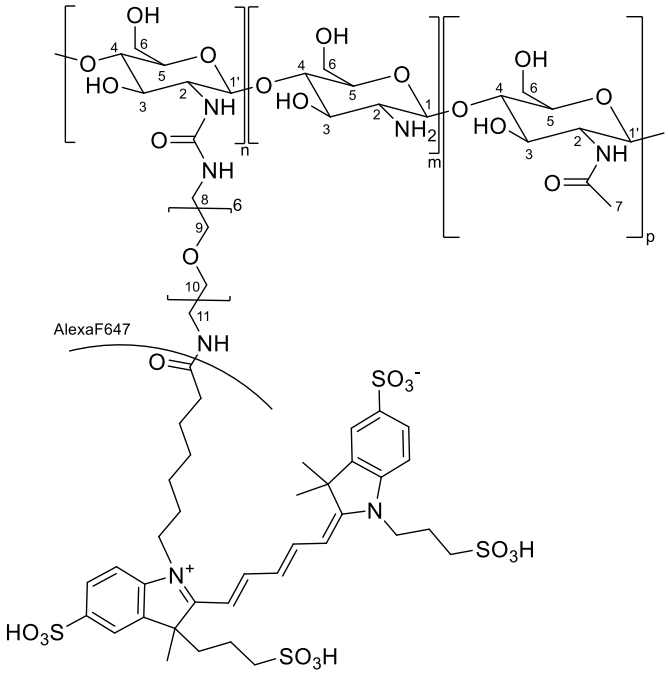

The reaction was performed in the dark to avoid bleaching of the fluorophore. To a brown-glass round-bottom flask containing 2 mL of distilled water, was added **dCS-NPEG$_{44}$-NH$_2$** (DD 72%, GD$_{PEG}$ 7 %, 20 mg, 4.50 µmol of reactive units, 1.0 equiv.). Et$_3$N (1.20 µL, 4.50 µmol, 2.0 equiv.) was added in order to reach pH 8. Alexa Fluor 647-NHS ester (1.20 mg, 1.13 µmol, 0.250 equiv.) was then added to the reaction mixture. After 22 h at rt, the blue mixture was dialyzed (MWCO 3.5 kDa) against water in the dark for 2.5 days. After centrifugation (4700 rpm, 20 °C, 10 min), the resulting blue supernatant was lyophilized. **dCS-NPEG$_{44}$-AlexaF647** was obtained as a blue aerated solid (16.2 mg, GD$_{AlexaF647}$ ≤ 2%). **^{1}H NMR (500 MHz, D$_2$O):** δ 8.20 (br, H$_{AF647}$), 7.93 (br, H$_{AF647}$), 7.87 (br, H$_{AF647}$), 7.42 (br, H$_{AF647}$), 6.73 (br, H$_{AF647}$), 6.46 (br, H$_{AF647}$), 4.54 (br, 1 H, H1/1'), 4.24 (br, H$_{AF647}$), 4.05 – 3.27 (m, 183 H, H3-4-5-6-9-10-11), 3.23 (t, 2 H, H8), 3.07 (br, H$_{AF647}$), 2.78 (br, 1 H, H2), 2.26 (br, H$_{AF647}$), 2.07 (s, 3 H, H7), 1.76 (br, H$_{AF647}$), 1.34 (br, H$_{AF647}$).

^{1}H NMR spectrum of **dCS-NPEG$_{44}$-AlexaF647** (500 MHz, D$_2$O)

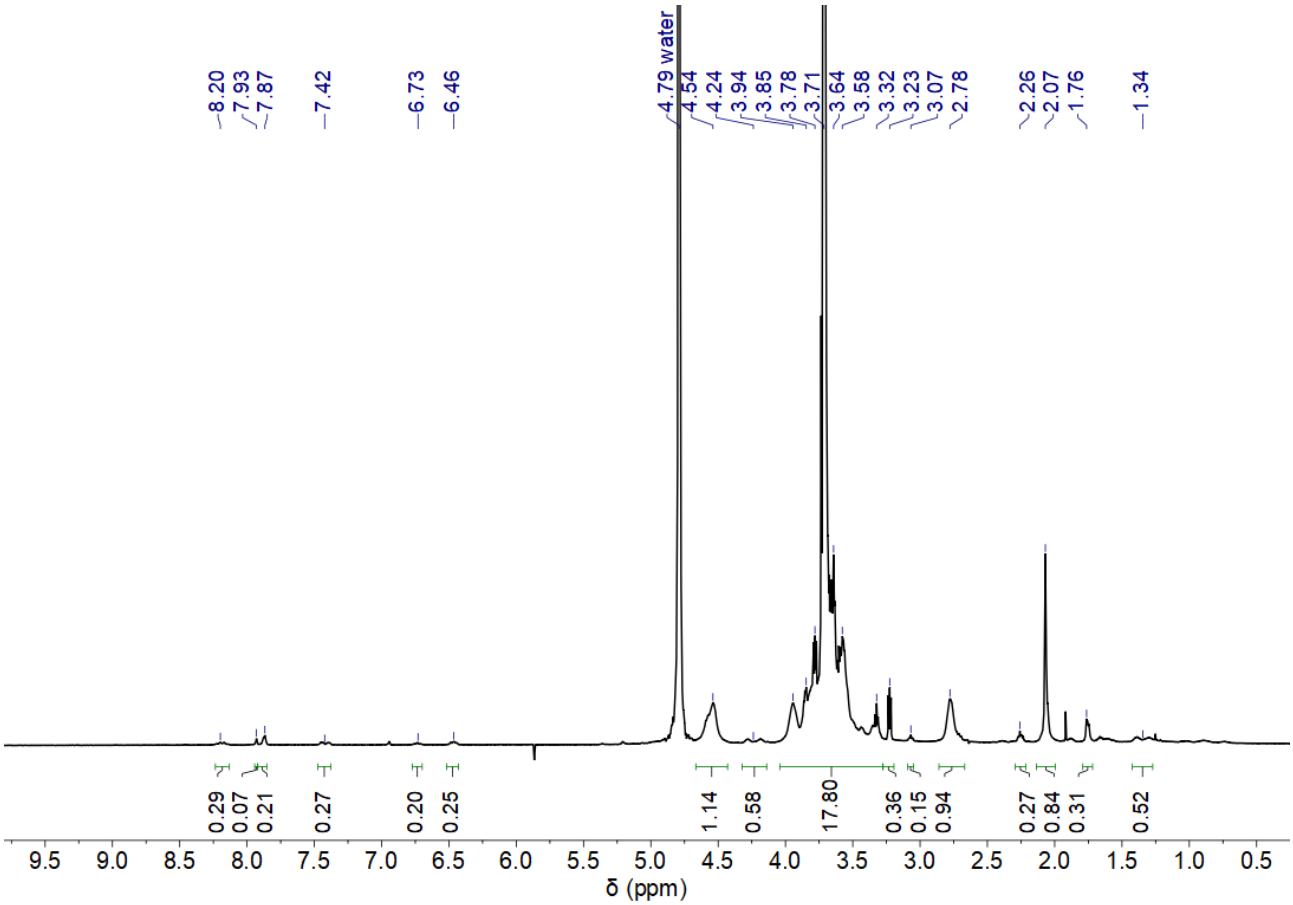

2D-DOSY NMR spectrum of **dCS-NPEG$_{44}$-AlexaF647** (500 MHz, D_2O)

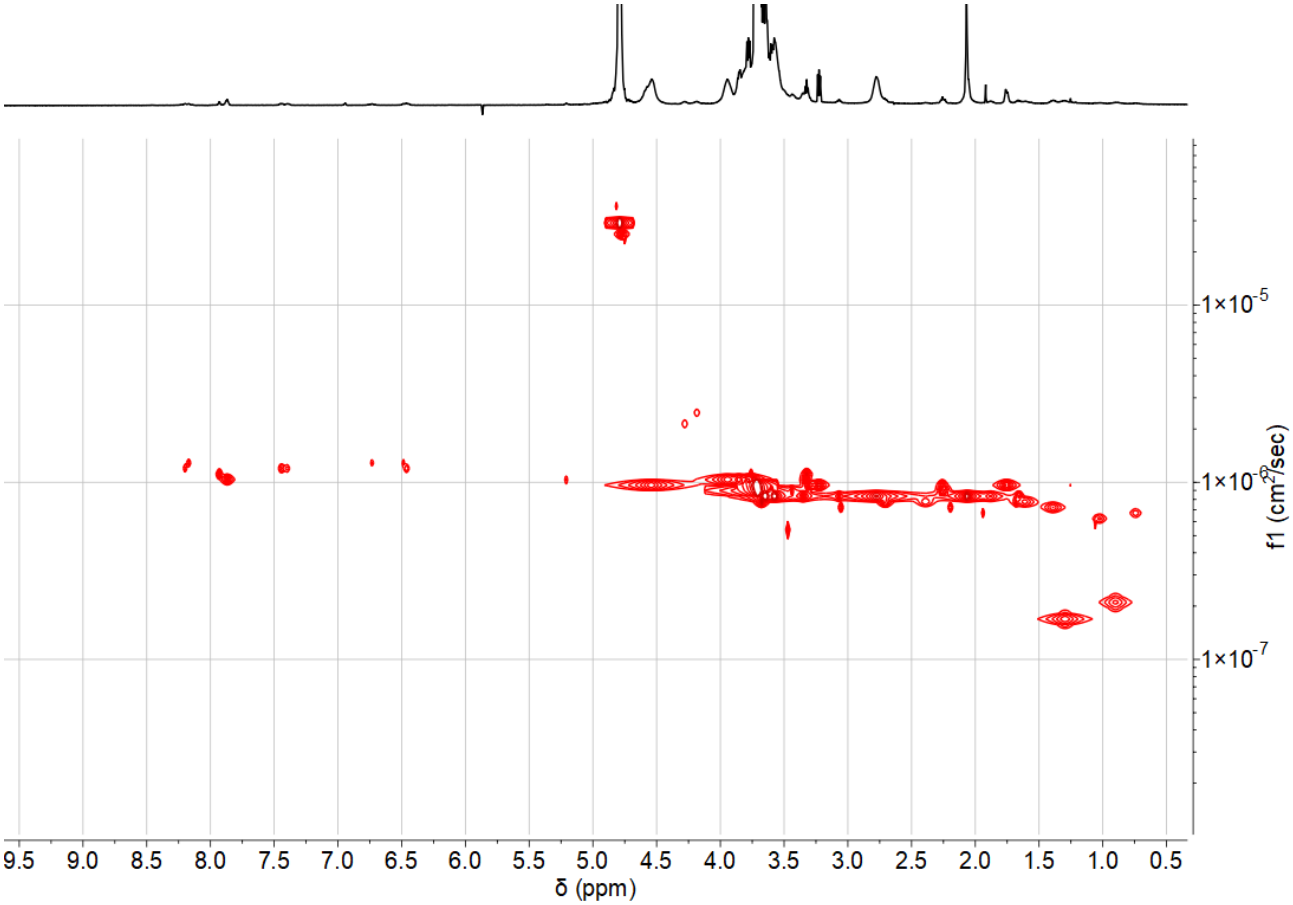

Calculation of the number of mol of reactive units (e.g. pegylated glucosamine units) of dCS-NPEG$_{44}$-NH$_2$ (n(reactive units)):

As GD_{PEG} = 7% and based on calculations explained in the previous step, the molar mass of one average unit of dCS-NPEG$_{44}$-NH$_2$ is M(dCS-NPEG$_{44}$-NH$_2$) = 314.6 g/mol, hence:

n(average units) = $\frac{m(dCS-NPEG44-NH2)}{M(dCS-NPEG44-NH2)} = \frac{0.020}{314.6}$ = 0.0636 mmol and as only 7% of units are considered to be reactive (because GD_{PEG} = 7%), n(reactive units) = 0.0636 x 0.07 = 0.0045 mmol

Estimation of the grafting degree of Alexa Fluor 647 on dCS-NPEG$_{44}$-NH$_2$ ($GD_{AlexaF647}$):

When integrating the peaks assigned to Alexa Fluor 647 on the spectrum, we found $GD_{AlexaF647}$ of 12% which is not realistic as the maximal GD that could be reached would be 2%. This result probably came from the very small and thus imprecise integral values of Alexa Fluor 647. $GD_{AlexaF647}$ was therefore estimated as inferior or equal to 2% of the total number of dCS units.

Estimation of the molecular weight of one dCS-NPEG$_{44}$-AlexaF647 chain (MW(dCS-NPEG$_{44}$-AlexaF647)):

MW(dCS-NPEG$_{44}$-AlexaF647) = Mw(dCS) + GD_{PEG} x MW(PEG) x nb(dCS units) + $GD_{AlexaF647}$ x $M_{AlexaF647}$ x nb(dCS units)

= 5800 + 0.07 x 2024 x 34 + 0.02 x 826 x 34

= 11.2 kDa

with 34 being the number of units per dCS chain (*cf.* dCS characterization for more details).

dCS-NSuc-LPEI-AlexaF647

The reaction was performed in the dark to avoid bleaching of the fluorophore. To a brown-glass round-bottom flask containing 3 mL of distilled water, was dissolved **dCS-NSuc-LPEI** (DD 79%, GD_{Suc} 63%, GD_{LPEI} 14%, 30.0 mg, 0.00720 mmol, 1.0 equiv.). 24 µL of 1 M HCl aqueous solution were added to the heterogenous mixture to decrease the pH from 9 to 8. After 30 min at rt, Alexa Fluor 647-NHS ester (1.70 mg, 0.00180 mmol, 0.25 equiv.) was introduced into the reaction mixture. 2 mL of rinsing distilled water were added and the blue mixture was stirred at rt for 22 h before being dialyzed (MWCO 3.5 kDa) against water in the dark for 3.5 days. The blue and homogenous solution was then centrifuged (4700 rpm, 20 °C, 10 min) and the supernatant was lyophilized. **dCS-NSuc-LPEI-AlexaF647** was obtained as

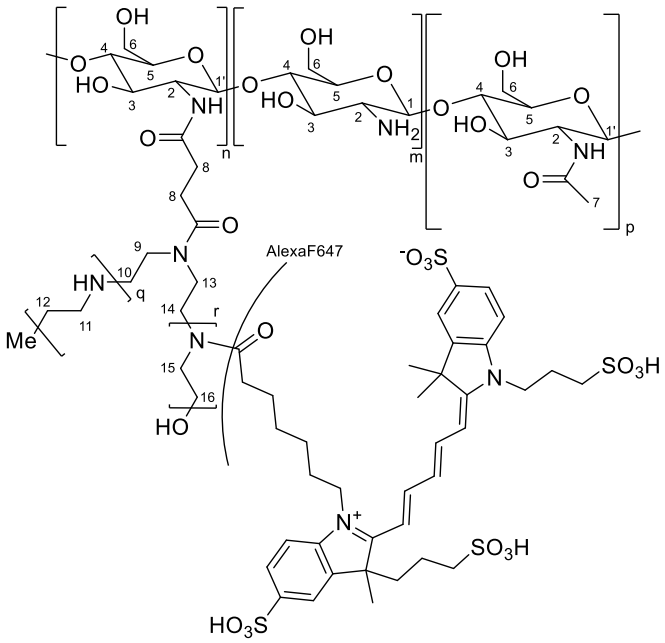

a blue aerated solid (15.3 mg, GD_{AF647} ≤ 3%). **^{1}H NMR (500 MHz, D_2O/CD_3COOD 1:1):** δ 9.35 (br, H_{AF647}), 7.92 (br, H_{AF647}), 7.40 (br, H_{AF647}), 6.44 (br, H_{AF647}), 4.94 (br, 0.16 H, H1), 4.60 (br, 0.84 H, H1'), 4.15 – 2.87 (m, 238 H, H2-3-4-5-6-9-10-11-12-13-14-15-16), 2.86 – 2.52 (br, 4 H, H8), 2.29 (br, H_{AF647}), 1.75 (br, H_{AF647}), 1.62 (br, H_{AF647}). δ 2.48, 1.24, 1.09 ppm are present in all commercial batches of LPEI.

^{1}H NMR spectrum of **dCS-NSuc-LPEI-AlexaF647** (500 MHz, D_2O/CD_3COOD 1:1)

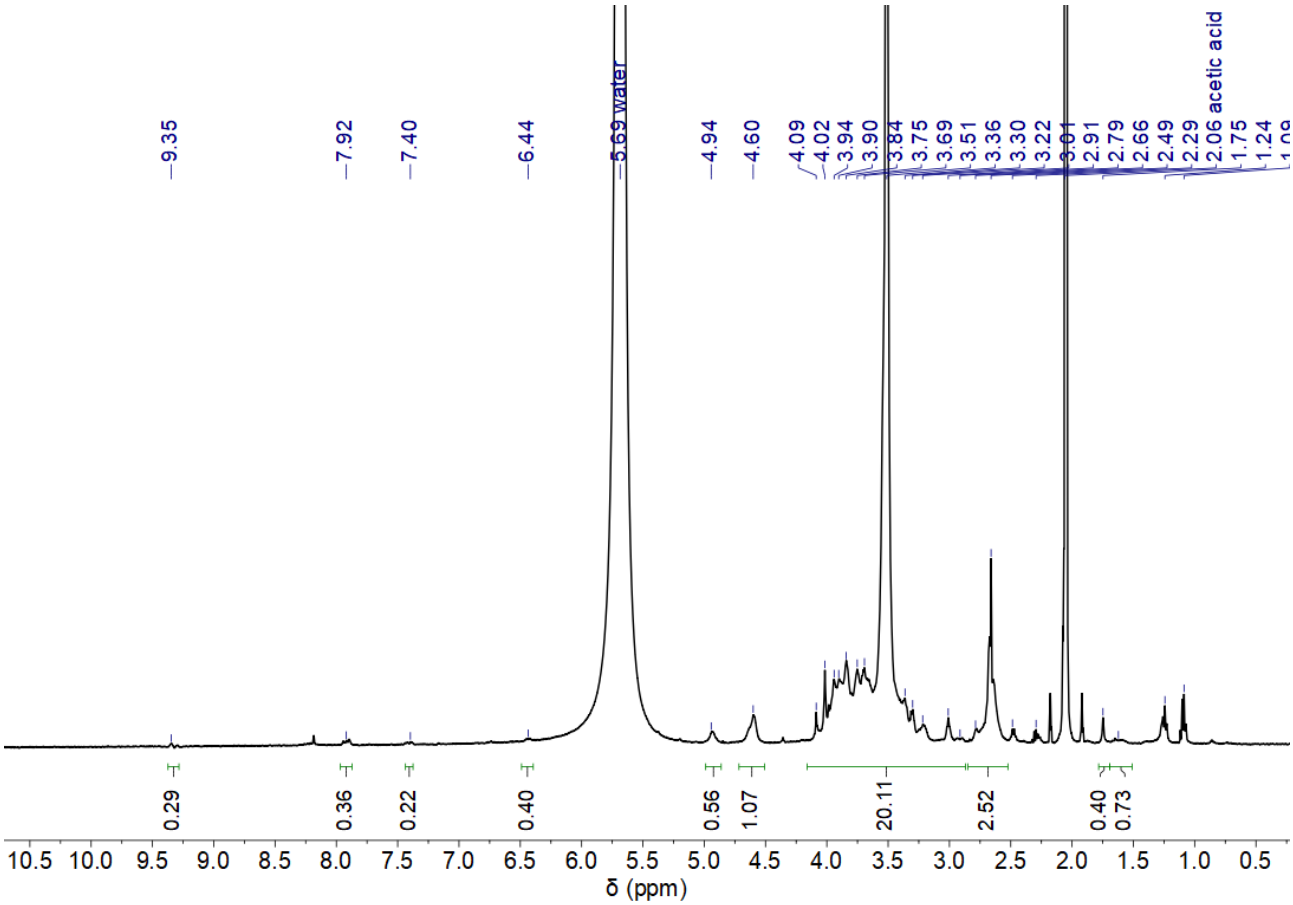

2D-DOSY NMR spectrum of **dCS-NSuc-LPEI-AlexaF647** (500 MHz, D_2O/CD_3COOD 1:1)

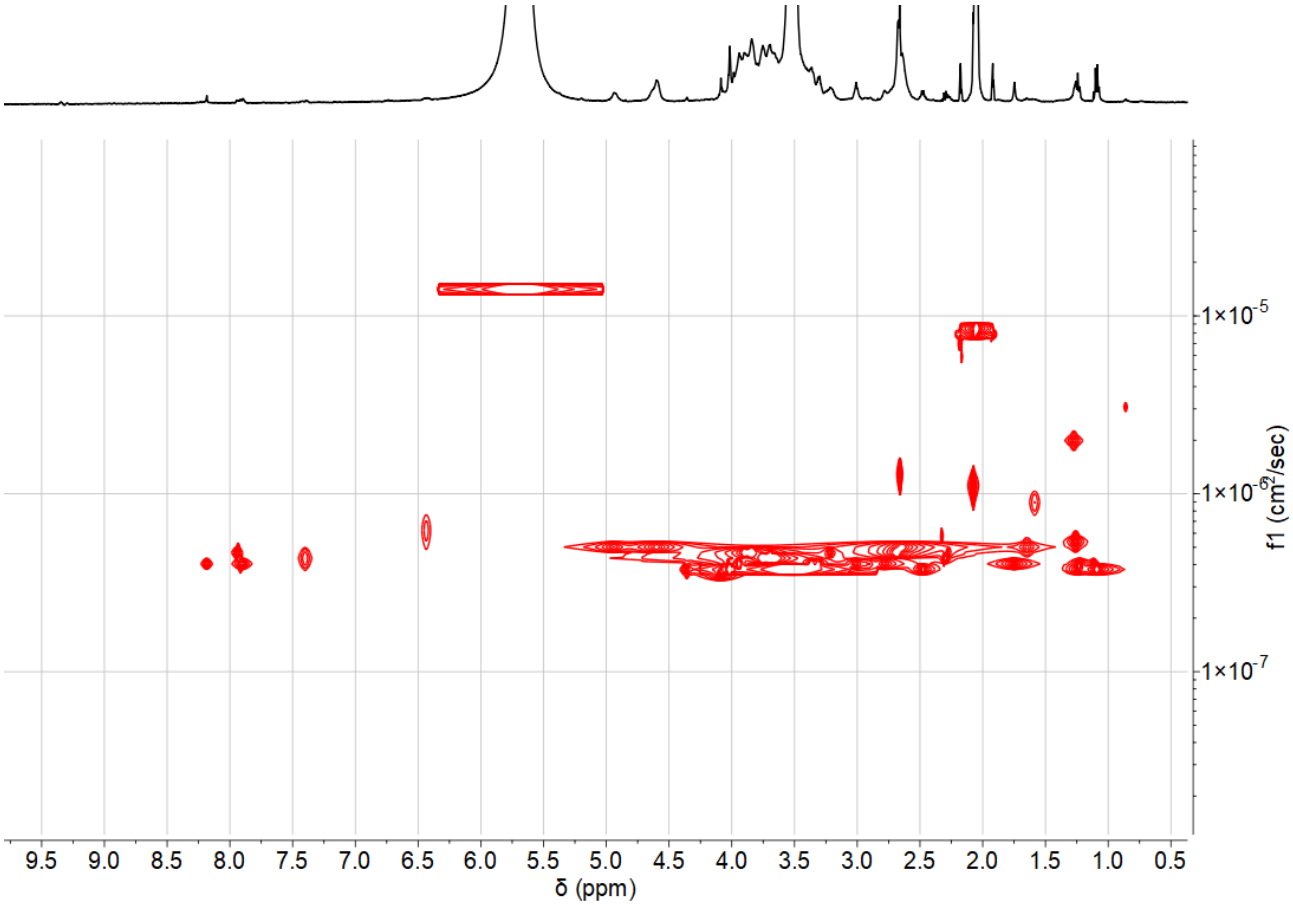

Calculation of the number of mol of reactive units (e.g. succinylated glucosamine units grafted with LPEI) of dCS-NSuc-LPEI (n(reactive units)):

As GD_{Suc} = 63%, GD_{LPEI} = 14% and DD = 79%, the molar mass of one average unit of dCS-NSuc-LPEI is M(dCS-NSuc-LPEI) = 583.0 g/mol (cf. characterization of dCS-NSuc-LPEI for more details), hence:

n(average units) = $\frac{m(\text{dCS-NSuc-LPEI})}{M(\text{dCS-NSuc-LPEI})} = \frac{0.03}{583.0}$ = 0.0515 mmol and as only 14% of units are reactive (because GD_{LPEI} = 14%), then n(reactive units) = 0.0515 x 0.14 = 0.00720 mmol

Note: we considered that only one amine of each LPEI chain was reacting with the fluorophore but it was in order to simplify the math. There were actually 58 times more amines from each chain that could have reacted with Alexa Fluor 647.

Estimation of the grafting degree of Alexa Fluor 647 on dCS-NSuc-LPEI ($GD_{AlexaF647}$):

When integrating the peaks assigned to Alexa Fluor 647 on the spectrum, we found $GD_{AlexaF647}$ to be superior to the maximal GD that could be reached (3%). This result probably came from the very small and thus imprecise integral values of Alexa Fluor 647. $GD_{AlexaF647}$ was therefore estimated as inferior or equal to 3% of the total number of dCS units.

Estimation of the molecular weight of one dCS-NSuc-LPEI-AlexaF647 chain (MW(dCS-NSuc-LPEI-AlexaF647)):

MW(dCS-NSuc-LPEI-AlexaF647) = Mw(dCS) + GD_{Suc} x M_{Suc} x nb(dCS units) + GD_{LPEI} x MW(LPEI) x nb(dCS units) + $GD_{AlexaF647}$ x $M_{AlexaF647}$ x nb(dCS units)

= 8300 + 0.63 x 101.1 x 49 + 0.14 x 2500 x 49 + 0.03 x 826 x 49

= 29.8 kDa

with 49 being the number of units per dCS chain (*cf.* dCS characterization for more details).

5.2.7. Functionalization of shell polymers

5.2.7.1. Synthesis of folic-acid derived PEG derivatives

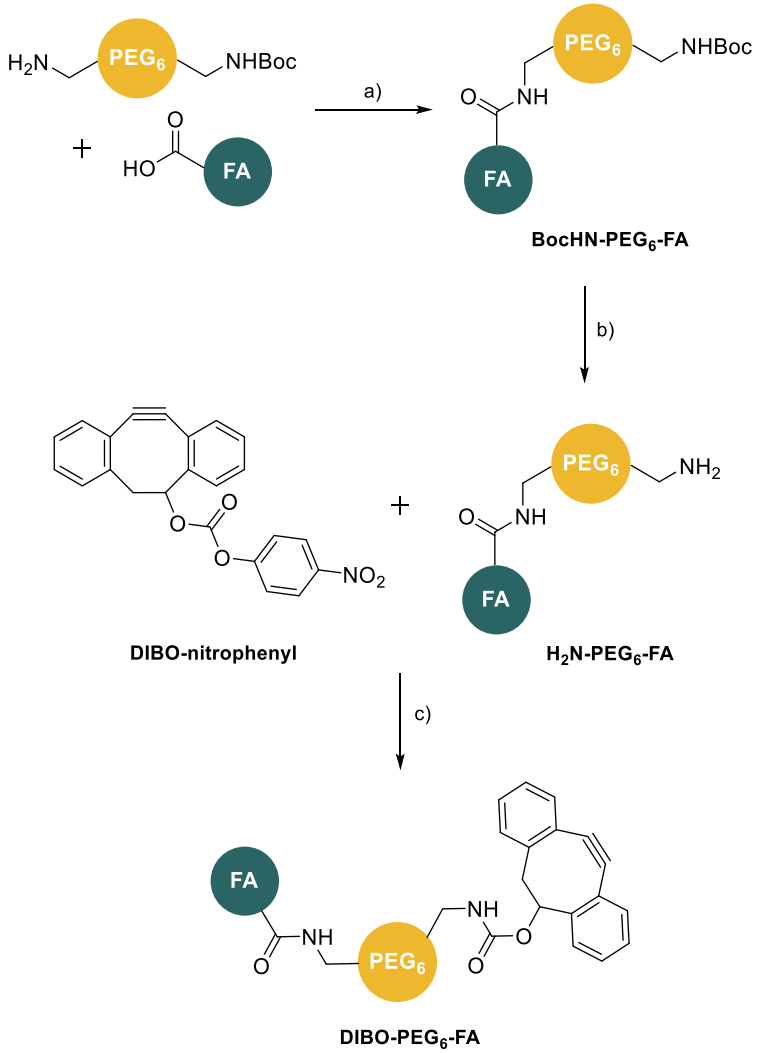

Scheme 33. Synthesis of DIBO-PEG_6-FA. a) TBTU, DIPEA, DMSO, rt, 16 h, 69%. b) 3 M HCl (aq.), rt, 3.5 h, 85%. c) Et_3N, DMSO, rt, 17 h, 40%.

BocHN-PEG$_6$-FA

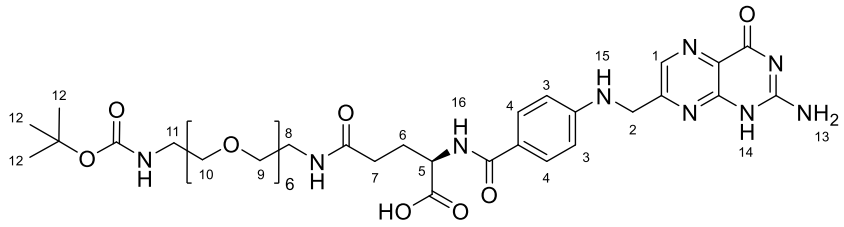

Folic acid (130 mg, 0.294 mmol, 1.0 equiv.) was dissolved at rt in 5 mL of dry DMSO. TBTU (90.0 mg, 0.280 mmol, 0.95 equiv.) and dry DIPEA (51 µL, 0.294 mmol, 1.0 equiv.) were then introduced into the homogenous orange solution. After 15 min of stirring at rt, a solution of H_2N-PEG$_6$-NHBoc (150 mg, 0.353 mmol, 1.2 equiv.) in 1 mL of DMSO was added dropwise to the reaction mixture. After 16 h of stirring at rt, the solution was dialyzed (MWCO 0.1 – 0.5 kDa) against water for 3 days. The product instantly precipitated after contact with distilled water. After dialysis, the heterogeneous orange solution was freeze dried to yield a yellow aerated solid (172 mg, 69%). **^{1}H NMR (400 MHz, DMSO-d$_6$):** 8.63 (s, 1 H, H1), 8.03 – 7.78 (m, 2 H, H14-15), 7.63 (br, 2 H, H4), 6.98 – 6.67 (m, 3 H, H13-16), 6.63 (br, 2 H, H3), 4.56 – 4.17 (m, 3 H, H2-5), 3.68 – 3.10 (m, 26 H, H8-9-10), 3.05 (br, 2 H, H11), 2.36 – 1.71 (m, 4 H, H6-7), 1.36 (t, 9 H, H12).

^{1}H NMR spectrum of **BocHN-PEG$_6$-FA** (400 MHz, DMSO-d$_6$)

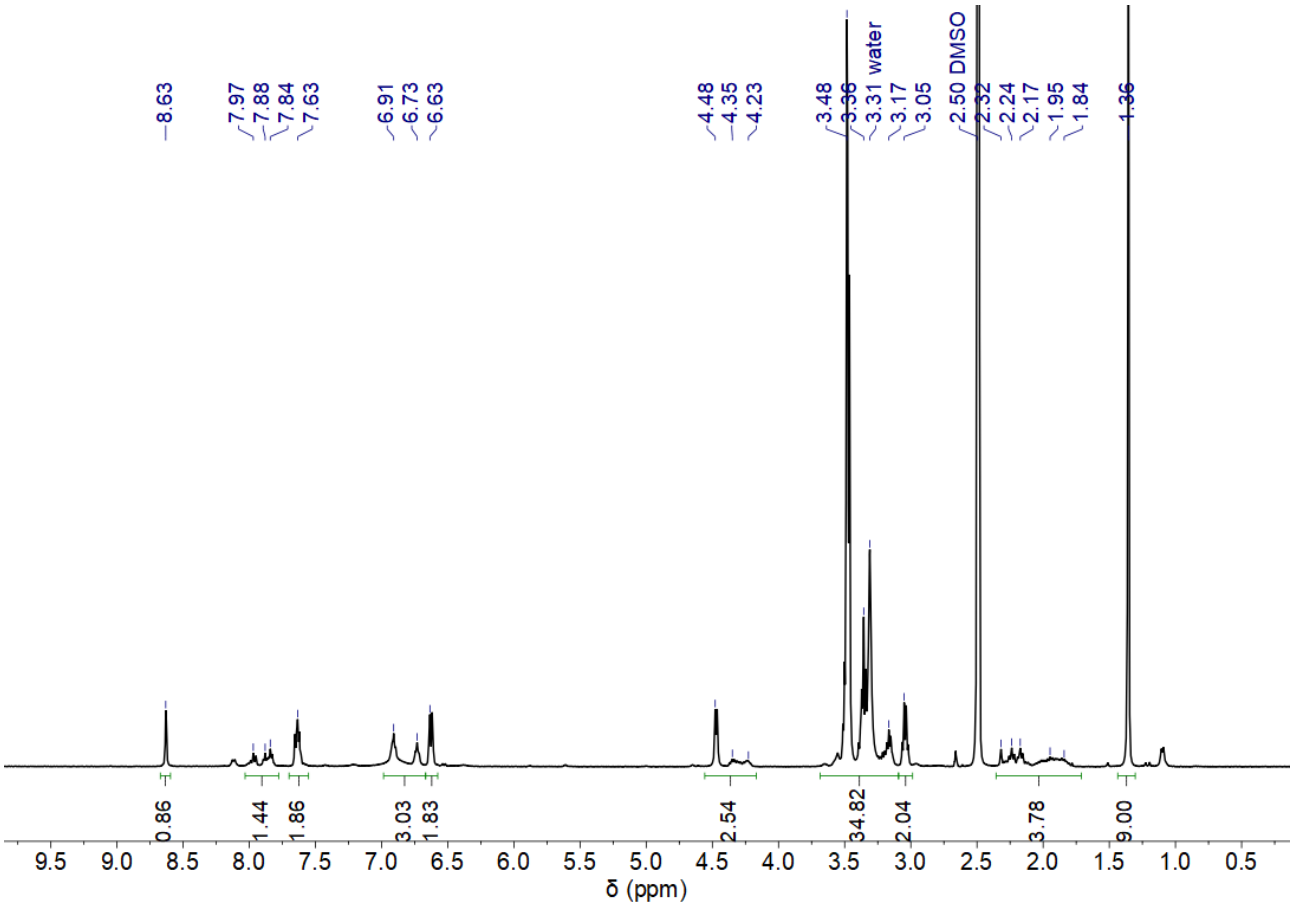

HRMS (ESI/QTOF): *m/z* calculated for $C_{38}H_{59}N_{10}O_{12}^+$ ([M + H]$^+$): 848.4076; Found 848.4157.

IR (cm^{-1}): 3283, 3107, 2869, 1686, 1635, 160, 1510, 1452, 1414, 1392, 1366, 1296, 1247, 1172, 1092, 969, 946, 838, 818, 768, 738.

H_2N-PEG_6-FA

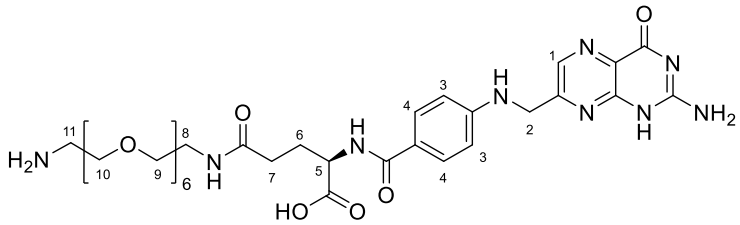

BocHN-PEG_6-FA (170 mg, 0.227 mmol) was dissolved in 9 mL of 3 M HCl (aq.) solution (≈ 20 mg/mL) at rt. After 3 h 30 of stirring at rt, the orange homogenous solution was transferred to dialysis (MWCO 0.1 – 0.5 kDa) against water for 3 days. **H_2N-PEG_6-FA** was obtained as an orange aerated solid after freeze drying (127 mg, 85%). **^{1}H NMR (400 MHz, D_2O):** δ 8.84 – 8.55 (br, 1 H, H1), 7.75 – 7.52 (br, 2 H, H4), 6.93 – 6.58 (br, 2 H, H3), 4.68 – 4.26 (m, 3 H, H2-5), 3.88 – 3.10 (m , 28 H, H-8-9-10-11), 2.55 – 1.93 (m, 4 H, H6-7). δ 1.34 ppm is assigned to remaining traces of Boc group.

^{1}H NMR spectrum of **H_2N-PEG_6-FA** (400 MHz, D_2O)

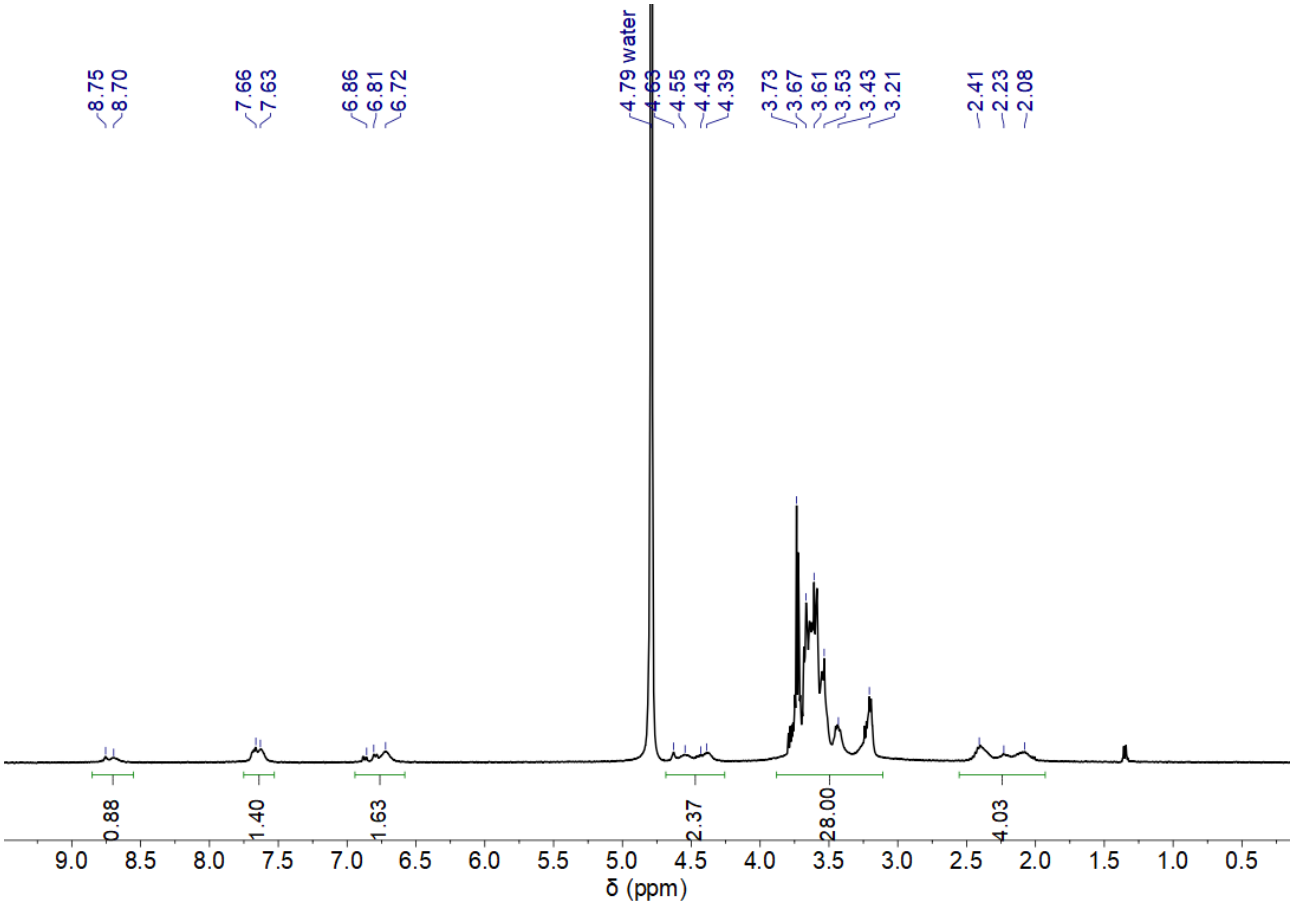

HRMS (ESI/QTOF): *m/z* calculated for $C_{33}H_{50}N_9O_{11}^+$ ([M + H]$^+$): 748.3624; Found 748.3637.

IR (cm^{-1}): 3259, 3086, 2872, 1725, 1685, 1603, 1508, 1451, 1402, 1298, 1191, 1084, 969, 945, 838, 818, 767, 737.

DIBO-PEG$_6$-FA

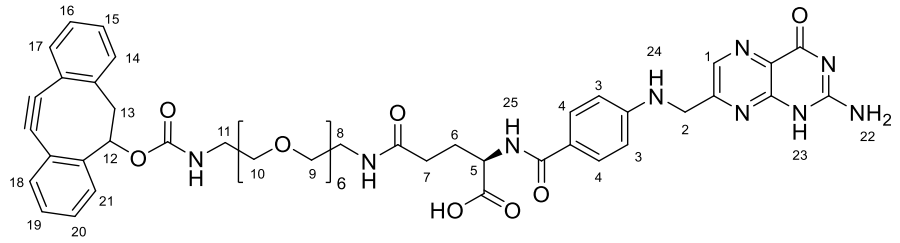

DIBO-nitrophenyl was synthesized according to a previously reported procedure.[212] To a solution of **DIBO-nitrophenyl** (12.1 mg, 0.0315 mmol, 1.0 equiv.) in 2 mL of dry DMSO, were successively added Et_3N (13.2 µL, 0.0945 mmol, 3.0 equiv.) and then **H_2N-PEG$_6$-FA** (23.5 mg, 0.0315 mmol, 1.0 equiv.). The resulting orange solution was stirred at rt for 17 h before being transferred to dialysis (MWCO 0.1 – 0.5 kDa) against water for 2 days. After freeze-drying, 19.8 mg of product were recovered and were directly redissolved in a 10% EtOH aqueous solution to remove remaining impurities. The product was dialyzed a second time against EtOH/water (10/90 v/v) for 1 day. After freeze-drying of the resulting solution, **DIBO-PEG$_6$-FA** was obtained as a yellow aerated solid (12.5 mg, 40%). **^{1}H NMR (400 MHz, DMSO-d$_6$):** δ 8.64 (s, 1 H, H1), 8.09 – 7.78 (m, 2 H, H23-24), 7.72 – 7.27 (m, 10 H, H4-14-15-16-17-18-19-20-21), 7.03 – 6.69 (m, 3 H, H22-25) , 6.63 (br, 2 H, H3), 5.28 (br, 1 H, H12), 4.58 – 4.19 (m, 3 H, H2-5), 3.71 – 2.70 (m, 30 H, H8-9-10-11-13), 2.38 – 1.76 (m, 4 H, H6-7). δ 1.10 ppm is assigned to remaining traces of an unknown impurity.

^{1}H NMR spectrum of **DIBO-PEG$_6$-FA** (400 MHz, DMSO-d$_6$)

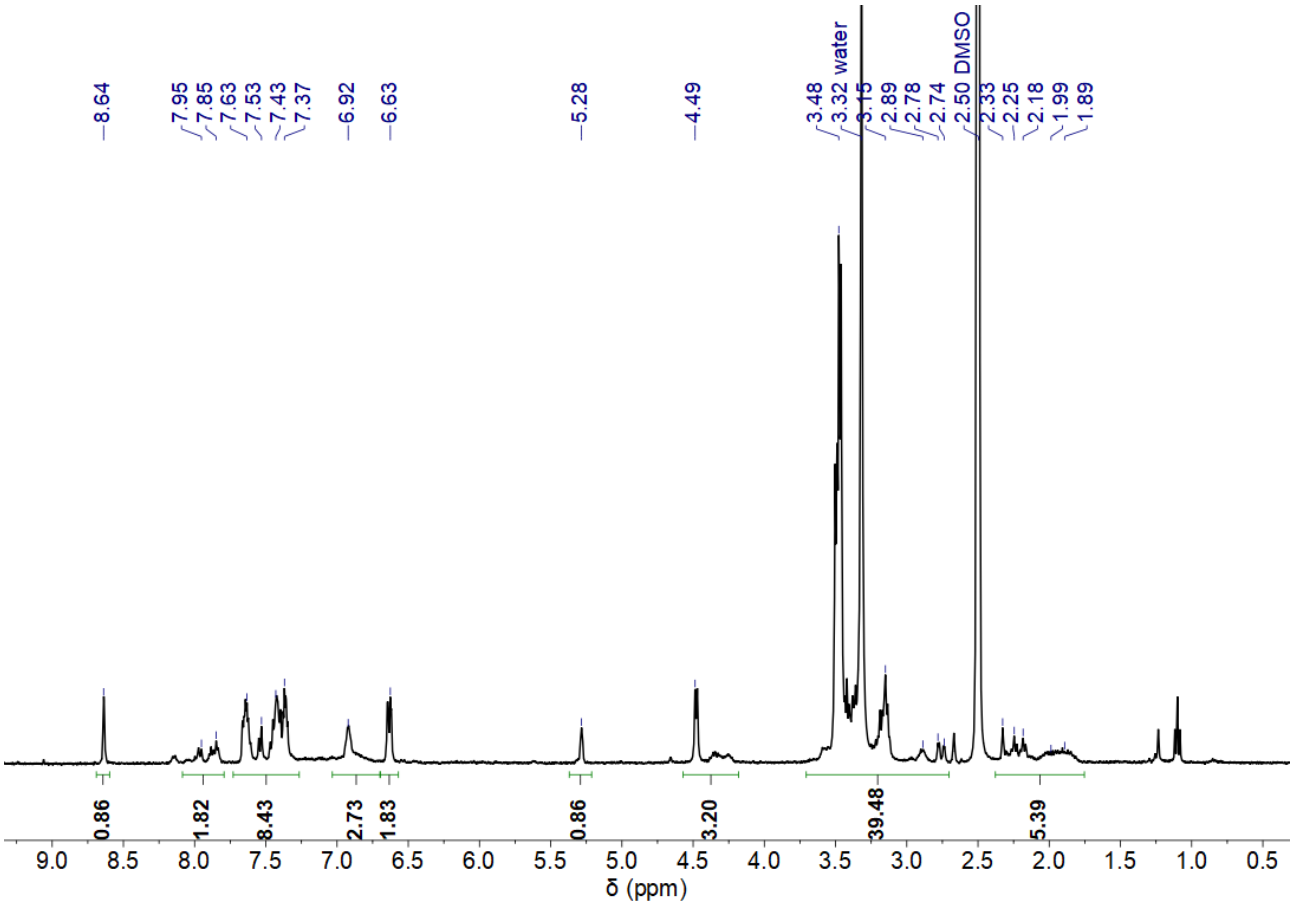

2D-DOSY NMR spectrum of **DIBO-PEG$_6$-FA** (500 MHz, DMSO-d$_6$)

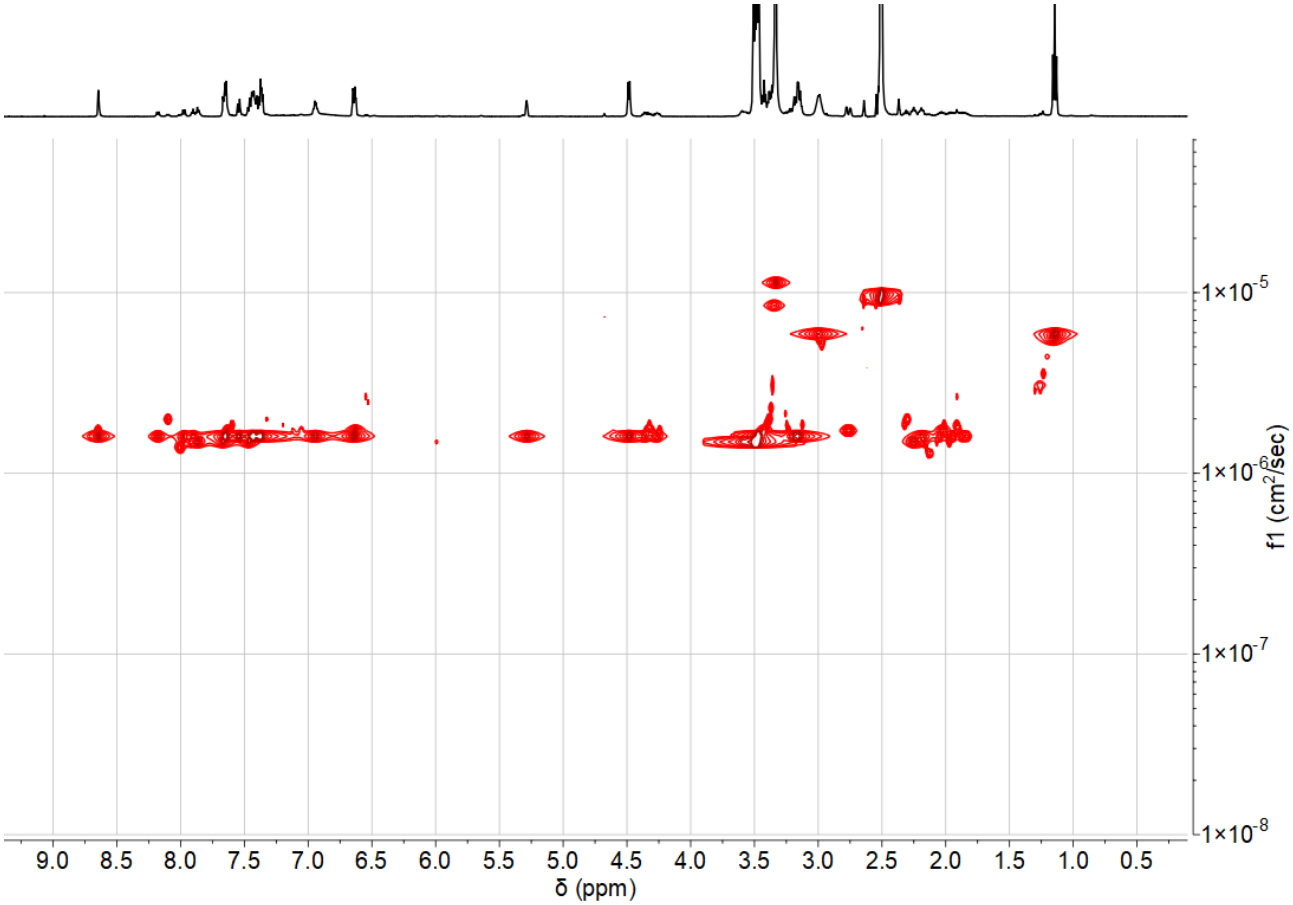

The peaks at δ 1.10 and 2.96 ppm representing the unknown impurity leads to spots on the 2D spectrum that are clearly not aligned with the spots of the desired product. This impurity was almost completely removed after the second dialysis (see ^{1}H NMR spectrum).

HRMS (ESI/QTOF): *m/z* calculated for $C_{50}H_{59}N_9NaO_{13}^+$ ([M + Na]$^+$): 1016.4125; Found 1016.4138.

5.2.7.2. Synthesis of asparagusic acid-derived PEG derivatives

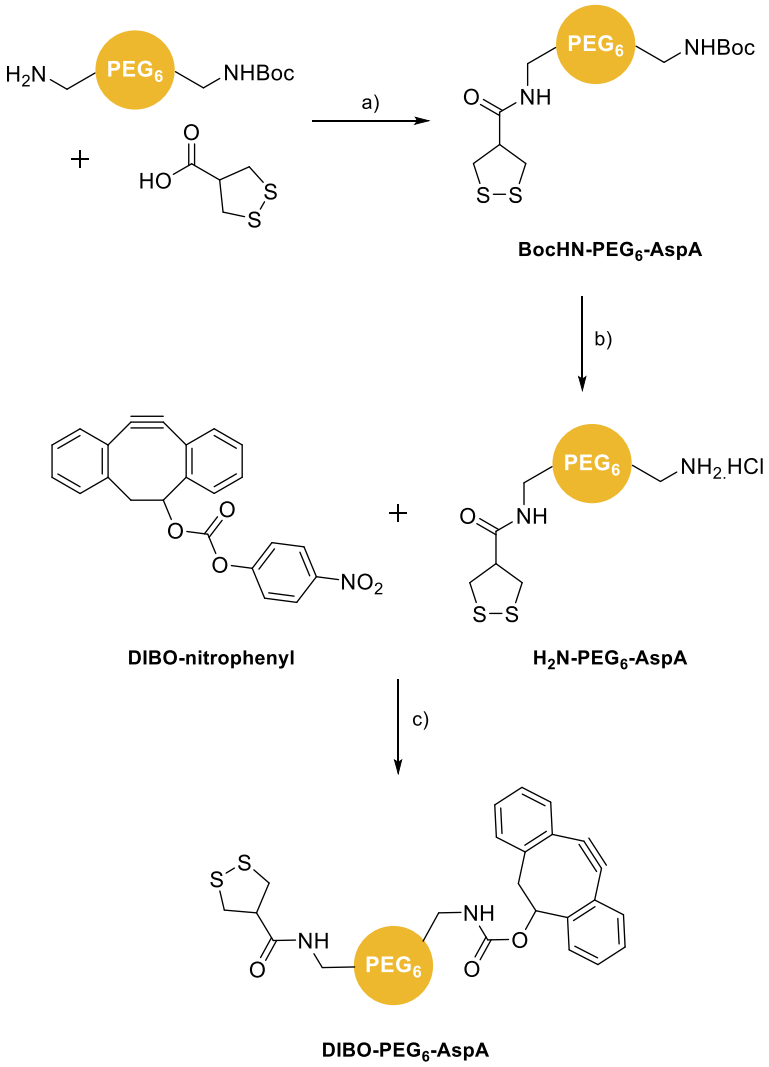

Scheme 34. Synthesis of DIBO-PEG$_6$-AspA. a) TBTU, DIPEA, DMF, rt, 21 h, 52%. b) 4 M HCl in dioxane, rt, 1.5 h, quant. c) Et$_3$N, DMSO, rt, 19 h, 13%.

BocHN-PEG$_6$-AspA

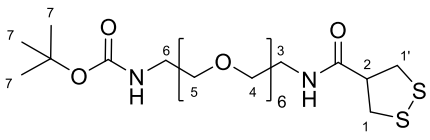

Asparagusic acid (50 mg, 0.333 mmol, 1.0 equiv.) was dissolved in 1.5 mL of dry DMF at rt. To this yellow solution were added successively TBTU (102 mg, 0.316 mmol, 0.95 equiv.) and dry DIPEA (58 µL, 0.333 mmol, 1.0 equiv.). After 15 min of stirring at rt, a solution of H_2N-PEG$_6$-NHBoc (141

mg, 0.333 mmol, 1.0 equiv.) in 0.5 mL of dry DMF was added dropwise to the reaction mixture. Following 21 h of stirring at rt, the yellow solution was then concentrated under reduced pressure. The crude was first purified by FCC (gradient DCM/MeOH 10/0 to 9/1). Fractions containing the desired product were then collected and purified again *via* preparative TLC (DCM/MeOH 9/1). Using UV revelation, **BocHN-PEG$_6$-AspA** could be finally recovered as a yellow oil (m = 70 mg, 52%). **^{1}H NMR (400 MHz, CDCl$_3$):** δ 3.75 – 3.43 (m, 26 H, H3-4-5), 3.36 (m, 4 H, H1/1'), 3.31 (t, 2 H, H6), 3.18 (m, 1 H, H2), 1.44 (s, 9 H, H7).

^{1}H NMR spectrum of **BocHN-PEG$_6$-AspA** (400 MHz, CDCl$_3$)

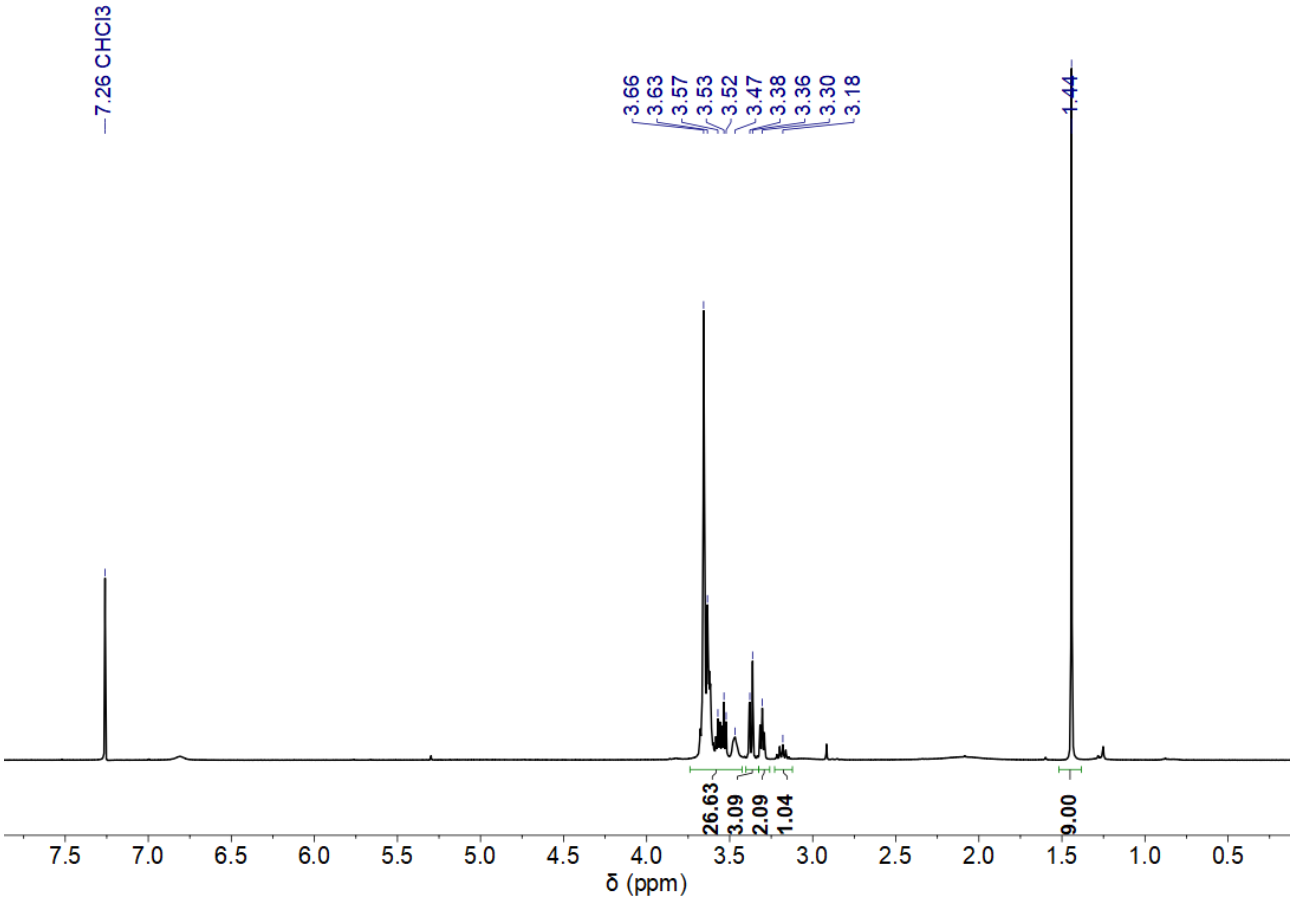

HRMS (ESI/QTOF): *m/z* calculated for $C_{23}H_{44}N_2NaO_9S_2^+$ ([M + Na]$^+$): 579.2380; Found 579.2386.

IR (cm^{-1}): 3575, 3317, 2870, 1706, 1662, 1525, 1455, 1391, 1365, 1249, 1170, 1095, 949, 863, 779, 756.

HCl.H$_2$N-PEG$_6$-AspA

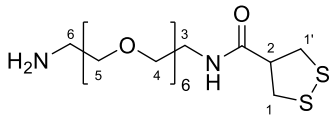

BocHN-PEG$_6$-AspA (70 mg, 0.126 mmol) was dissolved in 2 mL of a solution of 4 M HCl in dioxane at rt. After 1.5 h of stirring, the reaction mixture was concentrated under reduced pressure allowing the removal of the side products coming from the deprotection. **HCl.H$_2$N-PEG$_6$-AspA** was obtained as a pale yellow oil (m = 64.07 mg, quant.). **^{1}H NMR (400 MHz, D$_2$O + 2 drops DCl):** δ 3.58 – 3.27 (m, 26 H, H4-5-6), 3.17 – 2.86 (m, 6 H, H1/1'-3), 2.69 (br, 1 H, H2).

^{1}H NMR spectrum of **HCl.H$_2$N-PEG$_6$-AspA** (400 MHz, D$_2$O + 2 drops DCl)

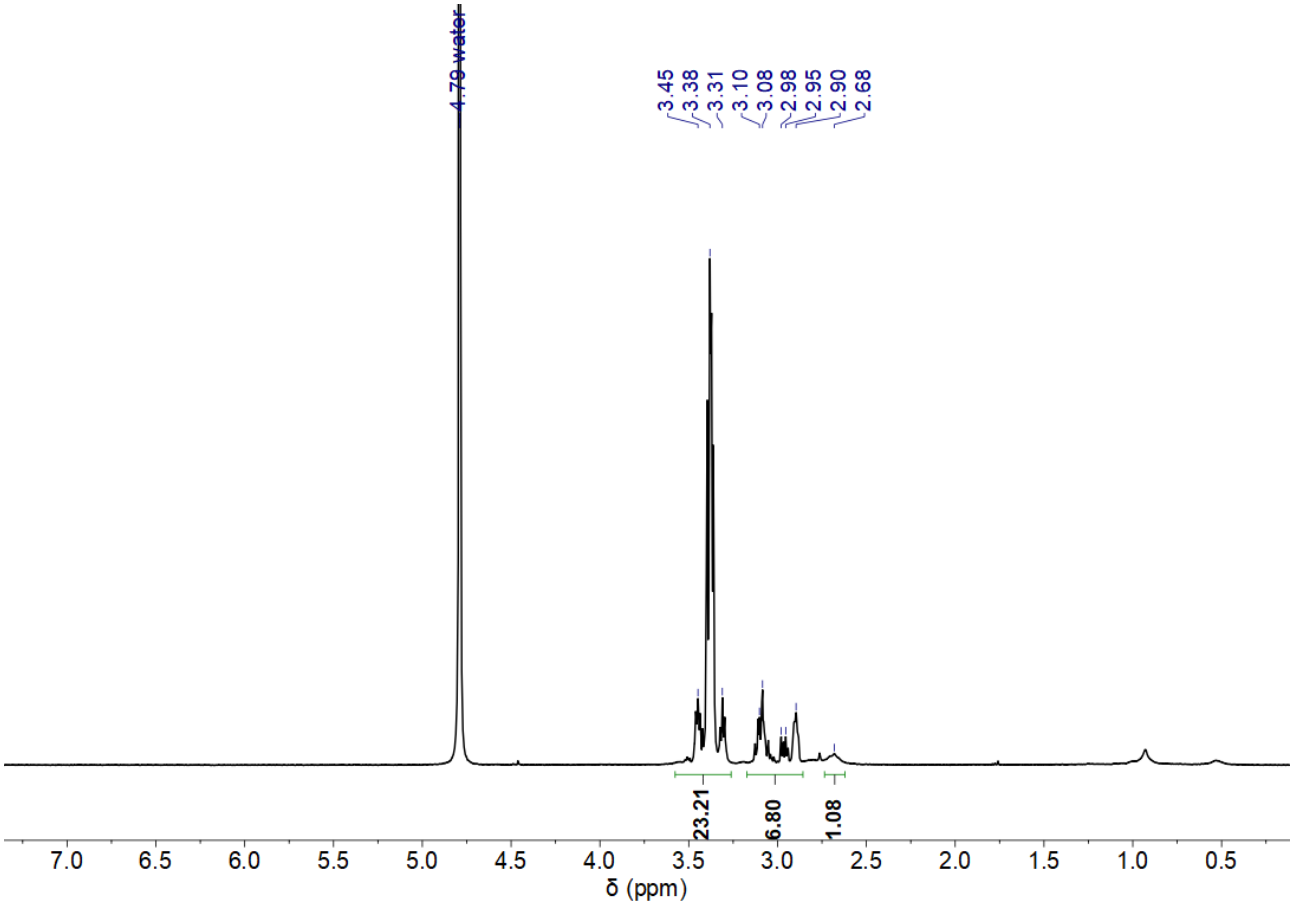

HRMS (ESI/QTOF): *m/z* calculated for $C_{18}H_{37}N_2O_7S_2^+$ ([M + H]$^+$): 457.2037; Found 457.2039.

IR (cm^{-1}): 3382, 2919, 2069, 1644, 1538, 1458 1350, 1251, 1085, 946.

DIBO-PEG6-AspA

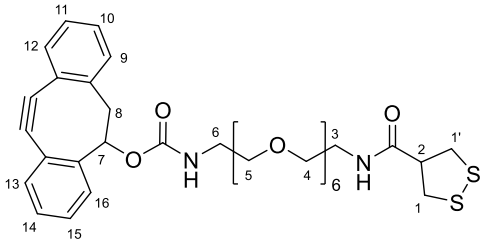

DIBO-nitrophenyl was synthesized according to a previously reported procedure.[212] To a solution of DIBO-nitrophenyl (39 mg, 0.101 mmol, 1.0 equiv.) in 3 mL of dry DMSO, was added dry Et$_3$N (56 µL, 0.405 mmol, 4.0 equiv.) and the solution turned green. Then, **HCl.H$_2$N-PEG$_6$-AspA** (50 mg, 0.101 mmol, 1.0 equiv.) dissolved in 3 mL of dry DMSO was added dropwise to the reaction mixture, which turned yellow. After 19 h of stirring at rt, the homogenous solution was dialyzed (MWCO 0.1 – 0.5 kDa) against EtOH/water 10/90 for the first six hours and then against pure distilled water for the next 2 days. After freeze-drying, 9 mg of **DIBO-PEG6-AspA** were recovered (13%). **^{1}H NMR (800 MHz, DMSO-d$_6$):** δ 7.70 – 7.30 (m, 9 H, H9-10-11-12-13-14-15-16), 5.28 (br, 1 H, H7), 3.63 – 2.71 (m, 35 H, H1/1'-2-3-4-5-6-8). δ 3.06 and 1.18 ppm are assigned to remaining traces of an unknown impurity.

^{1}H NMR spectrum of **DIBO-PEG6-AspA** (800 MHz, DMSO-d$_6$)

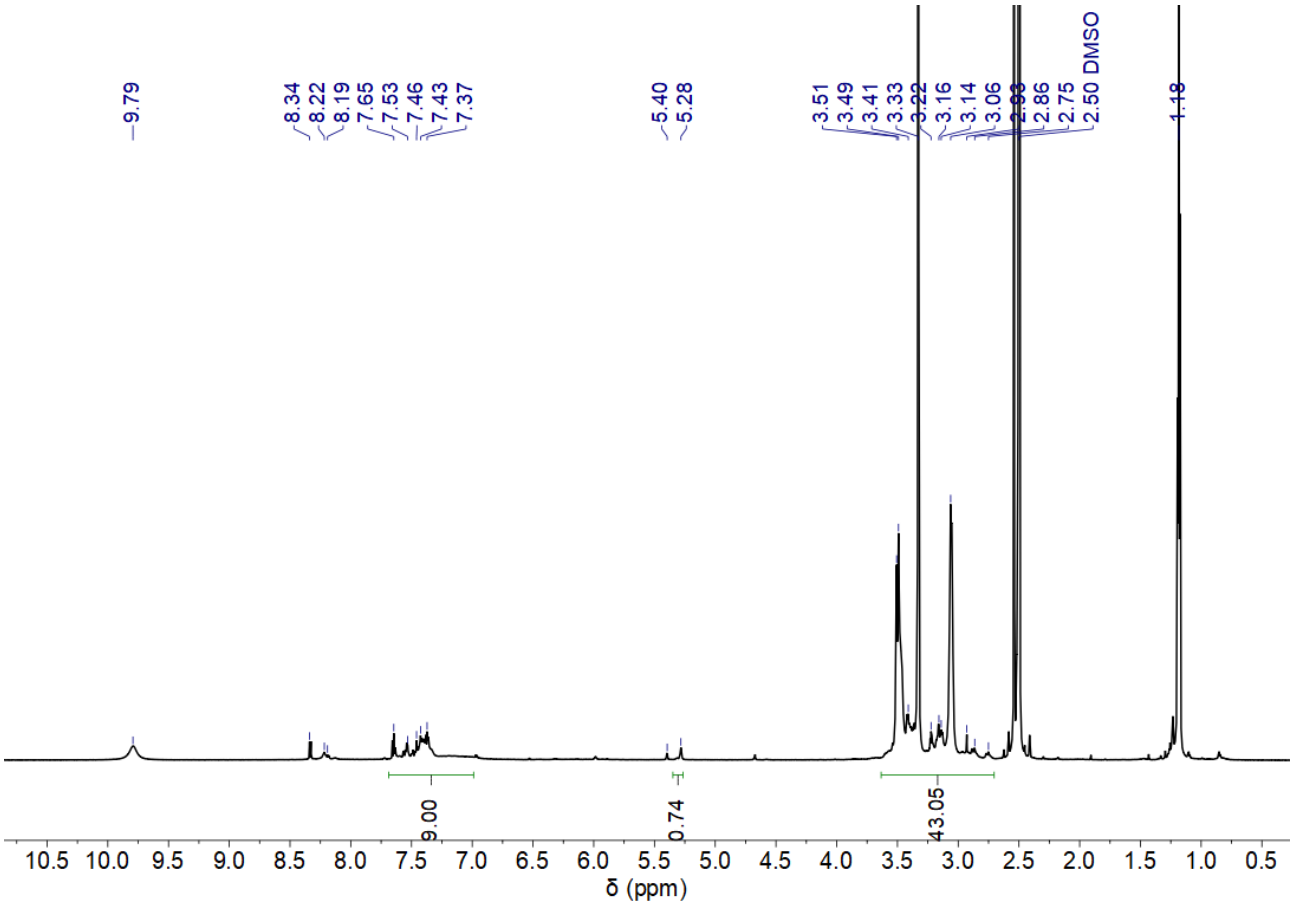

HRMS (ESI/QTOF): *m/z* calculated for $C_{35}H_{46}N_2NaO_9S_2^+$ ([M + Na]$^+$): 725.2537; Found 725.2532.

5.2.7.3. Synthesis of folic acid- and asparagusic acid-derived shell polymers

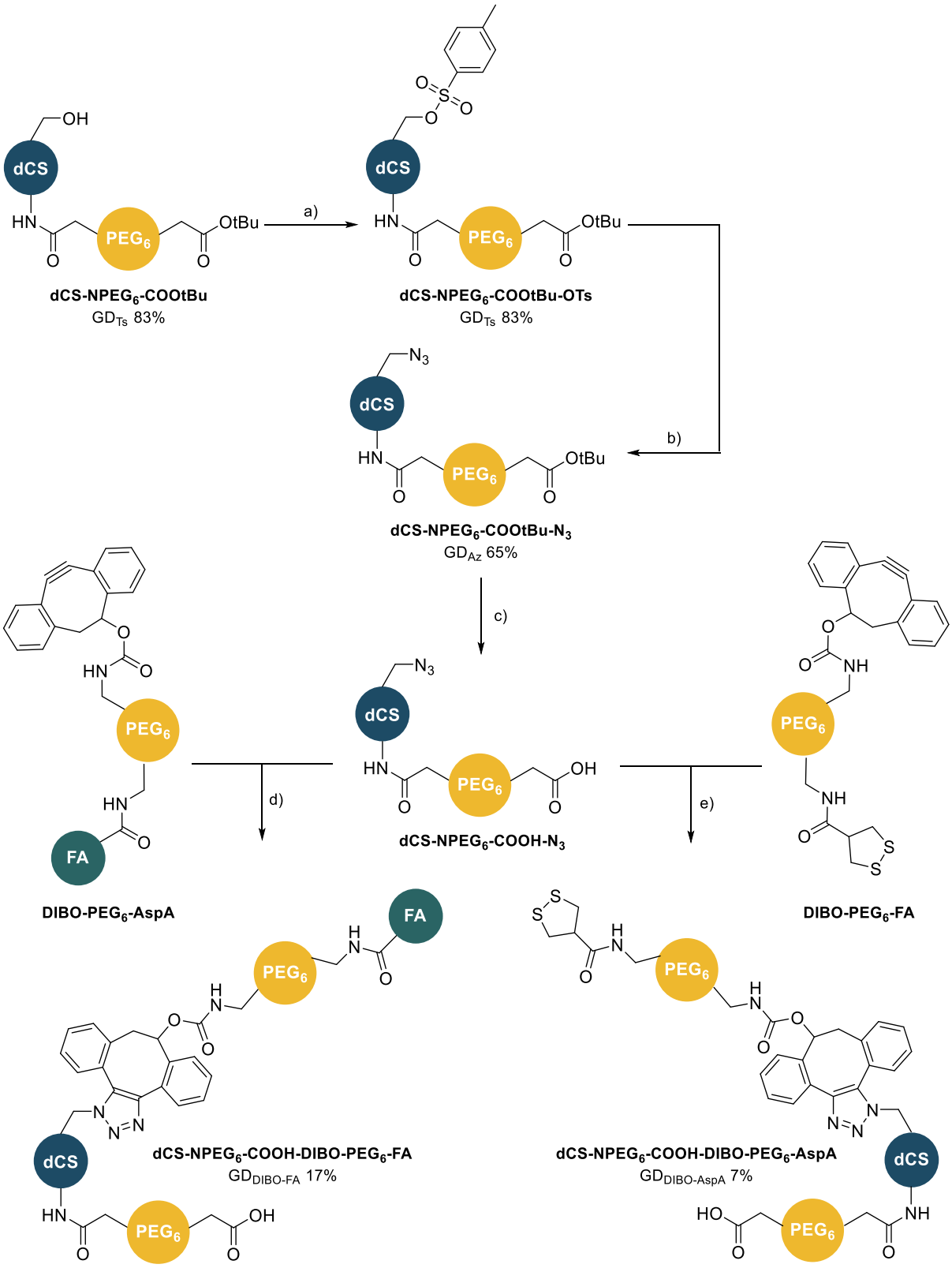

Scheme 35. Synthesis of folic acid- and asparagusic acid-derived shell polymers. a) TsCl, pyridine, rt, 48 h. b) NaN_3, DMSO, 60 °C, 48 h. c) 3 M HCl (aq.), rt, 5 h. d) DMSO, 60 °C, 18 h. e) DMSO, 60 °C, 18 h.

dCS-NPEG$_6$-COOtBu-OTs

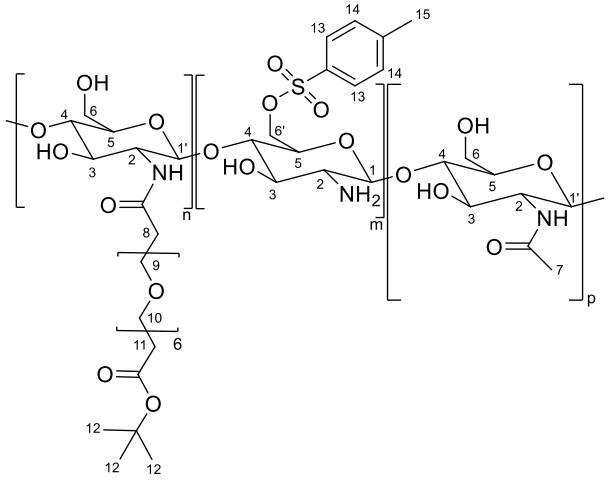

dCS-NPEG$_6$-COOtBu (DD 77%, GD$_{PEG}$ 50%, 55 mg, 0.147 mmol, 1.0 equiv.) was dissolved at rt in 3 mL of dry pyridine. After the addition of TsCl (56 mg, 0.294 mmol, 2.0 equiv.), the solution turned instantly yellow. The reaction mixture was stirred at rt for 48 h before being dialyzed (MWCO 3.5 kDa) against water for 2.5 days. After 24 h of dialysis, 1 mL of a solution of NaCl (aq.) (20 mg/mL) was added into the dialysis bag to help removing the unreacted TsOH. After lyophilization, **dCS-NPEG$_6$-COOtBu-OTs** was obtained as a white aerated solid (61 mg, GD$_{Ts}$ ≈ 83%). **^{1}H NMR (500 MHz, DMSO-d$_6$):** δ 7.79 (br, 2 H, H13), 7.47 (br, 2 H, H14), 4.94 – 3.91 (m, 6 H, H1/1'-3-4-5-6/6'), 3.75 – 3.14 (m, H2-9-10), 2.41 (m, 7 H, H8-11-15), 1.84 (s, 3 H, H7), 1.38 (s, 9 H, H12).

^{1}H NMR spectrum of **dCS-NPEG$_6$-COOtBu-OTs** (500 MHz, DMSO-d$_6$)

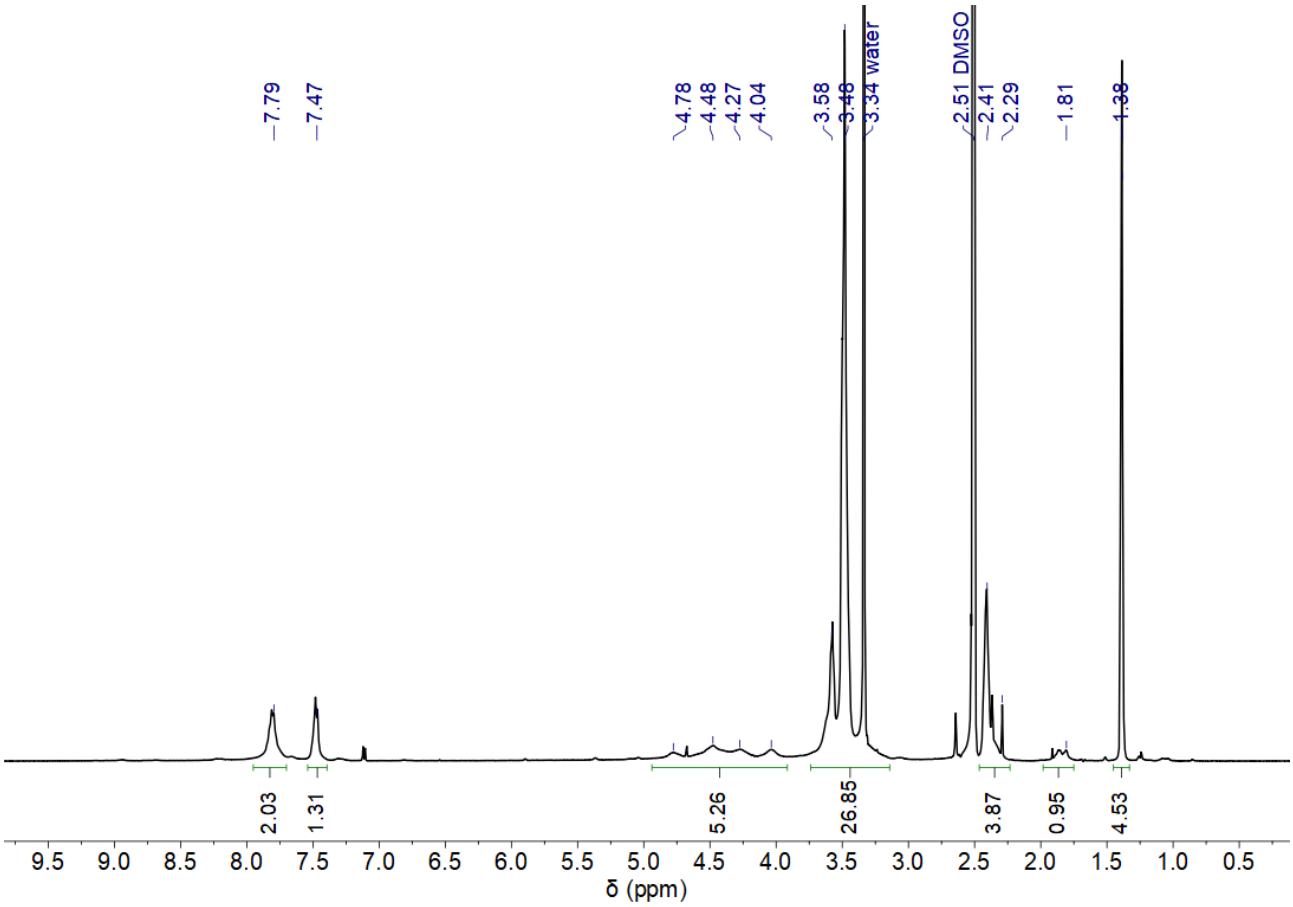

2D-DOSY NMR spectrum of **dCS-NPEG$_6$-COOtBu-OTs** (500 MHz, DMSO-d$_6$)

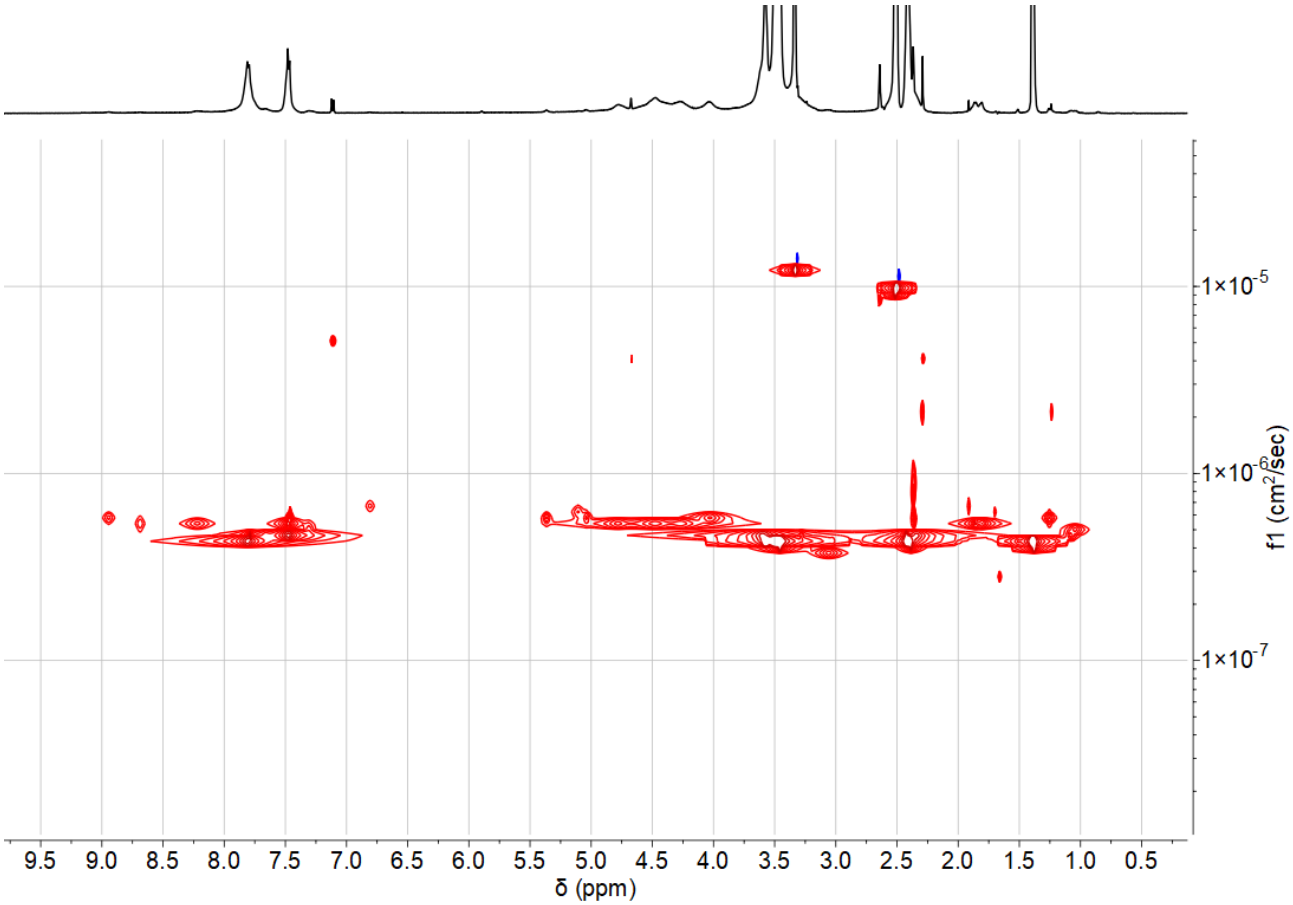

Calculation of the number of mol of reactive units (e.g. all dCS units) of dCS-NPEG$_6$-COOtBu (n(average units)):

As DD = 77% and GD$_{PEG}$ = 50%, the molar mass of one average unit of dCS-NPEG$_6$-COOtBu is M(dCS-NPEG$_6$-COOtBu) = 374.1 g/mol (cf. dCS-NPEG$_6$-COOtBu characterization for more details), hence:

$$n(\text{average units}) = \frac{m(dCS-NPEG6-COOtBu)}{M(dCS-NPEG6-COOtBu)} = \frac{0.055}{374.1} = 0.147 \text{ mmol}$$

Estimation of the grafting degree of the tosyl moiety on dCS-NPEG$_6$-COOtBu (GD$_{Ts}$):

From the ^{1}H NMR spectrum, the peak for the *tert*-butoxyl group (δ 1.38 ppm) is used as the reference peak. As GD$_{PEG}$ = 50 %, the integration for this peak is 4.50 (cf. dCS-NPEG$_6$-COOtBu characterization for more details). The peaks at δ 7.79 and 7.47 ppm are assigned to H13 and H14 and the sum of their integrations leads to a total number of 3.33 H.

Hence, $GD_{PEG} = \frac{3.33}{4} \times 100 = 83\%$

Note: The value of this GD is a rough estimation because it relies on GD$_{PEG}$ which by essence is already an approximation of the reality. The superimposition of the residual water peak (δ 3.34 ppm) with dCS-NPEG$_6$-COOtBu shifts prevents the determination of a more precise value.

Calculation of the molar mass of one average unit of dCS-NPEG$_6$-COOtBu-OTs (M(dCS-NPEG$_6$-COOtBu-OTs)):

M(dCS-NPEG$_6$-COOtBu-OTs) = DD x M(glucosamine) + AD x M(acetylglucosamine) + GD_{PEG} x MW(HOOC-PEG$_6$-COOtBu) + GD_{Ts} x M_{Ts}

= 0.77 x 161.2 + 0.23 x 203.2 + 0.50 x 406.5 + 0.83 x 154.2

= 502.1 g/mol with AD = (1 – DD)

dCS-NPEG$_6$-COOtBu-N$_3$

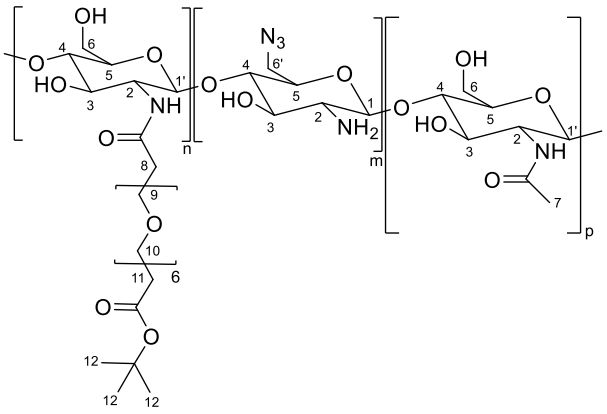

dCS-NPEG$_6$-COOtBu-OTs (DD 79%, GD_{PEG} 36%, GD_{Ts} 56%, 164 mg, 0.407 mmol, 1.0 equiv.) was dissolved at rt in 15 mL of dry DMSO. NaN_3 (265 mg, 4.07 mmol, 10 equiv.) was then added and the reaction mixture was heated up to 60 °C for 48 h. After cooling down, the homogenous solution was dialyzed (MWCO 3.5 kDa) against water for 2.5 days. After lyophilization of the purified solution, **dCS-NPEG$_6$-COOtBu-N$_3$** was obtained as a white aerated solid (122 mg, GD_{N3} ≈ 40%). **^{1}H NMR (800 MHz, DMSO-d^6):** δ 5.09 – 4.17 (6 H, H1/1'-3-4-5-6/6'), 3.78 – 3.20 (m, H2-9-10), 2.44 – 2.22 (m, 4 H, H8-11), 1.82 (s, 3 H, H7), 1.39 (s, 9 H, H12). δ 7.89 ppm is assigned to residual traces of tosyl moiety that was not converted to azide. δ 7.46, 7.10 and 2.29 ppm are assigned to residual traces of free TsOH trapped in the polymeric network.

^{1}H NMR spectrum of **dCS-NPEG$_6$-COOtBu-N$_3$** (800 MHz, DMSO-d^6)

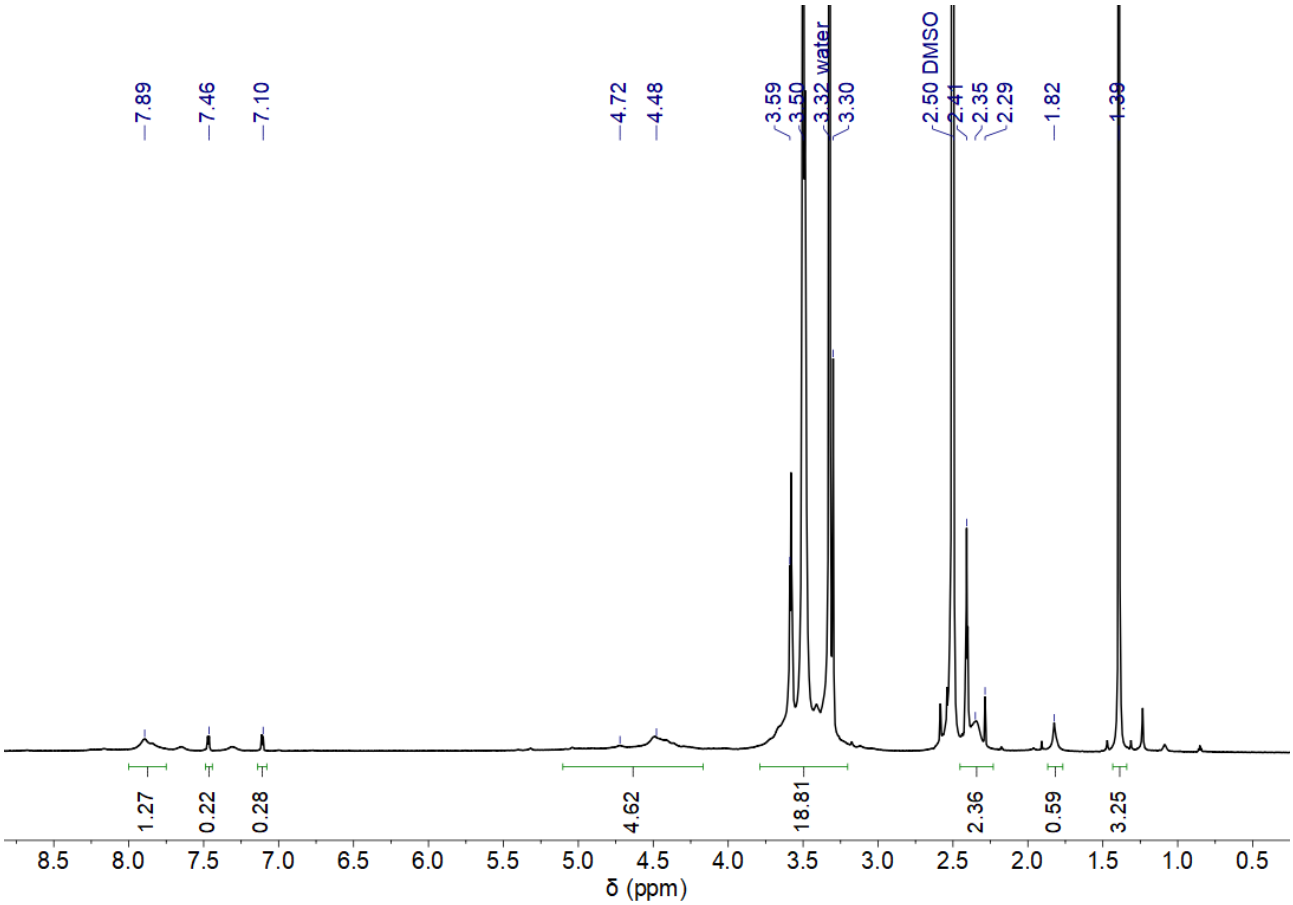

2D-DOSY NMR spectrum of **dCS-NPEG$_6$-COOtBu-N$_3$** (800 MHz, DMSO-d$_6$)

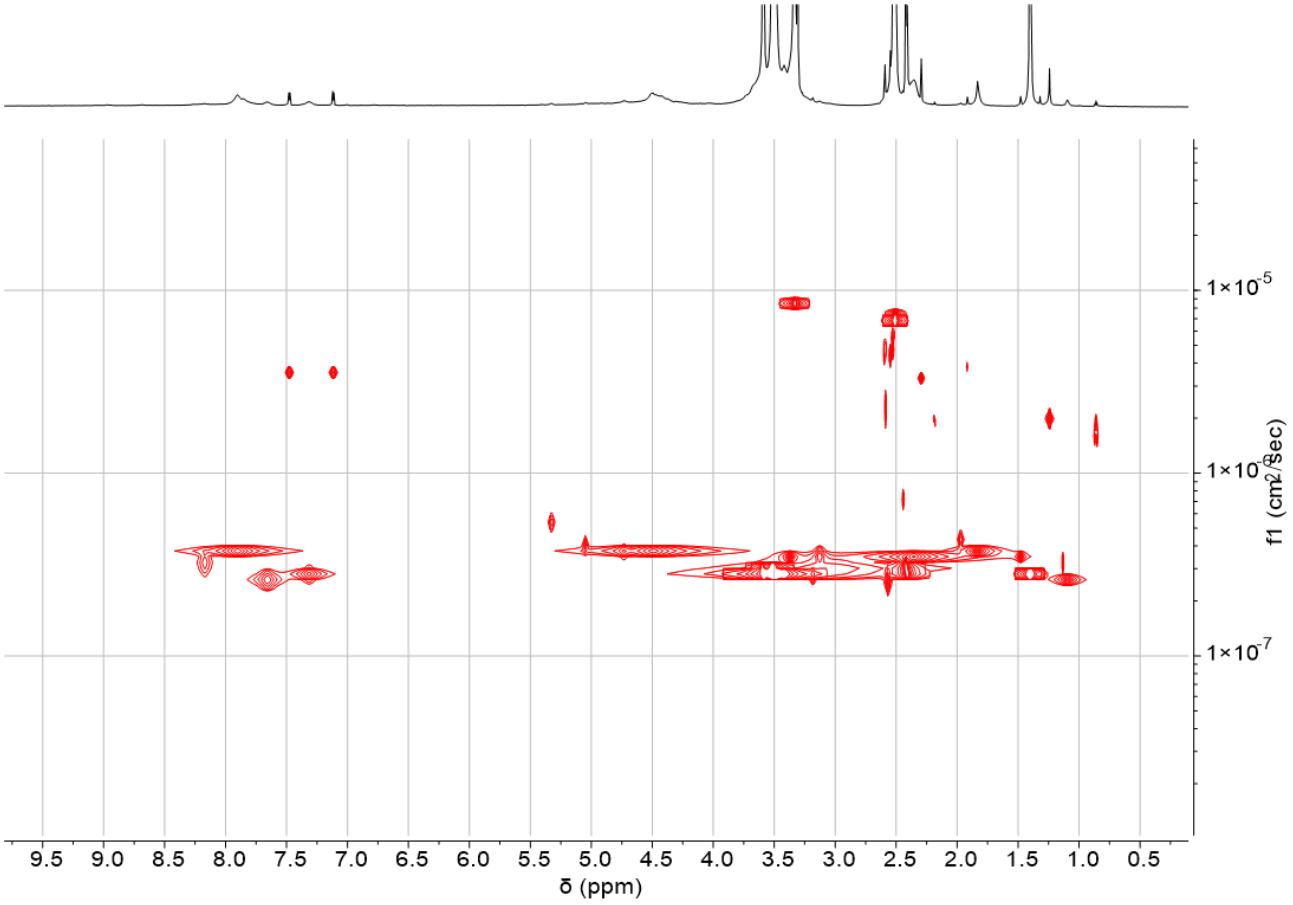

IR(cm^{-1}): 3294, 2871, 2108, 1726, 1654, 1546, 1367, 1284, 1251, 1154, 1063, 948, 847, 669.

Calculation of the number of mol of dCS-NPEG$_6$-COOtBu-OTs (n(average units)):

As DD = 79%, GD_{PEG} = 36% and GD_{Ts} = 56%, the molar mass of one average unit of dCS-NPEG$_6$-COOtBu-OTs is M(dCS-NPEG$_6$-COOtBu-OTs) = 402.7 g/mol (*cf.* dCS-NPEG$_6$-COOtBu-OTs characterization for more details), hence:

$$n(\text{average units}) = \frac{m(dCS-NPEG6-COOtBu-OTs)}{M(dCS-NPEG6-COOtBu-OTs)} = \frac{0.164}{402.7} = 0.407 \text{ mmol}$$

Estimation of the grafting degree of the azide moiety on dCS-NPEG$_6$-COOtBu (GD_{N3}):

The peak assigned to C*H*$_2$-N_3 cannot be properly differentiated from C*H*$_2$-OTs nor C*H*$_2$-OH as they are all superimposed in the massif at δ 5.09 – 4.17 ppm. We can only rely on the disappearance of the peak assigned to H13 and H14 in the aromatic region. As observed on the ^{1}H NMR spectrum, the peak δ 7.89 ppm fits to the tosyl moiety, therefore GD_{N3} is roughly estimated at 40%.

Calculation of the molar mass of one average unit of dCS-NPEG$_6$-COOtBu-N$_3$ (M(dCS-NPEG$_6$-COOtBu-N$_3$)):

M(dCS-NPEG$_6$-COOtBu-N_3) = DD x M(glucosamine) + AD x M(acetylglucosamine) + GD_{PEG} x MW(HOOC-PEG$_6$-COOtBu) + GD_{N3} x M_{N3}

= 0.79 x 161.2 + 0.21 x 203.2 + 0.36 x 406.5 + 0.40 x 25

= 326.3 g/mol with AD = (1 – DD)

dCS-NPEG$_6$-COOH-N$_3$

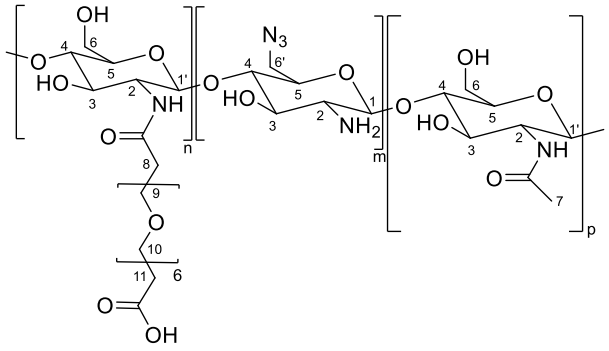

dCS-NPEG$_6$-COOtBu-N$_3$ (DD 79%, GD_{PEG} 36%, GD_{N3} ≈ 40%, 117 mg, 0.359 mmol) was dissolved in 12 mL of 3 M HCl (aq) solution at rt. After 5 h of stirring, the reaction mixture was dialyzed (MWCO 3.5 kDa) against water for 3 days. The purified solution was then centrifuged (4700 rpm, 20 °C, 10 min) and the supernatant was freeze-dried. **dCS-NPEG$_6$-COOH-N$_3$** was obtained as a white aerated solid (60 mg). **^{1}H NMR (500 MHz, D$_2$O):** δ 4.59 (br, 1 H, H1/1'), 4.05 – 3.23 (m, 29 H, H3-4-5-6/6'-9-10), 2.61 (m, 5 H, H2-8-11), 2.04 (s, 3 H, H7).

^{1}H NMR spectrum of **dCS-NPEG$_6$-COOH-N$_3$** (500 MHz, D_2O)

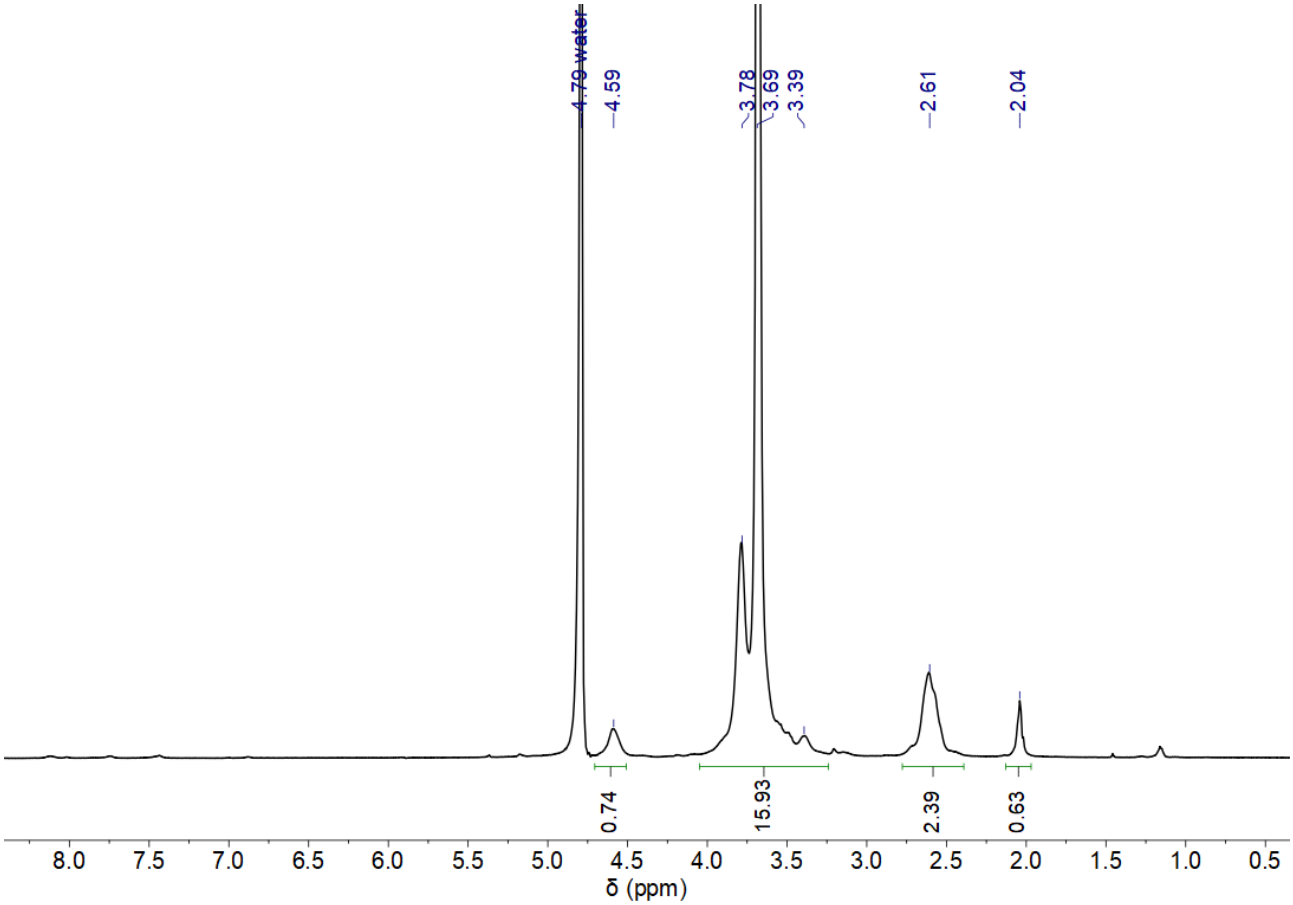

2D-DOSY NMR spectrum of **dCS-NPEG$_6$-COOH-N$_3$** (500 MHz, D_2O)

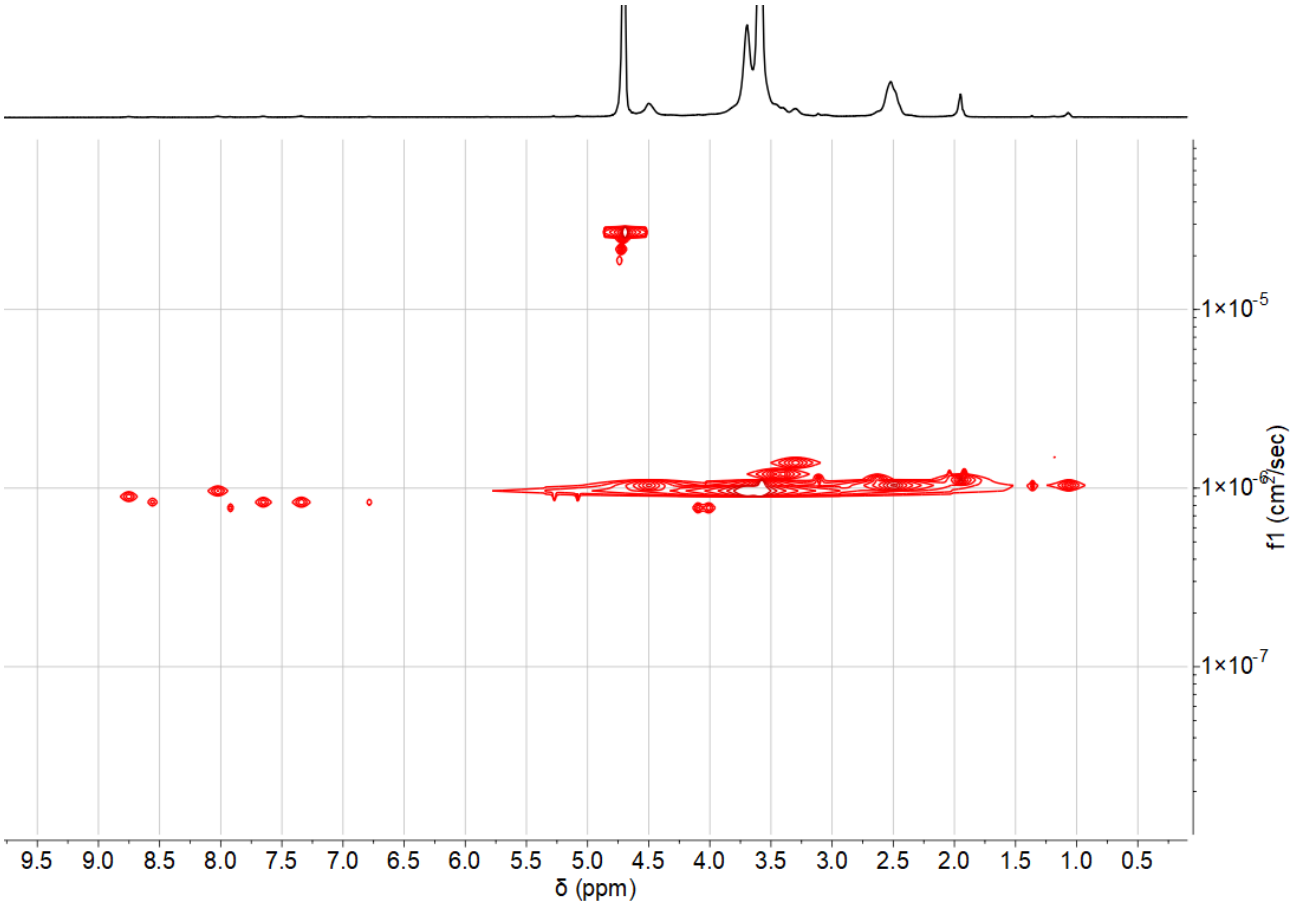

IR (cm^{-1}): 3288, 2873, 2108, 1728, 1651, 1549, 1373, 1286, 1249, 1201, 1064, 946, 840, 667.

Calculation of the number of mol of dCS-NPEG$_6$-COOtBu-N$_3$ (n(average units)):

As DD = 79%, GD$_{PEG}$ = 36% and GD$_{N3}$ = 40%, the molar mass of one average unit of dCS-NPEG$_6$-COOtBu-N$_3$ is M(dCS-NPEG$_6$-COOtBu-N$_3$) = 326.3 g/mol (*cf.* dCS-NPEG$_6$-COOtBu-N$_3$ characterization for more details), hence:

$$n(\text{average units}) = \frac{m(dCS-NPEG6-COOtBu-N3)}{M(dCS-NPEG6-COOtBu-N3)} = \frac{0.117}{326.3} = 0.359 \text{ mmol}$$

Calculation of the molar mass of one average unit of dCS-NPEG$_6$-COOH-N$_3$ (M(dCS-NPEG$_6$-COOH-N$_3$)):

M(dCS-NPEG$_6$-COOH-N$_3$) = DD x M(glucosamine) + AD x M(acetylglucosamine) + GD$_{PEG}$ x MW(HOOC-PEG$_6$-COOH) + GD$_{N3}$ x M$_{N3}$

= 0.79 x 161.2 + 0.21 x 203.2 + 0.36 x 364.5 + 0.40 x 25

= 311.2 g/mol with AD = (1 – DD)

dCS-NPEG$_6$-COOH-DIBO-PEG$_6$-FA

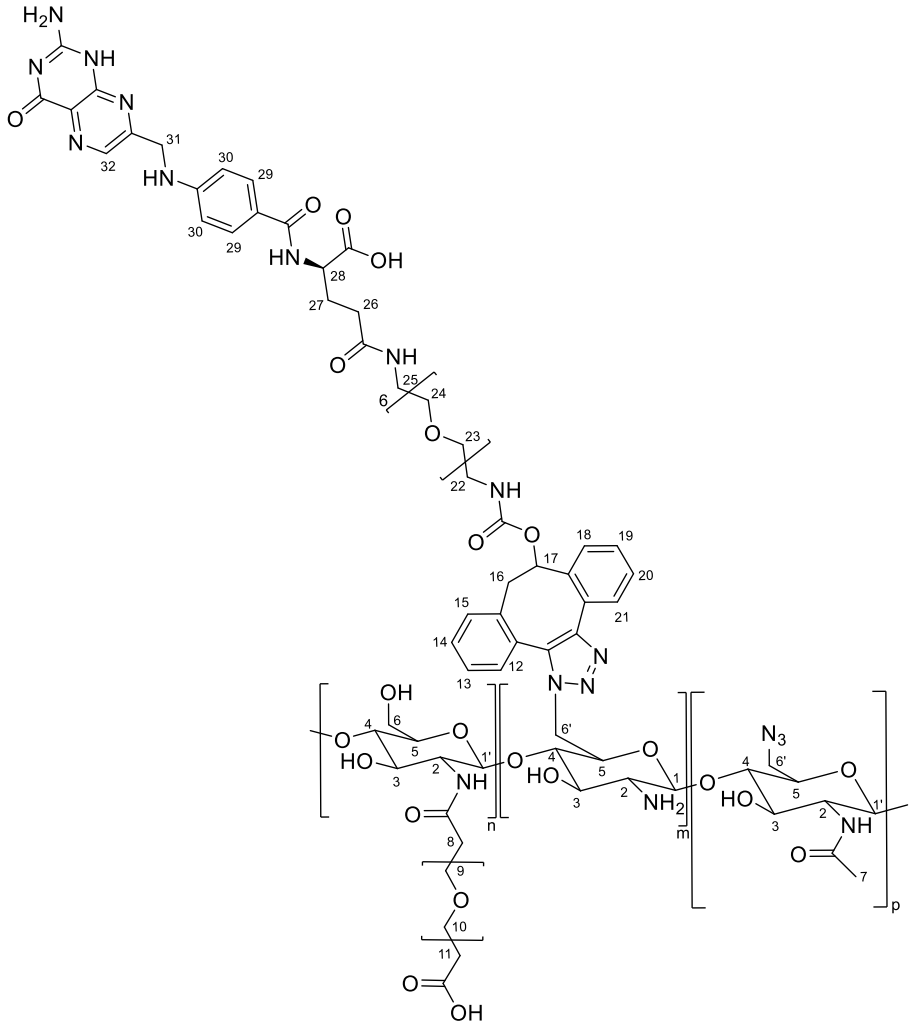

To a solution of **dCS-NPEG$_6$-COOH-N$_3$** (DD 78%, GD$_{PEG}$ 48%, GD$_{N3}$ ≈ 70%, 39.0 mg, 0.0763 mmol, 1.0 equiv.) in 4 mL of dry DMSO, was added **DIBO-PEG$_6$-FA** (21.4 mg, 0.0215 mmol, 0.3 equiv.) at rt. The yellow solution was heated up to 60 °C over 18 h. After cooling down, the orange solution was dialyzed (MWCO 3.5 kDa) against water for 3 days. After centrifugation (4700 rpm, 20 °C, 10 min) of the resulting solution, the supernatant was recovered and lyophilized. **dCS-NPEG$_6$-COOH-DIBO-PEG$_6$-FA** was obtained as a yellow aerated solid (54 mg, GD$_{DIBO-FA}$ = 17%). **^{1}H NMR (500 MHz, D$_2$O):** δ 7.45 (br, 14 H, H12-13-14-15-17-18-19-20-21-29-30-32), 4.59 (br, 1 H, H1/1'), 4.17 – 2.46 (m, 71 H, H2-3-4-5-6/6'-8-9-10-11-16-22-23-24-25-26-27-28-31), 2.04 (br, 3 H, H7).

^{1}H NMR spectrum of **dCS-NPEG$_6$-COOH-DIBO-PEG$_6$-FA** (500 MHz, D$_2$O)

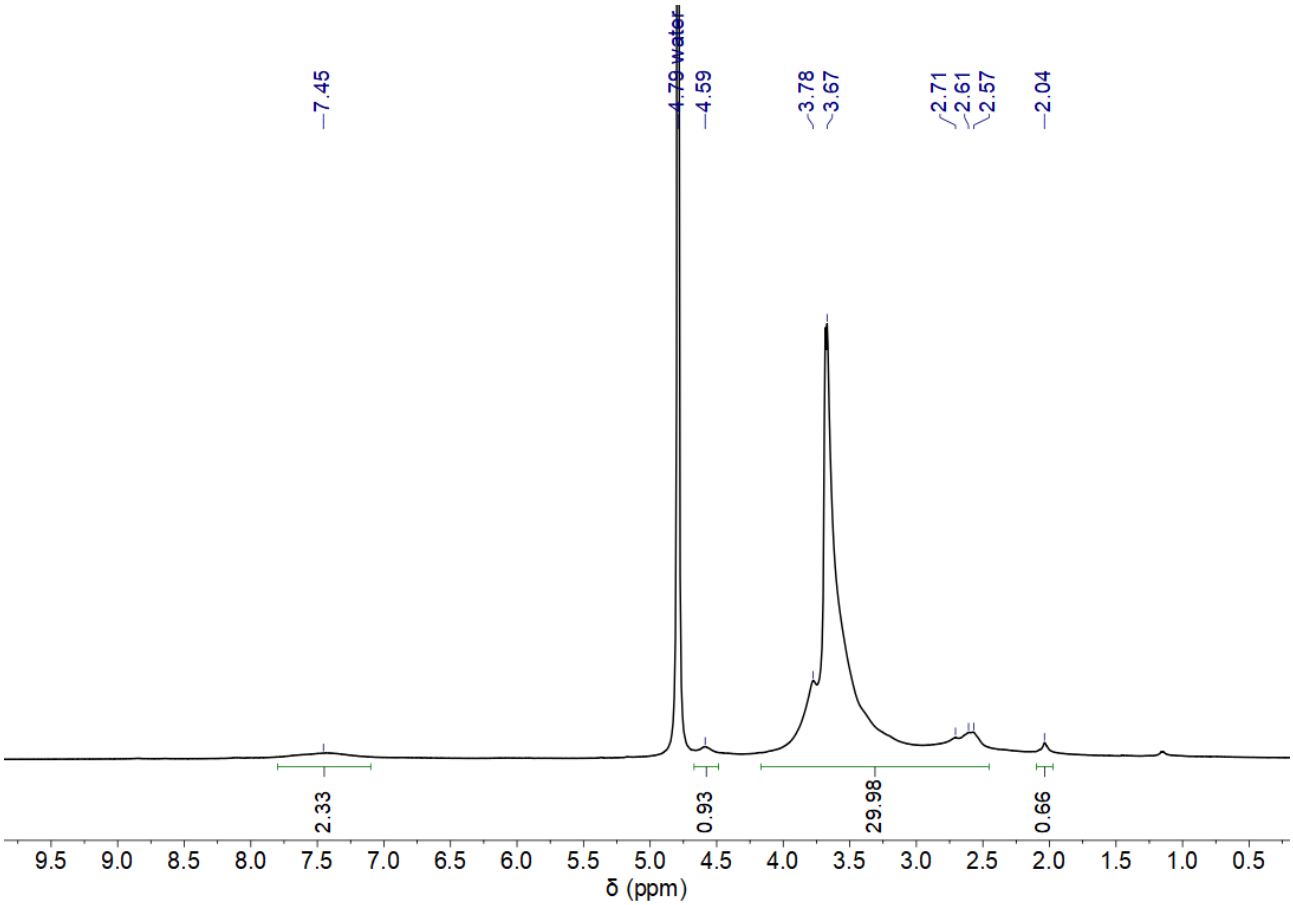

2D-DOSY NMR spectrum of **dCS-NPEG$_6$-COOH-DIBO-PEG$_6$-FA** (500 MHz, D_2O)

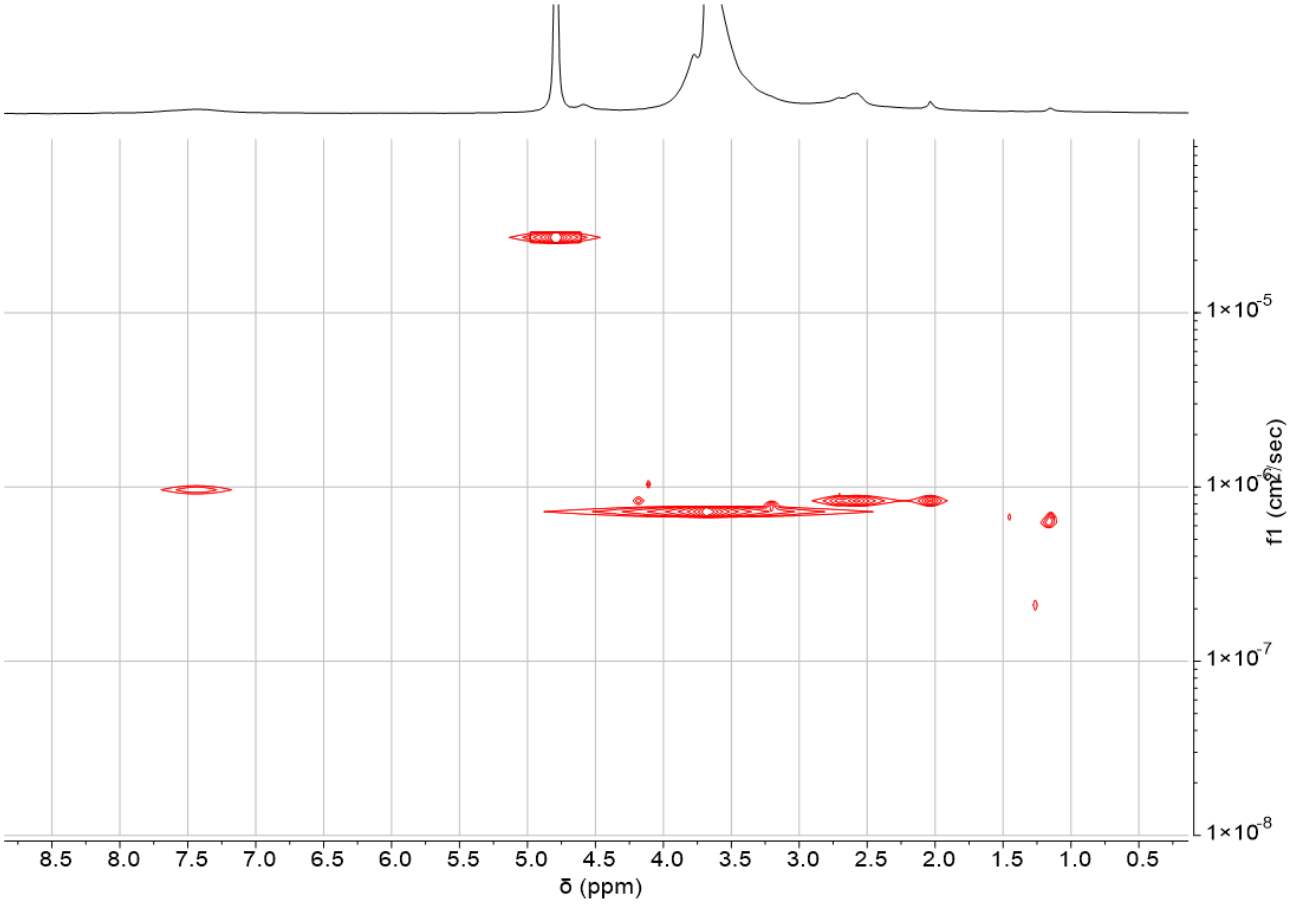

IR (cm^{-1}): 3302, 2871, 2106, 1651, 1608, 1538, 1349, 1250, 1196, 1089, 946, 840, 768.

Calculation of the number of mol of reactive units (e.g. all azidated-dCS units) of dCS-NPEG$_6$-COOH-N$_3$ (n(reactive units)):

As DD = 78%, GD_{PEG} = 48% and GD_{N3} ≈ 70%, the molar mass of one average unit of dCS-NPEG$_6$-COOH-N$_3$ is M(dCS-NPEG$_6$-COOH-N$_3$) = 362.9 g/mol (cf. dCS-NPEG$_6$-COOH-N$_3$ characterization for more details), hence:

n(average units) = $\frac{m(dCS-NPEG6-COOH-N3)}{M(dCS-NPEG6-COOH-N3)} = \frac{0.039}{362.9}$ = 0.109 mmol but as there are only about 70% of reactive units (meaning azidated dCS units), then n(reactive units) = 0.109 x 0.7 = 0.0763 mmol

Estimation of the grafting degree of DIBO-PEG$_6$-FA on dCS-NPEG$_6$-COOH ($GD_{DIBO-FA}$):

From the ^{1}H NMR spectrum, the peak for the acetyl group (δ 2.04 ppm) is used as the reference peak. As DD = 78 %, the integration for this peak is 0.66 (cf. dCS characterization for more details). The broad peak at δ 7.75 ppm is assigned to the aromatic protons from DIBO and FA, leading to a total of 14 H. On the ^{1}H NMR spectrum, its integration leads to a total number of 2.33 H.

Hence, $GD_{DIBO-FA} = \frac{2.33}{14}$ x 100 = 17%

Note: The value of this GD is again a rough estimation because the intensities of the different peaks of the polymer are very low.

Estimation of the molecular weight of one dCS-NPEG$_6$-COOH-DIBO-PEG$_6$-FA chain (MW(dCS-NPEG$_6$-COOH-DIBO-PEG$_6$-FA)):

MW(dCS-NPEG$_6$-COOH-DIBO-PEG$_6$-FA) = Mw(dCS) + GD_{N3} x M_{N3} x nb(dCS units) + GD_{PEG} x MW(HOOC-PEG$_6$-COOH) x nb(dCS units) + $GD_{DIBO-FA}$ x $M_{DIBO-FA}$ x nb(dCS units)

= 6480 + 0.7 x 25 x 38 + 0.48 x 364.5 x 38 + 0.17 x 994.1 x 38 = 20.2 kDa

with 38 being the number of units per dCS chain (*cf.* dCS characterization for more details).

dCS-NPEG$_6$-COOH-DIBO-PEG$_6$-AspA

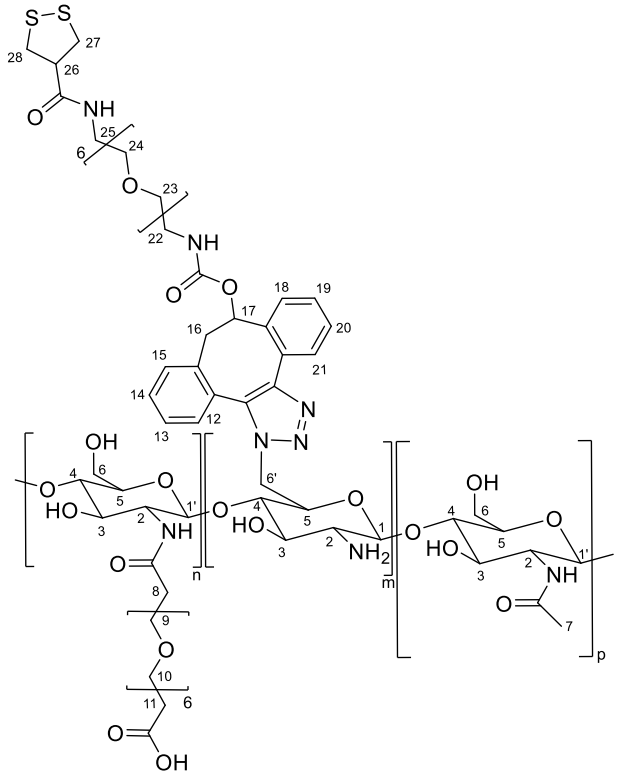

To a solution of **dCS-NPEG$_6$-COOH-N$_3$** (DD 79%, GD$_{PEG}$ 36%, GD$_{N3}$ ≈ 40%, 40.0 mg, 0.0514mmol, 1.0 equiv.) in 1.5 mL of dry DMSO, was added a solution of **DIBO-PEG$_6$-AspA** (14.5 mg, 0.0206 mmol, 0.4 equiv.) in 2.5 mL of dry DMSO at rt. The reaction mixture was heated up to 60 °C over 18 h. After cooling down, the solution was dialyzed (MWCO 3.5 kDa) against water for 3 days. After centrifugation (4700 rpm, 20 °C, 10 min) of the resulting solution, the supernatant was recovered and lyophilized. **dCS-NPEG$_6$-COOH-DIBO-PEG$_6$-AspA** was obtained as a white aerated solid (34 mg, GD$_{DIBO-AspA}$ = 5-10%). **^{1}H NMR (500 MHz, D$_2$O):** δ 7.44 (m, 8 H, H12-13-14-15-18-19-20-21), 4.53 (br, 1 H, H1/1'), 4.03 – 2.37 (m, 70 H, H2-3-4-5-6/6'-8-9-10-11-16-17-22-23-24-25-26-27-28), 2.04 (s, 3 H, H7). δ 1.16 ppm is assigned to remaining traces of an unknown impurity.

^{1}H NMR spectrum of **dCS-NPEG$_6$-COOH-DIBO-PEG$_6$-AspA** (500 MHz, D$_2$O)

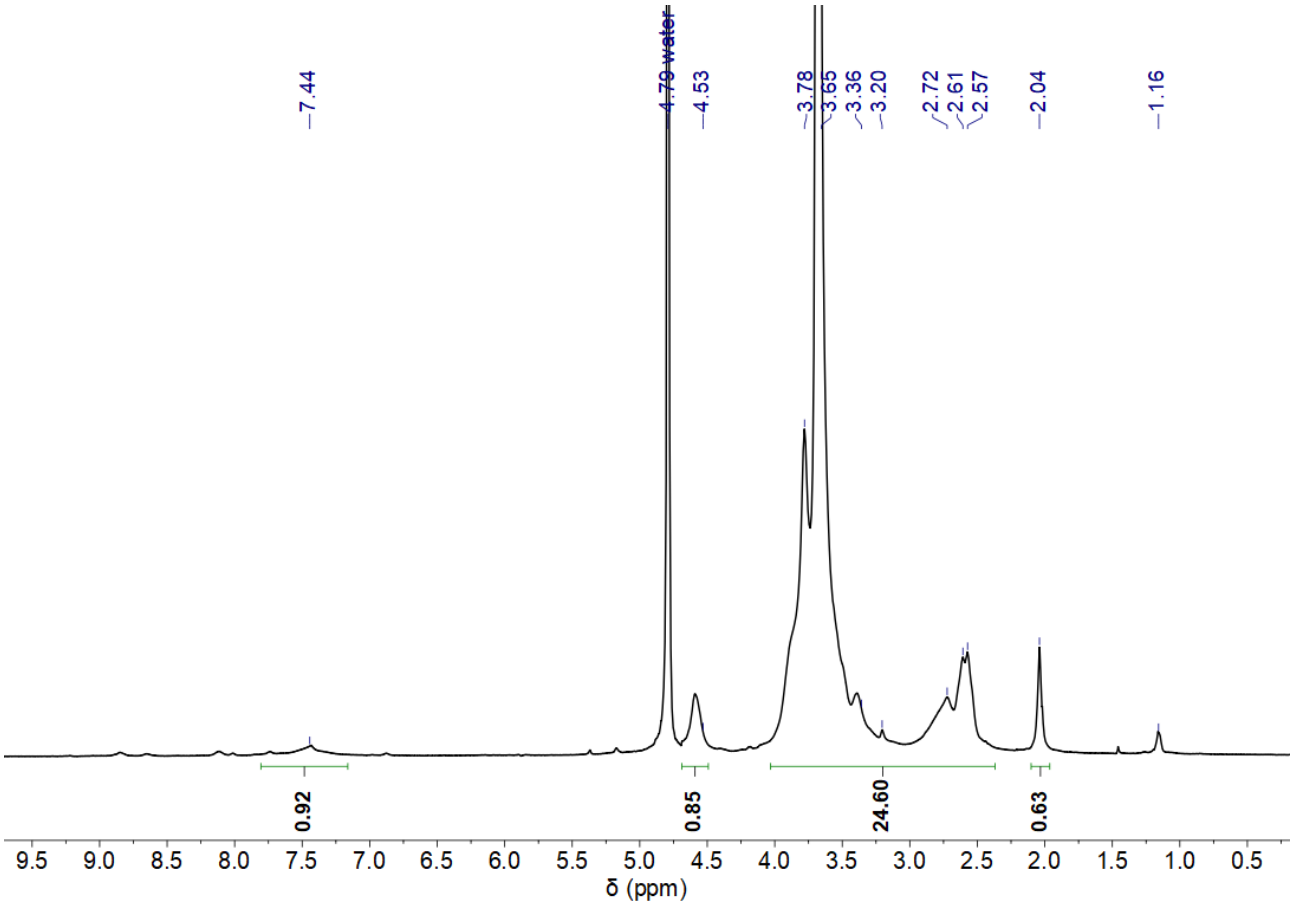

2D- DOSY NMR spectrum of **dCS-NPEG$_6$-COOH-DIBO-PEG$_6$-AspA** (500 MHz, D_2O)

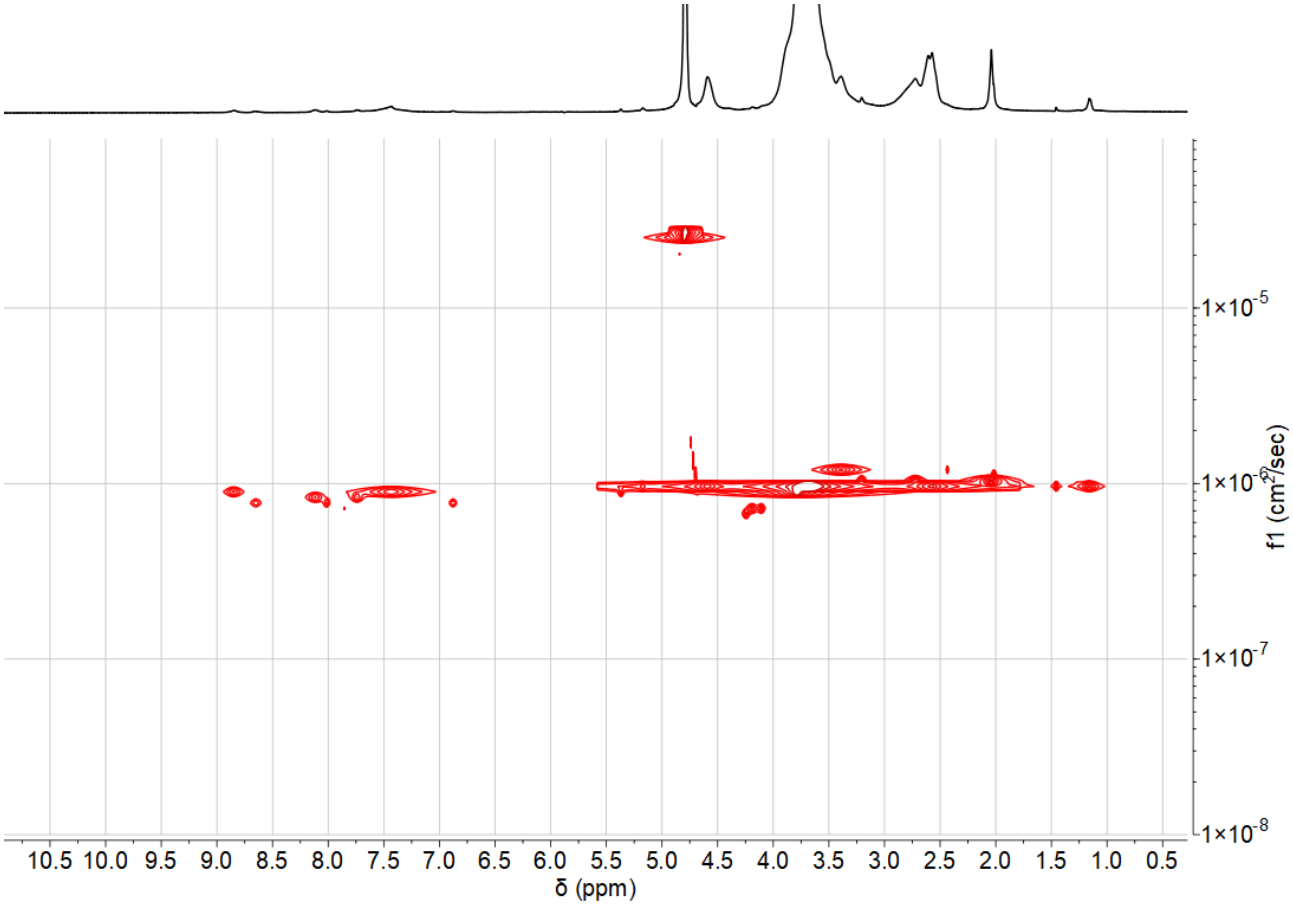

IR (cm^{-1}): 3291, 2872, 2109, 1725, 1651, 1547, 1351, 1285, 1249, 1201, 1066, 946, 841, 672.

Calculation of the number of mol of reactive units (e.g. all azidated-dCS units) of dCS-NPEG$_6$-COOH-N$_3$ (n(reactive units)):

As DD = 79%, GD_{PEG} = 36% and GD_{N3} = 40%, the molar mass of one average unit of dCS-NPEG$_6$-COOH-N$_3$ is M(dCS-NPEG$_6$-COOH-N$_3$) = 311.2 g/mol (*cf.* dCS-NPEG$_6$-COOH-N$_3$ characterization for more details), hence:

n(average units) = $\frac{m(dCS-NPEG6-COOH-N3)}{M(dCS-NPEG6-COOH-N3)} = \frac{0.040}{311.2}$ = 0.128 mmol but as there are only about 40% of reactive units (meaning azidated dCS units), then n(reactive units) = 0.128 x 0.4 = 0.0514 mmol

Estimation of the grafting degree of DIBO-PEG$_6$-AspA on dCS-NPEG$_6$-COOH ($GD_{DIBO-AspA}$):

From the ^{1}H NMR spectrum, the peak for the acetyl group (δ 2.04 ppm) is used as the reference peak. As DD = 79 %, the integration for this peak is 0.63 (cf. dCS characterization for more details). The broad peak at δ 7.44 ppm is assigned to the aromatic protons from DIBO, leading to a total of 8 H. On the ^{1}H NMR spectrum, its integration leads to a total number of 0.92 H.

Hence, $GD_{DIBO-FA} = \frac{0.92}{8}$ x 100 = 11%

However, this value is probably overestimated as the peak is very small in intensity leading to significant error when performing the integration. $GD_{DIBO-FA}$ is consequently estimated between 5 and 10% (7% on average).

Estimation of the molecular weight of one dCS-NPEG$_6$-COOH-DIBO-PEG$_6$-AspA chain (MW(dCS-NPEG$_6$-COOH-DIBO-PEG$_6$-AspA)):

MW(dCS-NPEG$_6$-COOH-DIBO-PEG$_6$-AspA) = Mw(dCS) + GD_{N3} x M_{N3} x nb(dCS units) + GD_{PEG} x MW(HOOC-PEG$_6$-COOH) x nb(dCS units) + $GD_{DIBO-AspA}$ x $M_{DIBO-AspA}$ x nb(dCS units)

= 6760 + 0.4 x 25 x 40 + 0.36 x 364.5 x 40 + 0.07 x 702.9 x 40 = 14.4 kDa

with 40 being the number of units per dCS chain (*cf.* dCS characterization for more details).

5.2.8. Biological assessments

Biological assesments of the polymeric derivatives were conducted both at the Univeristy of Basel and Children's University Hospital of Zürich. In order to have a global overview of the project, summarized versions of the most important procedures used are reported below.

5.2.8.1. Nanoparticles formation and *in vitro* procedures

5.2.8.1.1. Nanoparticles formation and DNA accessibility

The synthetized polymers were reconstituted in purified water and supported with HCl, when required, to a minimum pH of four. The polymer was diluted in glucose solution and added to the DNA, vortexed, resulting in a final 5% (w/v) glucose solution, before incubating for 15 min at room temperature. The ability of polymers to condense DNA was confirmed by agarose gel electrophoresis. To 20 µl polyplexes at various c/p ratios with a final concentration of 15 µg DNA/ml, 4 µl DNA sample-buffer was added (15% Ficoll400 and 0.1% Bromophenol blue) and administered to electrophoresis on a 0.7% agarose gel (including 1 µg/mL ethidium bromide) during 90 min at an electric potential of 90 V in tris-borate-EDTA buffer (TBE). A molecular-wight size marker (Precision Plus Protein Dual Color Standards, Bio-Rad, Hércules, CA) was included as reference. DNA bands were imaged with ChemiDoc MP Imaging system using Image lab V6.1 software (Bio-Rad). To evaluate the accessibility of complexed DNA, a DNA exclusion assay was performed. Polyplex solutions at various c/p ratios were added to 20 µg DNA/mL and SYBR Gold nucleic acid staining solution (1:400, invitrogen, Carlsbad, CA).

5.2.8.1.2. Transfection experiments

Transfection experiments were assessed in 24-multiwell plates with $2*10^4$ HuH-7 cells/well. Subsequently, 100 µl polymer solution was added per well at a final concentration of 10 µg DNA/ml. Luciferin assay was conducted to determine transgene expression. 48 hours after addition of polyplex solution encoding firefly luciferase, cells were washed with phosphate-buffered saline (PBS) and lysed with 60 µl luciferase cell culture lysis reagent (25 mM Tris-phosphate pH 7.8, 2 mM DTT, 2 mM DCTA, 50% glycerol, 5% Triton X-100) on ice for 15 min. Cell lysate was centrifuged (21'000 g, 3 min) and 20 µl supernatant was measured using a bioluminescence microplate reader after addition of 100 µl D-luciferin solution (570 µM). Transfection experiments were normalized to protein concentration of cell lysate supernatants. Protein concentration was quantified by UV-absorption at 280 nm.

Quantification of delivered DNA was conducted by quantitative polymerase-chain reaction (qPCR). Twenty-four hours after addition of polyplex solution with nanovector-DNA encoding firefly luciferase, transfected DNA was extracted using QIAprep Spin Miniprep Kit (Quiagen, Venlo, Netherlands) according to manufacturer's protocol. Subsequently, qPCR was performed using KAPA SYBR Fast qPCR Master Mix (KAPA Biosystems, Wilmington, MA), equal voluminal of isolated DNA, and the following primers: Luciferase forward 5'-AACAGGTTGAACTGCTGATCC-3' and Luciferase reverse 5'-ACAAGATGTGCGAACTCGATATT-3'. qPCR reactions were performed applying 40 cycles of 95 °C for 15 seconds and 60 °C for 1 min, using a Rotor-Gene Cycler (Corbett research, Sydney, New South Wales, Australia). Readout data were normalized to DNA calibration curve.

The number of transfected cells was quantified using flow cytometry. Forty-eight hours after addition of polyplex solution encoding eGFP, cells were trypsinized and resuspended in FACS-Buffer (1% FCS, 2.5 mM EDTA, 0.05% NaN_3 in PBS) containing 7 aminoactinomycin D (7-AAD, 2 µg/ml) and annexin V (1 µg/ml). For the flow cytometry, singlets, 7-AAD, and Annexin V negative cells were gated and

analyzed for eGFP expression. A total of 10'000 cells per sample was analyzed using FACS Canto II (BD Bioscience, San Jose, CA) and data was subsequently processed using FlowJo software (TreeStar, Ashland, OR).

5.2.8.2. *In vivo* procedures

5.2.8.2.1. Retrograde Intrabiliary Infusion in mice

Animal experiments conducted under license ZH082/19 (31232), were approved by the State Veterinary Office of Zurich (approved on 29 August 2019) and carried out according to the guidelines of the Swiss Law of Animal Protection, the Swiss Federal Act on Animal Protection (1978), and the Swiss Animal Protection Ordinance (1981). Wild-type C57BL/6JRccHsd male mice aged 6–8 weeks (20–24 g) were obtained from Envigo, Horst, Netherlands. Mice were maintained under a 12-h dark–light cycle at a standardized environment with controlled humidity and temperature. They had ad libitum access to standard chow and water. 15 hours prior to the surgical intervention, mice were administered i.p. a single dose of 10 mg/kg dexamethasone (Mephameson, Mepha Pharma AG, Basel Switzerland). For pain relief, mice received a combination of 0.1 mg/kg buprenorphine (Temgesic, Indivior Schweiz AG, Baar, Switzerland) and 5 mg/kg carprofen (Rimadyl, Pfizer, New York, NY, USA) subcutaneously 30 min before and after surgery. A nose mask was fixed with continued treatment of 2–3% isoflurane for anesthesia. Following a midline laparotomy, polyethylene tubing (Smiths Medical, Adliswil, Switzerland) was carefully inserted into the gallbladder and placed just proximal to the junction of the cystic duct. A silk tie was used to secure the infusion tubing. The common bile duct was obstructed by a micro vessel clamp (60 g; Fine Science Tools, Heidelberg, Germany) to ensure fluid-injection directly into the liver and at the same time to prevent fluid from entering the pancreas and duodenum. A total volume of 400 µL containing either *in vivo*-jetPEI at N/P 1.1 (Polyplus, Illkirch, France) or dCS-NSuc-LPEI at c/p 2 and dCS-NPEG$_6$-COOH at c/p 1, each encapsulating 0.1 or 1 µg of Nanoplasmid™ n.P3Luc1 in 5% glucose solution, were administered. Duration of infusion was 10 min using an infusion pump (Harvard Apparatus, Holliston, MA, USA) and an infusion rate of 0.04 mL/min. After infusion, the micro vessel clamp was removed from the common bile duct. The infusion tubing was withdrawn from the gallbladder, the cystic duct was ligated, and a cholecystectomy was performed.

5.2.8.2.2. In vivo imaging and hepatotoxicity

Mice were injected intraperitoneally. with 150 mg/kg of D-luciferin potassium salt (Gold Biotechnology, St. Louis, MO, USA). After D-luciferin injection, bioluminescence was monitored using a bioimaging system (IVIS 200, Perkin Elmer, Santa Clara, CA, USA). Signals were quantified using Living Image 3.2 software (Perkin Elmer). After termination of the experiment on day 3, blood samples were collected from the vena cava. Alanine aminotransferase (ALT), alkaline phosphatase (ALP), and direct/total bilirubin levels in serum samples were analyzed as indicated by the manufacturer (Abbott Alinity C System, Abbot Laboratories, Chicago, IL, USA).

Chapter 6 References

[1] D. Ibraheem, A. Elaissari, H. Fessi, *Int. J. Pharm.* **2014**, *459*, 70–83.

[2] C. E. Dunbar, K. A. High, J. K. Joung, D. B. Kohn, K. Ozawa, M. Sadelain, *Science (80-.).* **2018**, *359*, eaan4672.

[3] X. M. Anguela, K. A. High, *Annu. Rev. Med.* **2019**, *70*, 273–288.

[4] A. V. Anzalone, L. W. Koblan, D. R. Liu, *Nat. Biotechnol.* **2020**, *38*, 824–844.

[5] L. Teboul, Y. Herault, S. Wells, W. Qasim, G. Pavlovic, *Mol. Ther.* **2020**, *28*, 1422–1431.

[6] D. Matsumoto, W. Nomura, *Bioconjug. Chem.* **2021**, *32*, 639–648.

[7] J. Conniot, S. Talebian, S. Simões, L. Ferreira, J. Conde, *Biomater. Sci.* **2021**, *9*, 1065–1087.

[8] C. Hardee, L. Arévalo-Soliz, B. Hornstein, L. Zechiedrich, *Genes* **2017**, *8*, 65.

[9] R. N. Aravalli, J. D. Belcher, C. J. Steer, *Liver Transplant.* **2015**, *21*, 718–737.

[10] M. L. Lugin, R. T. Lee, Y. J. Kwon, *ACS Nano* **2020**, *14*, 14262–14283.

[11] B. Santos-Carballal, E. Fernández Fernández, F. Goycoolea, *Polymers* **2018**, *10*, 444.

[12] U. Lächelt, E. Wagner, *Chem. Rev.* **2015**, *115*, 11043–11078.

[13] N. Bono, F. Ponti, D. Mantovani, G. Candiani, *Pharmaceutics* **2020**, *12*, 183.

[14] J. Lu, F. Zhang, S. Xu, A. Z. Fire, M. A. Kay, *Mol. Ther.* **2012**, *20*, 2111–2119.

[15] A. M. Darquet, B. Cameron, P. Wils, D. Scherman, J. Crouzet, *Gene Ther.* **1997**, *4*, 1341–1349.

[16] X. H. Hou, X. Y. Guo, Y. Chen, C.-Y. He, Z.-Y. Chen, *Mol. Ther. Methods Clin. Dev.* **2015**, *2*, 14062.

[17] C. P. Hodgson, A. E. Carnes, J. A. Williams, *Cell Gene Ther. Insights* **2017**, *3*, 95–101.

[18] J. M. Wilson, *Mol. Genet. Metab.* **2009**, *96*, 151–157.

[19] C. C. Ma, Z. L. Wang, T. Xu, Z. Y. He, Y. Q. Wei, *Biotechnol. Adv.* **2020**, *40*, 107502.

[20] A. Shahryari, M. S. Jazi, S. Mohammadi, H. R. Nikoo, Z. Nazari, E. S. Hosseini, I. Burtscher, S. J. Mowla, H. Lickert, *Front. Genet.* **2019**, *10*, 868.

[21] H. Yin, R. L. Kanasty, A. A. Eltoukhy, A. J. Vegas, J. R. Dorkin, D. G. Anderson, *Nat. Rev. Genet.* **2014**, *15*, 541–555.

[22] Y. Suzuki, H. Ishihara, *Drug Metab. Pharmacokinet.* **2021**, *41*, 100424.

[23] M. T. S. Lin, L. Pulkkinen, J. Uitto, K. Yoon, *Int. J. Dermatol.* **2000**, *39*, 161–170.

[24] C. Watkins, J. Hopkins, G. Harkiss, *Vaccine* **2005**, *23*, 4247–4256.

[25] X. Gao, K.-S. Kim, D. Liu, *AAPS J.* **2007**, *9*, E92–E104.

[26] X.-F. Ding, M. Fan, *Gene Therapy for Neurological Disorders*, Springer International Publishing, **2016**, 297–306.

[27] B. D. Hornstein, D. Roman, L. M. Arévalo-Soliz, M. A. Engevik, L. Zechiedrich, *PLoS One* **2016**, *11*, e0167537.

[28] J. Li, T. Yang, D. Huang, Y. Chen, Y. Huang, Z. Li, in *2020 IEEE 33rd Int. Conf. Micro Electro Mech. Syst.*, IEEE, **2020**, 372–375.

[29] X. Du, J. Wang, Q. Zhou, L. Zhang, S. Wang, Z. Zhang, C. Yao, *Drug Deliv.* **2018**, *25*, 1516–1525.

[30] B. L. Helfield, X. Chen, B. Qin, S. C. Watkins, F. S. Villanueva, *Ultrasound Med. Biol.* **2017**, *43*, 2678–2689.

[31] J. M. Escoffre, P. Campomanes, M. Tarek, A. Bouakaz, *Ultrason. Sonochem.* **2020**, *64*, 104998.

[32] M. Bez, J. Foiret, G. Shapiro, G. Pelled, K. W. Ferrara, D. Gazit, *Nat. Protoc.* **2019**, *14*, 1015–1026.

[33] T. Suda, D. Liu, *Mol. Ther.* **2007**, *15*, 2063–2069.

[34] M. Huang, R. Sun, Q. Huang, Z. Tian, *Front. Pharmacol.* **2017**, *8*, 591.

[35] F. Stoller, A. Schlegel, H. M. Viecelli, V. Rüfenacht, N. Cesarovic, C. Viecelli, S. Deplazes, R. Bettschart, K. Hurter, P. Schmierer, X. Sidler, P. Kron, P. Dutkowski, R. Graf, B. Thöny, J. Häberle, *Hum. Gene Ther. Methods* **2015**, *26*, 181–192.

[36] K. Xu, J. Sun, S. Chen, Y. Li, X. Peng, M. Li, Y. Li, *Biochem. Biophys. Res. Commun.* **2019**, *508*, 198–202.

[37] C. H. Sum, S. M. Shortall, S. Wong, S. D. Wettig, *Nanomedicine: Gene Delivery, Imaging and Evaluation Systems*, Springer International Publishing, **2018**, 3–68.

[38] G. Lin, L. Li, N. Panwar, J. Wang, S. C. Tjin, X. Wang, K. T. Yong, *Coord. Chem. Rev.* **2018**, *374*, 133–152.

[39] M. Riley, W. Vermerris, *Nanomaterials* **2017**, *7*, 94.

[40] M. A. Mintzer, E. E. Simanek, *Chem. Rev.* **2009**, *109*, 259–302.

[41] P. L. Felgner, T. R. Gadek, M. Holm, R. Roman, H. W. Chan, M. Wenz, J. P. Northrop, G. M. Ringold, M. Danielsen, *Proc. Natl. Acad. Sci. U. S. A.* **1987**, *84*, 7413–7417.

[42] A. V. Oliveira, A. M. Rosa da Costa, G. A. Silva, *Mater. Sci. Eng. C* **2017**, *77*, 1275–1289.

[43] J. P. Behr, B. Demeneix, J. P. Loeffler, J. Perez-Mutul, *Proc. Natl. Acad. Sci. U. S. A.* **1989**, *86*, 6982–6986.

[44] M. S. Al-Dosari, X. Gao, *AAPS J.* **2009**, *11*, 671–681.

[45] H. Lv, S. Zhang, B. Wang, S. Cui, J. Yan, *J. Control. Release* **2006**, *114*, 100–109.

[46] L. Jin, X. Zeng, M. Liu, Y. Deng, N. He, *Theranostics* **2014**, *4*, 240–255.

[47] M. A. Zanta, O. Boussif, A. Adib, J. P. Behr, *Bioconjug. Chem.* **1997**, *8*, 839–844.

[48] Y. Q. Wang, J. Su, F. Wu, P. Lu, L. F. Yuan, W. E. Yuan, J. Sheng, T. Jin, *Int. J. Nanomedicine* **2012**, *7*, 693–704.

[49] B. Singh, S. Maharjan, T.-E. Park, T. Jiang, S.-K. Kang, Y.-J. Choi, C.-S. Cho, *Macromol. Biosci.* **2015**, *15*, 622–635.

[50] G. Y. Wu, C. H. Wu, *J. Biol. Chem.* **1988**, *263*, 14621–14624.

[51] J. J. Virgen-Ortíz, J. C. S. dos Santos, Á. Berenguer-Murcia, O. Barbosa, R. C. Rodrigues, R. Fernandez-Lafuente, *J. Mater. Chem. B* **2017**, *5*, 7461–7490.

[52] A. P. Pandey, K. K. Sawant, *Mater. Sci. Eng. C* **2016**, *68*, 904–918.

[53] R. Kircheis, L. Wightman, E. Wagner, *Adv. Drug Deliv. Rev.* **2001**, *53*, 341–358.

[54] L. Tauhardt, K. Kempe, K. Knop, E. Altuntaş, M. Jäger, S. Schubert, D. Fischer, U. S. Schubert, *Macromol. Chem. Phys.* **2011**, *212*, 1918–1924.

[55] J. H. Jeong, S. H. Song, D. W. Lim, H. Lee, T. G. Park, *J. Control. Release* **2001**, *73*, 391–399.

[56] O. Boussif, F. Lezoualc'h, M. A. Zanta, M. D. Mergny, D. Scherman, B. Demeneix, J. P. Behr, *Proc. Natl. Acad. Sci.* **1995**, *92*, 7297–7301.

[57] A. Hall, U. Lächelt, J. Bartek, E. Wagner, S. M. Moghimi, *Mol. Ther.* **2017**, *25*, 1476–1490.

[58] S. A. Smith, L. I. Selby, A. P. R. Johnston, G. K. Such, *Bioconjug. Chem.* **2019**, *30*, 263–272.

[59] D. Pei, M. Buyanova, *Bioconjug. Chem.* **2019**, *30*, 273–283.

[60] S. Venkiteswaran, T. Thomas, T. J. Thomas, *ChemistrySelect* **2016**, *1*, 1144–1150.

[61] J. Chen, K. Wang, J. Wu, H. Tian, X. Chen, *Bioconjug. Chem.* **2018**, *30*, 338–349.

[62] D. Fischer, Y. Li, B. Ahlemeyer, J. Krieglstein, T. Kissel, *Biomaterials* **2003**, *24*, 1121–1131.

[63] A. Hall, A. K. Larsen, L. Parhamifar, K. D. Meyle, L. P. Wu, S. M. Moghimi, *Biochim. Biophys. Acta - Bioenerg.* **2013**, *1827*, 1213–1225.

[64] A. Hall, L. Parhamifar, M. K. Lange, K. D. Meyle, M. Sanderhoff, H. Andersen, M. Roursgaard, A. K. Larsen, P. B. Jensen, C. Christensen, J. Bartek, S. M. Moghimi, *Biochim. Biophys. Acta - Bioenerg.* **2015**, *1847*, 328–342.

[65] O. M. Merkel, R. Urbanics, P. Bedocs, Z. Rozsnyay, L. Rosivall, M. Toth, T. Kissel, J. Szebeni, *Biomaterials* **2011**, *32*, 4936–4942.

[66] K. Morimoto, M. Nishikawa, S. Kawakami, T. Nakano, Y. Hattori, S. Fumoto, F. Yamashita, M. Hashida, *Mol. Ther.* **2003**, *7*, 254–261.

[67] T. Thomas, H. Tajmir-Riahi, C. Pillai, *Molecules* **2019**, *24*, 3744.

[68] G. Navarro, C. Tros de ILarduya, *Nanomedicine Nanotechnology, Biol. Med.* **2009**, *5*, 287–297.

[69] H. Liu, H. Wang, W. Yang, Y. Cheng, *J. Am. Chem. Soc.* **2012**, *134*, 17680–17687.

[70] Y. Gao, X. L. Liu, X. R. Li, *Int. J. Nanomedicine* **2011**, *6*, 1017–1025.

[71] A. I. S. van den Berg, C. O. Yun, R. M. Schiffelers, W. E. Hennink, *J. Control. Release* **2021**, *331*, 121–141.

[72] R. Kumar, C. F. Santa Chalarca, M. R. Bockman, C. Van Bruggen, C. J. Grimme, R. J. Dalal, M. G. Hanson, J. K. Hexum, T. M. Reineke, *Chem. Rev.* **2021**, *121*, 11527–11652.

[73] M. M. Frank, L. F. Fries, *Immunol. Today* **1991**, *12*, 322–326.

[74] M. Ruponen, P. Honkakoski, M. Tammi, A. Urtti, *J. Gene Med.* **2004**, *6*, 405–414.

[75] J. S. Suk, Q. Xu, N. Kim, J. Hanes, L. M. Ensign, *Adv. Drug Deliv. Rev.* **2016**, *99*, 28–51.

[76] G. Chen, K. Wang, Y. Wang, P. Wu, M. Sun, D. Oupický, *Adv. Healthc. Mater.* **2018**, *7*, 1700978.

[77] A. Sizovs, L. Xue, Z. P. Tolstyka, N. P. Ingle, Y. Wu, M. Cortez, T. M. Reineke, *J. Am. Chem. Soc.* **2013**, *135*, 15417–15424.

[78] Z. P. Tolstyka, H. Phillips, M. Cortez, Y. Wu, N. Ingle, J. B. Bell, P. B. Hackett, T. M. Reineke, *ACS Biomater. Sci. Eng.* **2016**, *2*, 43–55.

[79] A. Abuchowski, J. R. McCoy, N. C. Palczuk, T. van Es, F. F. Davis, *J. Biol. Chem.* **1977**, *252*, 3582–3586.

[80] S. V. Vinogradov, T. K. Bronich, A. V. Kabanov, *Bioconjug. Chem.* **1998**, *9*, 805–812.

[81] M. Ogris, S. Brunner, S. Schüller, R. Kircheis, E. Wagner, *Gene Ther.* **1999**, *6*, 595–605.

[82] S. Mishra, P. Webster, M. E. Davis, *Eur. J. Cell Biol.* **2004**, *83*, 97–111.

[83] H. Hatakeyama, H. Akita, H. Harashima, *Adv. Drug Deliv. Rev.* **2011**, *63*, 152–160.

[84] M. Ogris, P. Steinlein, S. Carotta, S. Brunner, E. Wagner, *AAPS PharmSci* **2001**, *3*, E21.

[85] A. Gabizon, J. Szebeni, *ACS Nano* **2020**, *14*, 7682–7688.

[86] Q. Yang, T. M. Jacobs, J. D. McCallen, D. T. Moore, J. T. Huckaby, J. N. Edelstein, S. K. Lai, *Anal. Chem.* **2016**, *88*, 11804–11812.

[87] K. Takeda, S. Akira, *Int. Immunol.* **2005**, *17*, 1–14.

[88] J. R. Cubillos-Ruiz, X. Engle, U. K. Scarlett, D. Martinez, A. Barber, R. Elgueta, L. Wang, Y. Nesbeth, Y. Durant, A. T. Gewirtz, C. L. Sentman, R. Kedl, J. R. Conejo-Garcia, *J. Clin. Invest.* **2009**, *119*, 2231–2244.

[89] H. R. Phillips, Z. P. Tolstyka, B. C. Hall, J. K. Hexum, P. B. Hackett, T. M. Reineke, *Biomacromolecules* **2019**, *20*, 1530–1544.

[90] C. Plank, K. Mechtler, F. C. Szoka, E. Wagner, *Hum. Gene. Ther.* **1996**, *7*, 1437–1446.

[91] P. R. Dash, M. L. Read, L. B. Barrett, M. A. Wolfert, L. W. Seymour, *Gene Ther.* **1999**, *6*, 643–650.

[92] R. J. Stockert, *Physiol. Rev.* **1995**, *75*, 591–609.

[93] N. Mishra, N. P. Yadav, V. K. Rai, P. Sinha, K. S. Yadav, S. Jain, S. Arora, *Biomed Res. Int.* **2013**, 382184.

[94] D. Stokmaier, O. Khorev, B. Cutting, R. Born, D. Ricklin, T. O. G. Ernst, F. Böni, K. Schwingruber, M. Gentner, M. Wittwer, M. Spreafico, A. Vedani, S. Rabbani, O. Schwardt, B. Ernst, *Bioorg. Med. Chem.* **2009**, *17*, 7254–7264.

[95] S. Alonso, *J. Control. Release* **2018**, *287*, 216–234.

[96] Q. Pan, Y. Lv, G. R. Williams, L. Tao, H. Yang, H. Li, L. Zhu, *Carbohydr. Polym.* **2016**, *151*, 812–820.

[97] F. Kong, C. Tang, C. Yin, *Bioconjug. Chem.* **2020**, *31*, 2446–2455.

[98] A. M. Gazzali, M. Lobry, L. Colombeau, S. Acherar, H. Azaïs, S. Mordon, P. Arnoux, F. Baros, R. Vanderesse, C. Frochot, *Eur. J. Pharm. Sci.* **2016**, *93*, 419–430.

[99] F. Zhao, H. Yin, Z. Zhang, J. Li, *Biomacromolecules* **2013**, *14*, 476–484.

[100] B. Shi, H. Zhang, J. Bi, S. Dai, *Colloids Surf. B.* **2014**, *119*, 55–65.

[101] E. P. Rondon, H. A. Benabdoun, F. Vallières, M. S. Petrônio, M. J. Tiera, M. Benderdour, J. C. Fernandes, *Int. J. Nanomedicine* **2020**, *15*, 6183–6200.

[102] C. Liu, Y. Xie, X. Li, X. Yao, X. Wang, M. Wang, Z. Li, F. Cao, *Mol. Biotechnol.* **2021**, *63*, 63–79.

[103] P. Midoux, G. Breuzard, J. Gomez, C. Pichon, *Curr. Gene Ther.* **2008**, *8*, 335–352.

[104] O. L. Mozley, B. C. Thompson, A. Fernandez-Martell, D. C. James, *Biotechnol. Prog.* **2014**, *30*, 1161–1170.

[105] Q. Laurent, R. Martinent, B. Lim, A.-T. Pham, T. Kato, J. López-Andarias, N. Sakai, S. Matile, *JACS Au* **2021**, *1*, 710–728.

[106] T. Bus, A. Traeger, U. S. Schubert, *J. Mater. Chem. B* **2018**, *6*, 6904–6918.

[107] J. Mercer, A. Helenius, *Nat. Cell Biol.* **2009**, *11*, 510–520.

[108] L. Pelkmans, A. Helenius, *Traffic* **2002**, *3*, 311–320.

[109] S. Boeckle, K. von Gersdorff, S. van der Piepen, C. Culmsee, E. Wagner, M. Ogris, *J. Gene Med.* **2004**, *6*, 1102–1111.

[110] S. Vaidyanathan, J. Chen, B. G. Orr, M. M. Banaszak Holl, *Mol. Pharm.* **2016**, *13*, 1967–1978.

[111] A. D. Frankel, C. O. Pabo, *Cell* **1988**, *55*, 1189–1193.

[112] M. Green, P. M. Loewenstein, *Cell* **1988**, *55*, 1179–1188.

[113] A. Joliot, C. Pernelle, H. Deagostini-Bazin, A. Prochiantz, *Proc. Natl. Acad. Sci. U. S. A.* **1991**, *88*, 1864–1868.

[114] B. Layek, L. Lipp, J. Singh, *Int. J. Mol. Sci.* **2015**, *16*, 28912–28930.

[115] G. Guidotti, L. Brambilla, D. Rossi, *Trends Pharmacol. Sci.* **2017**, *38*, 406–424.

[116] J. B. Rothbard, T. C. Jessop, R. S. Lewis, B. A. Murray, P. A. Wender, *J. Am. Chem. Soc.* **2004**, *126*, 9506–9507.

[117] S. Futaki, T. Suzuki, W. Ohashi, T. Yagami, S. Tanaka, K. Ueda, Y. Sugiura, *J. Biol. Chem.* **2001**, *276*, 5836–5840.

[118] T. Tashima, *Bioorganic Med. Chem. Lett.* **2017**, *27*, 121–130.

[119] H. J. P. Ryser, E. M. Levy, R. Mandel, G. J. DiSciullo, *Proc. Natl. Acad. Sci. U. S. A.* **1994**, *91*, 4559–4563.

[120] S. Aubry, F. Burlina, E. Dupont, D. Delaroche, A. Joliot, S. Lavielle, G. Chassaing, S. Sagan, *FASEB J.* **2009**, *23*, 2956–2967.

[121] E. K. Bang, G. Gasparini, G. Molinard, A. Roux, N. Sakai, S. Matile, *J. Am. Chem. Soc.* **2013**, *135*, 2088–2091.

[122] J. López-Andarias, J. Saarbach, D. Moreau, Y. Cheng, E. Derivery, Q. Laurent, M. González-Gaitán, N. Winssinger, N. Sakai, S. Matile, *J. Am. Chem. Soc.* **2020**, *142*, 4784–4792.

[123] E. Derivery, E. Bartolami, S. Matile, M. Gonzalez-Gaitan, *J. Am. Chem. Soc.* **2017**, *139*, 10172–10175.

[124] P. Yuan, X. Mao, K. C. Chong, J. Fu, S. Pan, S. Wu, C. Yu, S. Q. Yao, *Small* **2017**, *13*, 1700569.

[125] G. Gasparini, G. Sargsyan, E. K. Bang, N. Sakai, S. Matile, *Angew. Chemie Int. Ed.* **2015**, *54*, 7328–7331.

[126] D. Abegg, G. Gasparini, D. G. Hoch, A. Shuster, E. Bartolami, S. Matile, A. Adibekian, *J. Am. Chem. Soc.* **2017**, *139*, 231–238.

[127] R. Martinent, S. Tawffik, J. López-Andarias, D. Moreau, Q. Laurent, S. Matile, *Chem. Sci.* **2021**, *12*, 13922–13929.

[128] A. Tirla, P. Rivera-Fuentes, *Biochemistry* **2019**, *58*, 1184–1187.

[129] N. Chuard, G. Gasparini, D. Moreau, S. Lörcher, C. Palivan, W. Meier, N. Sakai, S. Matile, *Angew. Chemie Int. Ed.* **2017**, *56*, 2947–2950.

[130] G. L. Lukacs, P. Haggie, O. Seksek, D. Lechardeur, N. Freedman, A. S. Verkman, *J. Biol. Chem.* **2000**, *275*, 1625–1629.

[131] R. P. Kulkarni, K. Castelino, A. Majumdar, S. E. Fraser, *Biophys. J.* **2006**, *90*, L42–L44.

[132] K. Itaka, A. Harada, Y. Yamasaki, K. Nakamura, H. Kawaguchi, K. Kataoka, *J. Gene Med.* **2004**, *6*, 76–84.

[133] J. Cheng, R. Zeidan, S. Mishra, A. Liu, S. H. Pun, R. P. Kulkarni, G. S. Jensen, N. C. Bellocq, M. E. Davis, *J. Med. Chem.* **2006**, *49*, 6522–6531.

[134] N. Panté, M. Kann, *Mol. Biol. Cell* **2002**, *13*, 425–434.

[135] J. J. Ludtke, G. Zhang, M. G. Sebestyén, J. A. Wolff, *J. Cell Sci.* **1999**, *112*, 2033–2041.

[136] M. G. Sebestyén, J. J. Ludtke, M. C. Bassik, G. Zhang, V. Budker, E. A. Lukhtanov, J. E. Hagstrom, J. A. Wolff, *Nat. Biotechnol.* **1998**, *16*, 80–85.

[137] E. Hébert, *Biol. Cell* **2003**, *95*, 59–68.

[138] L. M. McLane, A. H. Corbett, *IUBMB Life* **2009**, *61*, 697–706.

[139] H. Bai, G. M. S. Lester, L. C. Petishnok, D. A. Dean, *Biosci. Rep.* **2017**, *37*, 20160616.

[140] D. A. Dean, *Exp. Cell Res.* **1997**, *230*, 293–302.

[141] A. B. Hill, M. Chen, C. K. Chen, B. A. Pfeifer, C. H. Jones, *Trends Biotechnol.* **2016**, *34*, 91–105.

[142] S. M. Joseph, S. Krishnamoorthy, R. Paranthaman, J. A. Moses, C. Anandharamakrishnan, *Carbohydr. Polym. Technol. Appl.* **2021**, *2*, 100036.

[143] M. Yadav, P. Goswami, K. Paritosh, M. Kumar, N. Pareek, V. Vivekanand, *Bioresour. Bioprocess.* **2019**, *6*, 8.

[144] V. P. Santos, N. S. S. Marques, P. C. S. V. Maia, M. A. B. de Lima, L. de O. Franco, G. M. de Campos-Takaki, *Int. J. Mol. Sci.* **2020**, *21*, 4290.

[145] H. Mittal, S. S. Ray, B. S. Kaith, J. K. Bhatia, Sukriti, J. Sharma, S. M. Alhassan, *Eur. Polym. J.* **2018**, *109*, 402–434.

[146] I. Younes, M. Rinaudo, *Mar. Drugs* **2015**, *13*, 1133–1174.

[147] M. N. V. R. Kumar, R. A. A. Muzzarelli, C. Muzzarelli, H. Sashiwa, A. J. Domb, *Chem. Rev.* **2004**, *104*, 6017–6084.

[148] X. Zhai, C. Li, D. Ren, J. Wang, C. Ma, A. M. Abd El-Aty, *Carbohydr. Polym.* **2021**, *266*, 118132.

[149] C. Marques, C. Som, M. Schmutz, O. Borges, G. Borchard, *Front. Bioeng. Biotechnol.* **2020**, *8*, 165.

[150] T. Kean, M. Thanou, *Adv. Drug Deliv. Rev.* **2010**, *62*, 3–11.

[151] S. C. W. Richardson, H. V. J. Kolbe, R. Duncan, *Int. J. Pharm.* **1999**, *178*, 231–243.

[152] M. Jumaa, F. H. Furkert, B. W. Müller, *Eur. J. Pharm. Biopharm.* **2002**, *53*, 115–123.

[153] Z. Guo, R. Chen, R. Xing, S. Liu, H. Yu, P. Wang, C. Li, P. Li, *Carbohydr. Res.* **2006**, *341*, 351–354.

[154] Y. Cao, Y. F. Tan, Y. S. Wong, M. W. J. Liew, S. Venkatraman, *Mar. Drugs* **2019**, *17*, 381.

[155] A. Fiamingo, J. A. D. M. Delezuk, S. Trombotto, L. David, S. P. Campana-Filho, *Ultrason. Sonochem.* **2016**, *32*, 79–85.

[156] W.-J. Jung, R.-D. Park, *Mar. Drugs* **2014**, *12*, 5328–5356.

[157] E. N. Chebotok, V. Y. Novikov, I. N. Konovalova, *Russ. J. Appl. Chem.* **2006**, *79*, 1162–1166.

[158] C. Q. Qin, Y. M. Du, L. Xiao, *Polym. Degrad. Stab.* **2002**, *76*, 211–218.

[159] C. T. Tsao, C. H. Chang, Y. Y. Lin, M. F. Wu, J. L. Han, K. H. Hsieh, *Carbohydr. Res.* **2011**, *346*, 94–

102.

[160] E. D. Freitas, C. F. Moura, J. Kerwald, M. M. Beppu, *Polymers* **2020**, *12*, 2878.

[161] A. Fabiano, D. Beconcini, C. Migone, A. M. Piras, Y. Zambito, *Int. J. Mol. Sci.* **2020**, *21*, 6617.

[162] A. Anitha, S. Maya, N. Deepa, K. P. Chennazhi, S. V. Nair, H. Tamura, R. Jayakumar, *Carbohydr. Polym.* **2011**, *83*, 452–461.

[163] M. S. Gularte, J. M. Anghinoni, L. Abenante, G. T. Voss, R. L. de Oliveira, R. A. Vaucher, C. Luchese, E. A. Wilhelm, E. J. Lenardão, A. R. Fajardo, *Carbohydr. Polym.* **2019**, *219*, 240–250.

[164] M. S. Hanafy, W. M. Desoky, E. M. Hussein, N. H. El-Shaer, M. Gomaa, A. A. Gamal, M. A. Esawy, O. W. Guirguis, *J. Biomed. Mater. Res. Part A* **2021**, *109*, 232–247.

[165] M. Gingras, I. Paradis, F. Berthod, *Biomaterials* **2003**, *24*, 1653–1661.

[166] J. Radwan-Pragłowska, Ł. Janus, M. Piątkowski, D. Bogdał, D. Matysek, *Polymers* **2020**, *12*, 792.

[167] E. Díaz-montes, R. Castro-muñoz, *Polymers* **2021**, *13*, 767.

[168] M. Usman, A. Ahmed, B. Yu, S. Wang, Y. Shen, H. Cong, *Carbohydr. Polym.* **2020**, *255*, 117486.

[169] B. G. K. Steiger, L. D. Wilson, *Int. J. Mol. Sci.* **2020**, *21*, 7130.

[170] J. Li, X. Tian, T. Hua, J. Fu, M. Koo, W. Chan, T. Poon, *ACS Appl. Bio Mater.* **2021**, *4*, 4014–4038.

[171] Z. Mohammadi, M. Eini, A. Rastegari, M. R. Tehrani, *Carbohydr. Polym.* **2021**, *256*, 117414.

[172] H. L. Jiang, Y. K. Kim, R. Arote, J. W. Nah, M. H. Cho, Y. J. Choi, T. Akaike, C. S. Cho, *J. Control. Release* **2007**, *117*, 273–280.

[173] D. Wu, Y. Zhang, X. Xu, T. Guo, D. Xie, R. Zhu, S. Chen, S. Ramakrishna, L. He, *Acta Biomater.* **2018**, *72*, 266–277.

[174] Y. Zhang, X. Tan, T. Ren, C. Jia, Z. Yang, H. Sun, *Carbohydr. Polym.* **2018**, *198*, 76–85.

[175] R. Feng, W. Wang, L. Zhu, H. Xu, S. Chen, Z. Song, *J. Biomed. Mater. Res. Part B Appl. Biomater.* **2020**, *108*, 3345–3355.

[176] K. Aiedeh, M. O. Taha, *Arch. Pharm.* **1999**, *332*, 103–107.

[177] X. Zhang, Y. Duan, D. Wang, F. Bian, *Carbohydr. Polym.* **2015**, *122*, 53–59.

[178] E. A. Kamoun, *J. Adv. Res.* **2016**, *7*, 69–77.

[179] G. W. Jeong, J. W. Nah, *Carbohydr. Polym.* **2017**, *178*, 322–330.

[180] J. Q. Gao, Q. Q. Zhao, T. F. Lv, W. P. Shuai, J. Zhou, G. P. Tang, W. Q. Liang, Y. Tabata, Y. L. Hu, *Int. J. Pharm.* **2010**, *387*, 286–294.

[181] M. Zhang, X. Qiao, W. Han, T. Jiang, F. Liu, X. Zhao, *Carbohydr. Polym.* **2021**, *266*, 118100.

[182] L. Yue, J. Li, W. Chen, X. Liu, Q. Jiang, W. Xia, *Carbohydr. Polym.* **2017**, *176*, 356–364.

[183] E. Olewnik-Kruszkowska, M. Gierszewska, S. Grabska-Zielińska, J. Skopińska-Wiśniewska, E. Jakubowska, *Int. J. Mol. Sci.* **2021**, *22*, 3329.

[184] J. Wang, L. G. Liu, W. Q. Jiao, H. Yang, J. Liu, D. Liu, *Carbohydr. Polym.* **2021**, *256*, 117497.

[185] L. Nicolle, C. M. A. Journot, S. Gerber-Lemaire, *Polymers* **2021**, *13*, 4118.

[186] E. Curti, D. de Britto, S. P. Campana-Filho, *Macromol. Biosci.* **2003**, *3*, 571–576.

[187] H. Chen, Y. Zhao, S. Cui, D. Zhi, S. Zhang, X. Peng, *J. Appl. Polym. Sci.* **2015**, *132*, 42469.

[188] M. Fathi, P. Sahandi Zangabad, J. Barar, A. Aghanejad, H. Erfan-Niya, Y. Omidi, *Int. J. Biol. Macromol.* **2018**, *106*, 266–276.

[189] M. Zheng, B. Han, Y. Yang, W. Liu, *Carbohydr. Polym.* **2011**, *86*, 231–238.

[190] L. Xia, S. Wang, Z. Jiang, J. Chi, S. Yu, H. Li, Y. Zhang, L. Li, C. Zhou, W. Liu, B. Han, *Carbohydr. Polym.* **2021**, *264*, 117965.

[191] C. Xu, S. Guan, J. Xu, W. Gong, T. Liu, X. Ma, C. Sun, *Carbohydr. Polym.* **2021**, *252*, 117210.

[192] K. Zhang, P. Zhuang, Z. Wang, Y. Li, Z. Jiang, Q. Hu, M. Liu, Q. Zhao, *Carbohydr. Polym.* **2012**, *90*, 1515–1521.

[193] M. Elsabahy, M. A. Hamad, *Mar. Drugs* **2021**, *19*, 50.

[194] J. Nie, Z. Wang, Q. Hu, *Sci. Rep.* **2016**, *6*, 36005.

[195] M. Yao, Y. Lu, T. Zhang, J. Xie, S. Han, S. Zhang, Y. Fei, Z. Ling, J. Wu, Y. Hu, S. Ji, H. Chen, B. Berglund, L. Li, *npj Biofilms Microbiomes* **2021**, *7*, 58.

[196] N. Sedyakina, A. Kuskov, K. Velonia, N. Feldman, S. Lutsenko, G. Avramenko, *Materials.* **2020**, *13*, 1989.

[197] L. Zhuang, X. Zhi, B. Du, S. Yuan, *ACS Omega* **2020**, *5*, 1086–1097.

[198] D. Shahdeo, V. Kesarwani, D. Suhag, J. Ahmed, S. M. Alshehri, S. Gandhi, *Carbohydr. Polym.* **2021**, *266*, 118138.

[199] U. Lichter-Konecki, L. Caldovic, H. Morizono, K. Simpson, N. Ah Mew, E. MacLeod, "Ornithine Transcarbamylase Deficiency," can be found under https://www.ncbi.nlm.nih.gov/books/NBK154378/, **2013**.

[200] H. M. Grisch-Chan, G. Schwank, C. O. Harding, B. Thöny, *Hum. Gene Ther.* **2019**, *30*, 1274–1283.

[201] C. M. A. Journot, L. Nicolle, Y. Lavanchy, S. Gerber-Lemaire, *Polymers* **2020**, *12*, 1274.

[202] M. Agirre, J. Zarate, E. Ojeda, G. Puras, J. Desbrieres, J. L. Pedraz, *Polymers* **2014**, *6*, 1727–1755.

[203] H. Lu, Y. Dai, L. Lv, H. Zhao, *PLoS One* **2014**, *9*, e84703.

[204] L. Nicolle, J. Casper, M. Willimann, C. M. A. Journot, P. Detampel, T. Einfalt, H. M. Grisch-Chan, B. Thöny, S. Gerber-Lemaire, J. Huwyler, *Int. J. Mol. Sci.* **2021**, *22*, 3828.

[205] I. Dmour, M. O. Taha, *Int. J. Pharm.* **2017**, *529*, 15–31.

[206] X. Zhao, R. Shen, L. Bao, C. Wang, H. Yuan, *Carbohydr. Polym.* **2020**, *245*, 116509.

[207] R. J. Pounder, M. J. Stanford, P. Brooks, S. P. Richards, A. P. Dove, *Chem. Commun.* **2008**, *44*, 5158–5160.

[208] M. J. Kade, D. J. Burke, C. J. Hawker, *J. Polym. Sci. Part A Polym. Chem.* **2010**, *48*, 743–750.

[209] A. C. Croce, A. Ferrigno, M. Vairetti, R. Bertone, I. Freitas, G. Bottiroli, *Photochem. Photobiol. Sci.* **2004**, *3*, 920–926.

[210] D. Wahler, O. Boujard, F. Lefèvre, J. L. Reymond, *Tetrahedron* **2004**, *60*, 703–710.

[211] K. J. Padiya, S. Gavade, B. Kardile, M. Tiwari, S. Bajare, M. Mane, V. Gaware, S. Varghese, D. Harel, S. Kurhade, *Org. Lett.* **2012**, *14*, 2814–2817.

[212] R. De Matos, J. Vuilleumier, C. Mas, S. Constant, D. Staedler, S. Gerber-Lemaire, *RSC Adv.* **2019**, *9*,

31659–31669.

[213] M. Rezaee, R. K. Oskuee, H. Nassirli, B. Malaekeh-Nikouei, *J. Control. Release* **2016**, *236*, 1–14.